PB-222 349

STEAM CAR CONTROL ANALYSIS

E. A. Mayer, et al

Bendix Corporation

Prepared for:

Environmental Protection Agency

July 1972

DISTRIBUTED BY:

NTIS

National Technical Information Service
U. S. DEPARTMENT OF COMMERCE
5285 Port Royal Road, Springfield Va. 22151

APTD-1545
PB 222 349

Steam Car Control Analysis

E.A. Mayer
G.W. Hurlong. Jr.

The Bendix Corporation
Research Laboratories
Southfield, Michigan

Final Report
July 1972

Prepared for

Steam Engine Systems Corporation
Watertown, Massachusetts

Prime Contract No. 68-04-0004
Division of Advanced Automotive Power Systems Development
Environmental Protection Agency
Ann Arbor, Michigan

Reproduced by
NATIONAL TECHNICAL
INFORMATION SERVICE
U S Department of Commerce
Springfield VA 22151

BRL Report No. 6329

Copy No. 25

181

BIBLIOGRAPHIC DATA SHEET

1. Report No. APTD-1545

2.

3. Recipient's Accession No. PB-222 349

4. Title and Subtitle

Steam Car Control Analysis

5. Report Date July 1972

6.

7. Author(s) E. A. Mayer and G. W. Hurlong, Jr.

8. Performing Organization Rept. No. BRL Report 6329

9. Performing Organization Name and Address

Steam Engine Systems Corporation, Watertown, Massachusetts
and
The Bendix Corporation, Southfield, Michigan

10. Project/Task/Work Unit No.

11. Contract/Grant No. 68-04-0004

12. Sponsoring Organization Name and Address

ENVIRONMENTAL PROTECTION AGENCY
Division of Advanced Automotive Power Systems Development
Ann Arbor, Michigan

13. Type of Report & Period Covered Final

14.

15. Supplementary Notes

16. Abstracts

The aims were the selection of the best control mode for steam-car power plant and experimental verification of the soundness of the concept through pre-prototype control hardware. A new control concept, the predictive flow-control system, was proposed; it includes the use of the expander as a positive-displacement machine to give an indication of instantaneous steam-flow requirements. A strong open-loop control system then adjusts both the burner power level and the feedwater supply system to satisfy this demand. Secondary closed-loop controls correct any deviations in the output pressure and temperature of the steam generator from the desired set points. The corrections are accomplished by an appropriate trim-control function in both the burner and feedwater supply systems. A wide-range, analytical model of the vapor generator was combined with an analytical description of the expander and all auxiliaries to form a hybrid-computer simulation. Results were compared with experimental data on the Steam Engine Systems Model-4 vapor-generating system. This included both steady-state and dynamic comparison. A closed-loop control-mode simulation test program also was conducted to verify the soundness of the proposed control concept. The facsimile control-system hardware was specially designed to allow a more extensive evaluation of the proposed control mode without the development costs essential for an in-car installation. The predictive control system can provide satisfactory power plant operation. The analytical model of the Rankine cycle power plant has sufficient steady state and dynamic accuracy for detailed design of the control system. Optimization of the control concepts depend very strongly on component performance characteristics; the complexity of control can be traded against component complexity.

17. Key Words and Document Analysis. 17a. Descriptors

Air pollution
Steam
Automobiles
Water
Flow rates
Pressure
Temperature
Mathematical models
Simulation
Tests
Process control
Motor vehicle engines

17b. Identifiers/Open-Ended Terms

17c. COSATI Field/Group 13B

18. Availability Statement Unlimited

19. Security Class (This Report) UNCLASSIFIED

20. Security Class (This Page) UNCLASSIFIED

21. No. of Pages ~~167~~ 181

22. Price 11.25

FORM NTIS-35 (REV. 3-72)

THIS FORM MAY BE REPRODUCED

USCOMM-DC 14952-P72

Steam Car Control Analysis

E.A. Mayer
G.W. Hurlong. Jr.

The Bendix Corporation
Research Laboratories
Southfield, Michigan

Final Report
July 1972

Prepared for

Steam Engine Systems Corporation
Watertown, Massachusetts

ia

ACKNOWLEDGMENTS

The authors gratefully acknowledge assistance from the following people:

Dr. Lawrence C. Hoagland and Dr. Joseph Gerstman of Steam Engine Systems Corporation, Watertown, Massachusetts, for their specific and detailed involvement in the development of the steam-generator analytical model and their continued review of the entire technical effort;

Mr. Lewis J. Plumley of the Electrodynamics Division of The Bendix Corporation, North Hollywood, California, for the analysis and design of the electric servo actuators used in the facsimile and control-mode test experiments;

Mr. James M. Kirwin and Mr. Elmer A. Haase of the Energy Controls Division of The Bendix Corporation, South Bend, Indiana, for the design of the RSA Fuel Controller;

Mr. Ray J. Brown of the Bendix Research Laboratories, Southfield, Michigan, for the programming of the hybrid computer.

TABLE OF CONTENTS

Page

SECTION 1 - SUMMARY 1-1

1.1 Program Definition and Summary of Results 1-1
1.2 Conclusions 1-3
1.3 Recommendations 1-4

SECTION 2 - PROTOTYPE CONTROL DESIGN 2-1

2.1 Historical Background 2-1
2.2 Predictive Flow Control Concept 2-3
2.3 Predictive-Control Concept Implementation with Variable-Speed Auxiliary Drive 2-7

SECTION 3 - FACSIMILE CONTROL DESIGN 3-1

3.1 Facsimile Control Concept 3-1
3.2 Burner Control 3-4
3.3 Fuel Control 3-20
3.4 Bypass Valve 3-31
3.5 Facsimile Design Verification Test Results 3-39

SECTION 4 - ANALYTICAL CONTROL EVALUATION 4-1

4.1 Hybrid Computer Model 4-1
4.2 Experimental Verification for Model SES-4 4-25
4.3 Prototype Results 4-34

NOMENCLATURE 4-59

SECTION 5 - CONTROL MODE SIMULATION EXPERIMENTS 5-1

5.1 Experimental System Description 5-1
5.2 Simulation-Hardware Design Test Results 5-3
5.3 Closed-Loop Steam Generator Test Results 5-6

The aims

SECTION 1

SUMMARY

1.1 PROGRAM DEFINITION AND SUMMARY OF RESULTS

Final Objective

The final objective of the entire program is the development of a control system for a steam-car power plant. The achievement of the overall operational simplicity, safety and convenience that is currently available in present-day spark-ignition automobiles serves as the guideline for design of the control system. Power plant controls are to be fully automatic with the only input required of the driver to be the operation of the accelerator pedal. The operating control for the power plant must then control not only the input of steam to the expander, but also automatically control the feedwater and heat inputs to the steam generator to satisfy the operator's power demand. The objectives of the program phase covered by this final report were the selection of the best control mode and experimental verification of the soundness of the concept through pre-prototype control hardware.

Accomplishments

The program plan for the 16-month program is shown in Figure 1-1. The plan denotes a good balance between analytical and experimental programs aimed at the fulfillment of the program objectives stated. An early examination of control concepts adaptable to the needs of a vehicular steam power plant indicated the need for new development. To fill this need, a new control concept, the predictive flow-control system, was proposed for the steam car. The salient features of this controller include the use of the expander as a positive-displacement machine to give an indication of instantaneous steam-flow requirements. A strong open-loop control system then adjusts both the burner power level and the feedwater supply system to satisfy this demand. Secondary closed-loop controls correct any deviations in the output pressure and temperature of the steam generator from the desired set points. The corrections are accomplished by an appropriate trim-control function in both the burner and feedwater supply systems.

A wide-range, analytical model of the vapor generator was combined with an analytical description of the expander and all auxiliaries to form a hybrid-computer simulation. This computer simulation then served as the design tool for the evaluation of the various control concepts. In order to increase the credibility of the analytical results, initial results were compared with ~~available~~ experimental data on the Steam Engine Systems Model-4 vapor-generating system. The experimental

to p. 1-3

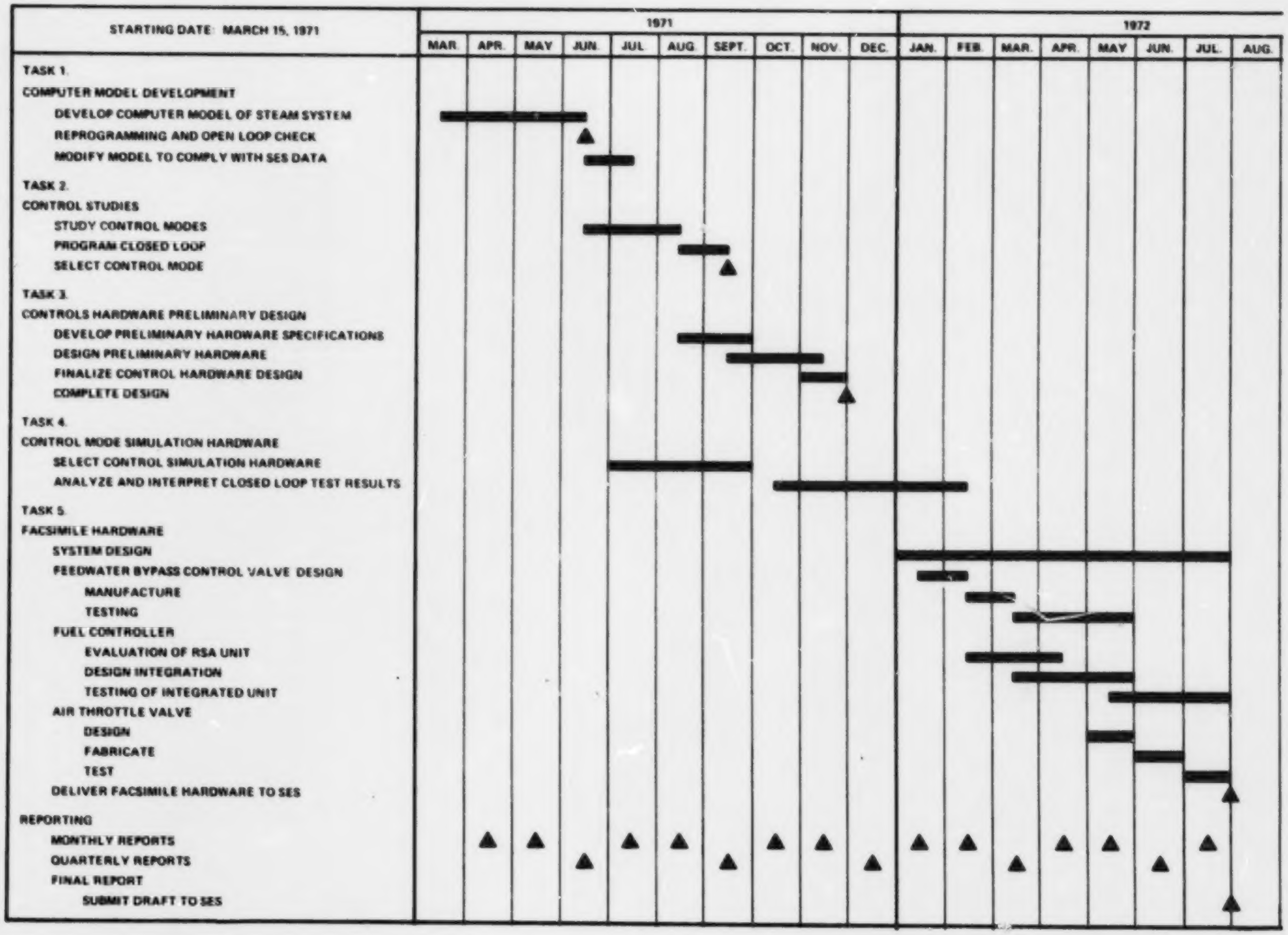

Figure 1-1 - Program Plan

from p 1.1

& Thus

verification included both steady-state and dynamic comparison between analytical predictions and known hardware performance. In addition to these open-loop verifications, a closed-loop control-mode simulation test program also was conducted to verify the soundness of the proposed control concept.

The facsimile control-system hardware was specially designed to allow a more extensive evaluation of the proposed control mode without the development costs essential for an in-car installation. The facsimile controllers made maximum use of commercially available components to test the concept. An electronic analytical signal processor was used to provide the necessary computations for the predictive signals. In addition, a laboratory-type feedwater meter was included in the vapor-generator feedwater system to predict the power level without relying on the expander for this function. A commercially available fuel controller was integrated with the system to provide the primary fuel-metering function to the burner. In the facsimile hardware program a feedwater bypass valve was also developed. This unit will serve to provide experimental design information for future, more advanced feedwater control hardware.

The program, thus concluded, will provide baseline information and the design tools necessary for the determination of design details needed for the development of the in-car control system.

1.2 CONCLUSIONS

On the basis of the completed program, the following conclusions are justified:

(1) Conventional closed-loop control of temperature and pressure is not satisfactory for the steam generator system. The complex interrelationship between pressure and temperature in the boiling section are combined with extremely long and variable response time in the vapor generator system. This combination becomes a source of control instability, particularly during operation at the low power levels and gain settings essential for safe and efficient operation of the power plant.

(2) The predictive control system with a closed-loop trim control in the temperature and pressure circuits can provide a satisfactory power plant operation.

(3) The analytical model of the Rankine cycle power plant has been verified by comparison with experimental data obtained by Steam Engine Systems Corporation. The model has sufficient steady state and dynamic accuracy for detailed design of the control system.

5
6
1-4

(4) The simplified hardware implementation of the predictive-control system does not provide satisfactory control over a 20:1 range of steam flow. To date, the control studies have not identified all the details of a system capable of operation over a flow range of at least 20:1.

(5) The program completed to date has developed an analytical tool that offers a realistic evaluation of details of the control design. The tradeoff studies conducted during the program also indicate that the optimization of the control concepts depend very strongly on component performance characteristics; ~~In other words~~, the complexity of control can be traded against component complexity. For example, the possible choice of a variable-displacement feedpump can reduce the control complexity through the elimination of the variable-ratio auxiliary drive and its control system.

1.3 RECOMMENDATIONS

On the basis of the experimental and analytical control studies conducted during the program covered by this report, a significant first step was made toward the successful proportional control of Rankine-cycle power plants. The most significant achievement, the establishment of a useful, analytical model of the Rankine-cycle power plant, is a basis for recommendations for continued work. The use of this tool offers a considerable savings both in time and development costs for the design of the Rankine-cycle power plant controls. The following specific recommendations can be made:

(1) Continue to use the analytical model as a design tool for the controls as the component selection is finalized. A blend of analytical and experimental programs, such as the one carried out during the completed phase of the program, should be continued for the purpose of maintaining a high confidence level in the design of the control system.

(2) Optimize the control concept for the selected hardware configuration and extend operation to meet the 20:1 operating range.

(3) Expand the initial facsimile control work and develop the required wide-range fuel-air ratio control for an external combustor system.

(4) In conjunction with development of the operating controls, develop the automatic startup and shutdown control system.

(5) Investigate alternate feedwater control concepts in addition to the present feedwater control concept.

(6) Investigate alternate control systems that would not require the use of the variable-ratio drive for the auxiliaries.

(7) Develop an electro-pneumatic servo for in-car combustion-air damper operation.

SECTION 2

PROTOTYPE CONTROL DESIGN

Examination of a steam-car bibliography indicates that the on-off type burner and feedwater controls dominated the early designs. Some references can be found describing proportional control. Valuable experimental performance evaluation reports were not available. On the basis of the adaptation of controls used on modern low-water-inventory steam generators, a predictive metering control is proposed in this program for the modern steam car. This control concept generates a measure of the instantaneous steam demand of the expander. On the basis of the steam flow information available, a strong predictive controller adjusts the burner firing rate to the known steady-state requirement of the steam generator plant. The feedwater flow input is also matched by the controller to the steam rate of the expander. Deviation in steam-generator output temperatures and pressures from the desired set points are independently corrected through closed-loop controls in the burner firing rate and feedwater supply systems respectively. Because the large variations in the variables are corrected by the open-loop predictive controller, the lower gains available in the closed-loop trim-control circuits can satisfactorily correct for deviation in plant characteristics and dynamic responses of the temperature and pressure control systems. Detailed implementation on the computer were evaluated using the expander as the flowmeter and an engine-driven, fixed-displacement, feedwater pump and combustion-air blower. The predictive control, in this case, was implemented through the use of a limited-range, variable-speed drive between the expander and the auxiliaries. Closed-loop pressure-trim control was accomplished through the use of a feedwater bypass valve. The temperature trim control was implemented through a combustion-air throttle valve. An independent fuel controller was used to maintain the air-fuel ratio at the desired level.

2.1 HISTORICAL BACKGROUND

The difficulty experienced by early steam car designers in automatic control of the monotube boiler becomes apparent on an examination of available bibliographies, such as the references listed at the end of this section. In addition to the slow thermal response from the boiler, the strongly intercoupled thermodynamic relations between pressure and temperature eliminate the possible use of the simple, independent, pressure and temperature controls. In the following, three typical monotube steam-generator control concepts will be reviewed.

Late-Model Doble Steam-Car Controls

Probably the most successful, and also most sophisticated, fully automatic boiler controls of early steam cars were developed by Abner

Doble. Several versions of controls can be found on the various models of Doble cars. A typical late control design uses an exhaust-steam-driven combustion-air blower, a feedpump and a condenser fan. The control is accomplished through the use of solenoid valves operated by a combination of pressure and temperature switches. The burner control is operated through a pressure sensor. At the low pressure limit (typically 1400 psi), the burner is turned on. As the steam pressure rises to the high limit setting (typically 1700 psi) of the burner control switch, the burner is turned off. An additional thermostat switch is set at the high temperature limit (such as 875°F) and the burner is turned off regardless of the value of the steam generator pressure. The steam-operated feedpump is controlled through a solenoid valve. The pump is turned off at the minimum temperature setting, such as 840°F. To improve the dynamic response of the steam generator, Doble uses a normalizer which injects feedwater near the entrance of the superheater at the time the feedwater flow to the boiler is increased. The flow through the normalizer helps to reduce the response time of the boiler. The fuel flow is controlled automatically through a simple carburetor equipped with a venturi injection supplied from a level-regulated fuel bowl. Further detailed descriptions of this and other Doble steam-car control concepts may be found in Reference 1.

The General Motors SE-101 Steam-Car Control

One of the most recent steam-car control designs can be found on the GM SE-101 Steam Car as reported in Reference 2. This control system includes a fully automatic turn-key starter sequence control. The operating control system is a three-level controller. This system uses a fixed-displacement engine-driven pump and solenoid bypass valves in the feedwater control circuit. The combustion air is supplied by an expander-driven combustion-air blower. The fuel system includes a fuel pump and a bypass solenoid. Air-fuel ratio essentially is controlled by the common mechanical drive of combustion-air blower and fuel pump. A three-level control mode, consisting of off, low and high outputs, is employed both in the combustion control and the feedwater control systems. Depending on a decision matrix, considering both output pressure and temperature, an electric decision network selects the appropriate level of operation for both the burner and the feedwater control. The use of a multilevel controller offers a more continuous operation of the steam generator and a better matching of steam output to the requirements of the vehicle.

Late-Model White Steam-Car Control System

One of the few attempts at proportional control of the monotube steam-car boiler is that of the late White system. The burner fuel supply is set to be proportional to the feedwater input to the steam generator by the "flowmotor." The flowmotor is a piston-spring combination. The differential pressure to the piston actuator is supplied from a pressure drop across a metering orifice in the feedwater system and correction is applied to the feedwater system. The steam-temperature correction signal is applied to the flowmotor as a separate input. Performance data, describing steady-state or dynamic operation of the White flowmotor system, was not found in any of the references.

These examples of steam-car control typify the development status of steam car controls. With emphasis placed on emissions, and also on vehicle performance, the capabilities of the On-Off controls fall short of the requirements. A continuously variable proportional control for the combustor becomes an essential part of the low-emission steam car. An examination of the controls used on modern low-water-inventory, high-response boilers indicates the use of highly sophisticated controls, expecially tailored to the operating characteristics of the boiler. In general, the fast-response controllers often employ some form of a control system that utilizes information defining the instantaneous operating level. This is often done by defining the steam output of the boiler and using this for at least one or both of the feedwater and thermal input controls. Using this background as the baseline, a predictive metering concept was developed for steam car control. This control concept is described in the following section.

2.2 PREDICTIVE FLOW CONTROL CONCEPT

A major requirement for the design of the steam-car control system is the achievement of the operational simplicity, safety and convenience that is currently available in present-day spark-ignition automobiles. In order to achieve this goal for the Rankine-cycle power plant, three types of controls will be essential:

(1) The operating control,

(2) Safety controls, and

(3) Automatic start and shutdown sequence controls.

It is apparent that the design of the automatic start and shutdown sequence controller is contingent on a near complete definition of the operating controls if maximum economy is to be realized. Safety controls will again have to interface with the operating controls. For this reason the control design effort to date has been focused on the development of the operating controls for the steam car.

The accelerator pedal is to be the only normal input required of the driver to control the Rankine-cycle power plant. The operating control system then must operate not only the steam input to the expander to produce the required accelerating torque from the power plant, but also automatically control the feedwater supply and heat input to the steam generator to satisfy the operator's demand. In order to accomplish this operating convenience, the control system must:

(1) Provide proper steam pressure, temperature and flow output from the boiler at all times.

(2) Regulate feedwater supply to the boiler and properly modulate the burner output.

(3) Maintain the burner air-fuel ratio at all times at the desired value to reduce exhaust emissions and maintain burner efficiency.

(4) Control the function of the condenser to keep up with continually varying steam output flow rejected by the expander.

(5) Satisfy the safety requirements at all times during the operation of the power plant.

(6) Have the capability for automation of the startup and shutdown functions to the extent that only turn-key operation is required of the vehicle operator.

The general concept of the metering control system is shown in the schematic of Figure 2-1. The essentials of the control concept include the use of the expander to determine the steam flow consumption. The steam flow signal thus generated is used to control the feedwater flow to the steam generator and also the combustion air flow to the burner at the proper level. The burner fuel flow is controlled independently on the basis of combustion air flow, thus maintaining an air-fuel ratio dictated by the combined requirements of low emissions and high burner efficiency. Several mechanizations of this basic concept are possible. The one shown in Figure 2-1 is an early concept of mechanization and utilizes an expander-driven feedpump and electrically driven combustion blower and combustion-air atomizing pump. The basic control concept readily can accommodate changes in auxiliary drives. The schematic of Figure 2-1 includes all functions necessary for the complete automatic control of the steam generator plant. A more detailed discussion of a selected implementation of the predictive flow metering concept is described in the next section.

During the program period, operating characteristics of the predictive steam-generator control system were evaluated both through analytical and experimental means. Details of the experiments are described in Section 5 under Control Mode Simulation Experiments. Typical results from this program are compared with the analytical predictions in Figure 2-2 to show the feasibility of the control concept just described. The figure shows closed-loop results of the predictive control concept when a step demand is made in throttle setting. The results indicate that successful control of the monotube steam generator is possible in spite of the relatively slow thermal response of the steam generator. The experimental setup used the same gain setting for the corrective trim temperature control loop that was predicted through the prior computer simulation of the system. The results shown are typical of the performance capabilities of the predictive controller. The controller is providing an approximate temperature control band of 75°F.

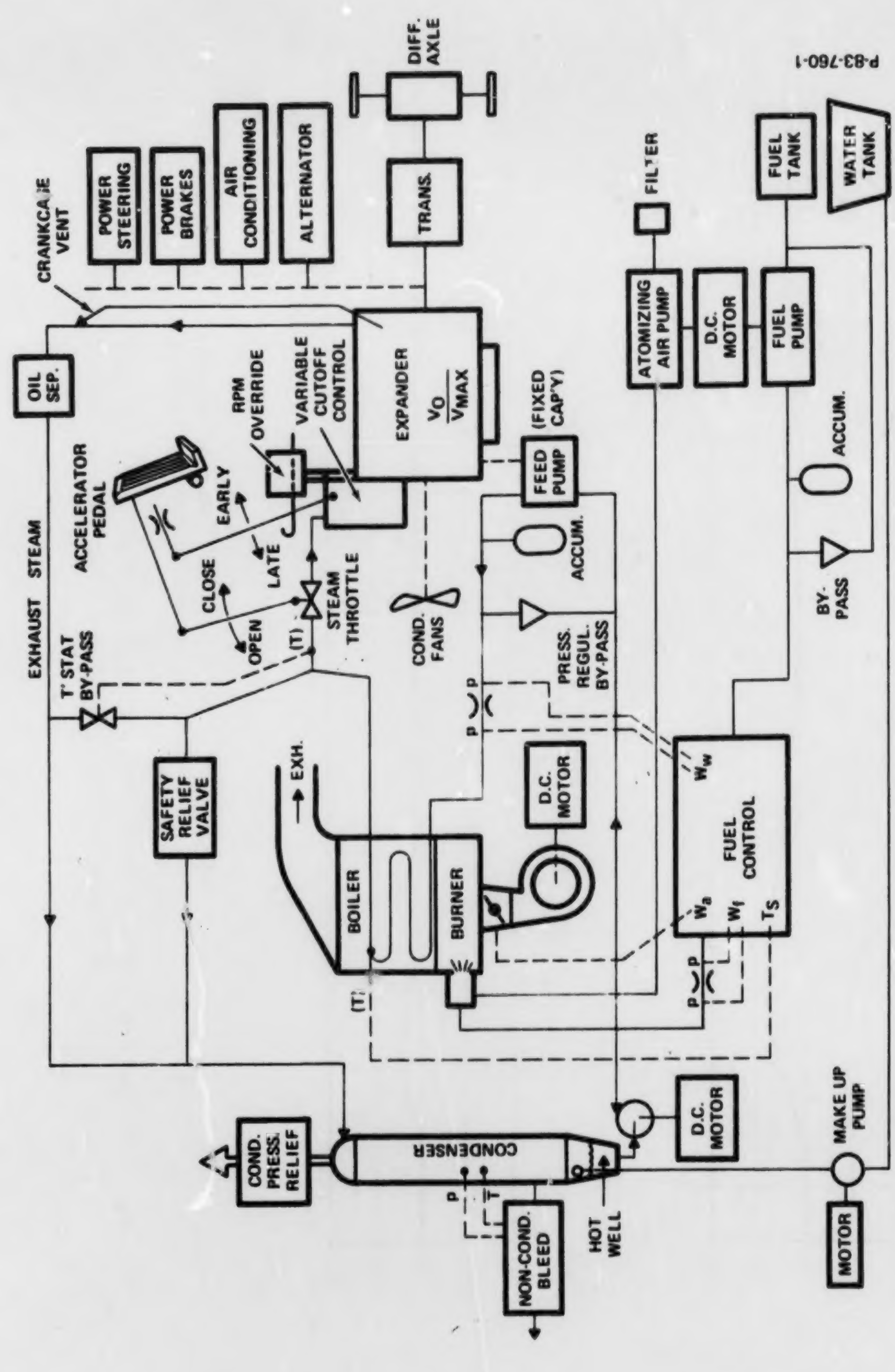
P-83-760-1
DIFF. AXLE
TRANS.
ALTERNATOR
AIR CONDITIONING
POWER BRAKES
POWER STEERING
CRANKCASE VENT
OIL SEP.
EXPANDER
V_O/V_{MAX}
VARIABLE CUTOFF CONTROL
RPM OVERRIDE
ACCELERATOR PEDAL
EARLY
LATE
CLOSE
OPEN
STEAM THROTTLE
(T)
EXHAUST STEAM
T' STAT BY-PASS
SAFETY RELIEF VALVE
EXH.
BOILER
BURNER
(T)
D.C. MOTOR
COND. FANS
FEED PUMP
(FIXED CAP'Y)
ACCUM.
PRESS. REGUL. BY-PASS
P
P
FUEL CONTROL
W_w
W_a
W_f
T_S
P
P
ATOMIZING AIR PUMP
D.C. MOTOR
FUEL PUMP
FILTER
FUEL TANK
WATER TANK
ACCUM.
BY-PASS
CONDENSER
COND. PRESS. RELIEF
P
T
NON-COND. BLEED
HOT WELL
D.C. MOTOR
MAKE UP PUMP
MOTOR

Figure 2-1 - Metering Control System Schematic

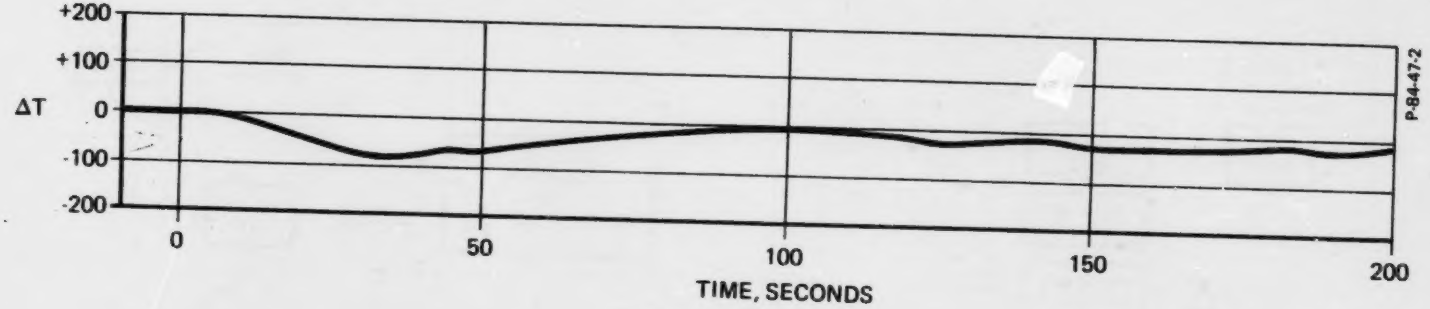

Experimental Results
SES-4 Steam Generator Manual Pressure Control
Predictive Temperature Control Nominal Setting

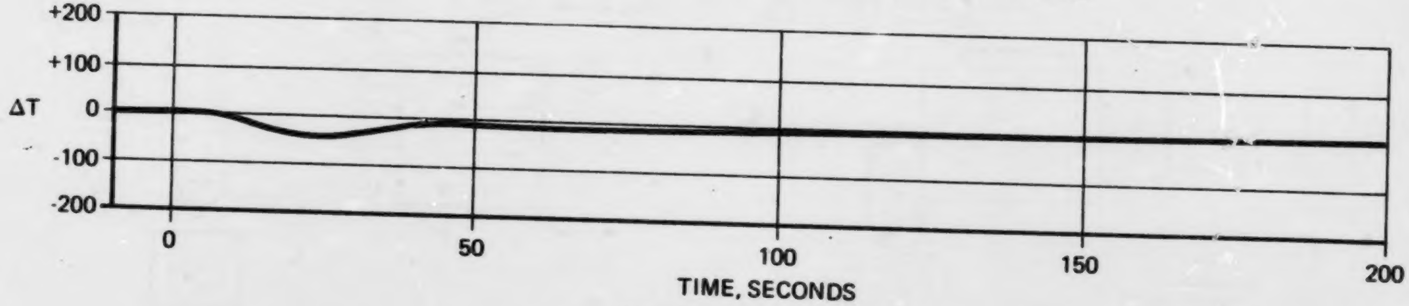

Hybrid Computer Results
SES-5 Steam Generator Bypass Pressure Control
Predictive Temperature Control Nominal Setting

Figure 2-2 - Effect of the Step Change From 39 to 56 Percent Flow Level in Steam Throttle Setting on Superheater Output Temperature

2.3 PREDICTIVE-CONTROL CONCEPT IMPLEMENTATION WITH VARIABLE-SPEED AUXILIARY DRIVE

The flow metering concept described functionally in the previous section can be implemented in many ways. The choice of power source for the feedpump and combustion-air blower has a significant effect on the type of controls that are practical. In general, several horsepower are required for auxiliary drives. Thus, the use of electric drive, although it would be desirable for controls, becomes bulky, because not only the electric motors are needed, but a significant increase in the size of the alternator used must be included in the package to provide the electric power generation in the steam car. Two other power sources remain attractive: mechanical power derived directly from the expander, or the steam output derived directly from the steam generator or from the exhaust of the expander. The use of mechanical power from the expander was selected for the initial concept evaluation. The use of steam-driven auxiliaries may be an attractive choice; however, at the present, the development status of these auxiliaries does not appear to fit the overall program timetable.

The schematic diagram of the predictive flow metering control concept is shown in Figure 2-3. The schematic includes only the operating controls. Both the feedpump and the combustion air blowers are driven by the expander through a variable-ratio transmission. The predictive control is limited to setting of the transmission ratio. The pressure trim control is accomplished through the use of a pressure-operated feedwater bypass valve. The temperature trim control on the superheater outlet temperature is accomplished through the use of an air damper located at the air-blower inlet. The fuel control for the concept maintains the desired air-fuel ratio independently. Condenser drive control and condenser shutter control are also independently operated. The only input from the driver is through the accelerator pedal. A power boost may be required to hold the oeprator's effort to a minimum level. The basic control unit is an electronic central controller. This unit, on the basis of expander speed and expander inlet-valve position, computes the instantaneous steam flow of the expander. When a positive displacement expander is used, this computation can be accomplished with sufficent accuracy for the predictive control loop. On the basis of this information, the transmission ratio is set to provide the proper speed to the auxiliaries. The use of a common variable transmission for both pump and blower drives compromises the prediction accuracy. The flow output of the pump is essentially proportional to pump speed. On the other hand, the combustion-air blower output is not a linear function of blower speed because of boundary effects over a wide flow range. This mismatch between the two functions must be corrected by the closed-loop trim controls. As long as the design speed variation of the expander is held within reasonable limits, such as the 3:1 to 4:1 speed range anticipated for the expander operation, it will be compatible with the corrective capabilities of the temperature and pressure trim controllers.

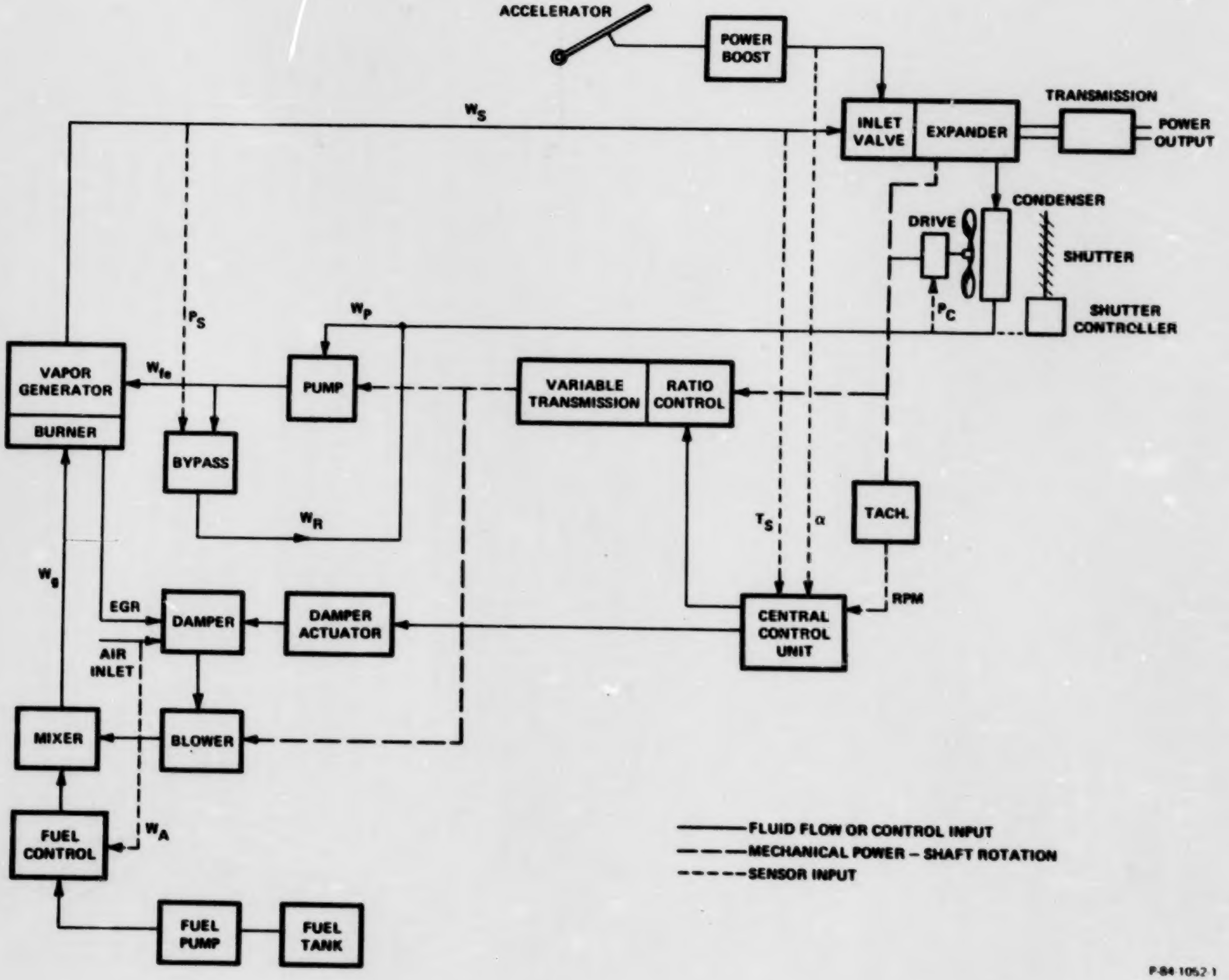
ACCELERATOR
POWER BOOST
INLET VALVE
EXPANDER
TRANSMISSION
POWER OUTPUT
CONDENSER
DRIVE
SHUTTER
SHUTTER CONTROLLER
W_S
P_S
W_P
P_C
VAPOR GENERATOR
BURNER
W_{fe}
PUMP
BYPASS
W_R
VARIABLE TRANSMISSION
RATIO CONTROL
T_S
α
TACH.
RPM
CENTRAL CONTROL UNIT
W_g
EGR
DAMPER
DAMPER ACTUATOR
AIR INLET
MIXER
BLOWER
FUEL CONTROL
W_A
FUEL PUMP
FUEL TANK
FLUID FLOW OR CONTROL INPUT
MECHANICAL POWER – SHAFT ROTATION
SENSOR INPUT
P-84-1052-1

Figure 2-3 - General Schematic Diagram of Predictive Flow Metering Concept

The concept shown in Figure 2-3 has been evaluated using an analytical model of the entire power plant. Details of the analytical model, and further results obtained through this study are given in Section 4. In the following, examples of the results obtained from this analytical control evaluation are given. These examples also point out operational peculiarities that appear at the two extremes of the steam-generator power range: the very low-level operation for idle and the very high-level operation near the maximum power point.

Typical results of the analysis are shown in Figures 2-4 and 2-5. The figures are reproductions of strip chart recordings showing simultaneous recordings of sixteen selected variables describing the responses of the power plant to a step input in throttle. The reduction of throttle position, α, from 38 degrees to 8 degrees initiates rapid response in the ratio setting, R_p, of the variable-speed auxiliary drive. This setting changes from an initial value of approximately 1.4 to 0.35. An examination of the feedwater input traces, W_{fe}, and the combustion-gas flow rates, W_g, indicates that the prediction circuit was properly predicting the new gas flow rate to the burner. Because of the singular prediction signal operating only the common variable-transmission ratio, the feedpump output was somewhat in excess of the requirements of the expander. The closed-loop pressure trim control, through operation of the bypass valve opening, x, reduced the bypass valve opening in order to maintain the steam-generator outlet pressure at the desired level. Examination of the additional traces shown in Figures 2-4 and 2-5 indicate satisfactory operation of the control concept as long as reasonable prediction accuracy is maintained. If, however, the system is operated beyond the range of the predictive system, the burden of control is shifted to the closed-loop trim controller.

An example of insufficient predictive control is shown in the analytical results given in Figures 2-6 and 2-7. A large error in the prediction signal causes excessive temperature oscillations. The error can be best visualized through examination of the combustion-gas flow rates, W_g. At the initiation of the transient, the initial, relatively rapid, reduction of the gas flow is the result of the prediction signal. Because of physical limitations in the simulated control system, this flow is almost four times the flow rate required for the steady-state operating point of the steam generator. The transient described was initiated at the beginning of the trace with a step input from high to low power by changing the throttle from the intake valve position, α, corresponding to 47 degrees to 23 degrees. The fluid flow level corresponding to the high intake-valve opening is 0.365 lbs/sec while the level corresponding to the lower intake-valve opening is 0.05 lbs/sec. Significant differences in the performance characteristics of the steam generator can be seen for the large transients. The first transient, taking place from the high power level operation is dominated by the slower thermal response of the boiler at the low-level operation. At the initiation of the transient, the predictor circuit rapidly reduces the speed ratio of the variable-speed drive. The reduction in auxiliary speeds can be noted as a rapid

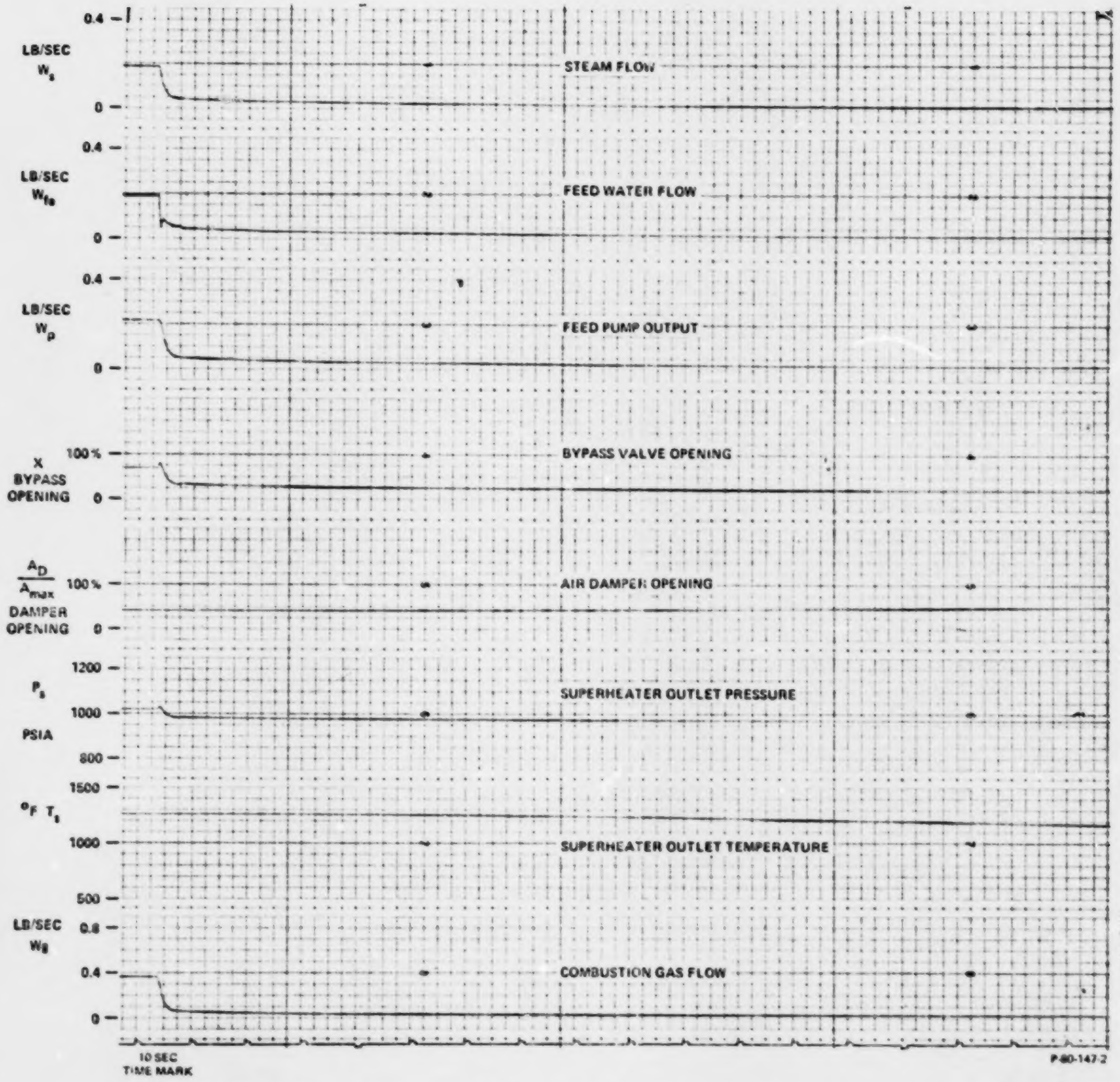

See following pages for greater detail.

Figure 2-4 - Hybrid-Computer Results; Fast Equal-Percentage Bypass Valve

Preceding page blank

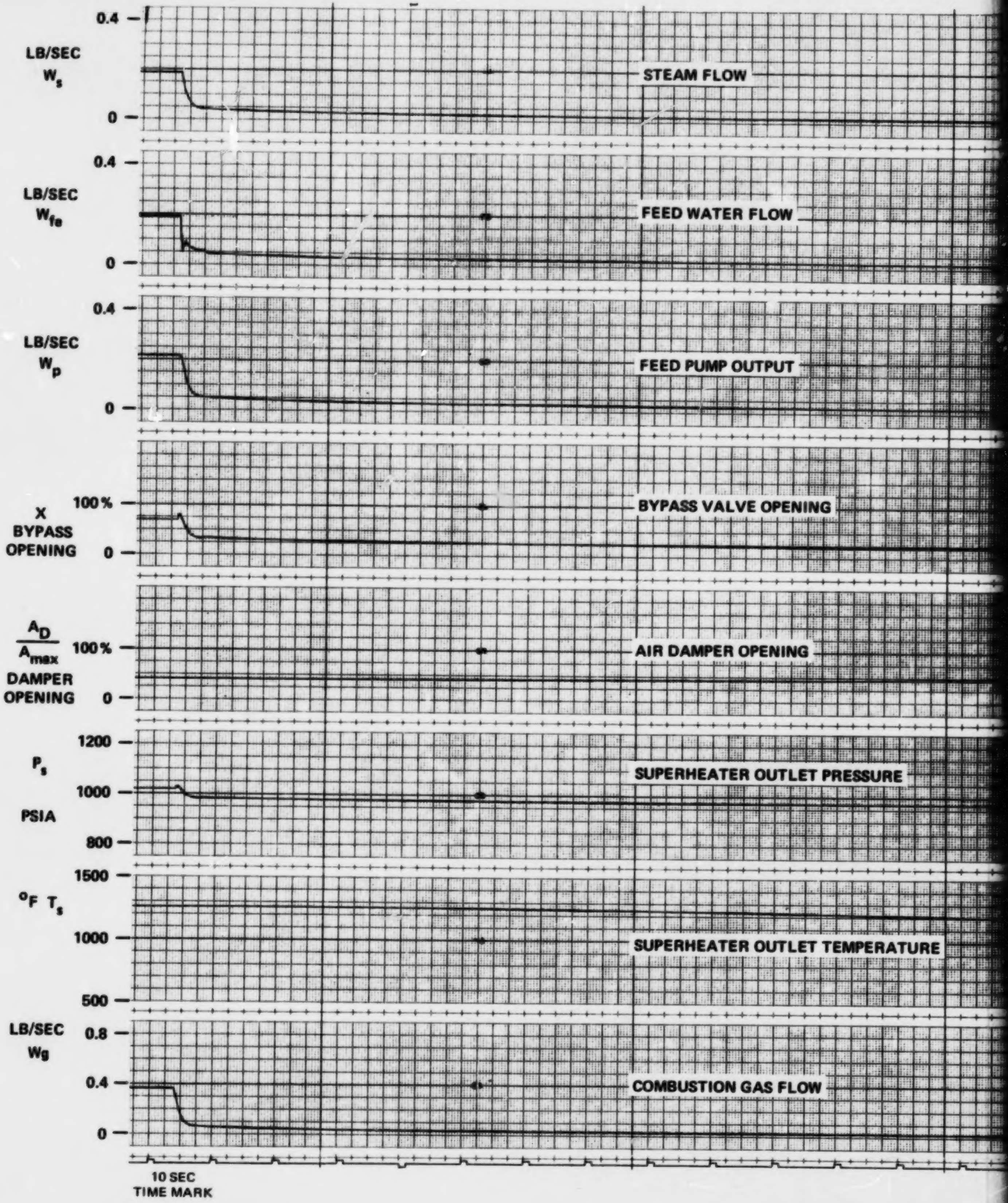

A

Figure 2-4 - Hybrid-Computer Results; Fast Equal-Percentage Bypass Valve

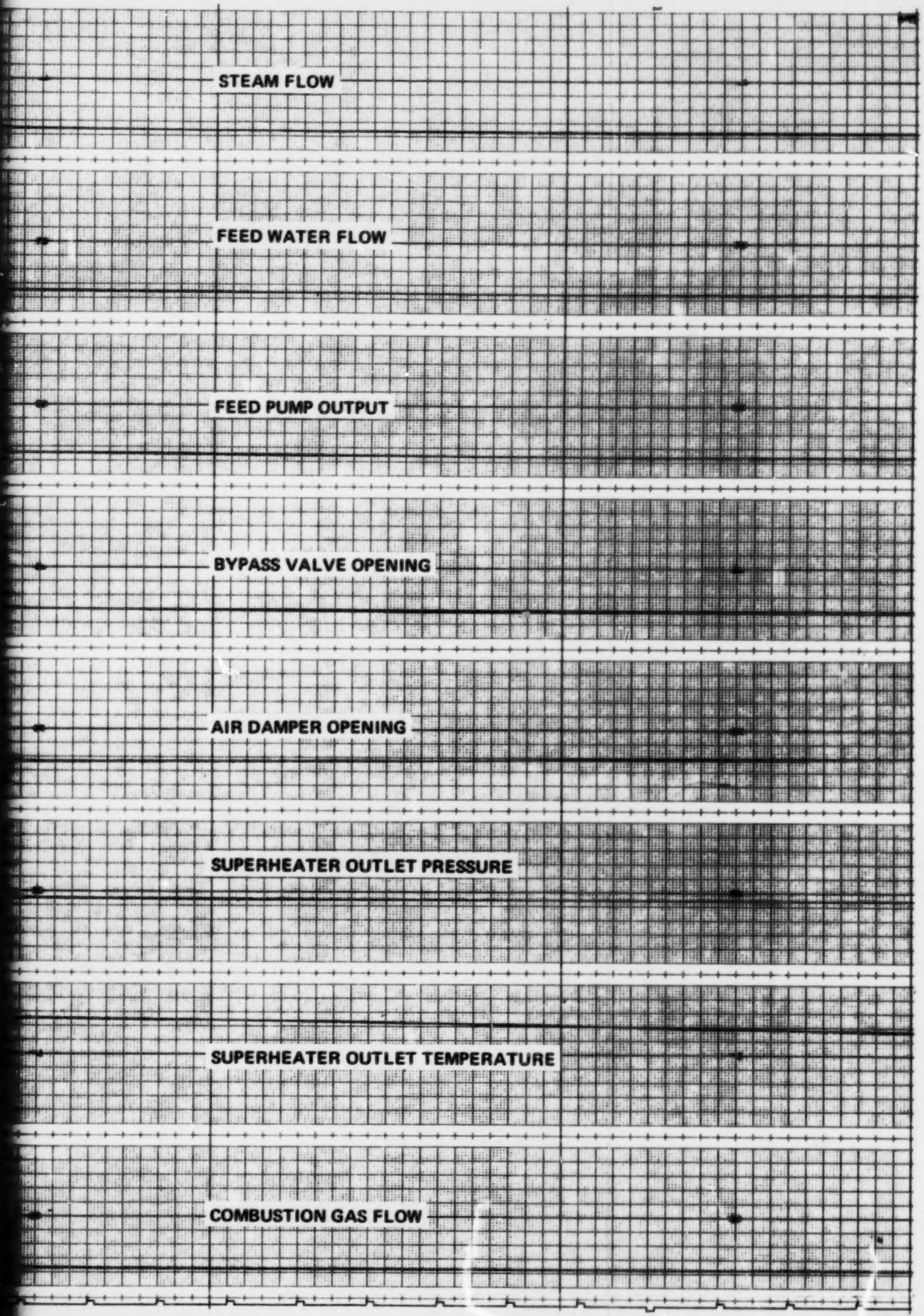

P-80-147-2

B

—Computer Results; Fast Equal-Percentage Bypass Valve

Preceding page blank

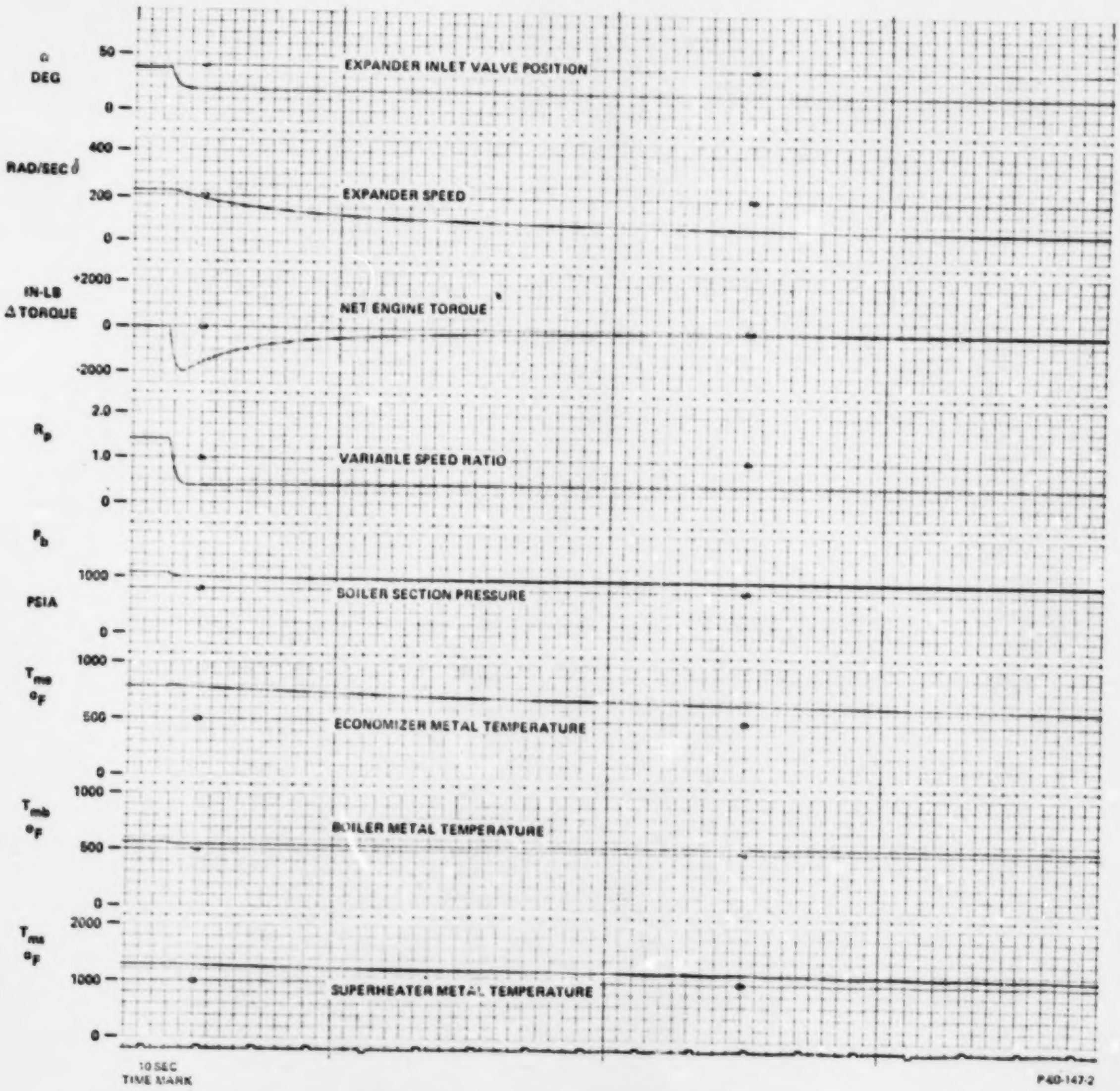

Figure 2-5 - Hybrid-Computer Results; Fast Equal-Percentage Bypass Valve

See following pages
for greater detail.

Preceding page blank

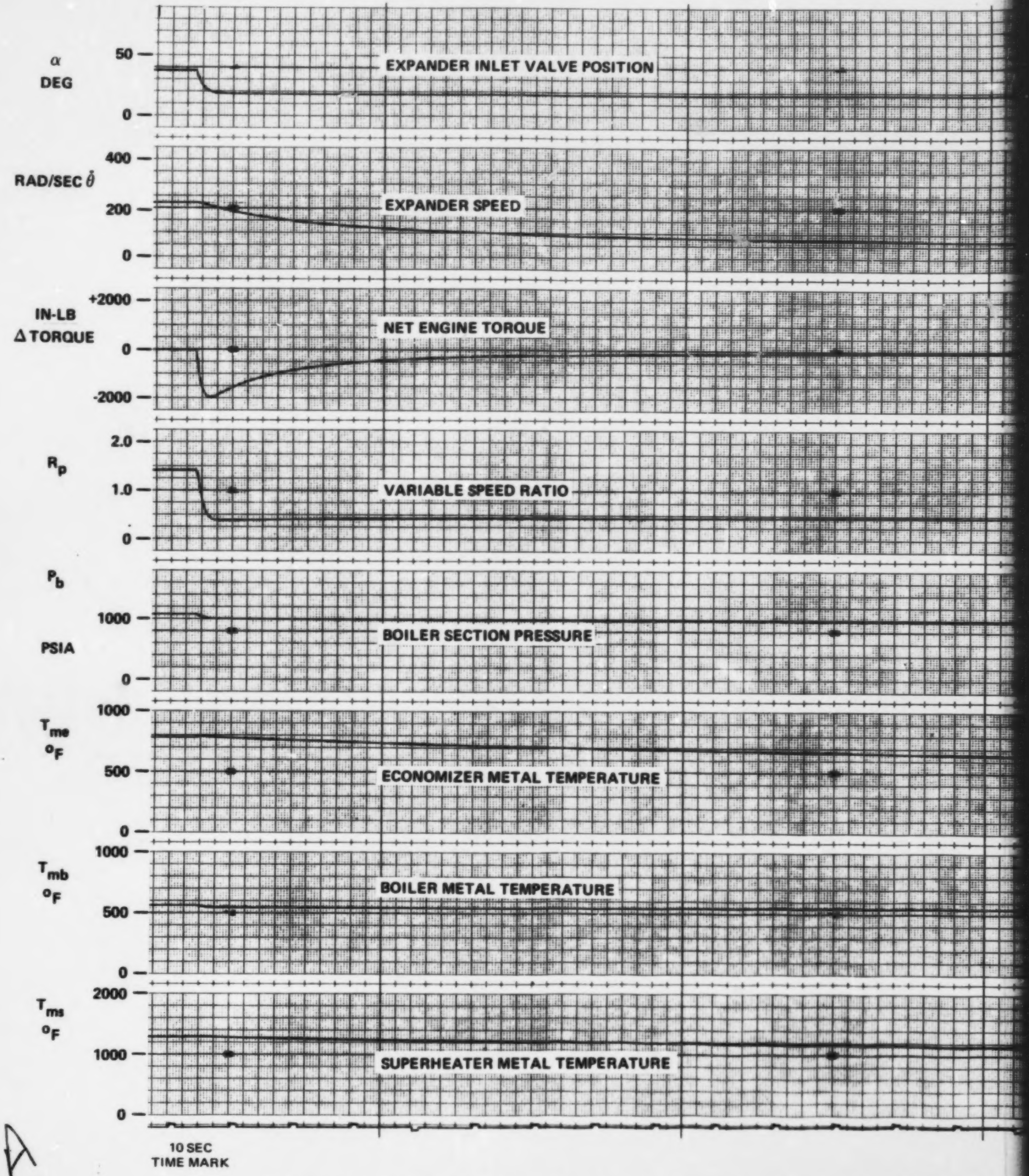

A

Figure 2-5 - Hybrid-Computer Results; Fast Equal-Percentage Bypass Valve

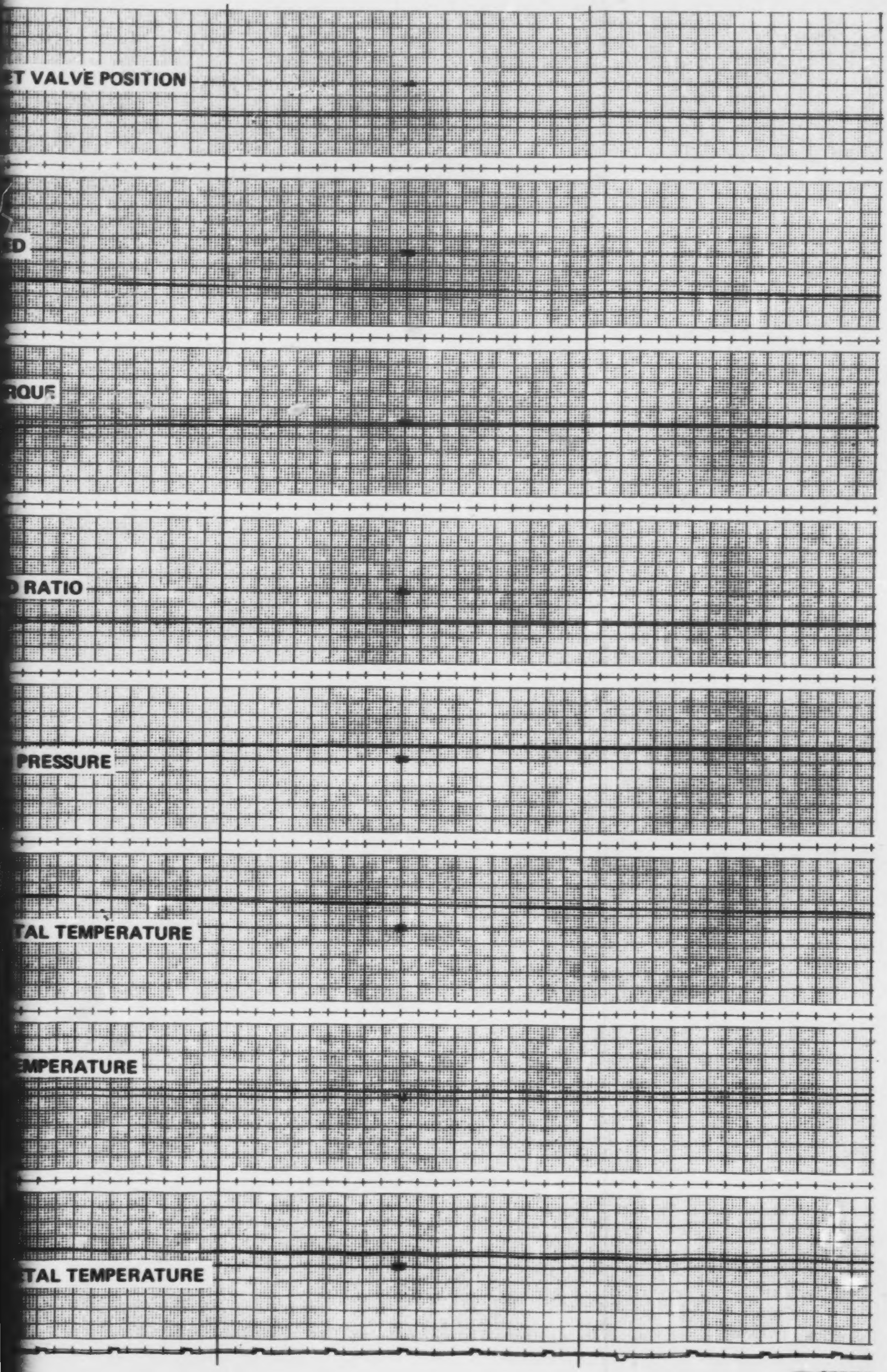

P-80-147-2

B

er Results; Fast Equal-Percentage Bypass Valve

Preceding page blank

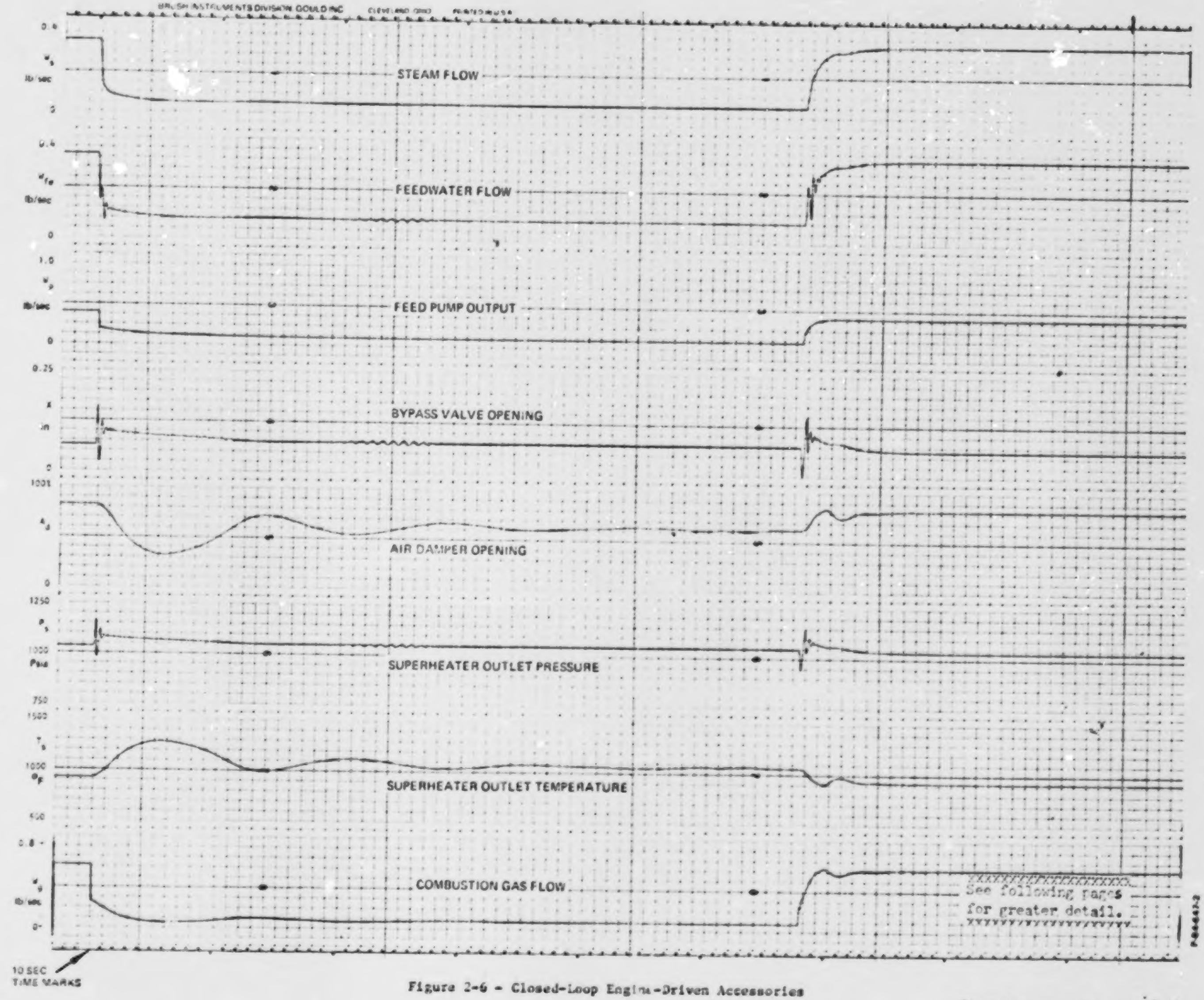

See following pages for greater detail.

Figure 2-6 - Closed-Loop Engine-Driven Accessories

Preceding page blank

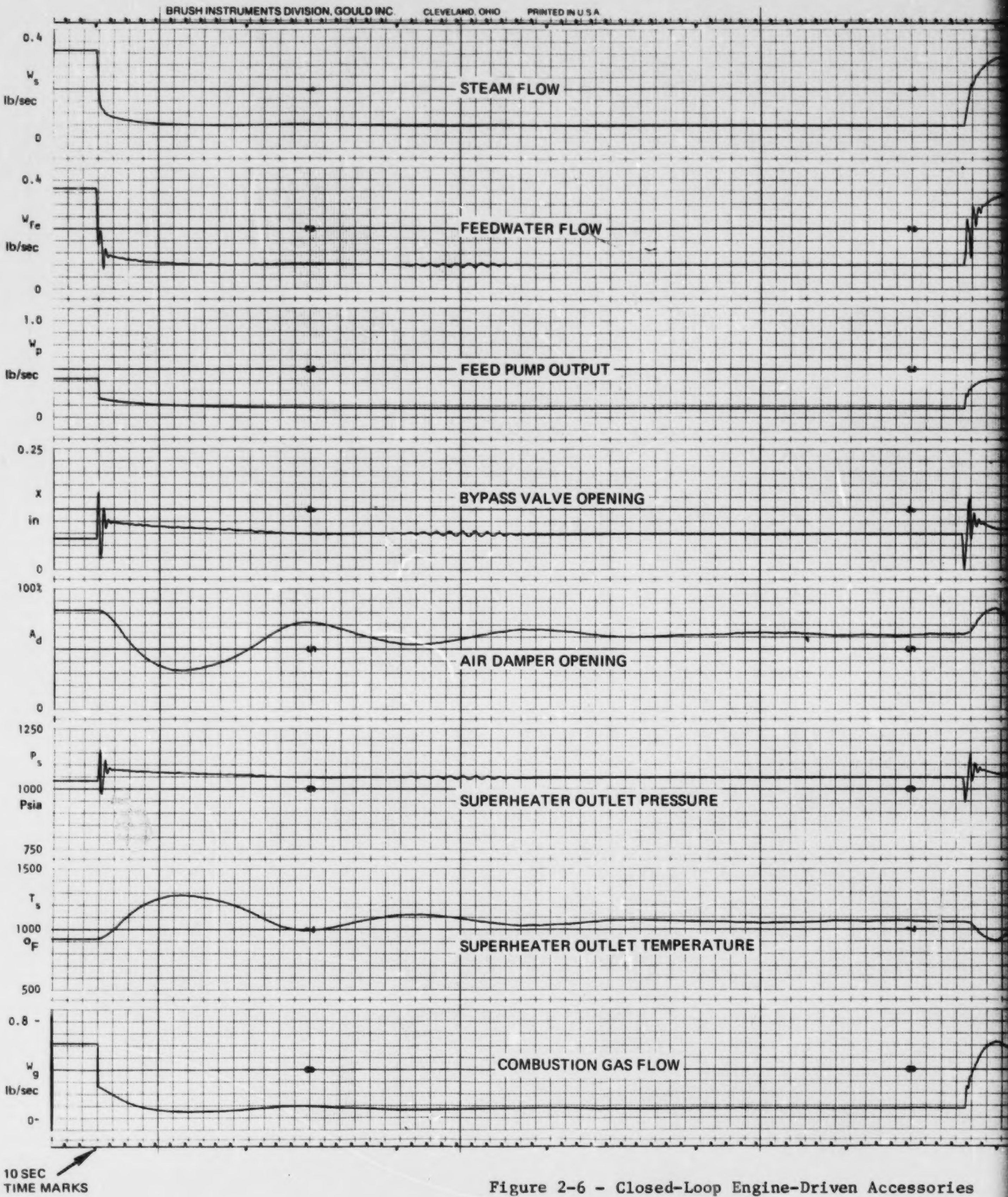

Figure 2-6 - Closed-Loop Engine-Driven Accessories

A

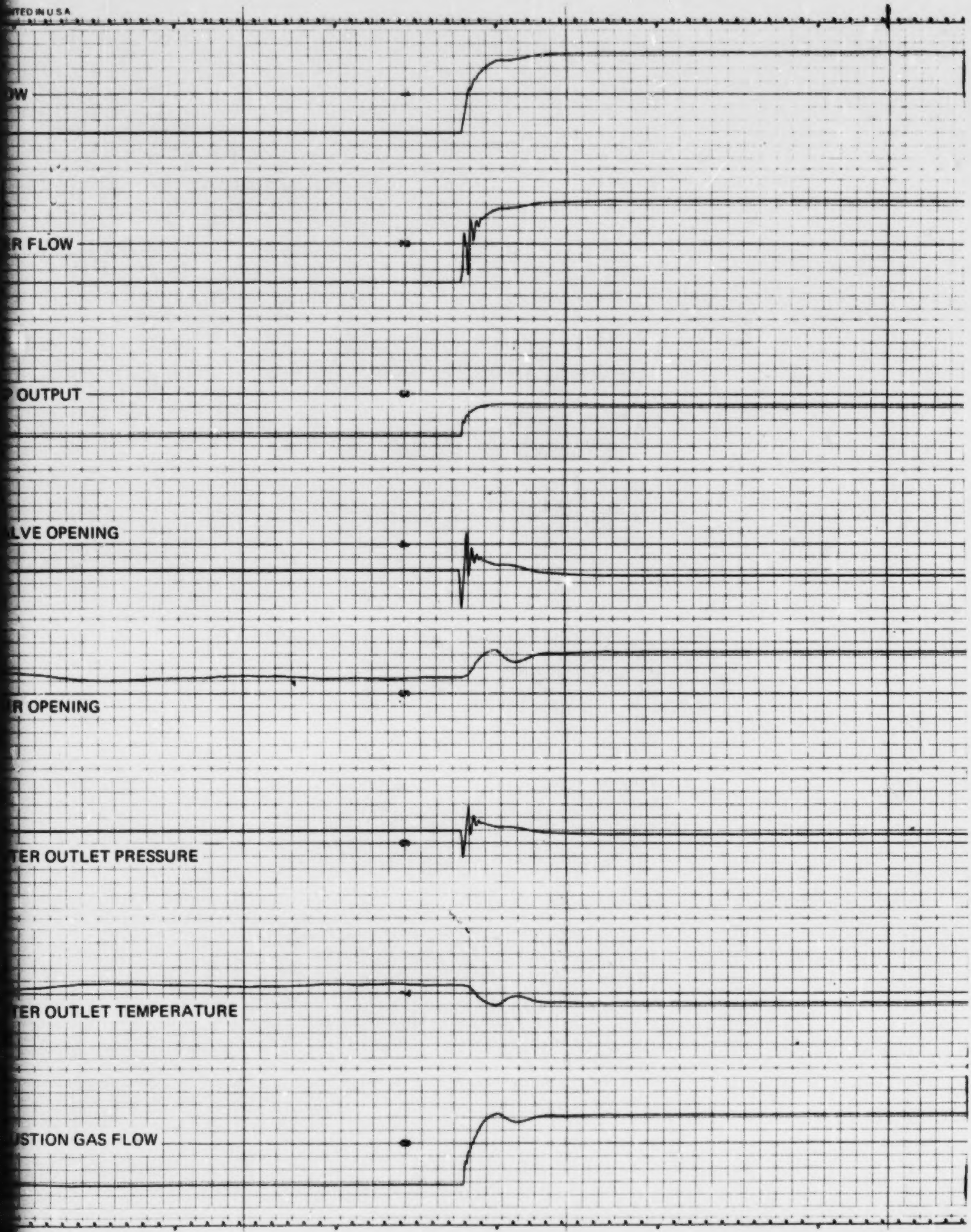

P-84-647-2

2-6 - Closed-Loop Engine-Driven Accessories

B

Preceding page blank

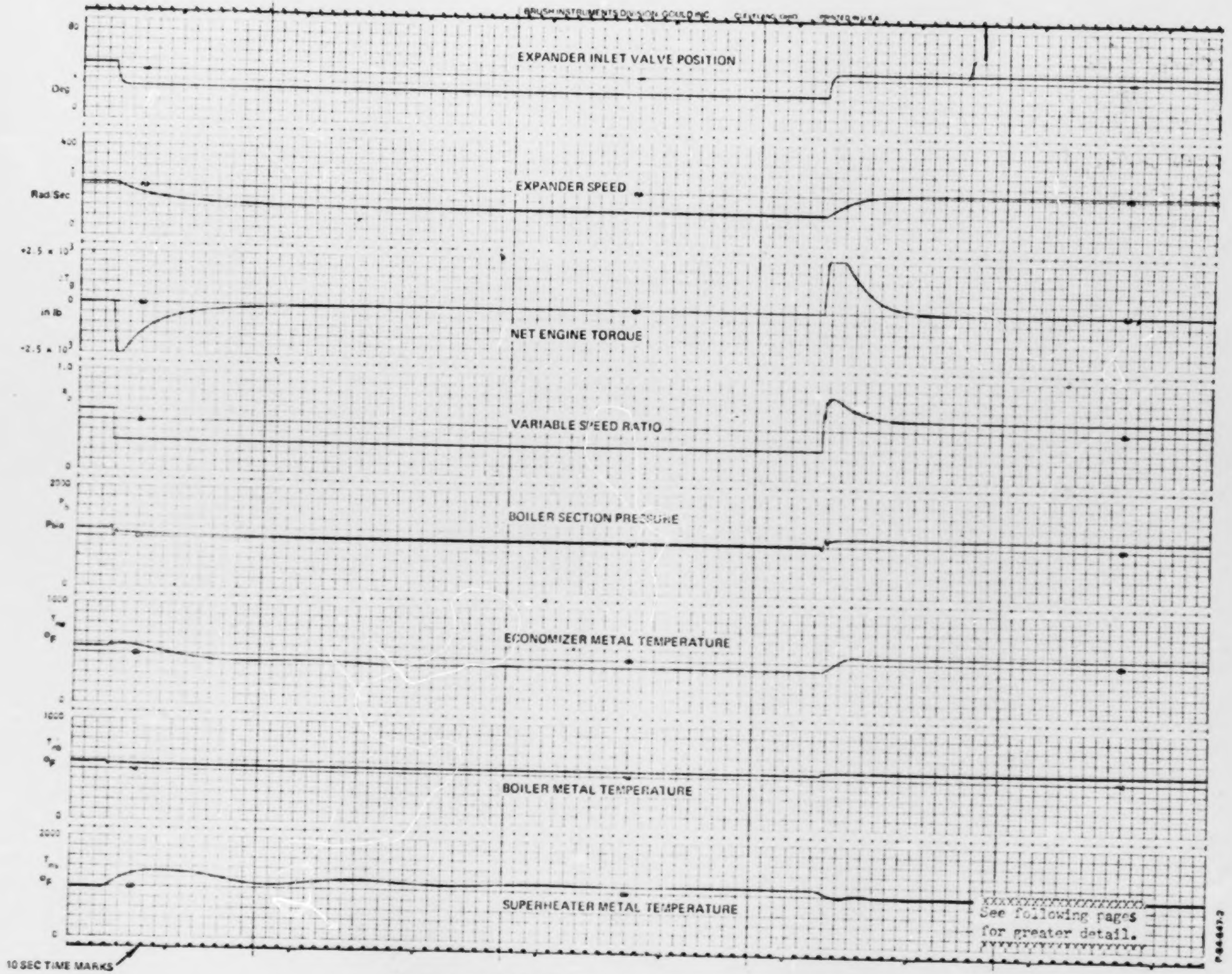

XXXXXXXXXXXXXXXXXXX
See following pages
for greater detail.
YYYYYYYYYYYYYYYYYYY

Figure 2-7 - Hybrid-Computer Results; Step Transients in Intake-Valve Position

Preceding page blank

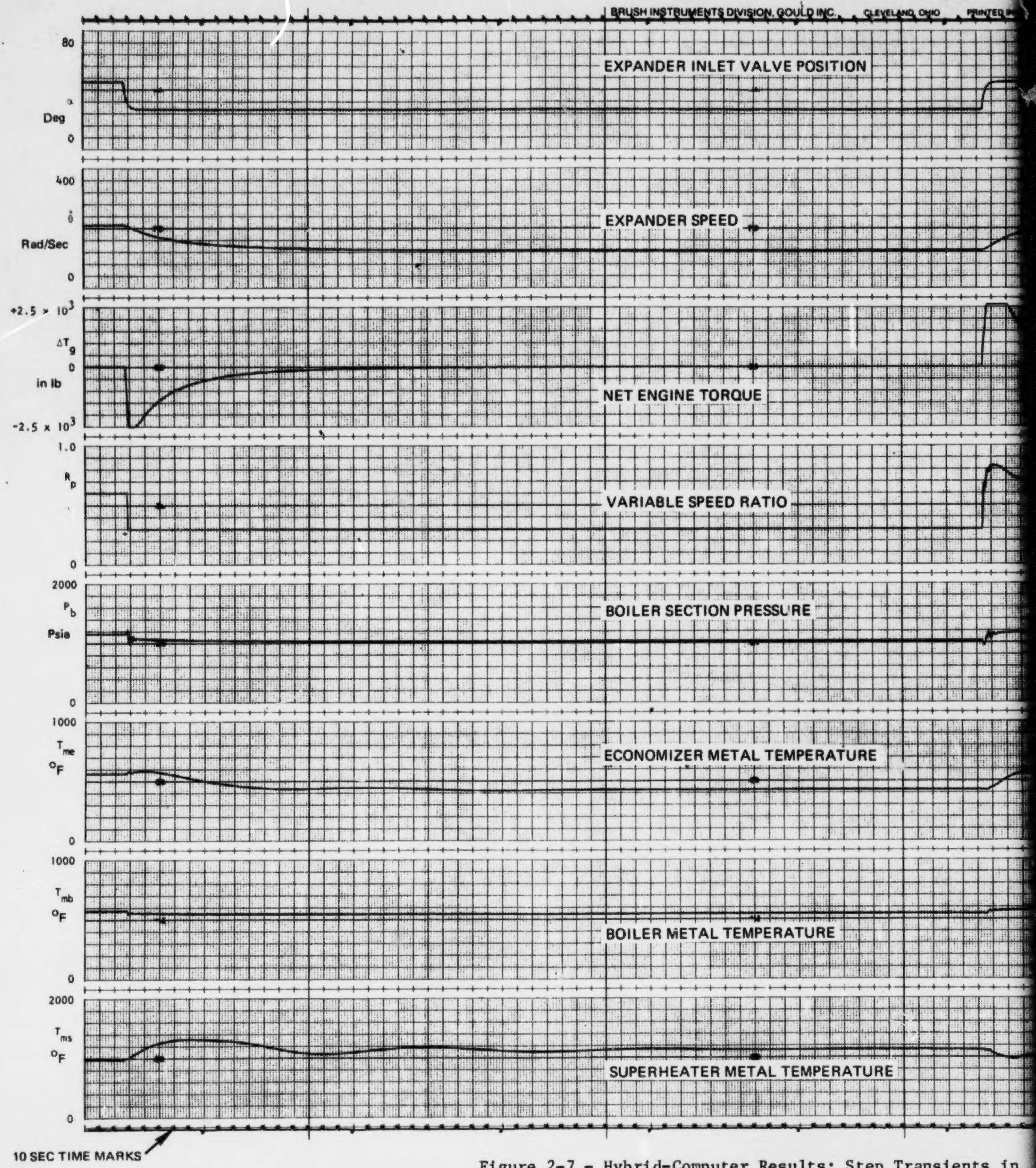

Figure 2-7 - Hybrid-Computer Results; Step Transients in Intake-Valve Position

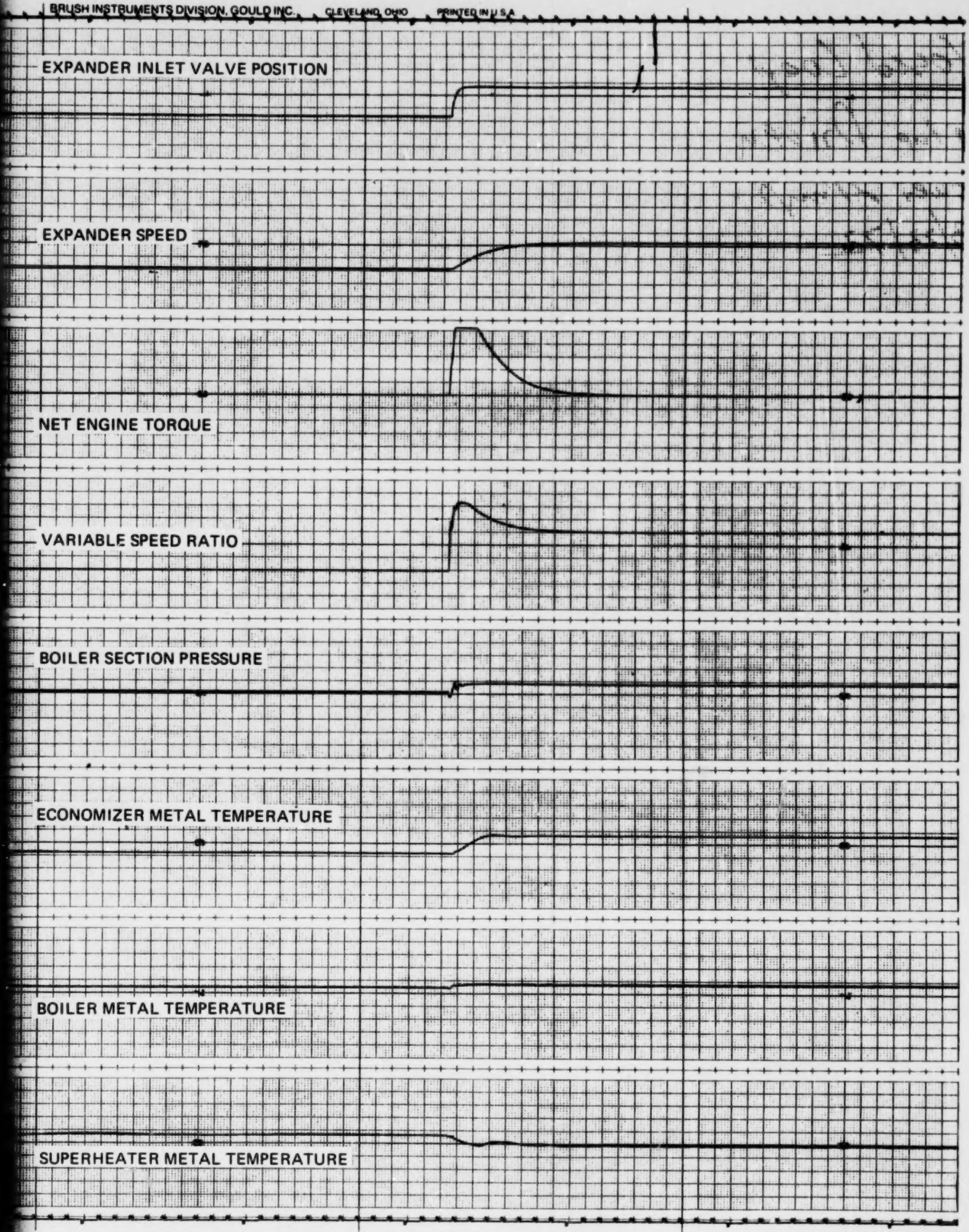

B

— Hybrid-Computer Results; Step Transients in Intake-Valve Position

Preceding page blank

decrease in both the feedpump output and also in the combustion gas flow. Because of limitations of the minimum ratio setting for the particular variable-speed drive employed in the analysis, the lower speed-ratio limit of the drive is reached. Thus, at the point of operation, both feedpump capacity and the combustion-air blower capacity exceeds the requirements of the steam generator, thereby calling for significant corrections by both the pressure and temperature trim controller. The slow thermal response at the low-level operating point of the boiler results in a larger temperature overshoot which is eventually corrected by the closed-loop temperature control operating through actuation of the air damper. As the temperature exceeds the trim control setting, the damper is closed and the superheater outlet temperature is corrected. Gain of the trim controller is near the stability limit as defined by the longer phase shift at the low-level operation of the boiler. For the second transient, going from this lower level back to the higher power plant operating level, the performance is significantly different. The prediction point for the variable-speed drive of the auxiliaries corresponds more closely to the required output for both the feedpump and the combustion gas flow. In addition, a significantly faster response time is evident for the steam generator at the higher operating level. For this reason, both the magnitude of the temperature and pressure errors and the time required to reach the final equilibrium condition is significantly less than for the down transient.

The maximum steam consumption of the expander must be limited by the controls to avoid the possibility of swamping the boiler. In vehicle operations, it is possible to demand a continuous power level from the expander that exceeds the maximum output of the steam generator. The need for limiting the maximum intake valve or cutoff angle as a function of RPM, is illustrated in the traces of Figures 2-8 and 2-9. Again, the same 16 selected variables are shown as a function of time for a step input in cutoff angle. When the steam demand of the expander becomes larger than the output capability of the steam generator, additional demand for power results in a drop of both steam pressure and steam temperature. In the particular transient shown, the steam pressure drops to 850 psi and the steam temperature drops to 650°F from the nominal 1,000 psi and 1000°F operating points. At the same time, in spite of the increase in intake valve settings, the expander speed remains at essentially the same level. The figures illustrate the definite need for a speed-sensitive limit on the maximum intake-valve position. It is believed that for practical reasons, this limit must be kept slightly under the maximum capacity of the steam-generator output. An alternate input to the limit controller could be the steam temperature. In other words, anytime steam temperature is below some acceptable minimum value, the cutoff angle must be reduced to avoid the possibility of demanding power in excess of the steam generator output.

The examples shown above indicate that proportional control of a monotube boiler for steam car application is feasible. However, it must be noted that care must be taken in component selections. For example,

Preceding page blank

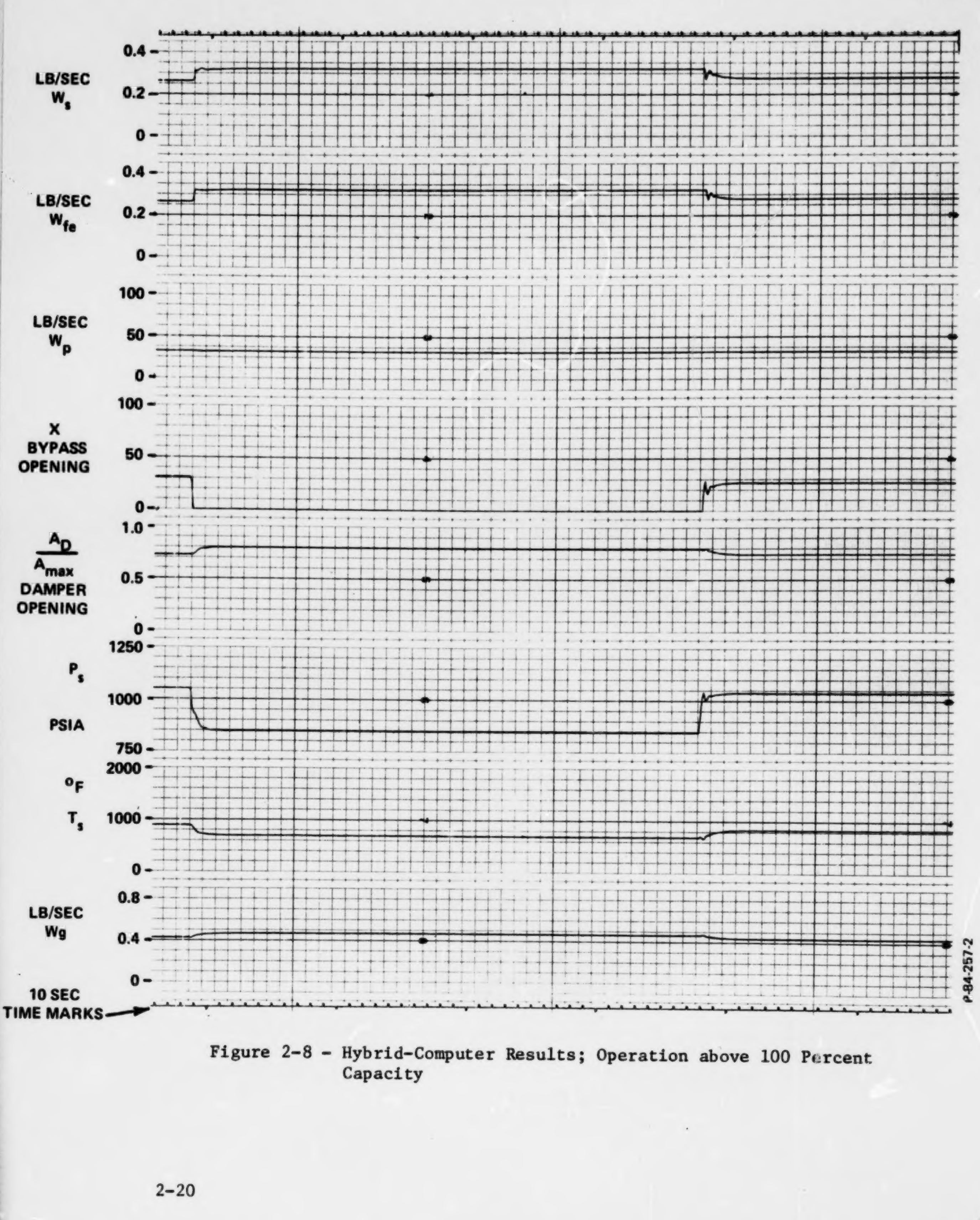

Figure 2-8 - Hybrid-Computer Results; Operation above 100 Percent Capacity

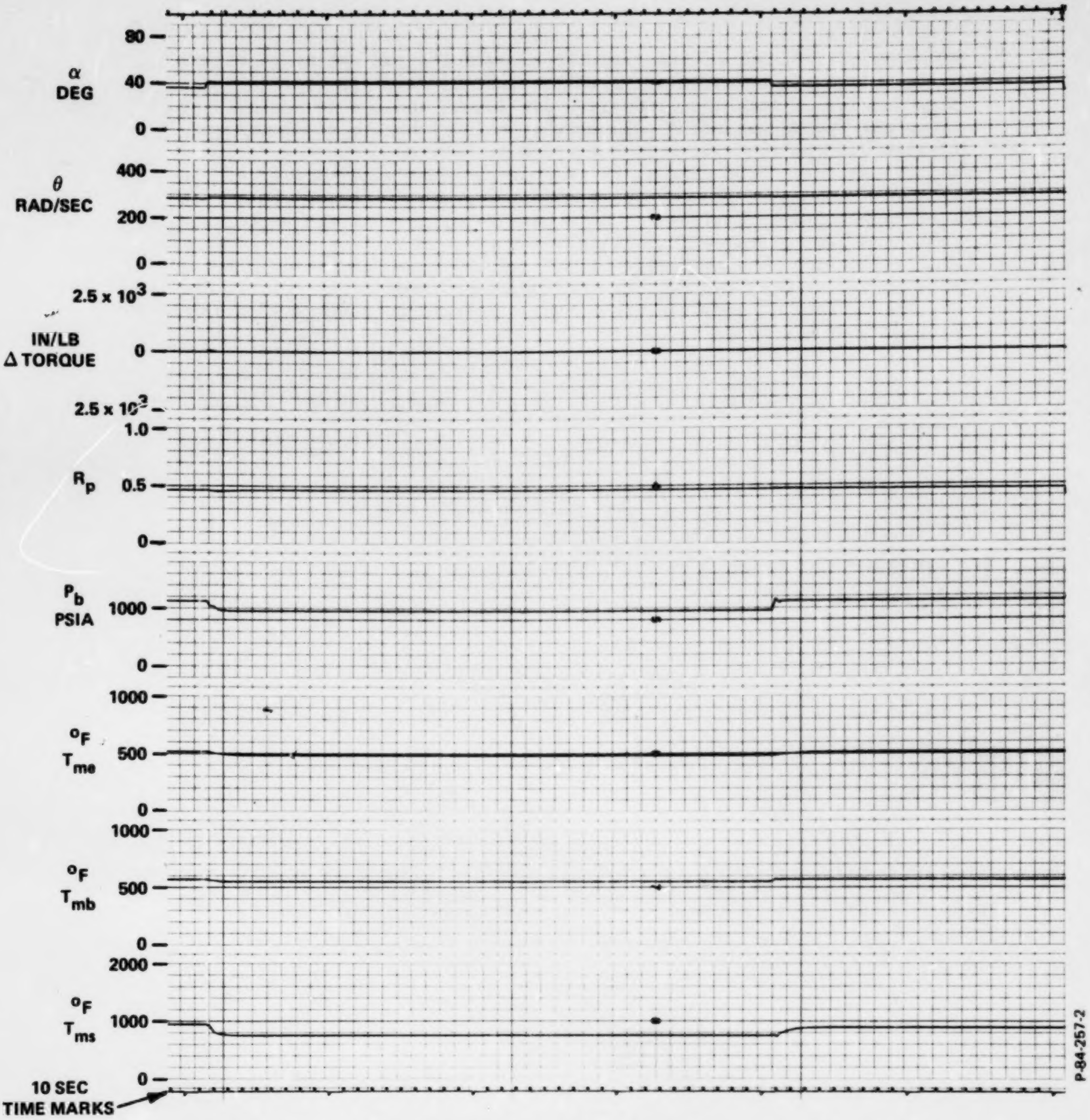

Figure 2-9 - Hybrid-Computer Results; Operation above 100 Percent Capacity

if range limitations of the variable-speed drive can not be eliminated, a more elaborate predictive controller must be developed and the predictive control of both the combustion air damper and the feedwater bypass valve may become essential. A somewhat more elaborate predictive controller for the air damper is described in Section 3 for the facsimile control system. In addition, it is apparent that some excess capacity of both feedpump and combustion air delivery system, above the steady-state power plant requirement, is needed to allow this system to recover from transient disturbances. This recovery capability of the power plant will affect the responsiveness or feel of the steam car power plant to accelerator command inputs from the operator. Additional results describing the effects of component selection on steam generator and power plant performances are given in Section 4 of the report.

REFERENCES

1. Walton, J. N., "Doble Steam Cars, Buses, Lorries and Railcars," *Light Steam Power*, Kirk Michael, Isle of Man, U.K., 1965.

2. Vickers, P. T., C. A. Amann, H. R. Mitchell, and W. Cornelius, "The Design Features of the GM SE-101 - A Vapor Cycle Powerplant," *SAE Paper No. 700163*, SAE Automotive Engineering Congress, Detroit, Michigan, January 1970.

3. Hoess, J. A., et al, "Study of Unconventional Thermal, Mechanical, and Nuclear Low-Pollution-Potential Power Sources for Urban Vehicles," *Summary Report, U.S. Department HEW Contract No. PH-86-67-109*, Battelle Memorial Institute, March 1968.

4. Garner, H. D., "Control of the Monotube Boiler," 1st Technical Meeting, Steam Automobile Club of America, Oak Ridge, Tennessee, September 1971.

5. Skinner, J. H., R. P. Shah, and W. A. Boothe, "Modeling, Analysis and Evaluation of Rankine Cycle Propulsion Systems," EPA Contract No. EHS-70-111, General Electric Co., February 1972.

SECTION 3

FACSIMILE CONTROL DESIGN

The purpose of the facsimile hardware is the demonstration of the overall control concept at a minimum cost. In order to minimize development costs, maximum utilization of available commercial components was made in implementing the predictive control concept. Electronic analog signal processing was selected as it offers maximum flexibility in the testing program at the lowest possible cost. The facsimile hardware design is an extension of the already tested temperature control concept. The results of this testing is reported in Section 5, Control Mode Simulation Experiments. The facsimile predictive control again relies on a laboratory-type feedwater flowmeter to monitor the power level of the steam generator. On the basis of feedwater flow and instantaneous blower speed, the analog signal processor predicts the desired air damper position. This prediction concept is sufficiently flexible to accommodate both the expander-driven auxiliary configuration and also independently driven auxiliary configurations currently planned for the initial testing phase. For an in-car installation, the feedwater flow would not be used and the expander speed and cut-off valve position would be used to produce the predictive damper signal. A commercially available Bendix RSA fuel controller was modified through the addition of an electric servo positioner for the idle-mixture control. This combination then becomes the forerunner of a two-stage fuel control system believed to be essential for the wide 20:1, possibly 40:1, operating range required for the prototype fuel controller. The command signal to the idle-mixture position servo is again obtained through the use of the electronic signal processor by combining air damper position with air-damper differential pressure to obtain an air flow signal in the idle range. An additional piece of hardware is a direct-pressure-operated bypass valve for the facsimile steam-generator feedwater control. The bypass valve does not include a predictive signal. The feedwater pump controller must bear the burden of the predictive control to establish stable operation of the feedwater control. In the following, a more detailed description of the individual component design and design verification test results of the major components will be presented.

3.1. FACSIMILE CONTROL CONCEPT

The schematic of the control circuit is shown in Figure 3-1. The feedwater supply to the vapor generator is measured with a turbine-type flowmeter. The flowmeter is designed to simulate the steam flow signal that normally would be obtained on the basis of expander characteristics. Using blower speed and, calculated or experimentally established, flow characteristics of the throttle valve, the throttle position corresponding to the required steady-state firing rate is predicted. A linear electric positioner loop is used to actuate the throttle plate and position it to the predicted position. The circuit also corrects the prediction signal for the actual blower speed. The closed-loop temperature trim-control signal modifies the position command to the throttle valve. Superheater outlet temperature in excess of the desired set point will introduce a corrective signal at this point into this circuit that results in a reduction of combustion air flow by commanding a reduction of valve opening. The use of the tachometer signal allows the use of a simple linear servo positioning actuator in the throttle-plate control loop. Although blower speed is not a precise indicator of combustion air flow, it will give an accuracy that is acceptable for the predictive temperature control loop.

The RSA fuel control unit operates approximately over a 4:1 fuel flow range. In order to extend automatic air-fuel ratio control over the entire burner operating range, the use of the idle-mixture control valve was selected to control air-fuel ratio below 600 lbs/hr combustion-air flow rate. In normal aircraft application, this control valve is directly operated from a throttle lever linkage in the idle range. In an aircraft, sufficiently accurate relationship exists between air flow and throttle plate position near the idle range to use this information for the fuel control signal. However, in the case of an external combustor, large variations in blower speed are anticipated. Thus, the throttle position alone is not sufficient to be a direct indicator of combustion air flow. An additional parameter is required to calculate the air flow.

The present concept, shown in Figure 3-1, for the idle-mixture control signal was selected after considering other methods. Some of the more promising concepts and reasons for discarding them are given in the following. The use of a laboratory-type inlet-air flow meter was discarded because nearly all available flow meters have pressure losses that would be excessive for the present application. In addition, the use of this concept appears impractical for an on-road vehicle application. A second concept of combining throttle position signal with blower speed, similar to the manner used in the predictive circuit, was not believed to be sufficiently accurate for fuel metering, particularly when combustor emissions are likely to require stringent air-fuel ratio control. The use of throttle plate position with throttle-plate differential pressure combines simple mechanization using available components with a predicted accuracy that should be satisfactory for burner fuel flow control. In addition, this concept will allow a mechanization compatible with the fuel controller and may be the forerunner of a two-stage fuel control system. It is believed that this type of a system will be essential when combustion-gas flow variations on the order of 25:1, to possibly as high as 40:1, will be considered in the final vehicle application. An additional feature is the relative ease of addition of other information such as a trim control signal based on actual combustion gas temperature.

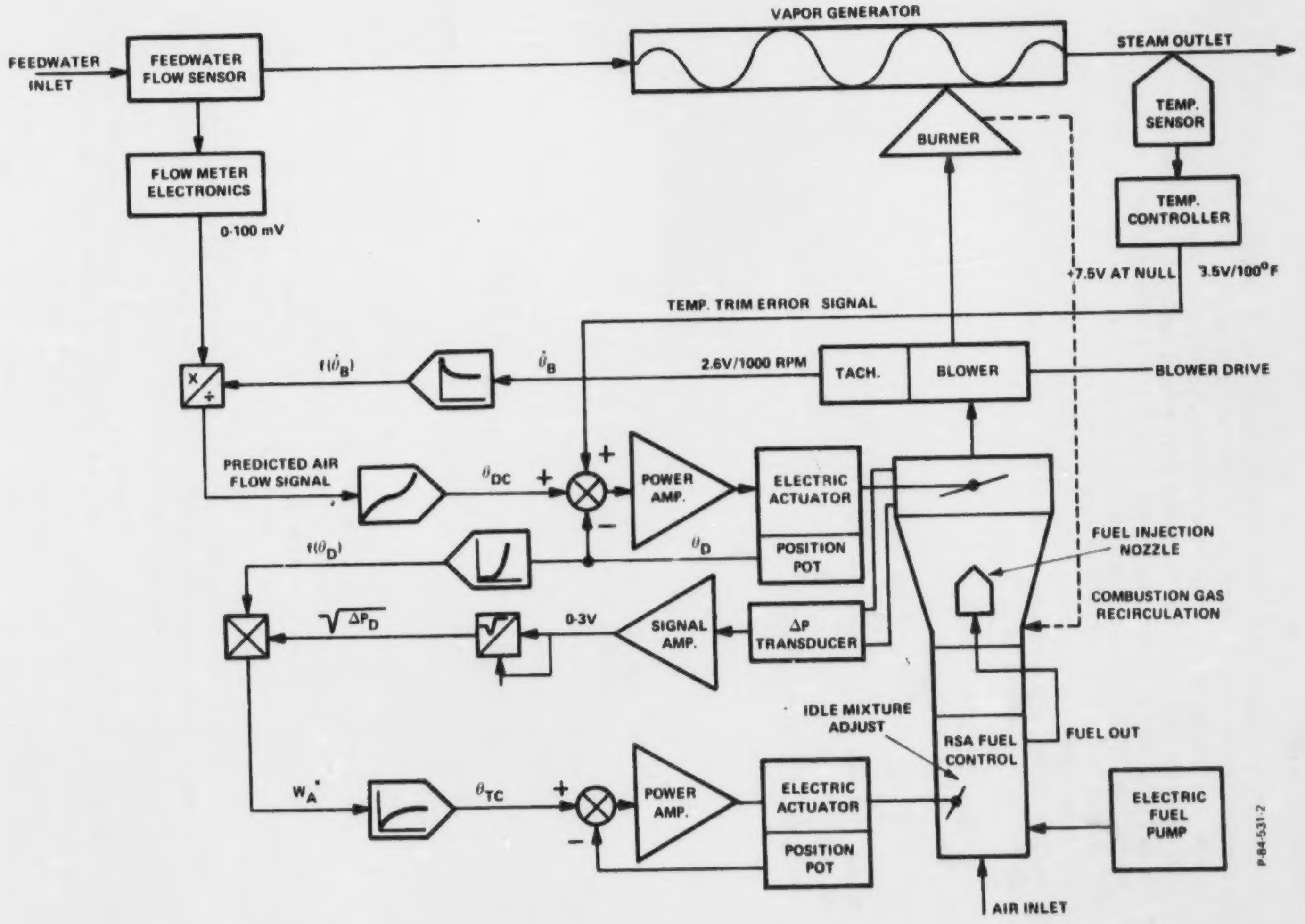
VAPOR GENERATOR
FEEDWATER INLET
FEEDWATER FLOW SENSOR
FLOW METER ELECTRONICS
0-100 mV
STEAM OUTLET
TEMP. SENSOR
TEMP. CONTROLLER
BURNER
+7.5V AT NULL
3.5V/100°F
TEMP. TRIM ERROR SIGNAL
2.6V/1000 RPM
TACH.
BLOWER
BLOWER DRIVE
$f(\dot{\theta}_B)$
$\dot{\theta}_B$
PREDICTED AIR FLOW SIGNAL
θ_{DC}
+
+
−
POWER AMP.
ELECTRIC ACTUATOR
POSITION POT
$f(\theta_D)$
θ_D
FUEL INJECTION NOZZLE
COMBUSTION GAS RECIRCULATION
$\sqrt{\Delta P_D}$
0-3V
SIGNAL AMP.
ΔP TRANSDUCER
IDLE MIXTURE ADJUST
RSA FUEL CONTROL
FUEL OUT
W_A^*
θ_{TC}
+
−
POWER AMP.
ELECTRIC ACTUATOR
POSITION POT
ELECTRIC FUEL PUMP
AIR INLET
P-84-531-2

Figure 3-1 - Predictive-Control Schematic

3.2 BURNER CONTROL

In order to quantitatively examine different mechanization of the predictive burner control concept, a simplified model of the burner air flow system was developed. The model includes the flexibility of handling any blower nonlinearities because the model uses a three-dimensional table of any suitable number of points to define the effects of both blower speed variations and combustion system flow resistance on the flow-pressure characteristics of the blower. As this model is of general use it is described in some detail. Following the general description of the burner simulation model, specific results as applicable to the facsimile burner control design are discussed.

3.2.1 Computer Simulation of the Burner System

In the development of models of any system, a first step is the derivation of the system equations. In general, the equations are based, in part, on certain assumptions which are made not only to facilitate the modeling task but also are those assumptions which result in the least sacrifice of accuracy. Some of the basic assumptions made concerning the present system model are:

- All gas flow through restrictors is proportional to the 1/2 power of the pressure drop except for the exhaust restrictor. Several exponents, including 1, 1/2, and 1/1.8, were evaluated for the exhaust restrictor.
- The specific heats of the recirculated combustion gas (CGR) and the inlet air-CGR mixture are assumed equal to the specific heat of the inlet air.
- The temperature rise in the combustor is fixed (3000°F).
- The air/fuel ratio is constant (20:1).
- Heat transfer from the burner system to the surroundings is neglected.
- Injected fuel is completely vaporized.

A schematic block diagram of the burner system is given in Figure 3-2. Gage pressures shown in the figure are those for maximum exhaust flow and were used to compute the orifice coefficients for the various restrictors. The symbols used in the block diagram, along with the variables and constants used in the equations to be presented, are all to be found in the nomenclature at the end of this section. For each symbol, the nomenclature includes a brief description of the symbol, the units, and, where applicable, the numerical value.

Basically, in the system model, incoming air, WA, at atmospheric temperature and pressure, is mixed with a prescheduled amount of recirculated combustion gas, WR. This gas then passes through the combustion air blower. Fuel, WF, is mixed with the air which then passes on to the combustor and is burned, producing a temperature rise, and is exhausted to atmosphere as WE. The exhaust restrictor, RC, represents

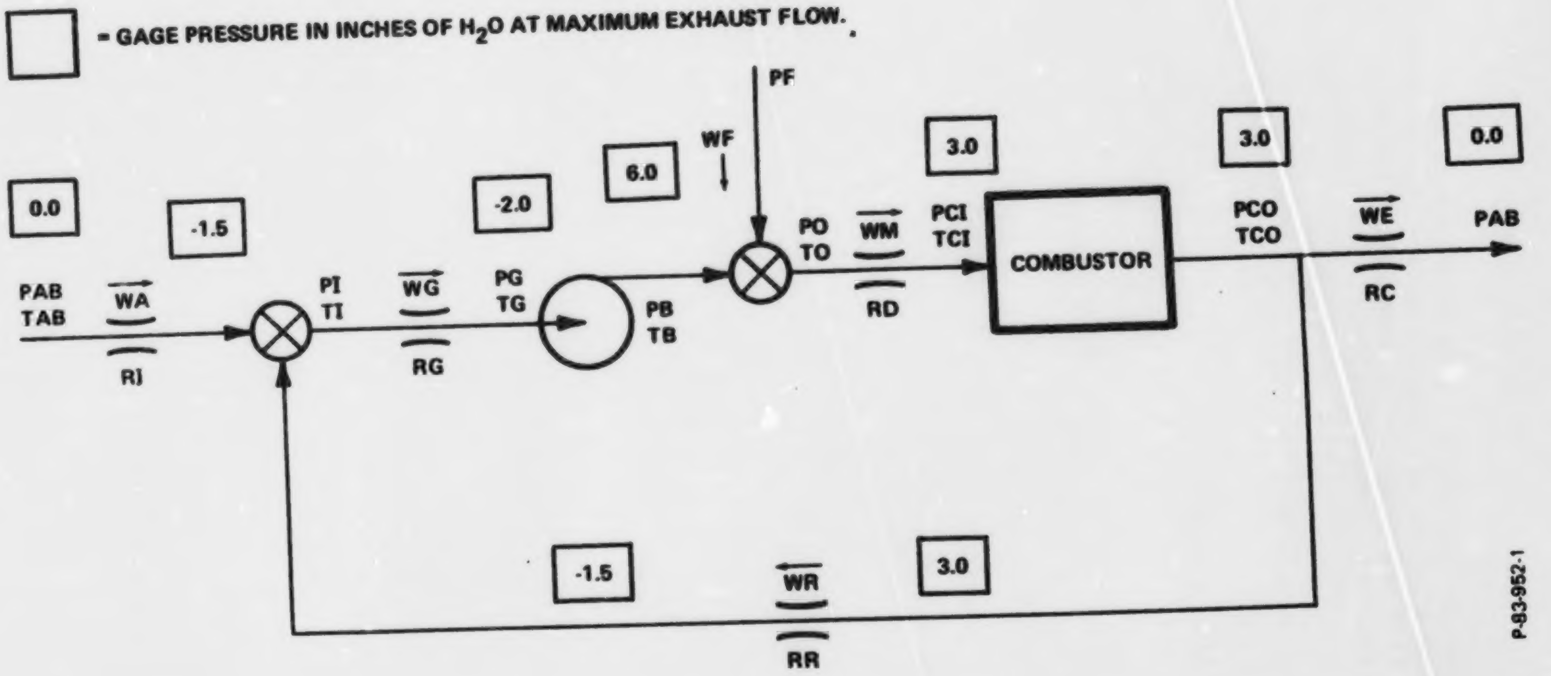
= GAGE PRESSURE IN INCHES OF H_2O AT MAXIMUM EXHAUST FLOW.
0.0
PAB
TAB
WA
RI
-1.5
PI
TI
WG
RG
-2.0
PG
TG
PB
TB
6.0
WF
PF
PO
TO
WM
RD
3.0
PCI
TCI
COMBUSTOR
3.0
PCO
TCO
WE
RC
0.0
PAB
-1.5
WR
RR
3.0
P-83-952-1

Figure 3-2 - Schematic Block Diagram of Burner System

the heat exchanger resistance. SES experimental evaluation indicates that an exponent of 1/1.8 is most representative for the design. Other designs may deviate from this value, with theoretical limits of 1.0 to 1/2. The system equations are presented below.

1. $WG = WA + WR$

2. $WM = WG + WF$

3. $WF = 0.05\ WA$

4. $WM = WE + WR$

5. $WA = \frac{(PAB - PI)^{1/2}}{RI}$

6. $WG = \frac{(PI - PG)^{1/2}}{RG}$

7. $WM = \frac{(PO - PCI)^{1/2}}{RD}$

8. $WE = \frac{(PCO - PAB)^{1/1.8}}{RC}$

9. $WR = \frac{(PCO - PI)^{1/2}}{RR}$

10. $PB = PO = PF$

11. $PCO = PCI$

12. $PB = PG + f(SP, VG)$

13. $$TI = \frac{WA \times CPA \times TAB + WR \times CPR \times TCO}{WA \times CPA + WR \times CPR}$$

14. $$TB = TI$$

15. $$TO = \frac{WG \times CPG \times TB + WF \times CPF \times TF - HLG \times WF}{WG \times CPG + WF \times CPF}$$

16. $$TCI = TO$$

17. $$TCO = TCI + 3000$$

18. $$VG = WG/D$$

19. $$D = \frac{PG \times 0.03613 \times 1728}{640 \times (460 + TG)}$$

The effects of this throttling scheme on exhaust gas flow versus blower speed is also shown in Figure 3-3 with the throttle angle given in parentheses. Examination of the results shows outflow to be quite linear with respect to blower speed for a given inlet area over the usable speed range of the blower.

From the results shown in Figure 3-3, a new set of curves may be derived. They are exhaust outflow versus blower inlet valve position, with blower speed as a parameter. These curves are the curves of constant blower speed shown in Figure 3-4. It can be inferred from the nonlinearity of these curves that some nonlinear response or curve shaping might be required for a shutter or throttle butterfly-valve inlet control.

The effect of changing the flow exponent to 1/1.8 was evaluated. This figure corresponds more closely to SES experimental results of steam generator pressure-flow tests. The calculation results, as far as pressure-flow relations are concerned, remained nearly unchanged, as shown in Figure 3-5.

The block diagram indicates that no active CGR valve exists and CGR flow is determined by system pressure distribution. Assuming no heat transfer from the gases, the 1/2 flow exponent model indicates a constant 218°F combustion inlet temperature. The 1/1.8 flow exponent model gives a blower inlet temperature of 247°F at minimum inlet flow and 216°F blower inlet temperature at the maximum inlet flow. At the extreme, if laminar flow conditions are assumed in the heat exchanger and a flow

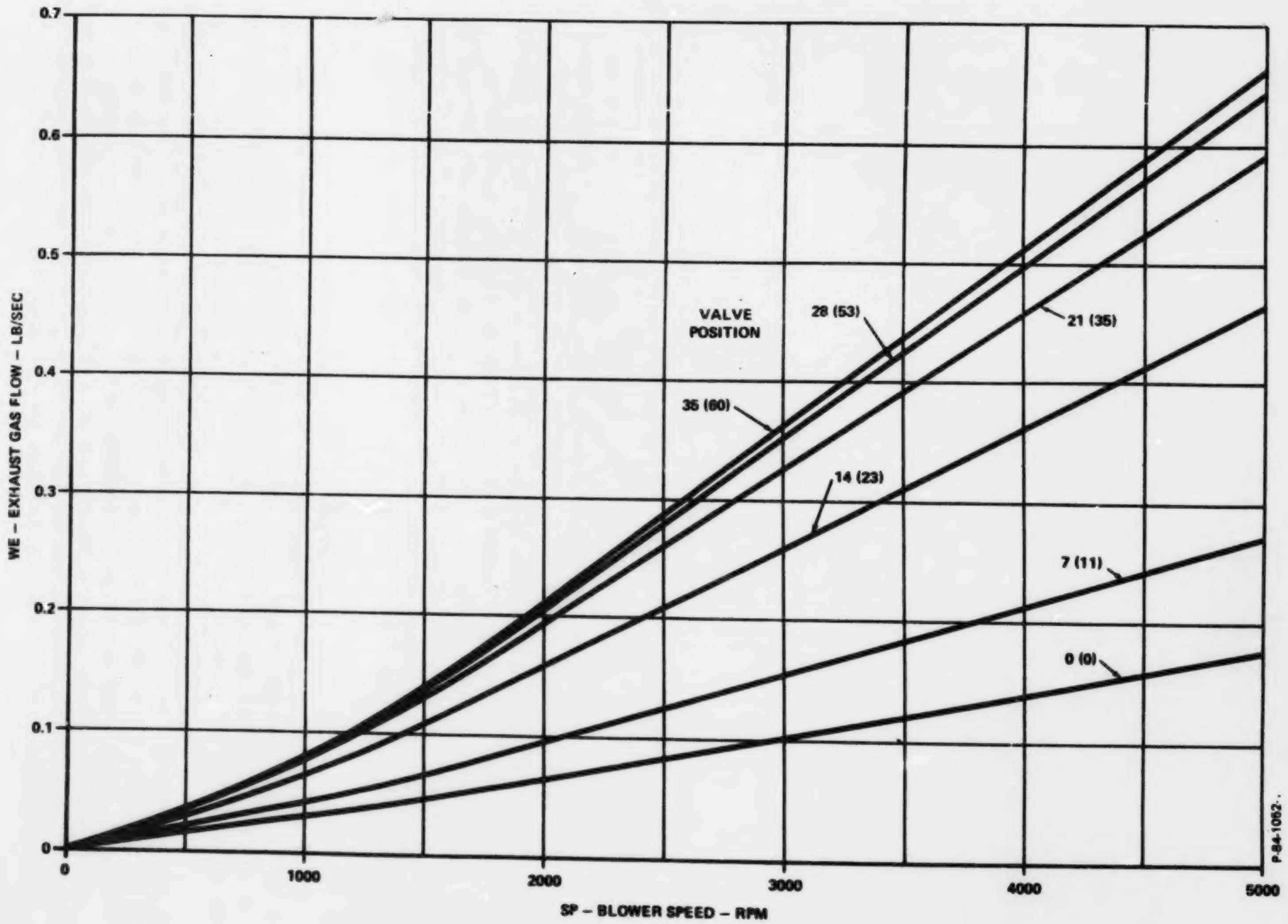

Figure 3-3 - Exhaust Gas Outflow versus Blower Speed

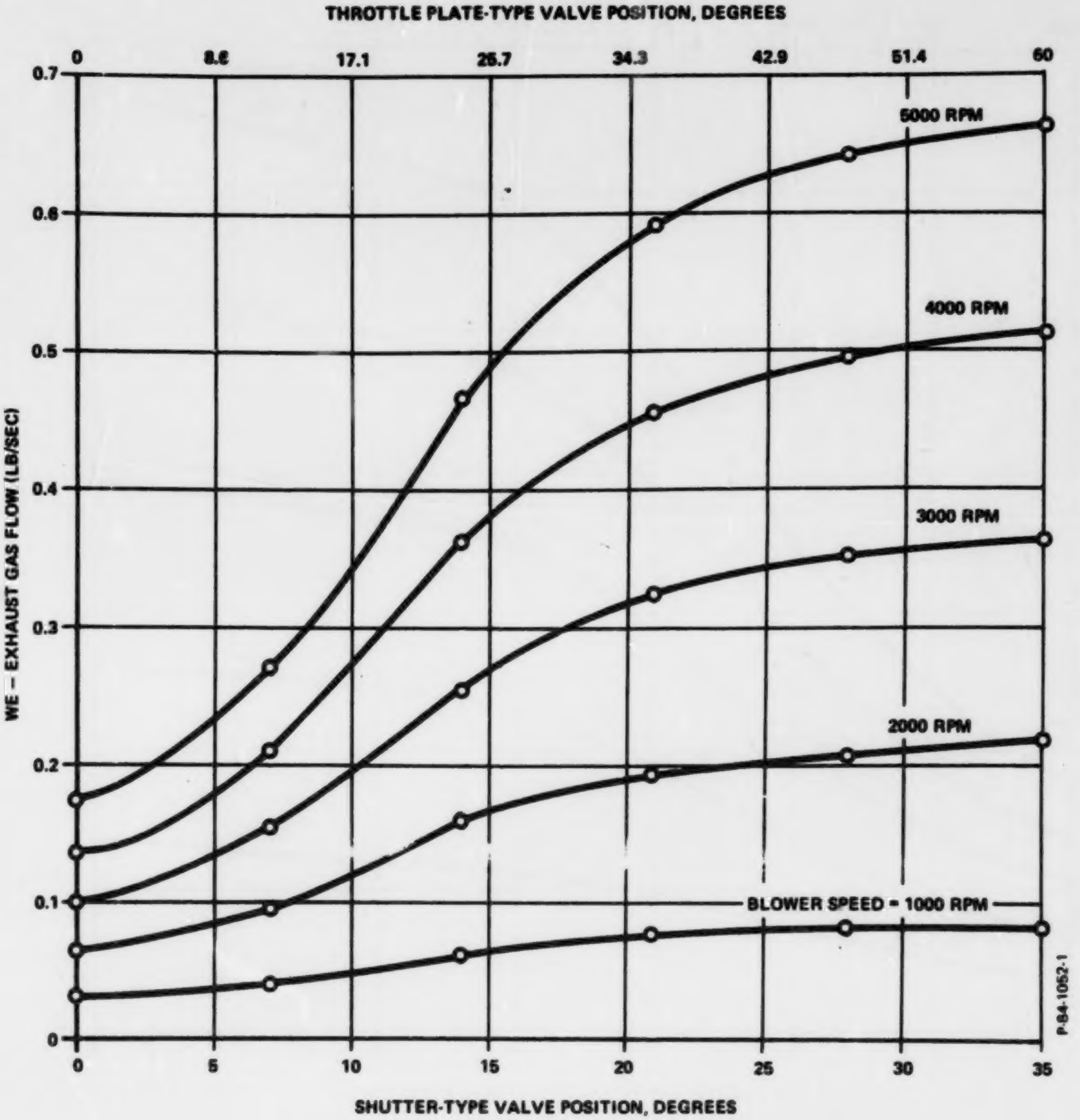

Figure 3-4 - Exhaust Gas Outflow versus Burner Inlet-Valve Position - Flow Exponent = 1.0

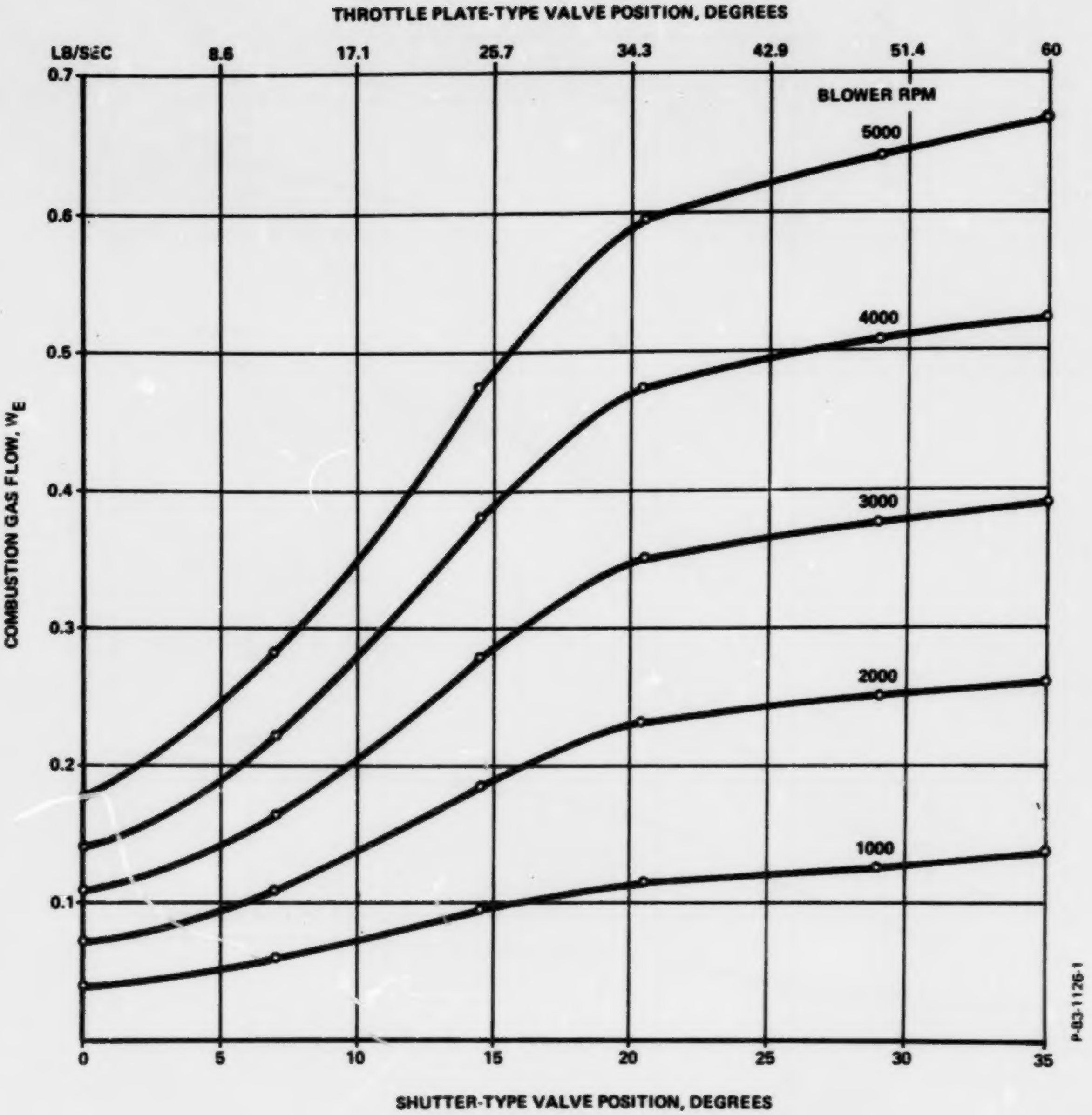

Figure 3-5 - Exhaust Gas Outflow versus Blower Inlet-Valve Position - Flow Exponent = 1.8

```
PRTGEN      9:18   04/18/72  TUE.


     BLOWER SIZING FACTOR          1.75
RI,RD,RR            2.3146        3.1174        76.3614
RC=           3.3136  D BFLY=          5.00

      S C A L E D  B Y   :           1.6002
     .00          .00       .50     1.00     1.50     2.00
CFM            RPM AT IN OF H20
     .00          .00 1043.00 1489.00 1853.00 2125.00
   87.50       325.00 1075.00 1514.00 1854.00 2143.00
  175.00       651.00 1189.00 1564.00 1876.00 2151.00
  262.50       976.00 1375.00 1710.00 1986.00 2232.00
  350.00      1302.00 1603.00 1894.00 2152.00 2379.00
  437.50      1627.00 1882.00 2108.00 2341.00 2553.00
  525.00      1953.00 2202.00 2351.00 2553.00 2749.00
  612.50      2278.00 2527.00 2640.00 2793.00 2965.00
  700.00      2604.00 2856.00 2958.00 3053.00 3205.00
  787.50      2929.00 3188.00 3280.00 3368.00 3452.00
  875.00      3255.00 3522.00 3606.00 3687.00 3765.00
  962.50      3580.00 3858.00 3935.00 4010.00 4082.00
 1050.00      3906.00 4194.00 4266.00 4336.00 4403.00
 1137.50      4231.00 4532.00 4599.00 4664.00 4727.00
 1225.00      4557.00 4871.00 4933.00 4994.00 5054.00



     .00         3.00     4.00     5.00     6.00     7.00
CFM            RPM AT IN OF H20
     .00      2617.00 3034.00 3402.00 3736.00 4044.00
   87.50      2627.00 3036.00 3396.00 3723.00 4024.00
  175.00      2624.00 3027.00 3383.00 3708.00 4007.00
  262.50      2662.00 3050.00 3392.00 3712.00 4007.00
  350.00      2772.00 3129.00 3444.00 3753.00 4037.00
  437.50      2930.00 3259.00 3559.00 3843.00 4105.00
  525.00      3104.00 3420.00 3709.00 3972.00 4221.00
  612.50      3296.00 3597.00 3875.00 4132.00 4373.00
  700.00      3502.00 3789.00 4053.00 4303.00 4536.00
  787.50      3733.00 3994.00 4247.00 4483.00 4712.00
  875.00      3975.00 4217.00 4453.00 4681.00 4895.00
  962.50      4223.00 4457.00 4672.00 4887.00 5097.00
 1050.00      4533.00 4702.00 4911.00 5106.00 5299.00
 1137.50      4849.00 4966.00 5150.00 5325.00 5501.00
 1225.00      5165.00 5230.00 5389.00 5544.00 5703.00



     .00         8.00     9.00    10.00    11.00
CFM            RPM AT IN OF H20
     .00      4331.00 4587.00 4835.00 5076.00
   87.50      4304.00 4567.00 4816.00 5053.00
  175.00      4286.00 4547.00 4795.00 5030.00
  262.50      4283.00 4541.00 4786.00 5018.00
  350.00      4301.00 4550.00 4792.00 5025.00
  437.50      4353.00 4601.00 4836.00 5060.00
  525.00      4464.00 4693.00 4910.00 5166.00
  612.50      4593.00 4811.00 5025.00 5272.00
  700.00      4757.00 4968.00 5153.00 5378.00
  787.50      4927.00 5125.00 5281.00 5484.00
  875.00      5105.00 5282.00 5409.00 5590.00
  962.50      5283.00 5439.00 5537.00 5696.00
 1050.00      5461.00 5596.00 5665.00 5802.00
 1137.50      5639.00 5753.00 5793.00 5908.00
 1225.00      5817.00 5910.00 5921.00 6014.00
```

Figure 3-6 - Pressure-Flow Characteristics of Blower

exponent of 1.0 is used, the blower inlet temperature varies from 502°F at minimum flow conditions to 212°F at maximum flow condition. The temperature calculation was made with no heat transfer to the surroundings. The effect of heat transfer, however, is believed to be significant and will affect the results. The prime purpose of the present study was the determination of pressure-flow control characteristics for the system studies, and did not require accurate temperature predictions.

3.2.2 Facsimile Burner Control System

Detailed design evaluation of the circuit described was carried out for the facsimile system. The blower characteristics of the combustion air blower used in the breadboard circuit were scaled to provide a blower input definition for the analysis. The flow-pressure characteristics at various speeds are shown in Figure 3-6. It is believed that for the purposes of the present design analysis, these curves are satisfactory and the design of the system is sufficiently flexible to accommodate any deviations that are expected in the performance characteristics of the blower to be selected by SES.

The calculations assumed the use of a simple butterfly-type valve for the throttle. System pressure drops specified by SES were used. Figure 3-7 shows the blower speed correction curve required for the predicted air flow calculation. The results indicate that for the specified blower characteristics a 4:1 blower speed range can be accommodated without the need for blower curve fitting. Also a simple two-segment curve can be used to accommodate a blower speed range in excess of 10:1 for the predicted position control of the air damper. The required air damper position for the blower speed corrected input signal is shown in Figure 3-8. This curve may be fitted with four straight segments to provide an accuracy better than that required for the predictive throttle-plate control system.

Computer Program Listing (1 of 3)

```
GASCK

100   CØMMØN DA(14),DB(15),DC(14,15)
110   READ,(DA(I),I=1,14)
120   READ,(DB(I),I=1,15)
130   READ,((DC(I,J),J=1,15),I=1,14)
140   READ,TAB,PAB,TF
150   READ,CPA,CPF,HLG
160   READ,RI,RD,RC,RR
162 XRC=1.8
164 RC=3**(1/XRC)
165 RC=RC/.65
166 PRINT"RC- ",RC
170    THE1=35.
180 122 CØNTINUE
190    PRINT,(',I=1,7)
200    CPR=CPA
210    CPG=CPA
220    AREA=1.5397+.018854*(THE1)**2.
230    RG=1./(.03724*AREA)
240    THE2=1.-((AREA-1.5397)/46.1926)
250    CPR=CPA
260    PRINT,(',I=1,5)
270    PRINT,RG,THE1,AREA
230    PRINT,THE2
290 PRINT
300    WA=.05
310  50 WR=(((1.05*RC*WA)**XRC+RI*RI*WA*WA)**.5)/RR
320    PWR=WR/WA*100.
330    WG=WA+WR
340    WF=.05*WA
350    WM=WF+WG
360    WE=WM-WR
370    A=WG*CPG+WF*CPF
380  TB=(WA*CPA*TAB*A+WR*CPR*(WF*CPF*TF-HLG*WF+3000.*A))/(A*(
390  +WA*CPA+WR*CPR)-WR*CPR*WG*CPG)
400  PG=PAB-(RI*WA)**2.-(RG*WG)**2.
410  PB=PAB+(RC*WE)**XRC+(RD*WM)**2
420  B=PB-PG
430  TØ=(WG*CPG*TB+WF*CPF*TF-HLG*WF)/A
440  TCØ=TØ+3000.
450  D=(.03613*1728.*PG)/(640.*(460.+TG))
460  C=WG*60./D
470  IF(11.-B)322,312,312
480  312 CØNTINUE
490  CALL INPØL(B,C,SP)
500  GØ TØ 329
510  322 SP=0.
520  GØ TØ 329
530  329 CØNTINUE
540  PRINT,WA,WG,WM,WE,WR,PWR,TB,TCØ,PG,PB,B,SP,C,D
550  PRINT
```

Computer Program Listing (2 of 3)

```
GASCK  CØNTINUED


560 WA=WA+.05
570 IF(.7-WA)230,230,50
580 230 CØNTINUE
590  IF(0.-THE1)372,379,379
600  372 THE1=THE1-7.
610 GØ TØ 122
620 379 CØNTINUE
630 END
640 SUBRØUTINE INPØL(XA,XB,XC)
650 CØMMØN AA(14),BB(15),CC(14,15)
660 I=1
670 40 IF(XA-AA(I))70,50,50
680 50 I=I+1
690 GØ TØ 40
700 70 M1=I-1
710 M2=I
720 I=1
730 100 IF(XB-BB(I))130,110,110
740 110 I=I+1
750 GØ TØ 100
760 130 N1=I-1
770 N2=I
780 GG=(XB-BB(N1))/(BB(N2)-BB(N1))
790 CLØ=CC(M1,N1)+(CC(M1,N2)-CC(M1,N1))*GG
800 CHI=CC(M2,N1)+(CC(M2,N2)-CC(M2,N1))*GG
810 XC=CLØ+(CHI-CLØ)*((XA-AA(M1))/(AA(M2)-AA(M1)))
820 RETURN
830 END
840 $DATA
850 0.,.5,1.,1.5,2.,3.,4.,5.,6.,7.,8.,9.,10.,11.
860 0.,50.,100.,150.,200.,250.,300.,350.,400.,450.,500.,
870 550.,600.,650.,700.
880 0.,325.,651.,976.,1302.,1627.,1953.,2278.,
890 2604.,2929.,3255.,3580.,3906.,4231.,4557.,
900 1043.,1075.,1189.,1375.,1603.,1882.,2202.,2527.,
910 2856.,3188.,3522.,3858.,4194.,4532.,4871.,
920 1489.,1514.,1564.,1710.,1894.,2108.,2351.,2640.,
930 2958.,3280.,3606.,3935.,4266.,4599.,4933.,
940 1853.,1854.,1876.,1986.,2152.,2341.,2553.,2793.,
950 3053.,3368.,3687.,4010.,4336.,4664.,4994.,
960 2125.,2143.,2151.,2232.,2379.,2553.,2749.,2965.,
970 3205.,3452.,3765.,4082.,4403.,4727.,5054.,
980 2617.,2627.,2624.,2662.,2772.,2930.,3104.,3296.,
990 3502.,3733.,3975.,4223.,4533.,4849.,5165.,
1000  3034.,3036.,3027.,3050.,3129.,3259.,3420.,3597.,
1010  3789.,3994.,4217.,4457.,4702.,4966.,5230.,
1020  3402.,3396.,3383.,3392.,3444.,3559.,3709.,3875.,
1030  4053.,4247.,4453.,4672.,4911.,5150.,5389.,
1040  3736.,3723.,3708.,3712.,3753.,3843.,3972.,4132.,
1050  4303.,4483.,4681.,4887.,5106.,5325.,5544.,
```

Computer Program Listing (3 of 3)

```
GASCK   CONTINUED


1060 4044.,4024.,4007.,4007.,4037.,4105.,4221.,4373.,
1070 4536.,4712.,4895.,5097.,5299.,5501.,5703.,
1080 4331.,4304.,4286.,4283.,4301.,4353.,4464.,4593.,
1090 4757.,4927.,5105.,5283.,5461.,5639.,5817.,
1100 4587.,4567.,4547.,4541.,4550.,4601.,4693.,4811.,
1110 4968.,5125.,5282.,5439.,5596.,5753.,5910.,
1120 4835.,4816.,4795.,4786.,4792.,4836.,4910.,5025.,
1130 5153.,5281.,5409.,5537.,5665.,5793.,5921.,
1140 5076.,5053.,5030.,5018.,5025.,5060.,5166.,5272.,
1150 5378.,5484.,5590.,5696.,5802.,5908.,6014.
1160 70.,407.,70.
1170 .243,.4,156.
1180 1.96,2.54,4.62,68.4
```

NOMENCLATURE

Symbol	Units	Value	Description
CPA	btu/lb°R	0.243	Specific heat of air
CPF	btu/lb°R	0.4	Specific heat of gasoline
CPG	btu/lb°R	---	Specific heat of inlet air and EGR mixture
CPR	btu/lb°R	---	Specific heat of EGR
D	lb/ft^3	---	Density of blower inlet gas
HLG	btu/lb	156	Heat of vaporization of gasoline
PAB	psia	14.7	Atmospheric pressure
PB	in H_2O	---	Blower outlet pressure
PCI	in H_2O	---	Combustor inlet pressure
PCO	in H_2O	---	Combustor outlet pressure
PF	in H_2O	---	Fuel pressure
PG	in H_2O	---	Blower inlet pressure
PI	in H_2O	---	Pressure of inlet air + EGR mixture
PO	in H_2O	---	Pressure of PI + fuel mixture
RC	$(in)^{1/1.8}$ (sec/lb)	2.83	Combustor restriction
RD	$\sqrt{in}$ sec/lb	2.54	Blower + duct outlet restriction
RG	$\sqrt{in}$ sec/lb	1.09	Blower inlet restriction
RI	$\sqrt{in}$ sec/lb	1.96	Inlet restriction
RR	$\sqrt{in}$ sec/lb	68.4	EGR duct restriction
SP	rev/min	---	Blower speed
TAB	°F	70	Inlet air temperature

Symbol	Units	Value	Description
TB	°F	---	Blower outlet temperature
TCI	°F	---	Combustor inlet temperature
TCO	°F	---	Combustor outlet temperature
TG	°F	---	Blower inlet temperature
TI	°F	---	Temperature of inlet air + EGR mixture
TO	°F	---	Temperature of TI + fuel mixture
WA	lb/sec	---	Inlet air flow
WE	lb/sec	---	Exhaust gas flow
WF	lb/sec	---	Fuel
WG	lb/sec	---	Inlet air + EGR flow
WM	lb/sec	---	WG + fuel mixture flow
WR	lb/sec	---	EGR flow
VG	ft^3/min	---	Blower volumetric flow rate

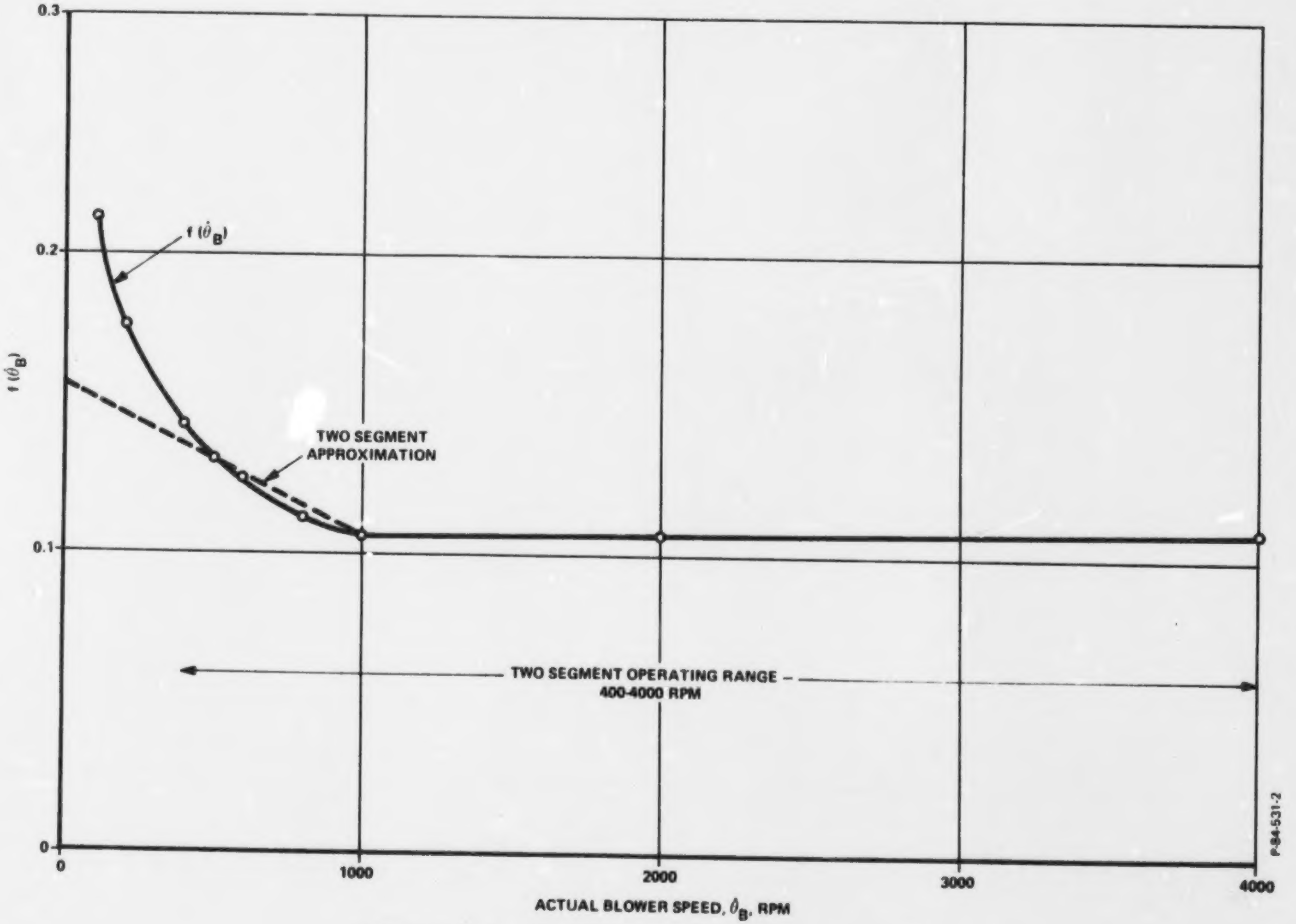

Figure 3-7 - Blower Speed Correction Curve

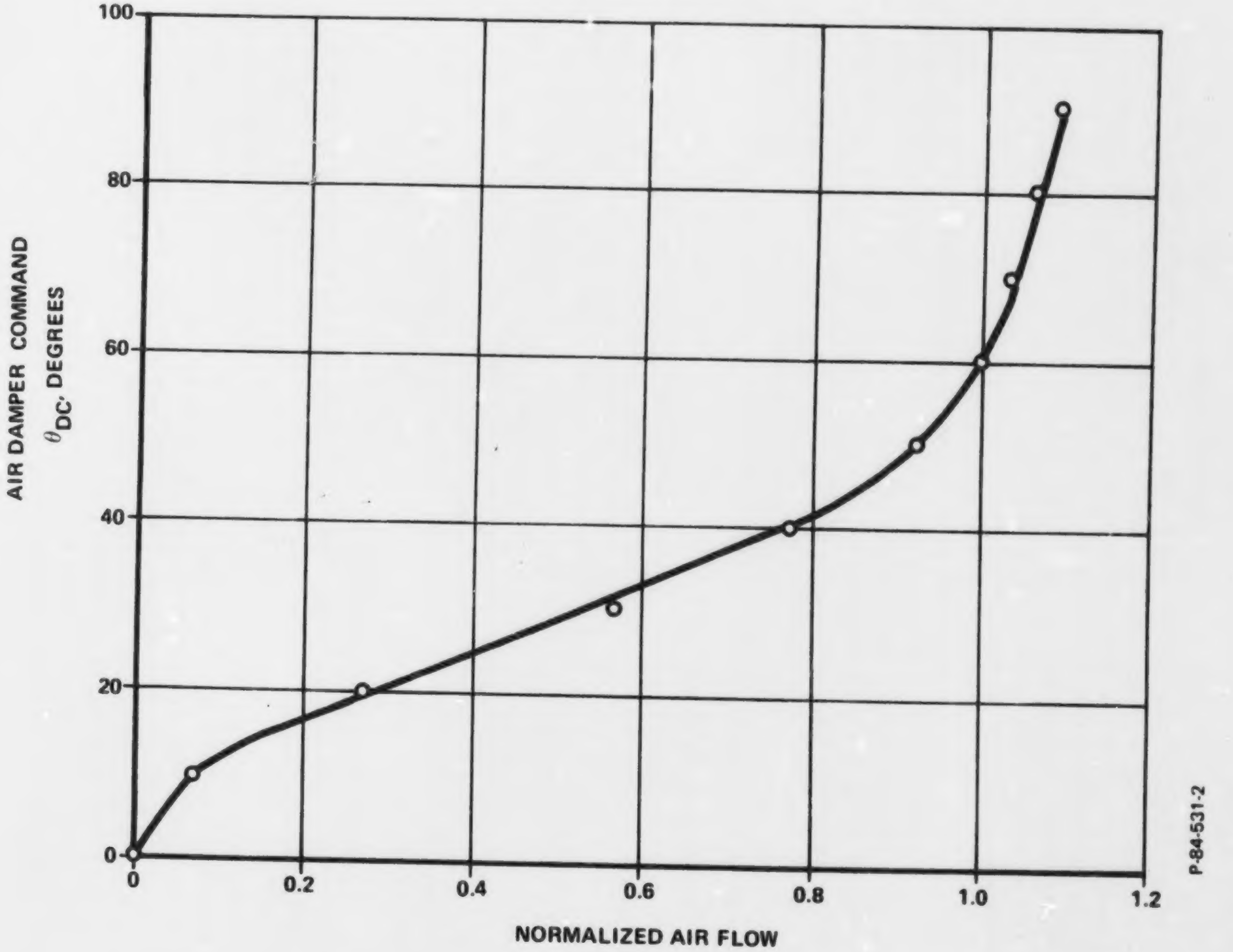

Figure 3-8 - Air Damper Command Signal Curve

3.3 FUEL CONTROL

The wide flow range of the external combustor falls beyond the reach of available fuel control systems. It is believed that an open-loop fuel metering scheme that relies on precise scheduling between air valve position and flow area opening of a fuel control valve would not be a practical device for mass fabrication techniques. In addition, when flow ranges in excess of 20:1 are considered, even with the ultimate in practical fuel filtering, erosion of the metering surfaces over an extended period of operation - such as a 50,000 mile vehicle operation - would alter the metering characteristics of this valve to a degree that is unacceptable for a low-emission combustor. On the basis of a brief evaluation of various fuel control concepts, a commercially available aircraft-type fuel injection system was selected to provide the primary fuel control function. One of the major factors influencing this decision again was the constraint of the time and funding schedule of the present program. It is quite possible that an alternate fuel control system could be the result of a more extended fuel control system program aimed at optimization for the external combustion system.

Carburetor-Type Fuel Control

A fuel control system relying on a constant-level fuel bowl for the fuel supply system and the air differential pressure developed in a venturi section has a limited range between maximum and minimum flow. If only inches of water is available as the maximum flow air differential pressure developed across the metering venturi, a specially designed variable-area fuel metering jet would become an essential part of this type of a metering system. At the present time, additional constraints, such as the use of an air atomizing nozzle believed to be essential for proper fuel vaporization, eliminate the carburetor-type fuel control system from consideration.

Pulsed-Type Fuel Metering

An intermittent or time-modulated fuel metering system, such as the electronic fuel injection system currently used on the VW 1600 cars, will offer a very flexible fuel metering system. The degree of sophistication will be limited only by cost considerations - primarily of the various sensors needed to mechanize a particular control scheme. It is believed that this concept may evolve to offer the ultimate in precision. The intermittent nature of the fuel flow may affect the emission characteristics of a continuous combustor. It was felt that combustion experiments would be essential to answer this question. Because neither funds not time were available to answer this uncertainty, the electronic fuel injection concept was not selected.

Continuous Fuel Injection

Continuous fuel injection has been in extensive use in the aircraft industry. This system offers the remote location of the fuel injection nozzle from the air metering and fuel control section. In addition, commercially available continuous fuel injection systems - often called pressure carburetors - include two independent mixture adjustments: the manual mixture control and the idle mixture control. An independent mechanization of either one of these two with a controller, such as an electric servo positioner, can easily convert the unit to a two-stage fuel metering system. Because of the ready availability of fuel injection units and the ease of modification that was found to be essential for thepresent application, this fuel control concept was selected for the facsimile fuel controller. A Bendix RSA fuel control device was selected as the prime component. In the following, the principle operation of this device and the operating characteristics of the particular unit incorporated in the facsimile fuel control system will be described in greater detail.

3.3.1 Operating Principles of the Bendix RSA Fuel Control Unit

A functional block diagram of the RSA fuel control system is shown in Figure 3-9. Briefly, the system operates as follows:

(1) Pressurized fuel from the fuel pump flows through the manual mixture control and idle cut-off valve to one side of both the enrichment valve and fuel diaphragms, and also to the enrichment and cruise jets.

(2) If the sum of the spring force and the pressure of the fuel from the enrichment jet exceeds the fuel pressure from the manual mixture control valve, the enrichment diaphragm moves to open the enrichment valve. Thus in the power range (manual idle valve open greater than idle setting), fuel may flow through the series combination of the fixed enrichment jet and variable enrichment valve and in parallel with the flow through the fixed cruise jet.

(3) Air is drawn into the unit through the inlet and boost venturi which causes a pressure drop. The differential pressure across the venturi is applied to either side of the air diaphragm. Thus the net force on the air diaphragm is a function of the air flow through the unit.

(4) Fuel leaving the manual idle valve is applied to the remaining side of the fuel diaphragm and the variable ball valve. The air and fuel diaphragms are constructed so that the fuel diaphragm opposes the force of the air diaphragm. Since the net force on the air diaphragm is totally dependent on air flow, and since the pressure on one side of the fuel

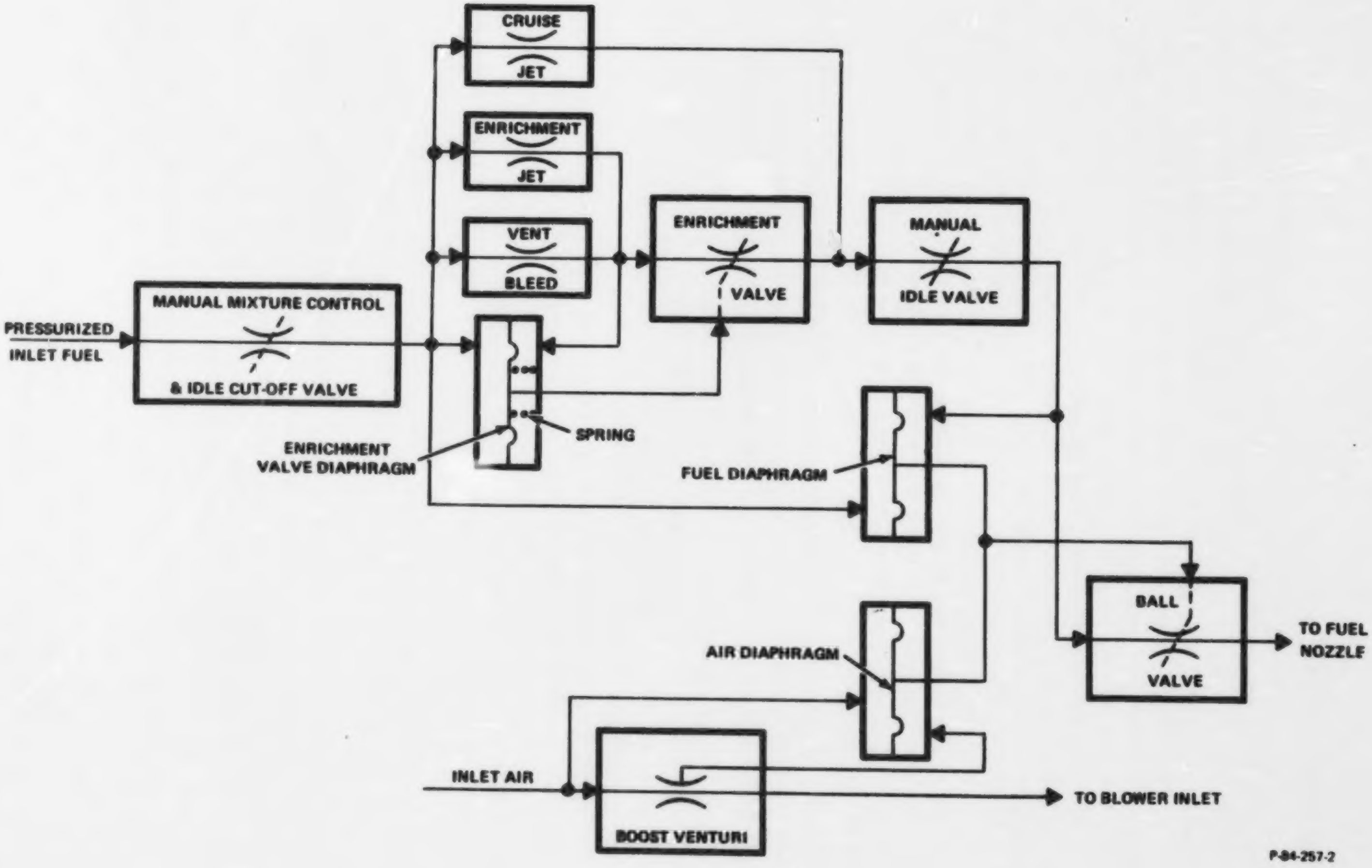
CRUISE
JET
ENRICHMENT
JET
VENT
BLEED
ENRICHMENT
VALVE
MANUAL
IDLE VALVE
PRESSURIZED
INLET FUEL
MANUAL MIXTURE CONTROL
& IDLE CUT-OFF VALVE
SPRING
ENRICHMENT
VALVE DIAPHRAGM
FUEL DIAPHRAGM
BALL
VALVE
TO FUEL
NOZZLE
AIR DIAPHRAGM
INLET AIR
BOOST VENTURI
TO BLOWER INLET
P-84-257-2

Figure 3-9 - Functional Block Diagram of RSA Unit

diaphragm is fixed at any point in time, the two diaphragms will balance only when the remaining fuel pressure, that to and through the ball valve, is of the proper valve, thus ensuring that fuel flow is a function of air flow.

From the above, it should be evident that the fuel control system is a closed-loop system with input air flow as an input control parameter. It should further be evident that by varying the sizes and taper of the enrichment jet and the spring which bears against the enrichment valve control diaphragm, the unit can be tailored to track nearly any fuel schedule.

3.3.2 RSA Fuel-Control Test Results

The Bendix RSA fuel control device was fabricated by Bendix Energy Controls Division in South Bend, Indiana. The unit initially was calibrated by ECD personnel and final tests, which will be described below, were performed in the presence and under the direction of Bendix Research Laboratories personnel at ECD. The overall performance of the unit was deemed satisfactory. A photograph of the unit is shown in Figure 3-10.

In order to test the effectiveness of the unit's regulation of fuel flow, the fuel outlet line was terminated with a variable orifice. Fuel flow and fuel pressure were then measured for constant values of air flow while the variable load resistance was varied from full open to a minimum opening. The data so obtained is shown in Figure 3-11. In all cases, the fuel inlet pressure was 30 psig, the test fluid was naphtha (specific gravity 0.735), and the ambient temperature was 70°F. It may be seen from the data that the operating characteristic of the unit is such as to provide a fuel flow appropriate to a given air flow, and to maintain this air/fuel ratio essentially constant over an extremely wide range of fuel outlet pressures. Thus, within reasonable bounds, the proper operation of the unit is unaffected by the choice of fuel atomizing nozzle.

Prior to the performance of the BRL-directed tests at ECD, preliminary data on the actual-unit fuel-schedule performance was submitted to BRL. This data is shown as the data points designated by the symbol "X" on Figure 3-12. Also shown on this figure is the desired fuel schedule (heavy line) and the ± air/fuel tolerance zone (area between the dashed lines). Data for the fuel schedule was taken by BRL personnel both with increasing air flow and decreasing air flow so that any hysteresis in the fuel schedule would be noted. The data points for increasing air flow are denoted by the symbol "o" in the figure, and the data points for decreasing air flow are denoted by the symbol "Δ". The fuel schedule data was taken with the manual idle valve in the full open position. No hysteresis was noted in the fuel schedule for air flow greater than 1000 lb/hr. Some hysteresis in the fuel schedule is noted for air flow of 1000 lb/hr and less. The maximum pressure drop across the RSA unit was 3.7 inches of H_2O at 2000 lb/hr air flow.

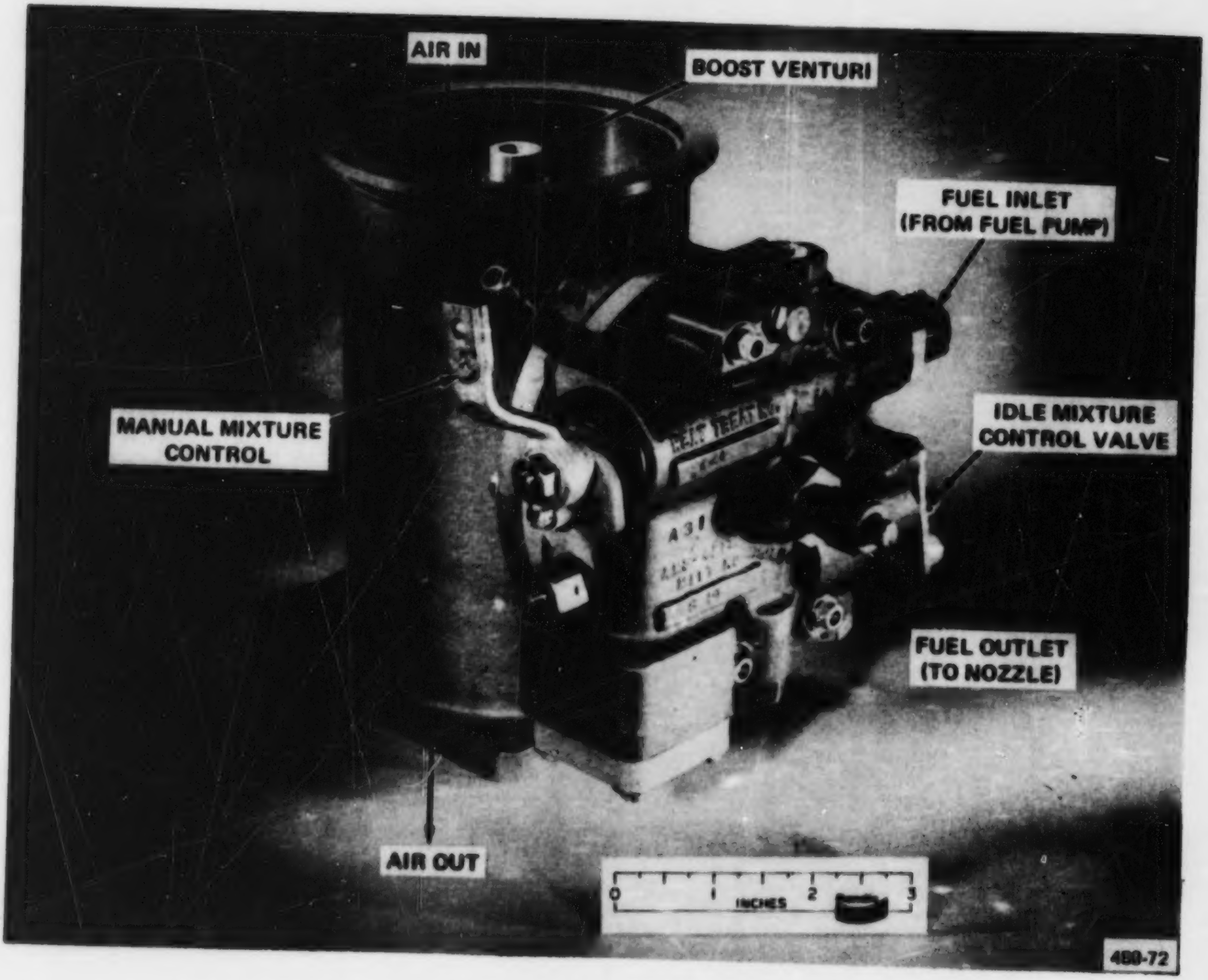
AIR IN
BOOST VENTURI
FUEL INLET (FROM FUEL PUMP)
MANUAL MIXTURE CONTROL
IDLE MIXTURE CONTROL VALVE
FUEL OUTLET (TO NOZZLE)
AIR OUT
0 1 INCHES 2 3
480-72

Figure 3-10 - Modified Bendix RSA-11 Fuel Control Device

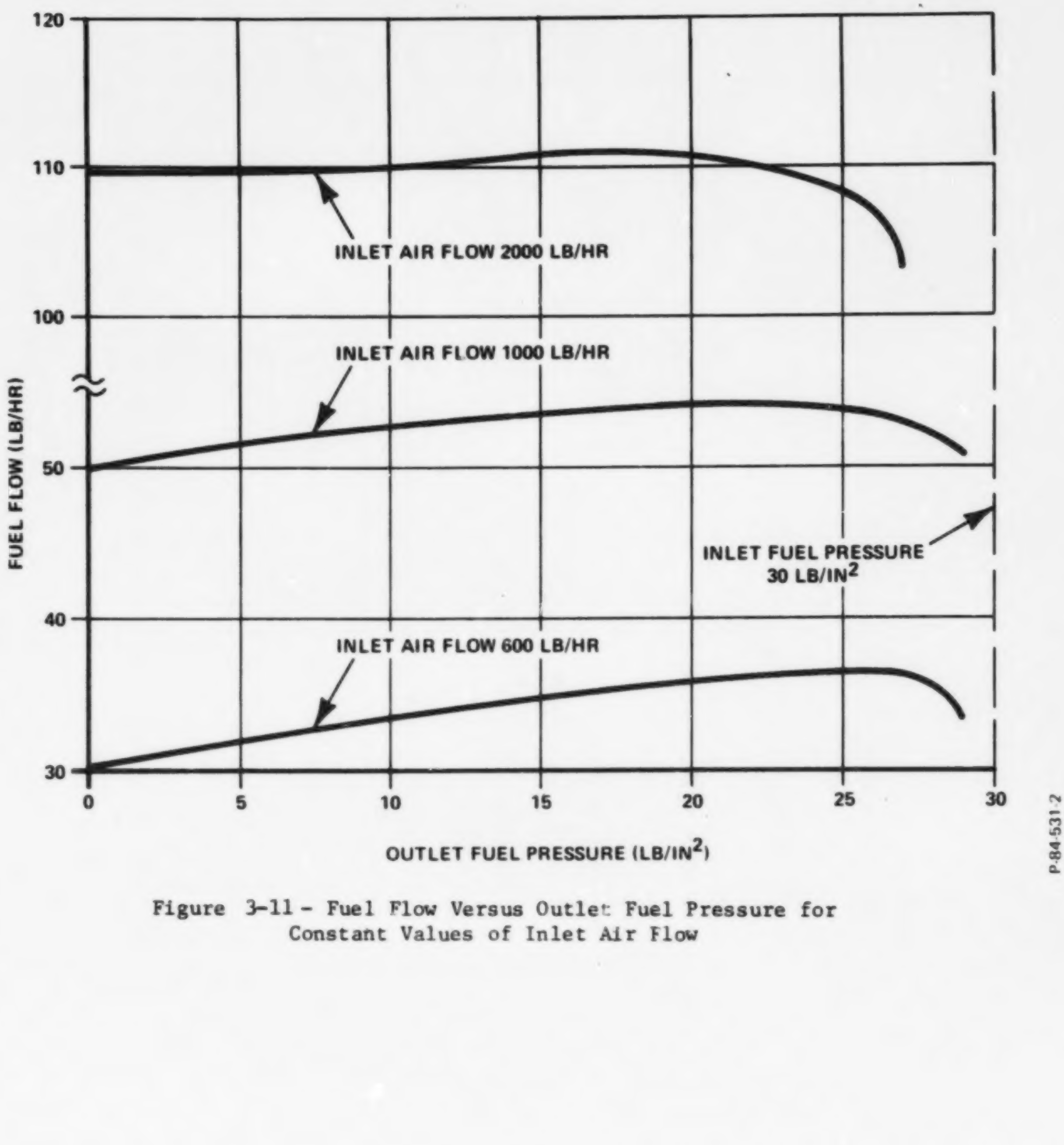

Figure 3-11 - Fuel Flow Versus Outlet Fuel Pressure for Constant Values of Inlet Air Flow

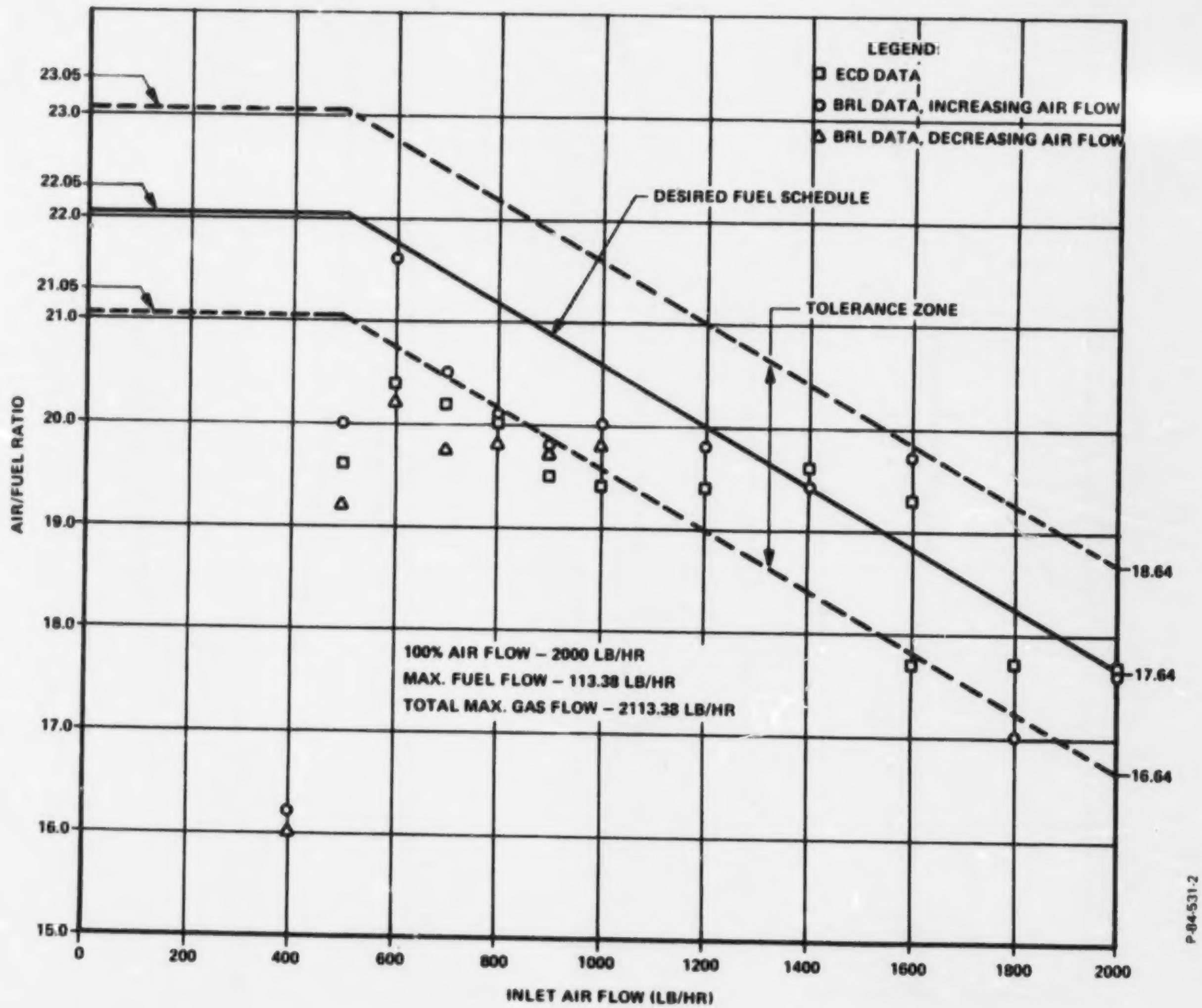

Figure 3-12 - Fuel Schedule - Air/Fuel Ratio Versus Inlet Air Flow

It may be seen that the fuel schedule data points lie within or near the tolerance zone for air flow in the range from 600 to 2000 lb/hr. It is also evident that the operation of the unit is such as to become increasingly fuel rich at lower values of air flow. This is because of the inability of the air and fuel diaphragms to respond to the extremely low control signals generated at low air-flow rates. The diaphragm materials used in this modified aircraft-type RSA unit are somewhat stiffer, to fulfill aircraft reliability requirements, than would be necessary in an automotive-type application. In addition, there is a small change in the effective area of the air and fuel diaphragms as they move in response to control signals. These small changes in effective area also tend to degrade the tracking accuracy of the unit at low air flow levels. In discussions between ECD and BRL personnel concerning the possibility of extended control range, ECD has assured BRL personnel that a modest diaphragm development program would most probably result in a unit which could track accurately down to approximately 350 lb/hr air flow.

The effect of the manual idle valve on fuel flow is shown in Figure 3-13. The data was taken at zero air flow, and the valve was more or less arbitrarily adjusted for 5 lb/hr minimum fuel flow. This minimum set point may be changed even to full cutoff by a simple mechanical adjustment without changing the maximum flow setting. It may be seen from the figure that the maximum fuel flow through the manual idle valve alone, as presently constructed, is 24.5 lb/hr. Referring again to the fuel schedule, Figure 3-12, it may be seen that the changeover to idle valve flow alone occurs at some value of air flow slightly less than 400 lb/hr. The control scheme for automatically operating the manual idle valve is described below. It is apparent that the RSA unit as presently modified will perform adequately in all respects and does conform to SES Specification SP-1041, dated 30 March 1972.

3.3.3 Idle Mixture Control

The air flow signal, below 600 lb/hr flow rates, is generated by combining the flow characteristics of the throttle valve with the square root of the pressure differential across the valve. Figure 3-14 gives a typical flow function for the throttle plate. The function shown is calculated; however, experimental corrections due to possible changes of C_d as a function of area configuration of the throttle plate can be accommodated readily in the design. The required idle-mixture control valve setting, as a function of a selected air flow signal, is shown in Figure 3-15. This curve was generated by combining the experimental results of the RSA fuel controller valve with results of the computer analysis of the combustion air delivery system. In general, the circuit offers the flexibility needed to accommodate possible final adjustments that may be needed to optimize burner emission characteristics. In addition, the overall concept lends itself to simplification and relatively low-cost manufacturing techniques once component tolerances are established for the entire fuel control system.

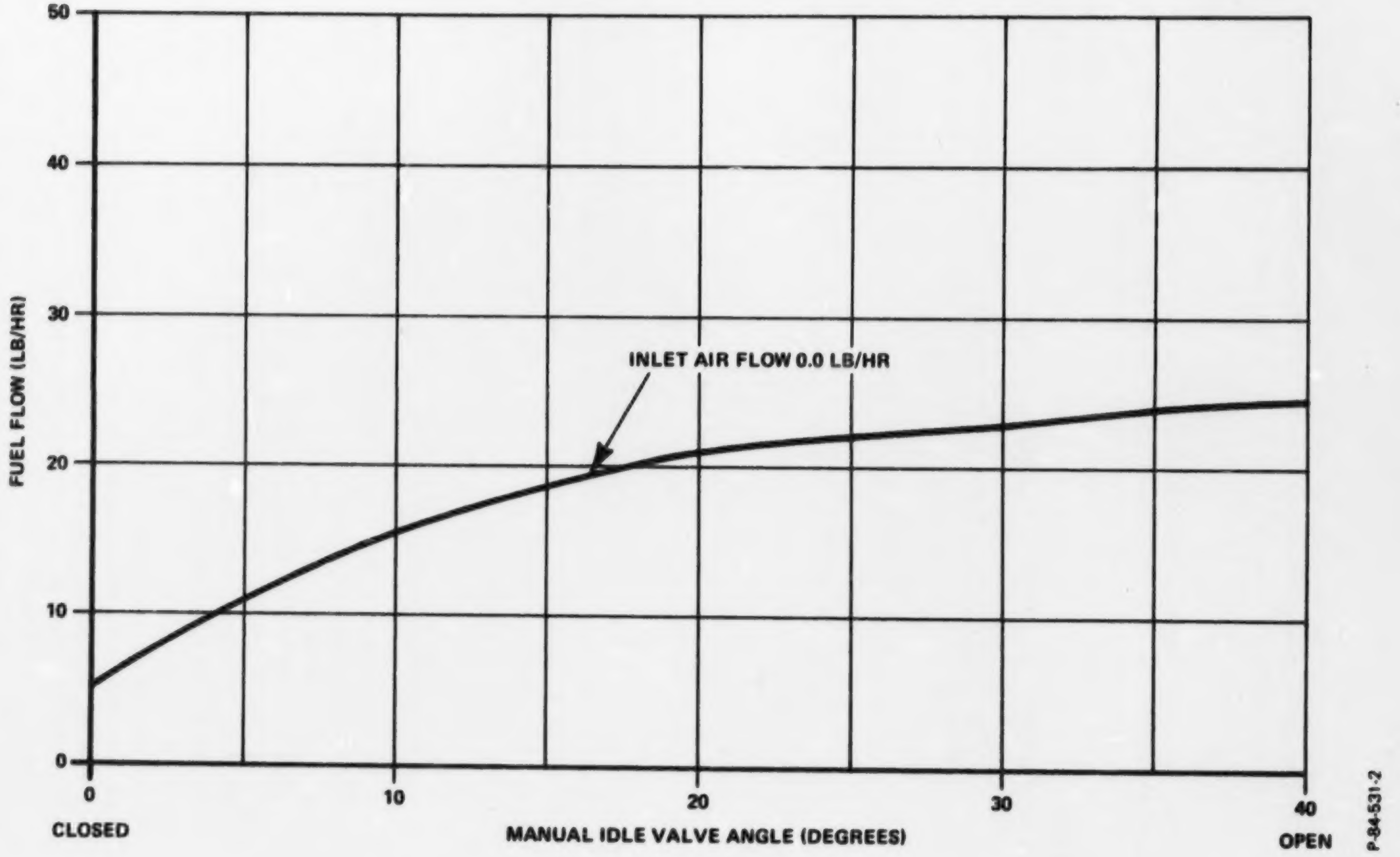

Figure 3-13 - Fuel Flow Versus Manual Idle Valve Angle at Zero Inlet Air Flow

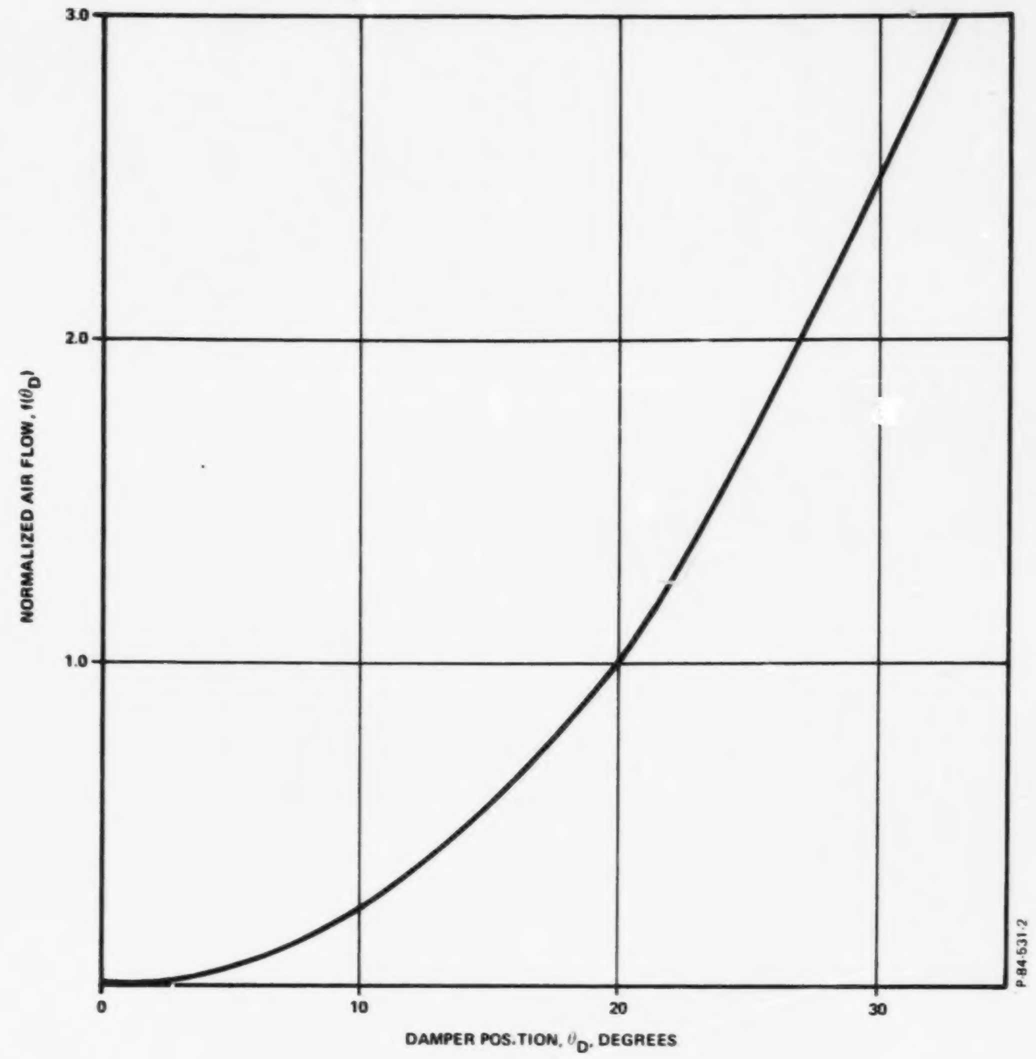

Figure 3-14 - Airflow Computer Function

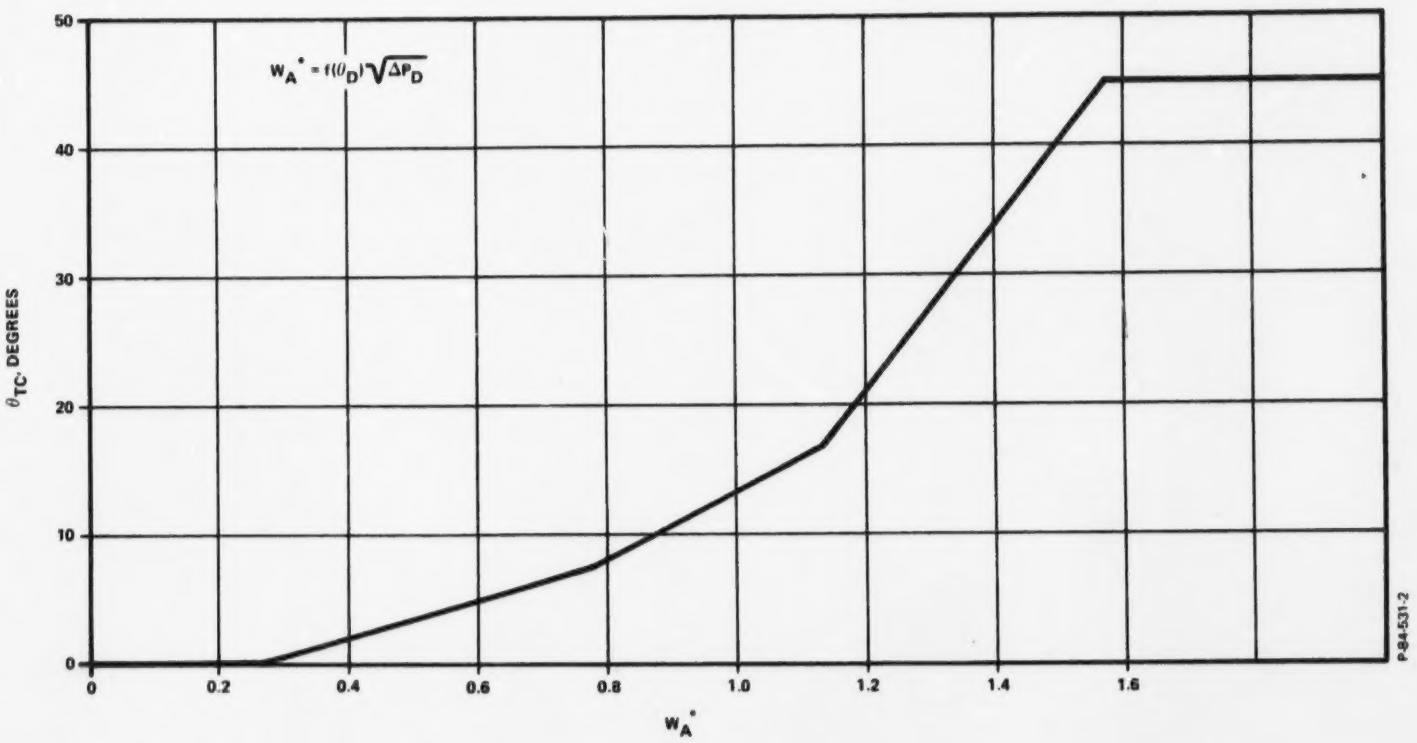

Figure 3-15 - Idle Fuel Control Valve Position Command

3.4 BYPASS VALVE

A single-stage, direct pressure-operated bypass valve is a separate piece of hardware designed for facsimile steam generator control. This bypass valve does not include a predictive signal. It is operated in the feedwater circuit by direct application of superheater outlet pressure. The use of the superheater pressure, instead of the inlet pressure for control, eliminates the shifting pressure at the outlet that would result from the ΔP variations caused by the variations in flow losses. The unit thus performs only the trim control function in the feedwater circuit. The feedwater pump controller must bear the burden of predictive control to achieve stable control of the feedwater circuit. An additional function of the bypass valve is the function of a safety device, as the full flow capability of the valve is 4 GPM, and exceeds the flow capacity of the feedwater pump. Thus the bypass valve is capable of pressure relief in the event of failure in the feedwater control circuit.

The valve was assembled and initial adjustments, to establish proper spring preloading and correct metering stem-to-seat closure, were made. A linear potentiometer, actuated by the valve control piston, has been provided to facilitate the acquisition of valve displacement data. Exploded and assembled views of the bypass valve are shown in Figure 3-16. Also provided, but not shown in the photographs, is an overpressure limit stop, the function of which is to limit, mechanically, the travel of the control piston to prevent extrusion and resultant damage to the piston seal in the event accidental overpressure of the valve occurs. In addition, two end caps, to accommodate springs varying from 2.5 to 6.0 inches in free length, have been fabricated. The test set up and results are described below.

The pressurized water source consisted of a pressure vessel filled with water and pressurized from a high-pressure nitrogen source through a constant-pressure regulator. The valve control pressure was obtained from the same nitrogen source through a second, independent, constant-pressure regulator. Pressure transducers were installed in the water and control pressure lines. A laboratory water flow meter was installed at the valve water inlet port. A voltage source was connected to the linear potentiometer. Thus, all control and operating parameters were available as electrical signals which were monitored simultaneously on a strip chart recorder. In addition, the water flow and control pressure signals were monitored, with expanded scale, on an X-Y plotter.

With a water supply pressure of 800 psi applied to the bottom port of the valve, that is, so that water flowed in through the seat and out of the side port, the control pressure was cycled slowly up to approximately 1060 psi and then down to 700 psi. The results of this test are shown in Figure 3-17. The data points denoted by the symbol '0' are those obtained from increasing pressures; the data points from decreasing pressure readings are denoted by the symbol 'Δ'. The best straight line approximations (graphically determined) to the increasing and decreasing

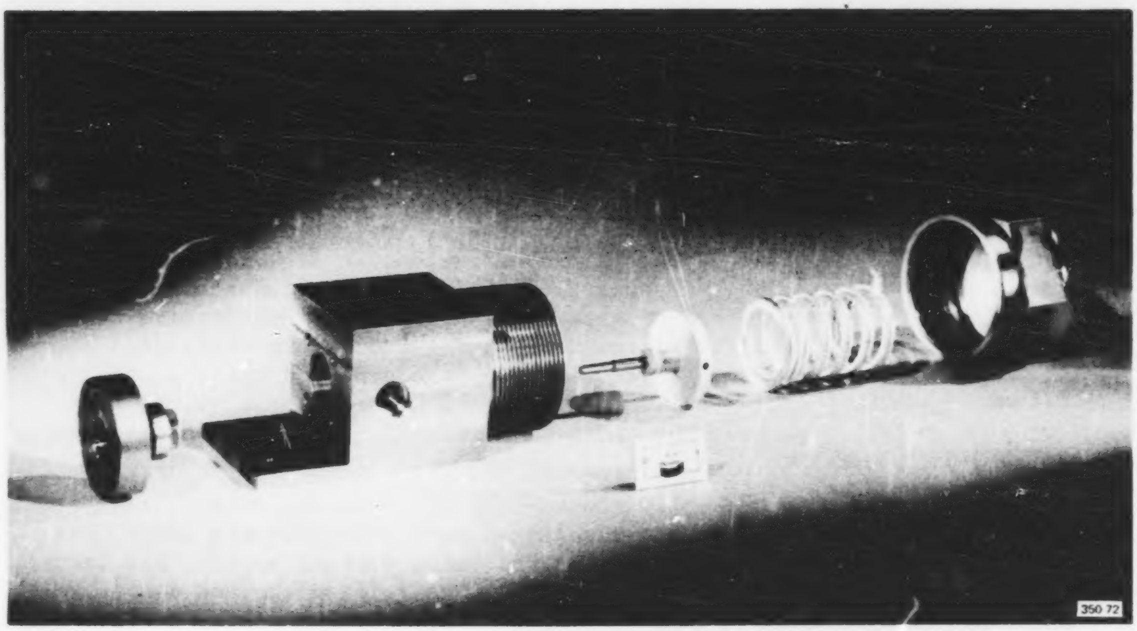

(a) Exploded View, Direct Pressure Operated Bypass Valve

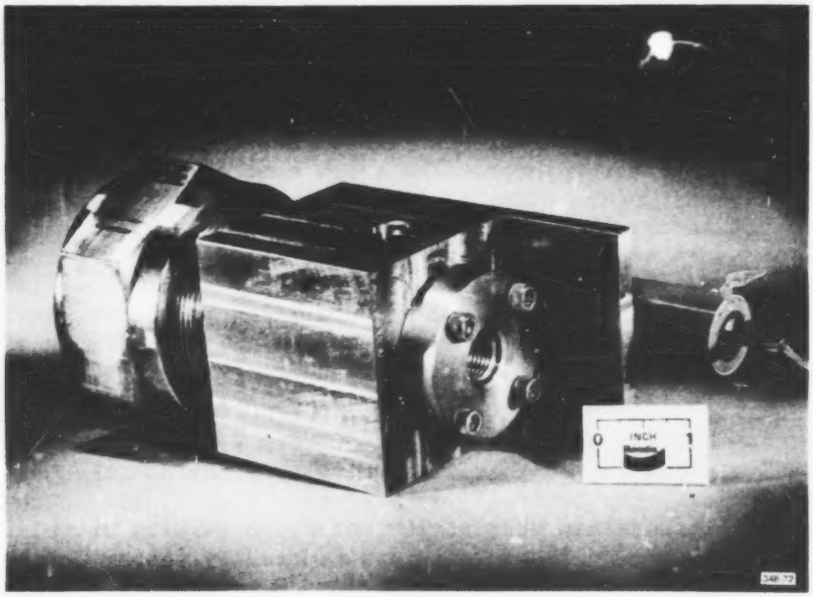
0
INCH
1
348 72

(b) Assembled View, Direct Pressure Operated Bypass Valve

Figure 3-16 - Direct Pressure Operated Bypass Valve

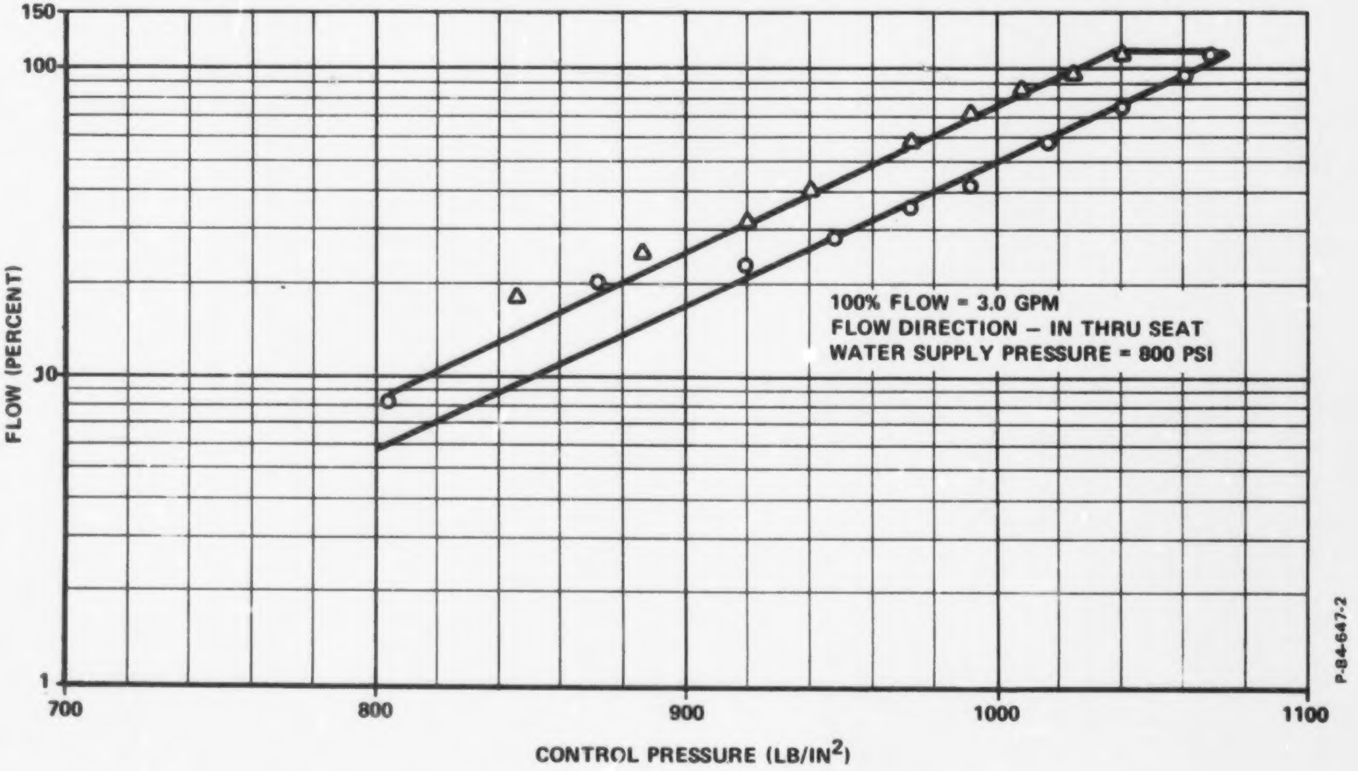

Figure 3-17 - Percent Flow Versus Control Pressure Showing Hysteresis

pressure points are also shown. A semilog scale (log percent flow versus linear pressure) was chosen because a perfect equal-percentage valve would yield a log percentage flow versus pressure plot which would be a perfectly straight line in these coordinates. Three gal/min was chosen as the 100 percent flow-point. Good linearity is noted at flows above the 10 percent (0.3 gpm) point. Repetitions of this test showed some variation in the valve cracking pressure because of stiction of the metering stem-control piston assembly. The valve displayed good repeatability, but the hysteresis caused by moving part friction, which is evident in Figure 2-17, was noted in these and all subsequent tests. The valve was then cycled as described above at constant water supply pressures of 600 and 1000 psi. The results of these tests are the mean value curves (hysteresis averaged out) shown in Figure 3-18. This data is repeated in Figure 3-19, but plotted as actual water flow versus control pressure in rectangular coordinates. The valve was then connected so that water flow was reversed, that is, in through the side port and out through the seat, and flow tests identical to those previously described were conducted. The results were the same as those previously obtained except in two respects:

(1) The valve cracking pressure was essentially constant at all supply pressures.

(2) Lower flow rates were obtained for a given supply and control pressure.

These effects are due primarily to the effect of the differential areas between the metering stem and control piston. The difference in flow rates are shown as the mean-value curves in Figure 3-20.

With the valve still connected so that the flow was out through the seat, the valve was tested dynamically by applying a control pressure of approximately 1050 psi, and then dropping the control pressure approximately 200 psi in 100 milliseconds. The results of the test are shown in Figure 3-21. Some delay in initial response is apparent, but subsequent control-pressure tracking and lack of overshoot or oscillation is noteworthy.

Closed-valve leakage tests were performed with 700 psi control pressure applied, and a water supply pressure of 1000 psi applied in both flow directions. With flow in through the seat, a leakage flow of 0.0324 gpm was obtained; with flow out through the seat, the leakage was 0.0306 gpm.

From the foregoing, it is believed that the valve will perform adequately and safely in the S.E.S. system. The safe operation of the system is enhanced by the fact that the maximum flow capacity of the bypass valve (approximately 4.1 gpm at 1000 psi pressure drop) exceeds the expected capacity of the feedwater pump. Therefore the valve, equipped with the spring and adjusted as in the tests reported above, has been delivered to S.E.S. A set of instructions for operation and adjustment has also been submitted. It is anticipated that any additional tests will be performed on the facsimile hardware at S.E.S.

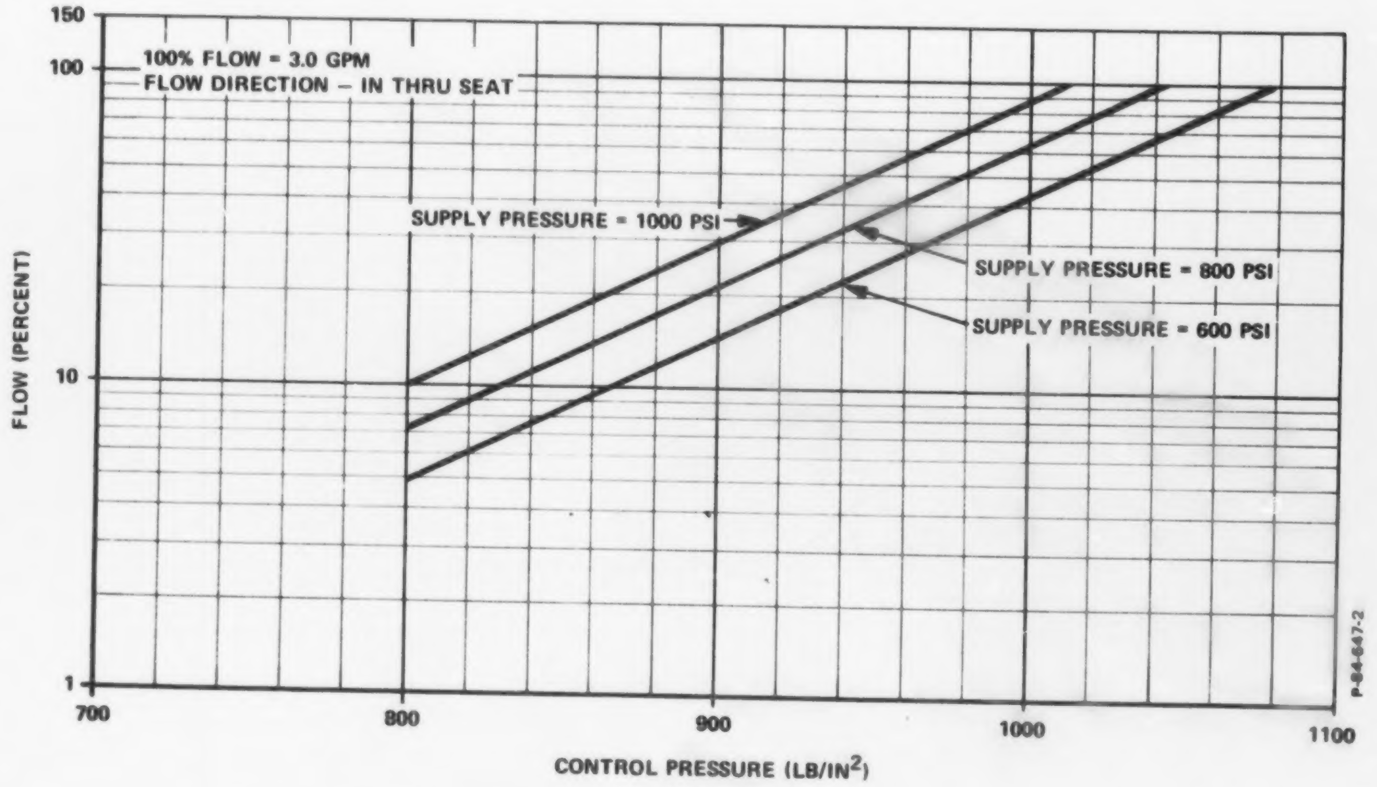

Figure 3-18- Mean Values of Percent Flow Versus Control Pressure for Constant Values of Water Supply Pressure

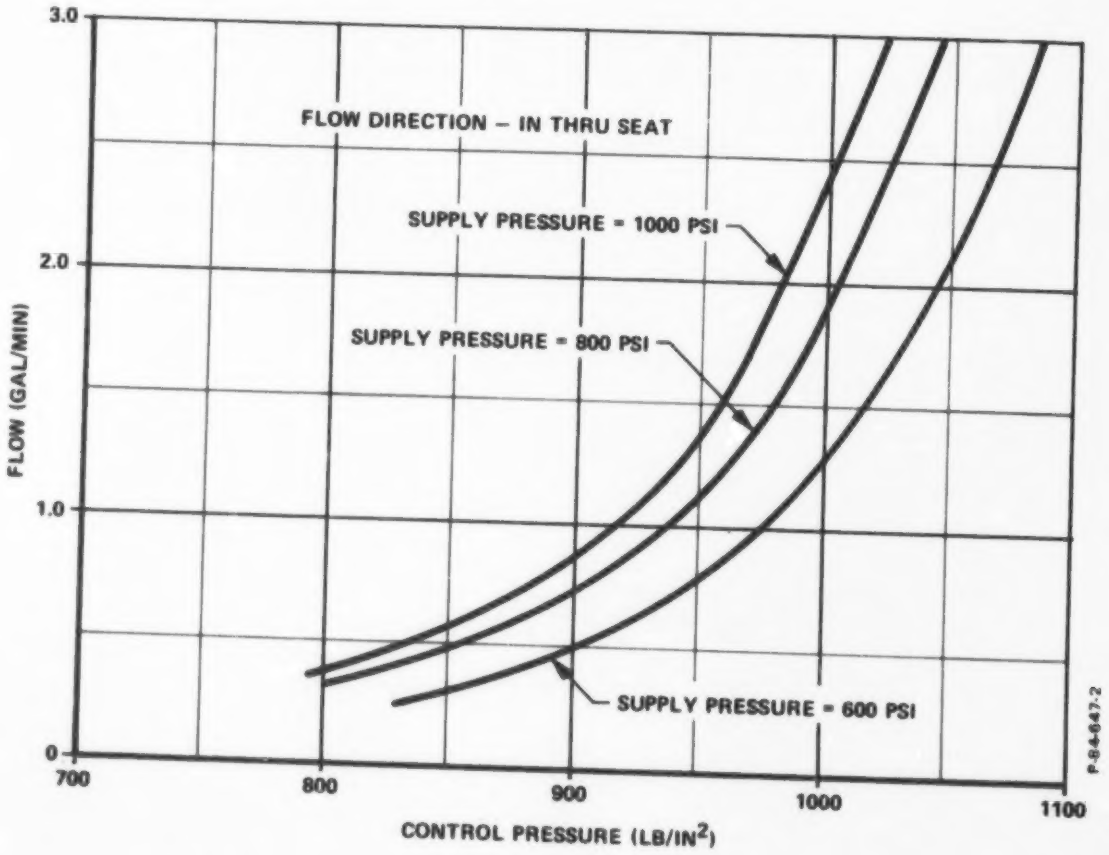

Figure 3-19 - Water Flow Versus Control Pressure for Constant Values of Water Supply Pressure

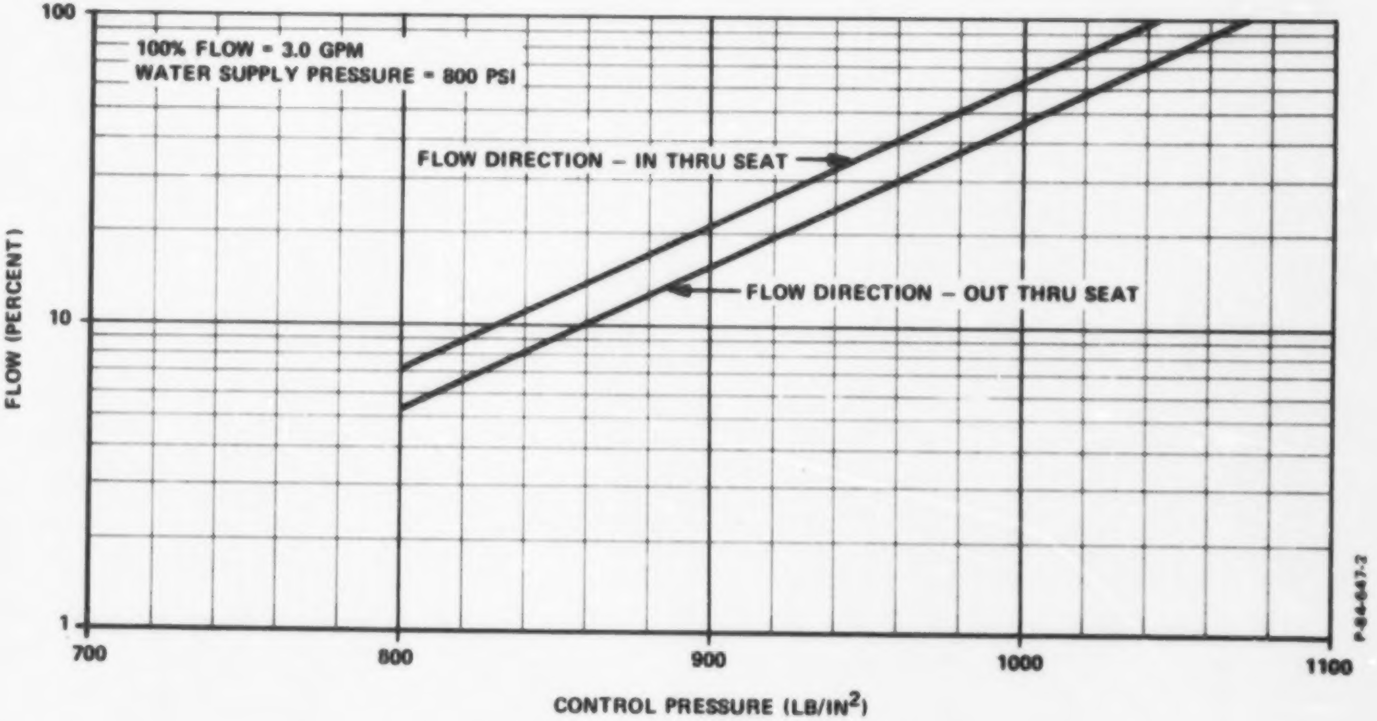

Figure 3-20 - Effect of Flow Direction on Flow Versus Control Pressure at Constant Supply Pressure

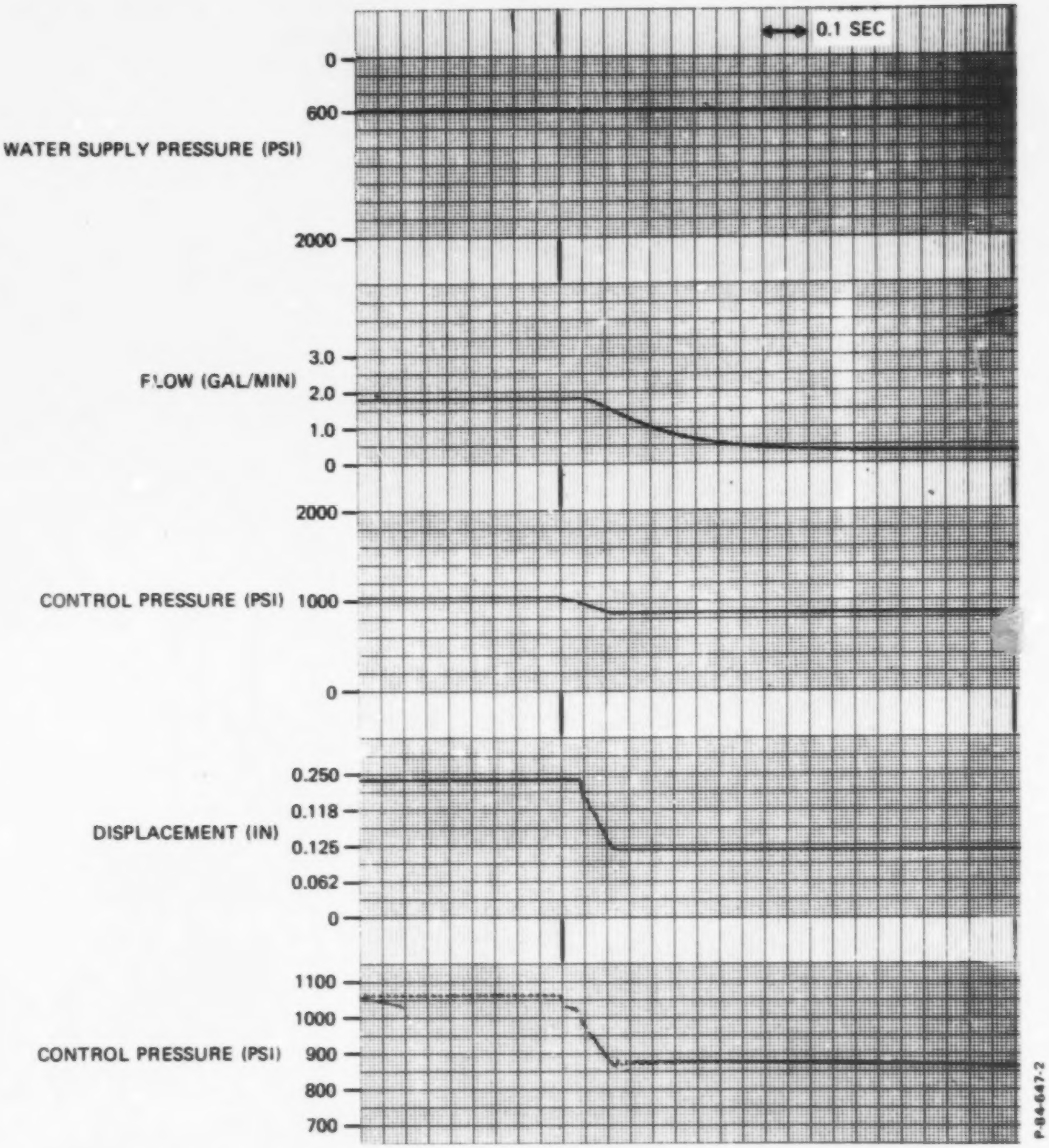

Figure 3-21 - Valve Response to a Step Change in Control Pressure

3.5 FACSIMILE DESIGN VERIFICATION TEST

A series of tests were conducted at the Bendix Research Laboratories to verify the operation of the facsimile burner control hardware. All input signals were activated either directly or through a simulated signal. All functional parts of the predictive controller and the fuel controller were tested. In addition, calibration curves for both the air flow circuit and the fuel control circuit were established. This section describes the test conditions and presents the results of the testing.

Figure 3-22 shows the complete test schematic. The RSA fuel control unit was connected through a transition section to the butterfly throttle valve. A suitable fuel source, using a Stoddard-T solvent as the working fluid, was used in the fuel circuit. An air-box vacuum system was used to provide the source for the air flow during the test program. Both the air-damper servo actuator system and the fuel trim-control servo actuator were fully energized and operated with both circuits simultaneously connected to the 809 analog signal processor. All signals, including both the throttle differential pressure input and the water flow signal, were also connected to the 809 analog signal processor. For the purposes of testing, low-pressure cold water was used to operate the water flowmeter. In order to simplify testing, a voltage source was substituted for the blower tachometer signal. A photograph of the test configuration is shown in Figure 3-23. A closeup of the throttle valve, the RSA fuel control, and the two electromechanical servo actuators are shown in Figure 3-24.

The calibration of the RSA unit, using the Stoddard-T solvent, was performed to verify the operating characteristics of the unit. The results, shown in Figure 3-25 verify the operating characteristics already established at an earlier date and reported in Section 3.3.2. The calibration curve for the fuel control trim servo at zero air flow was also established. The results are shown in Figure 3-26. The range of control and general smoothness of the curve indicates that the fuel control trim servo has the capability of controlling over the required fuel flow range.

The throttle-plate valve-position signal and differential pressure across the butterfly valve are used to compute the air flow signal for the low-range fuel controller. The calibration curve in terms of these two variables are shown in Figures 3-27 and 3-28. The first figure gives the overall calibration over the entire operating range. After the blower selection is finalized by SES, the operating characteristics of the blower can be combined with these curves to define the expected operating range of the fuel control system in terms of ΔP range and throttle-angle range.

Dynamic operating characteristics of the two servo actuators is shown in Figure 3-29. The response to a large step change in water flow signal is shown. It is believed that the signal rates indicated in the figure exceed the requirements of the SES facsimile plant.

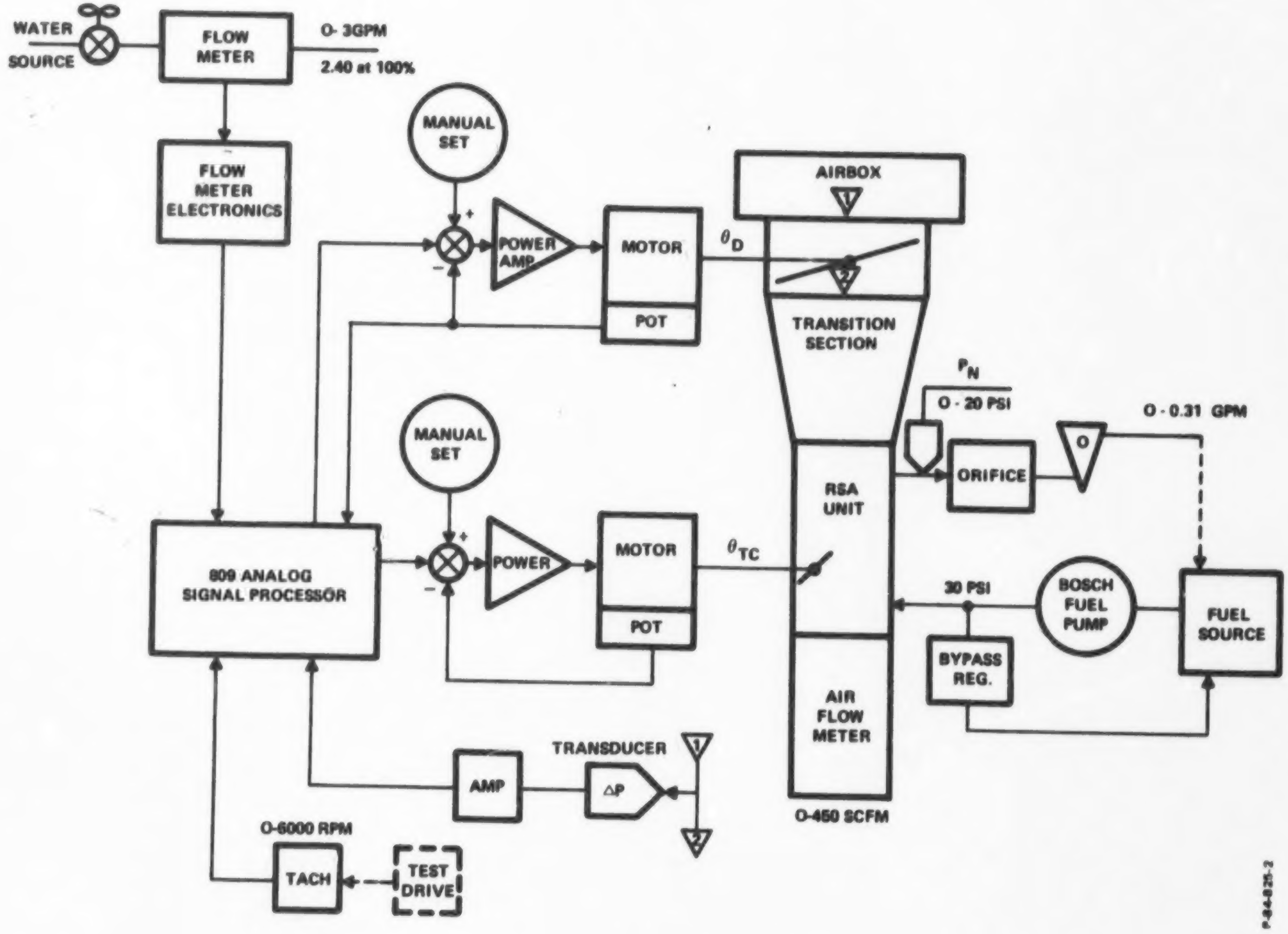
WATER
SOURCE
FLOW METER
O- 3GPM
2.40 at 100%
FLOW METER ELECTRONICS
MANUAL SET
+
−
POWER AMP
MOTOR
POT
θ_D
AIRBOX
1
2
TRANSITION SECTION
P_N
O - 20 PSI
ORIFICE
O
O - 0.31 GPM
RSA UNIT
MANUAL SET
+
−
POWER
MOTOR
POT
θ_{TC}
809 ANALOG SIGNAL PROCESSOR
30 PSI
BOSCH FUEL PUMP
FUEL SOURCE
BYPASS REG.
AIR FLOW METER
O-450 SCFM
TRANSDUCER
ΔP
AMP
1
2
O-6000 RPM
TACH
TEST DRIVE
P-84825-2

Figure 3-22 - Burner-Control Test Setup

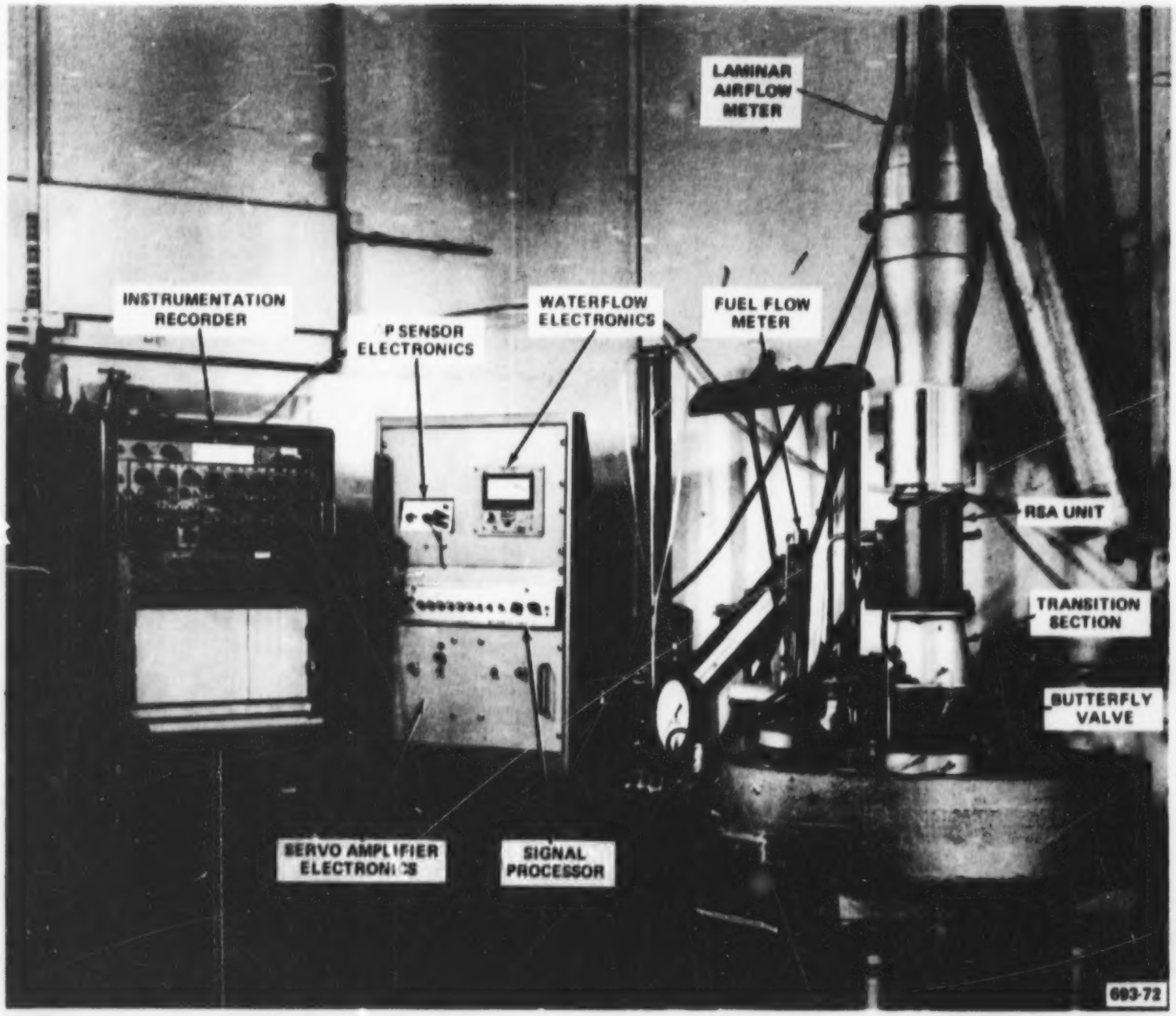
LAMINAR AIRFLOW METER
INSTRUMENTATION RECORDER
P SENSOR ELECTRONICS
WATERFLOW ELECTRONICS
FUEL FLOW METER
RSA UNIT
TRANSITION SECTION
BUTTERFLY VALVE
SERVO AMPLIFIER ELECTRONICS
SIGNAL PROCESSOR
693-72

Figure 3-23 - Facsimile Test Setup

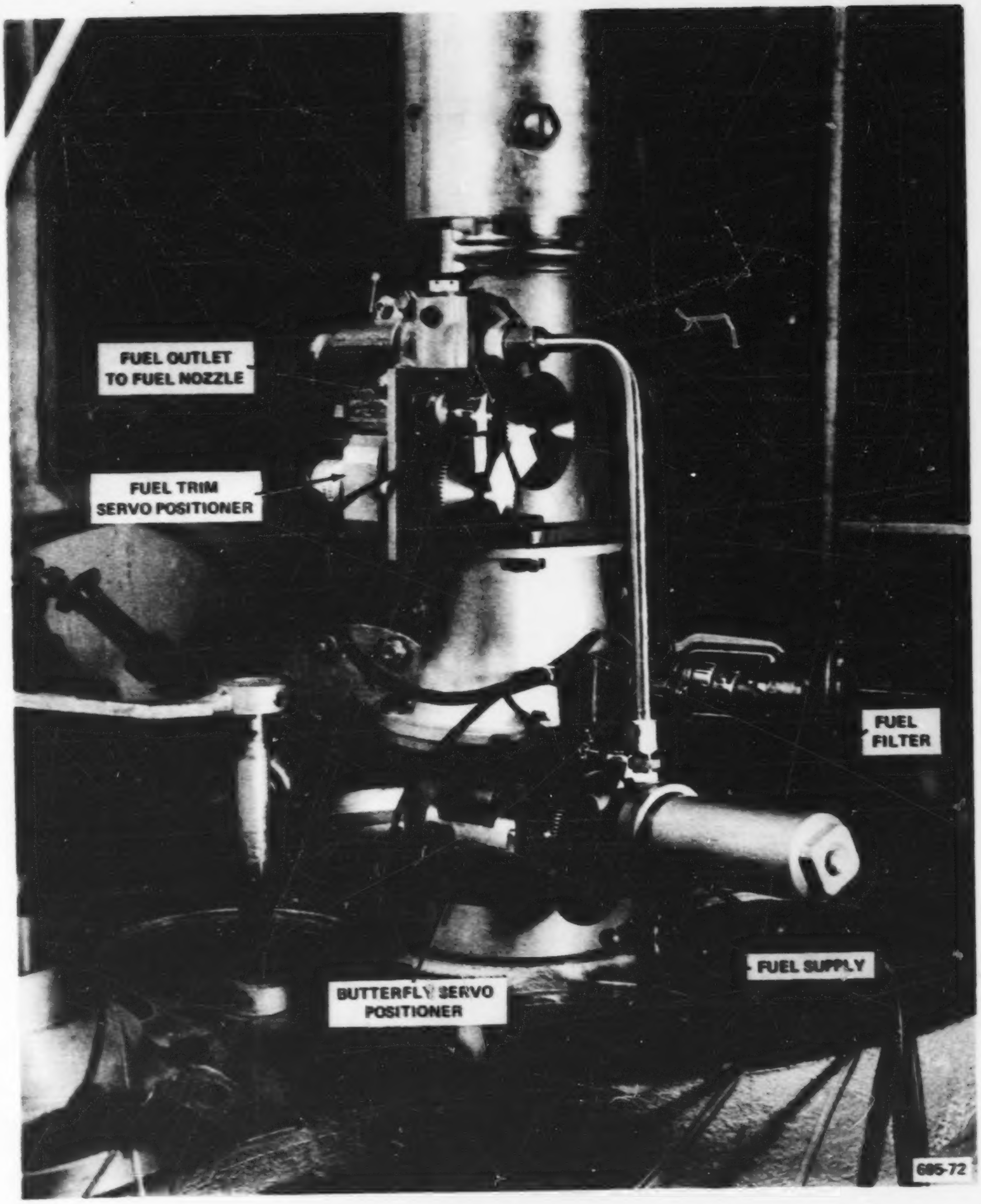
FUEL OUTLET TO FUEL NOZZLE
FUEL TRIM SERVO POSITIONER
FUEL FILTER
FUEL SUPPLY
BUTTERFLY SERVO POSITIONER
685-72

Figure 3-24 - RSA Fuel-Control Unit with Idle Circuit and Throttle-Plate Servoactuators

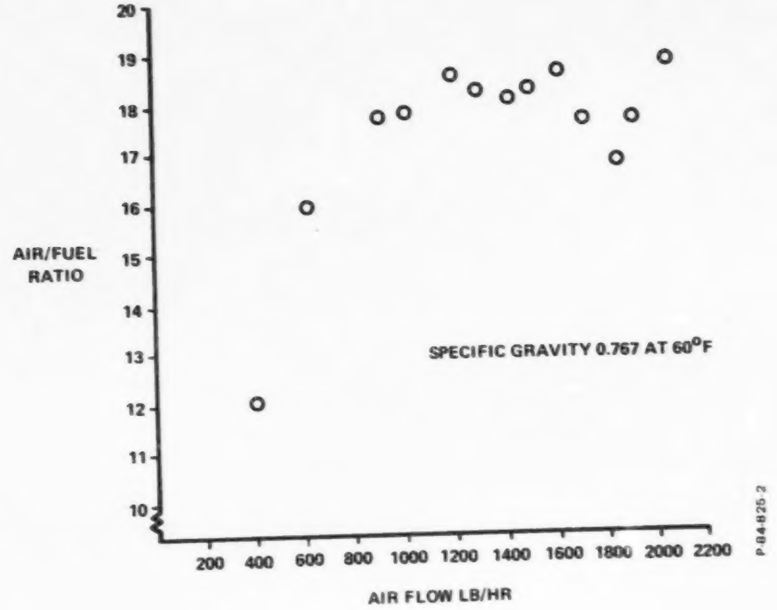

Figure 3-25 - RSA Unit Calibration Using Stoddard-T Solvent

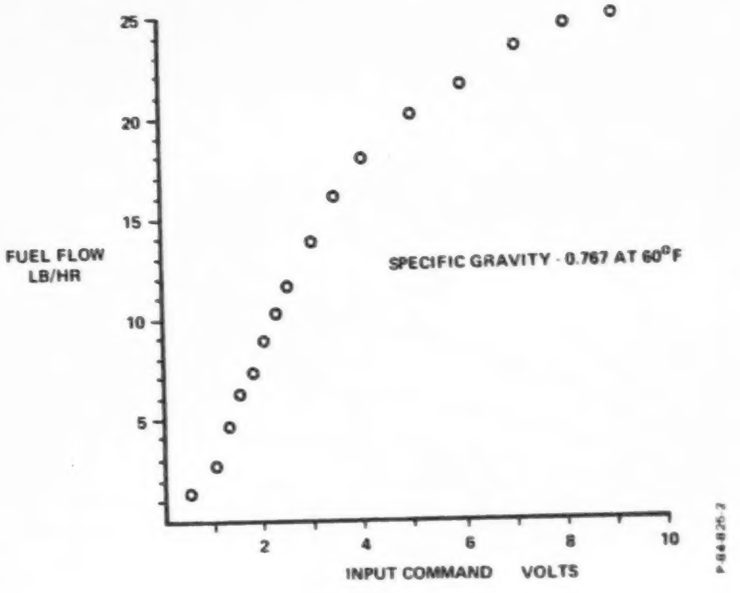

Figure 3-26 - Fuel-Control Trim-Servo Calibration

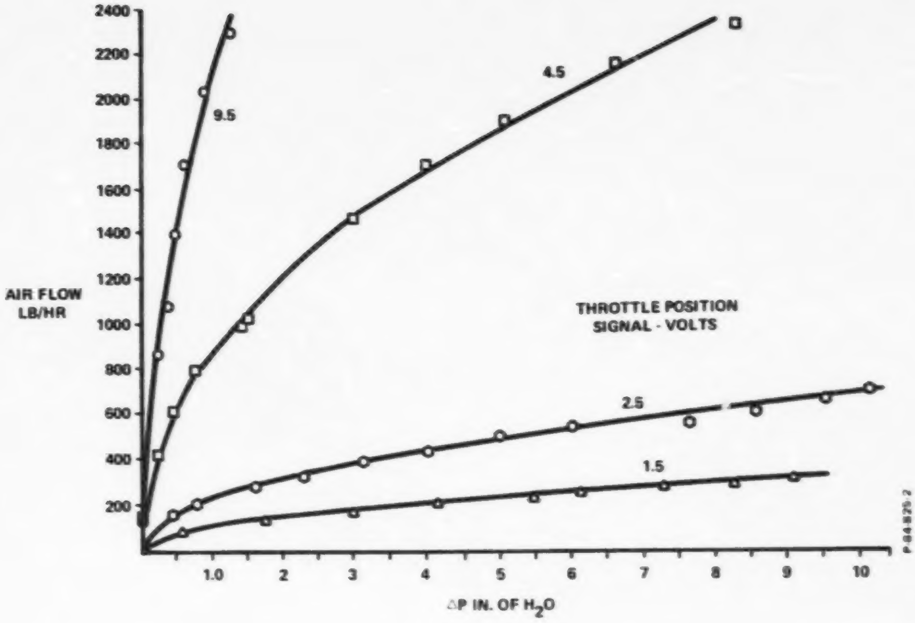

Figure 3-27 - High Flow Calibration of Throttle-Plate Valve

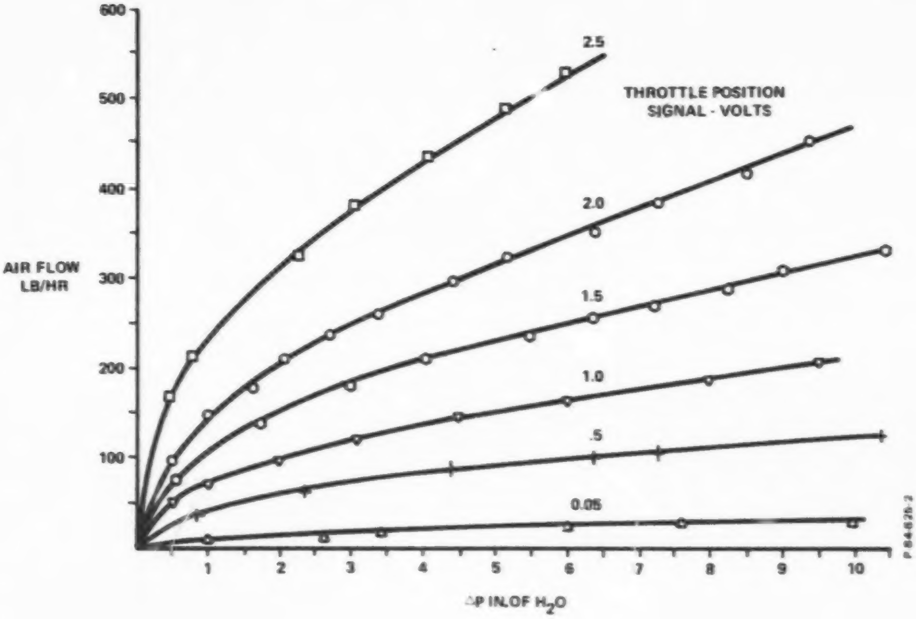

Figure 3-28 - Low Flow Calibration of Throttle Valve

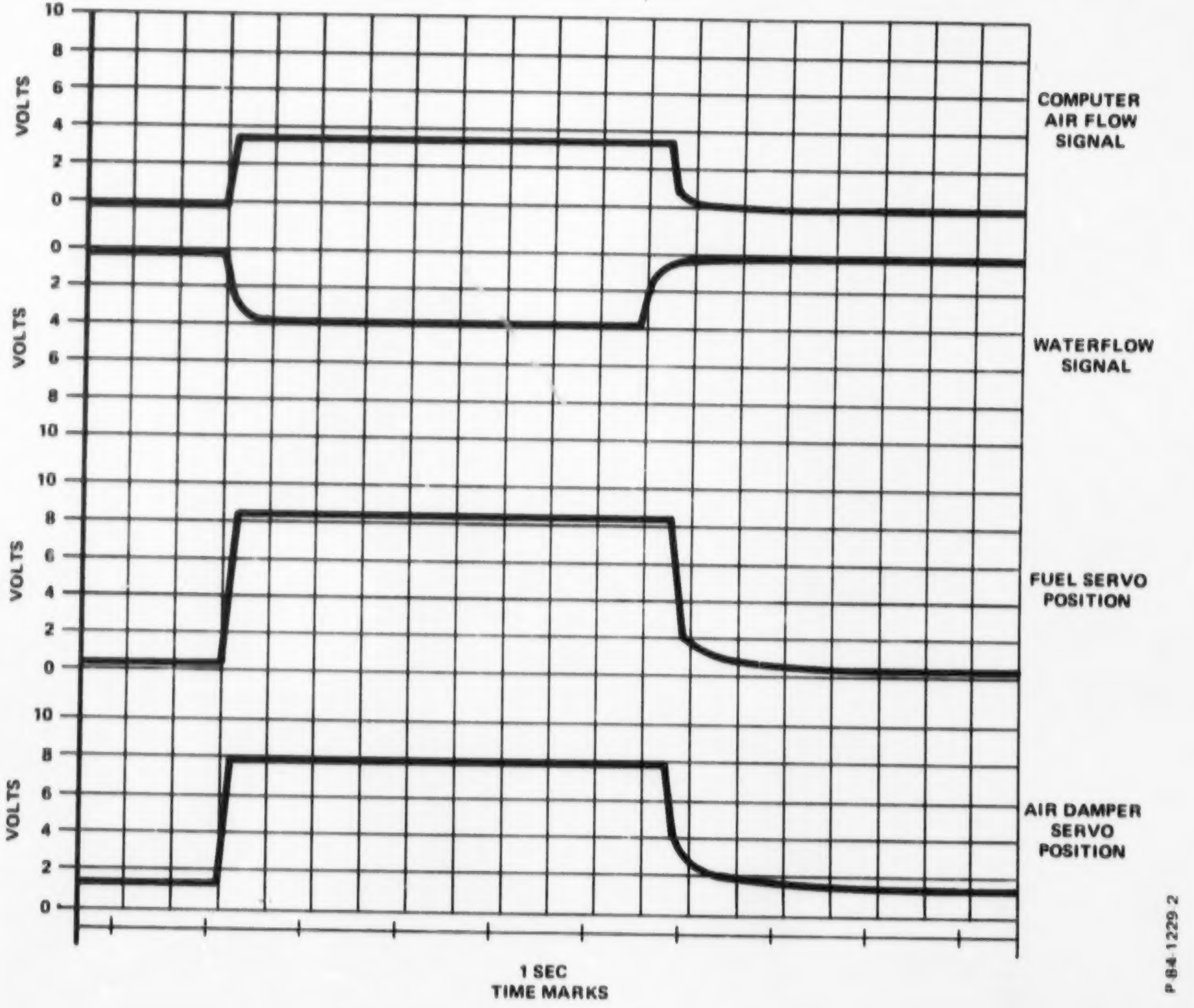

Figure 3-29 - Fuel Control and Air Damper Servo Dynamic Response

SECTION 4

ANALYTICAL CONTROL EVALUATION

The purpose of the analytical evaluation of closed-loop control concepts was the optimization of the operating controls for the steam-car vapor generator. Because no suitable analytical description of this class of monotube steam generators was available at the start of the program, a new analytical model of the boiler, to fit the time and cost frame of the project, had to be developed. It was assumed from the onset of the program that simplifying assumptions would be an essential part of this model to keep computer costs within reasonable limits. For this reason, a continued examination and comparison of analytical results with experimental data available from the ongoing burner-boiler experimental program conducted by SES on their model SES-4 vapor generator system was made a planned and significant part of the analytical program.

The analytical model of the entire power plant system was defined in terms of physical interfaces. This definition of individual components and subsystems offered maximum flexibility for evaluation of various control concepts including new evolutionary concepts that were not a part of the original planning. The model was designed to handle all significant nonlinearities in order to allow evaluations of both the system and the control concepts during large transients which are believed to be a significant part of automotive power plant operations.

The most significant part of the analytical model development was that of the vapor generator. A three-section model, characterizing fluid properties in the preheat, boiling, and superheat range, was selected. In each of these sections, heat transfer calculations from gas to metal and from metal to fluid were independently calculated on the basis of selected average temperatures. A simplified form of the equation of state was used in each of the three sections. In order to reduce inaccuracies resulting from shifts of the phase transition points, instead of using the fluid temperatures, the enthalpy of the fluid was used as the output variable denoting the thermal energy of the fluid at the outlet of each of the sections. In order to maintain a computer model offering simple and fast computations, both the expander and also engine-driven auxiliaries, such as the combustion blower, were described in terms of partial derivatives. The use of this model required some initial processing of the data for the main simulation. The amount of time and cost for this processing was minimal and repaid itself in the form of a greatly simplified system model.

The initial hybrid-computer simulation results were compared with the open-loop static and dynamic experimental results developed at SES for the quarter-scale model SES-4 vapor generator. This model was then used to develop the predicted closed-loop temperature control for this vapor generator. The resulting closed-loop experimental program is reported in further detail in Section 5. After the model was thus experimentally verified, two prototype vapor generators, the cross counterflow and also the counterflow vapor generator models, were simulated on the hybrid computer. The use of engine-driven auxiliaries operated through a variable-speed drive was also evaluated in this portion of the program.

4.1 HYBRID-COMPUTER MODEL

In the following, the final form of the hybrid-computer model is presented. This model, when used without the expander, and with simple models for the auxiliaries, such as the simplified gas-generator model described at the very beginning, was used during the initial parts of the program dealing with the model SES-4 vapor generator system. The model presented in the following thus describes the hybrid simulation including the steam generator, the expander, vehicle load and also the control concept based on the use of expander-driven auxiliaries through a variable-ratio drive. Following the general description of the model, results of the SES-4 unit are given. The section is then concluded by hybrid-computer results based on the prototype SES-5 design.

4.1.1 Steam-Generator Analytical Model

All variables used in the analytical models are described in alphabetical order by symbol in the nomenclature at the end of this section. In addition to a short description of the variable itself, the specific units required to be compatible with the other variables are listed. Also, when applicable, typical values of the variables describing the SES-4 and SES-5 steam generators are entered. It must be noted, however, that these values describe current design and some of the coefficients may be revised to reflect the final SES design.

Burner

The simplest burner model assumes constant air-fuel ratio:

$$W_g = W_F \, (1 + A/F) \tag{1}$$

$$T_g = \text{constant} \tag{2}$$

Gas residence time in the burner and boiler is assumed to be negligible compared to the boiler dynamics. In a later section, gas flow prediction using engine-driven auxiliaries will be described.

Feedwater Pump

Feed-pump characteristics may be elaborated during the program. For the present, description of a controllable, variable-displacement pump may be sufficient. A more detailed analytical description of an engine-driven, fixed-displacement pump is given in a later section.

$$T_{fei} = \text{constant} \tag{3}$$

$$W_{fei} = D_p \, \rho_{fei} \, \dot{\theta}_p \tag{4}$$

Other feedwater supply system characteristics such as the condenser model can be readily incorporated in the analysis.

Steam Generator

The steam-generator model is subdivided into three fixed-length sections: economizer, boiler and superheater sections. The information flow diagram representing the steam generator is shown in Figure 4-1.

Economizer

The flow through the economizer is nearly incompressible.

$$W_{fei} = W_{feo} = W_{fe} \tag{5}$$

The energy equation for the economizer section yields

$$m_{fe} \frac{d}{dt} h_e = Q_{mfe} + W_{fe} \left(h_{ei} - h_{eo} \right) \tag{6}$$

Pressure losses through the length of the economizer section are described in terms of viscous flow losses.

$$P_{ei} - P_{eo} = \frac{2 \, f_e \, L_e}{\rho_{fei} \, g_o \, D_e} \left(\frac{W_e^2}{A_{xe}^2} \right) \tag{7}$$

The metal-to-fluid heat flow is a function of the temperature difference between the metal and the fluid.

$$Q_{mfe} = u_{fe} \, A_{Hfe} \left(T_{me} - T_{fe} \right) \tag{8}$$

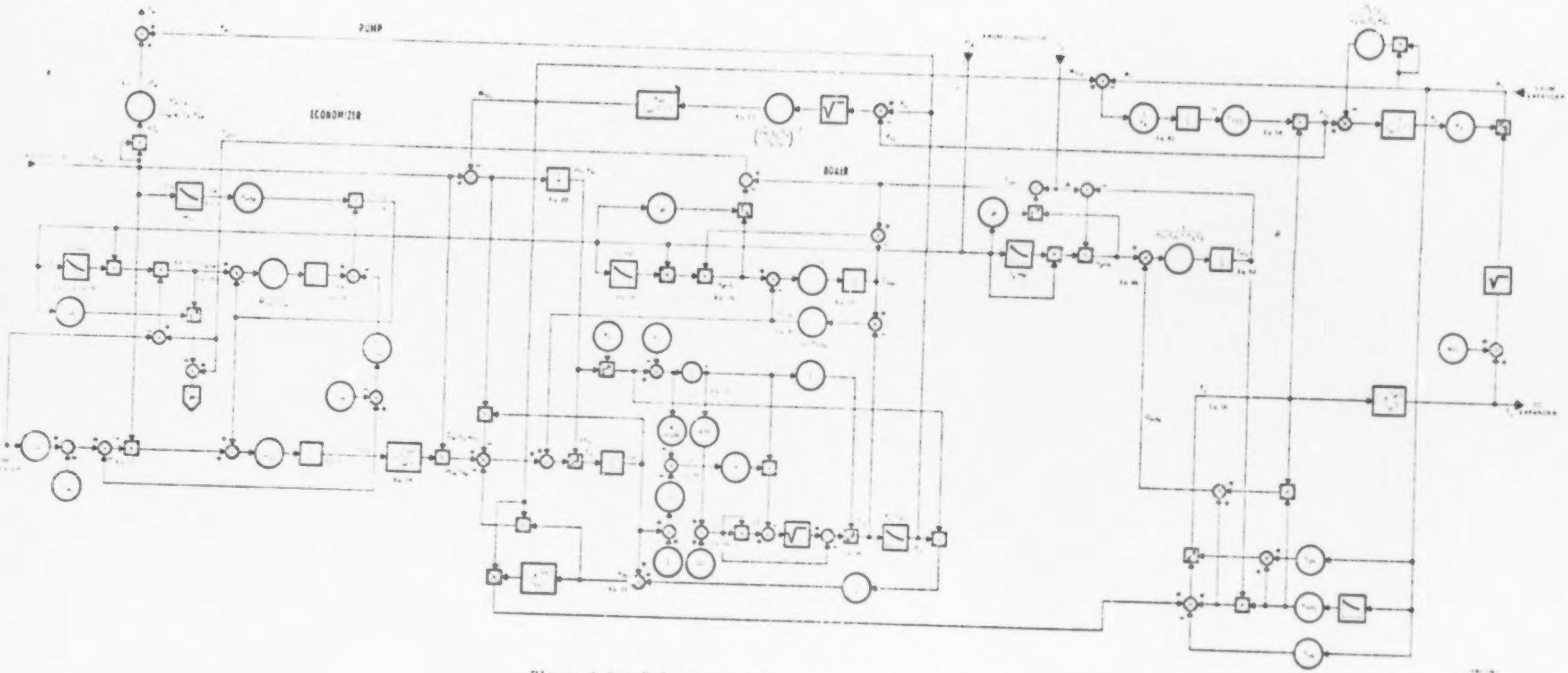
PUMP
ECONOMIZER
BOILER

Figure 4-1 - Information Flow Diagram - Steam Generator

See following pages
for greater detail.

Preceding page blank

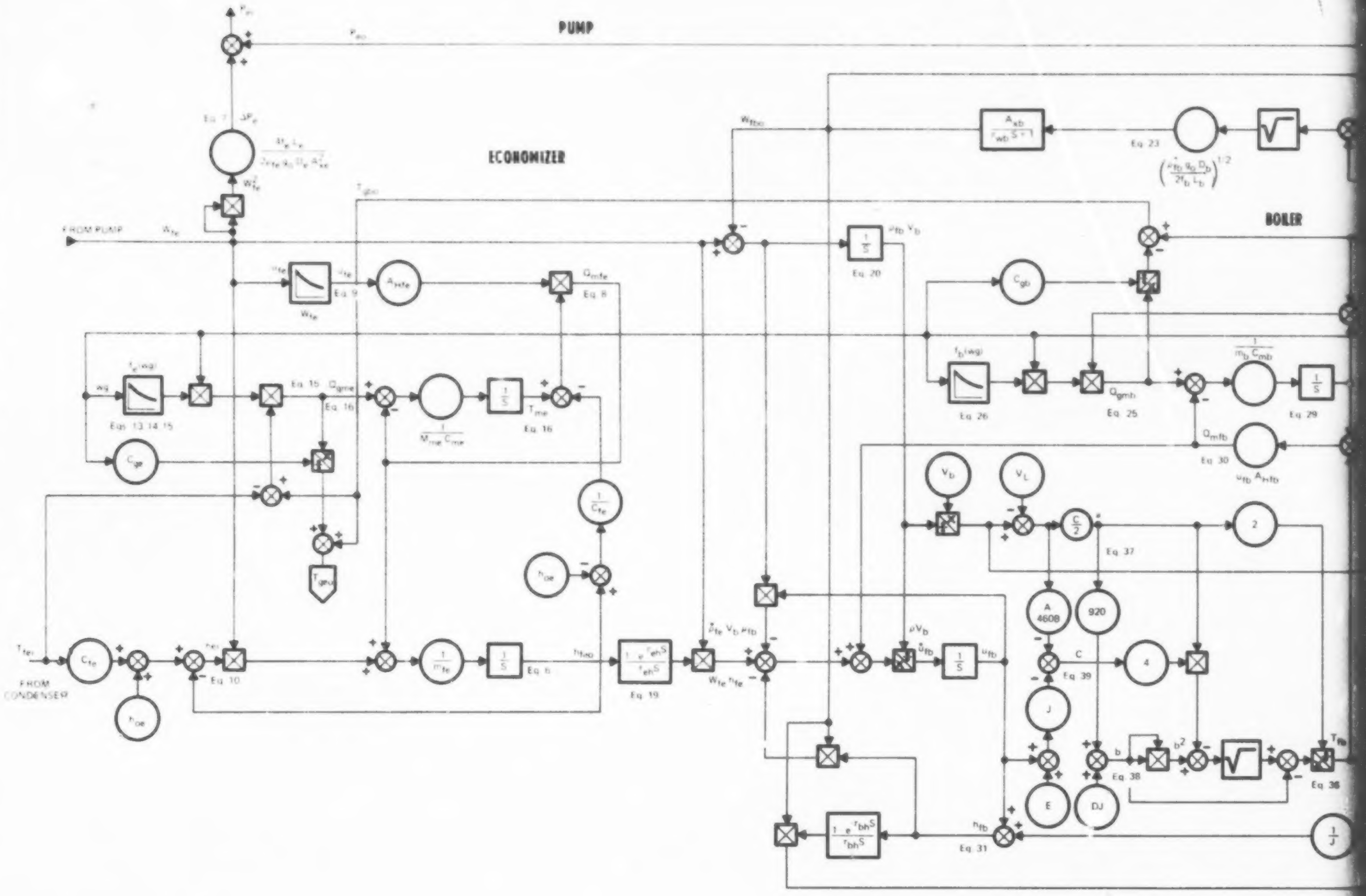
PUMP
ECONOMIZER
BOILER
FROM PUMP
FROM CONDENSER
Eq. 7
Eq. 8
Eq. 9
Eq. 10
Eqs. 13, 14, 15
Eq. 15
Eq. 16
Eq. 19
Eq. 20
Eq. 23
Eq. 25
Eq. 26
Eq. 29
Eq. 30
Eq. 31
Eq. 37
Eq. 38
Eq. 39
4608
920
2
4
J
E
DJ

Figure 4-1 - Information Flow Diagram -

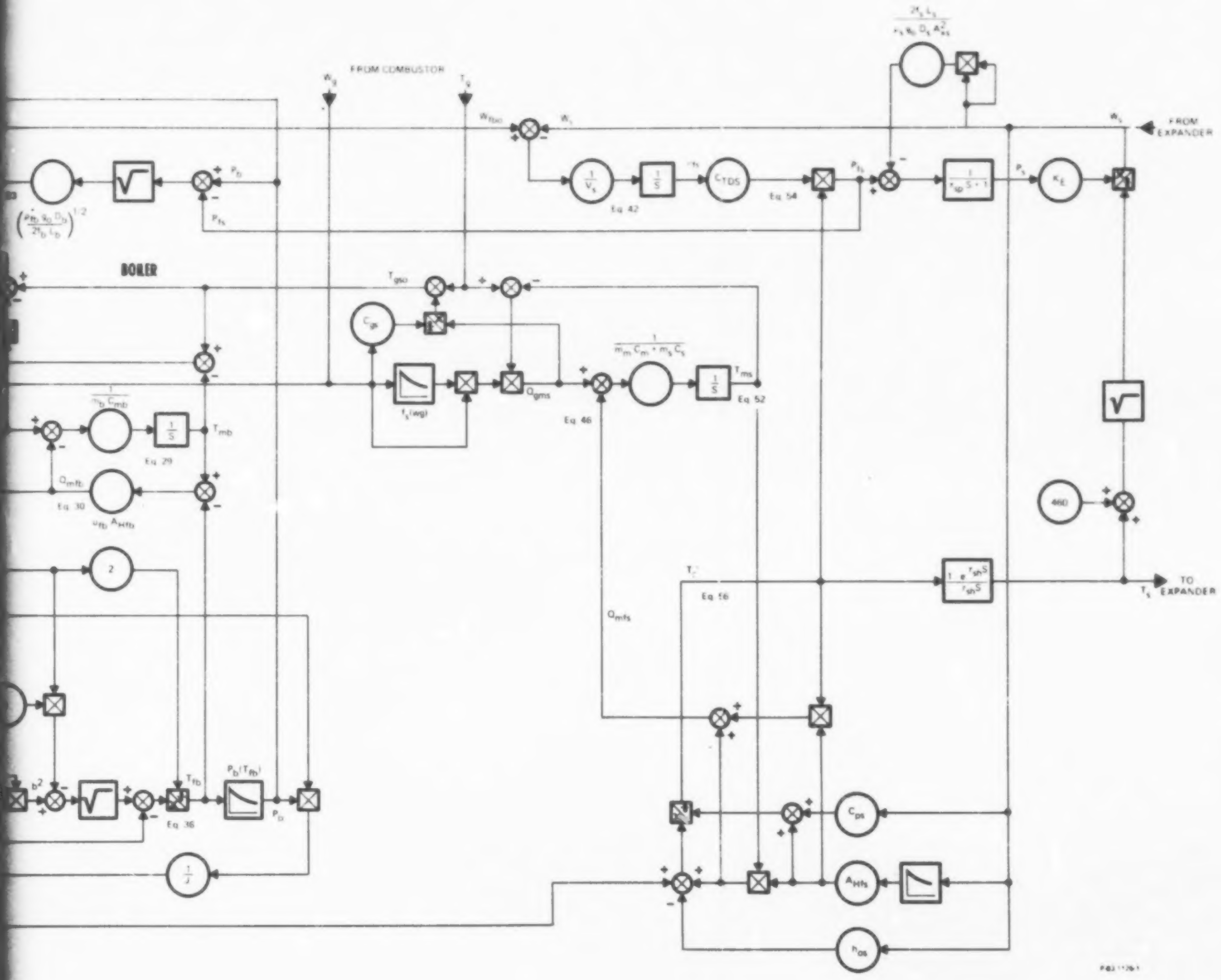
FROM COMBUSTOR
W_g
T_g
W_fbo
W_s
FROM EXPANDER
BOILER
T_gso
C_ps
f_s(wg)
Q_gms
T_ms
Eq 42
Eq 54
Eq 46
Eq 52
Eq 29
Eq 30
Eq 36
Eq 56
Q_mfb
Q_mfs
T_mb
T_fb
P_b(T_fb)
P_b
P_fs
P_s
C_TDS
K_E
460
2
T_s'
T_s
TO EXPANDER
A_Hfs
h_os
P83 1126-1

Flow Diagram - Steam Generator

B

Preceding page blank

$$u_{fe} = C_{1e} \left(\frac{W_{fe}}{W_{fe}^*} \right)^{0.8} \qquad (9)$$

The enthalpy of the inlet fluid is a nearly linear function of the fluid inlet temperature.

$$h_{ei} = C_{fe}\, T_{fei} + h_{oe} \qquad (10)$$

The gas-to-metal heat flow is based on the temperature difference between the inlet gas to the economizer and the metal temperature at the inlet. However, for the particular heat exchanger design, the inlet metal temperature is sufficiently close to the fluid temperature at the inlet so that the fluid inlet temperature, T_{fei}, may be substituted for the heat transfer calculations.

$$T_{gei} - T_{geo} = \varepsilon_e\, (T_{gei} - T_{fei}) = \Delta T_{ge} \qquad (11)$$

$$\varepsilon_e = \frac{1 - e^{\frac{-N\,T\,U_e}{2}}}{1 - \frac{1}{2}\, e^{\frac{-N\,T\,U_e}{2}}} \qquad (12)$$

$$N\,T\,U_e = 1.1 \left(\frac{W_g}{W_{ge}^*} \right)^{-0.4} \qquad (13)$$

For computation simplicity the above coefficients may be included into a single function describing the gas-to-metal heat conductance, f_e.

$$f_e\, (W_g) = C_{ge}\, \varepsilon_e \qquad (14)$$

$$W_g\, \Delta h_{ge} = C_{ge}\, (\Delta T_{ge})\, W_g = Q_{gme} = f_e\, (W_g)\, (T_{gei} - T_{fei})\, W_g \qquad (15)$$

Metal temperature calculation is based on the difference between the heat flow from gas to metal and metal to fluid in addition to the mass and specific heat of the metal.

Preceding page blank

$$m_{me} C_{me} \frac{d}{dt} T_{me} = Q_{gme} - Q_{mfe} \tag{16}$$

The fluid output temperature at the economizer outlet can be computed on the basis of outlet enthalpy.

$$T_{feo} = \frac{1}{C_{fe}} (h_{eo} - h_{oe}) \tag{17}$$

The model presented so far accomodates static heat transfer characteristics and primary dynamics of the economizer section. The distributed nature of the thermal wave is not sufficiently represented for the economizer section. An approximate description of the thermal wave propagation time was used.

$$\tau_{eh} = \frac{m_{me} C_{me}}{W_{fe} C_{fe}} \tag{18}$$

Equation (18) indicates that the thermal-wave propagation time is a function of fluid flow. During the anticipated operating range of the steam generator, the changes in thermal-wave propagation must be accommodated. The most convenient inclusion of the variable thermal wave propagation time was through the use of the digital portion of the hybrid computer. The outlet enthalpy of the economizer was thus delayed prior to use in the boiler energy equation.

$$h^*_{feo} = h_{feo} \frac{1 - e^{-\tau_{eh} s}}{\tau_{eh} s} \tag{19}$$

Inclusion of the thermal wave propagation time reuses the metal thermal inertia in addition to the account for m_{me} in equation (16). The repeated use of the metal mass resulted in a slower computer result than the experimental results indicated. Reducing the metal mass to 0.75 m_{me} in equation (16) offered a simple empirical solution to this problem. The same correction was also made in the boiler and superheater sections of the steam generator model.

Boiling Section

Conservation of mass in the fixed length representation of the boiling section may be stated as

$$V_b \frac{d}{dt} \rho_{fb} = W_{feo} - W_{fbo} \tag{20}$$

The energy equation for the boiling section defines the time rate of change of average fluid density and internal energy for the volume of the boiling section.

$$V_b \frac{d}{dt} (\rho_{fb} U_{fb}) = Q_{mfb} + W_{feo} h^*_{feo} - W_{fbo} h_{fbo} = V_b (\dot{\rho}_{fb} U_{fb} + \dot{U}_{fb} \rho_{fb}) \tag{21}$$

Thus the rate of change of internal energy in the boiling section is defined as

$$\dot{U}_{fb} = \frac{1}{\rho_{fb} V_b} (Q_{mfb} + W_{feo} h^*_{feo} - W_{fbo} h_{fbo} - \dot{\rho}_{fb} U_{fb} V_b) \tag{22}$$

The outlet flow from the boiler section is based on viscous flow calculations for the given length of pipe and the square root of pressure difference between boiler and superheater pressures.

$$W_{fbo} = \left(\frac{\rho^*_{fb} g_o D_b}{2 f_b L_b} \right)^{1/2} A_{xb} \sqrt{P_b - P_s} \tag{23}$$

The gas-to-metal heat flow rate is again defined as a function of temperature difference between the gas inlet temperature and the boiler metal temperature.

$$Q_{gmb} = W_g C_{gb} (T_{gbi} - T_{mb}) \left(1 - e^{-NTU_b \left(\frac{W_g}{W^*_{gb}} \right)^{-0.4}} \right) \tag{24}$$

This equation, again, may be simplified by representing the heat conductance by a single function, f_b.

$$Q_{gmb} = f_b (W_g) (T_{gbi} - T_{mb}) W_g \tag{25}$$

With f_b defined as follows:

$$f_b (W_g) = C_{gb} (1 - e^{-x}) \tag{26}$$

$$x = NTU_b \left(\frac{W_g}{W^*_{gb}} \right)^{-0.4} \tag{27}$$

The outlet gas temperature is calculated from the inlet gas temperature and the temperature loss due to the heat flow to the metal.

$$T_{gbo} = T_{gbi} - \frac{Q_{gmb}}{W_g \; C_{gb}} \tag{28}$$

The metal temperature time derivative is again related to the gas-to-metal and metal-to-fluid heat flow rate and the mass and specific heat of the metal of this section.

$$m_{mb} \; C_{mb} \frac{d}{dt} T_{mb} = Q_{gmb} - Q_{mfb} \tag{29}$$

Heat flow rate from the metal to the fluid in the boiler section is again governed by the temperature difference between the metal and the fluid of the boiler. The coefficient of heat conductance in this particular section may be assumed as a large constant, U_{fb}, due to the high heat transfer rate in the boiling section.

$$Q_{mfb} = u_{fb} \; A_{Hfb} (T_{mb} - T_{fb}) \tag{30}$$

The basic definition of enthalpy, as the sum of internal energy plus a PV term, is used to calculate enthalpy of the boiler fluid.

$$h_{fb} = U_{fb} + \frac{P_b}{J\ \rho_{fb}} \qquad (31)$$

The definition of specific volume and specific density of the fluid is used to calculate the specific volume of the fluid.

$$V_{fb} = 1/\rho_{fb} \qquad (32)$$

A simplified set of equations are used to describe the equation of state for the fluid in the boiling section. This simplified relationship was found to be satisfactory to evaluate the control characteristics of the boiler. Comparison with the experimental data obtained from the SES-4 boiler was used to establish the validity of this assumption. The pressure in the boiler is described as a function of the temperature.

$$P_b = A + B\ T_{fb} + \frac{C}{2}\ T_{fb}^{\ 2} \qquad (33)$$

On the basis of the Clapeyron relationship for the boiler

$$T_{fb} \frac{dP_b}{dT_{fb}} = \frac{(U_{fb} - U_L)\ J}{V_{fb} - V_L} + P_b \qquad (34)$$

The internal energy of the liquid is a linear function of temperature.

$$U_L = D\ T_{fb} - E \qquad (35)$$

Using the Clapeyron relationship, the temperature of the fluid in the boiler can be defined as follows:

$$T_{fb} = (-b + \sqrt{b^2 - 4\ ac})/2a \qquad (36)$$

$$a = \frac{C}{2} (V_{fb} - V_L) \tag{37}$$

$$b = 460C (V_{fb} - V_L) + DJ = 920a + DJ \tag{38}$$

$$c = -J (E + U_{fb}) - (V_{fb} - V_L) (A - 460 B) \tag{39}$$

The thermal wave propagation time is again included to improve the model's representation of the distributed thermal capacitance of the monotube steam generator.

$$\tau_{bh} = \frac{m_{mb} C_{mb}}{W_{fbo} C_{fb}} \tag{40}$$

The resulting thermal delay is again represented as a variable distributed delay time as a function of boiler outlet flow

$$h^*_{fbo} = h_{fbo} \frac{1 - e^{-\tau_{bh} s}}{\tau_{bh} s} \tag{41}$$

Superheater

Conservation of mass defines the change of density in the fixed section.

$$V_s \frac{d}{dt} \rho_{fs} = W_{fbo} - W_s \tag{42}$$

The energy equation in the superheater may be simplified because the contribution through the rate of change, ρU, is negligible.

$$V_s \frac{d}{dt} (\rho_{fs} U_{fs}) = Q_{mfs} + W_{fbo} h^*_{fbo} - W_s h_s = 0 \tag{43}$$

The superheater pressure loss is again calculated on the basis of viscous flow and the time constant relating the volumetric charge time of the superheater volume.

$$P_s = P_{fs} - \frac{2\ f_s\ L_s\ W_s^2}{\rho_s^*\ g_o\ D_s\ A_{xs}^2} \left(\frac{1}{\tau_{sp}\ S + 1} \right) \tag{44}$$

The heat flow rate from the gas to metal again is defined as a function of gas flow rate and temperature difference between the superheater inlet gas temperature and metal temperature.

$$Q_{gms} = W_g\ C_{gs}\ (T_{gsi} - T_{gso}) = W_g\ C_{gs}\ \varepsilon_s\ (T_{gsi} - T_{ms}) \tag{45}$$

This equation may be simplified as follows

$$Q_{gms} = f_s\ (W_g)\ (T_{gsi} - T_{ms})\ W_g \tag{46}$$

f_s flow function in the superheater section is defined as follows

$$f_s\ (W_g) = C_{gs}\ \varepsilon_s \tag{47}$$

$$\varepsilon_s = 0.7 \left(1 - 0.96\ e^{-NTU_s \left(\frac{W_g}{W^*_{gs}} \right)^{-0.4}} \right) \tag{48}$$

Outlet temperature of the gas leaving the superheater is calculated on the basis of heat loss.

$$T_{gso} = T_{gsi} - \frac{Q_{gms}}{W_g\ C_{gs}} \tag{49}$$

The metal-to-fluid heat flow rate is again calculated on the basis of temperature difference.

$$Q_{mfs} = u_{fs} A_{Hfs} (T_{ms} - T_s) \quad (50)$$

The heat transfer rate is defined as a 0.8 power of the fluid flow rate.

$$u_{fs} = C_{1s} \left(\frac{W_s}{W_s^*} \right)^{0.8} \quad (51)$$

The metal temperature is calculated on the basis of heat flow difference between the gas-to-metal and metal-to-fluid flow rates. In addition, a term describing the equivalent mass of the superheater steam and its specific heat is included in the equation. This correction, however, is small.

$$(m_{fs} C_{ps} + m_{ms} C_{ms}) \frac{d}{dt} T_{ms} = Q_{gms} - Q_{mfs} \quad (52)$$

The temperature of the working fluid in the superheater section is calculated on the basis of enthalpy and specific heat.

$$T_s = (h_s - h_{os})/C_{ps} \quad (53)$$

The superheater pressure is a nearly linear function of the superheater temperature.

$$P_{fs} = C_{Tps} T_{fs} \rho_{fs} \quad (54)$$

The superheater outlet temperature, T_s', may be solved by substituting the expression for Q_{mfs}, from equation (50), and the enthalpy, h_s, from equation (53), into the energy balance equation (43).

$$\left(C_{ps}\ T_s' + h_{os} - h^*_{fbo}\right)\ W_s = W_{fbo}\ h^*_{fbo} + U_{fs}\ A_{Hfs}\ \left(T_{ms} - T_s\right) \qquad (55)$$

Equation (55) now may be solved for the superheater outlet temperature

$$T_s' = \frac{1}{U_{fs}\ A_{Hfs} + W_s\ C_{ps}}\ \left(U_{fs}\ A_{Hfs}\ T_{ms} + W_{fbo}\ h^*_{fbo} - W_s\ h_{os}\right) \qquad (56)$$

The simplified equation of state used in the superheater section allows the insertion of the distributed effect of thermal propagation in series with the superheater outlet temperature.

$$T_s = T_s' \frac{1 - e^{-\tau_{sh} s}}{\tau_{sh} s} \qquad (57)$$

and similar to the economizer and boiler section

$$\tau_{sh} = \frac{m_{ms}\ C_{ms}}{W_s\ C_{fs}} \qquad (58)$$

The steam flow is normally calculated in the expander section, however, a choked-flow, variable-area throttle is used to compare steam generator operation independent from the expander to verify the analytical model with the experimental results. For the comparison, steam flow was calculated on the basis of throttle admittance and steam conditions.

$$W_s = K_E \frac{P_s}{\sqrt{T_s + 460}} \qquad (59)$$

4.1.2 Expander and Vehicle

For the purposes of control system evaluation, the expander may be characterized as a continuous flow device. This assumption is valid because the steam-generator dynamics are much slower than the individual flow pulsations that result from the opening and the closing of the intake valves on the four-cylinder expander. Engine output torque and mass flow consumed by an expansion device can be accurately predicted using the analytical model described by Taplin and Gregory*. Using this analytical model, the engine torque output, in general, is defined by a torque coefficient D_{MT}.

$$\text{Torque} = D_{MT} \times P \qquad (60)$$

The volumetric flow consumed by the expander is defined by a volumetric coefficient D_{MV}.

$$\text{Weight flow} = D_{MV}\ \rho_s\ \dot{\theta} \qquad (61)$$

In a variable-admission device, such as the SES expander, both D_{MT} and D_{MV} are also a function of the admission angle and engine RPM. It will be shown that a modified continuous flow model will simply and accurately describe the SES expander on the basis of available flow and indicated horsepower data. The information diagram for the combined expander and load dynamics and engine auxiliaries is shown in Figure 4-2.

The engine torque, T_E, is calculated on the basis of the D_{MT} model,

$$T_E = D_{MT} \left(P_s - P_c\right) \qquad (62)$$

where D_{MT} is a function of both engine speed and valve position

$$D_{MT} = D_{MT}\ (\alpha)\ D\ (\dot{\theta}) \qquad (63)$$

Similarly, the flow demand of the engine is computed

$$W = D_{MV} \frac{P_s}{\left(T_s + 460\right)\ R_s} \dot{\theta} \qquad (64)$$

---

*L. B. Taplin and A. J. Gregory, "Rotary Pneumatic Actuators," Control Engineering, December 1963.

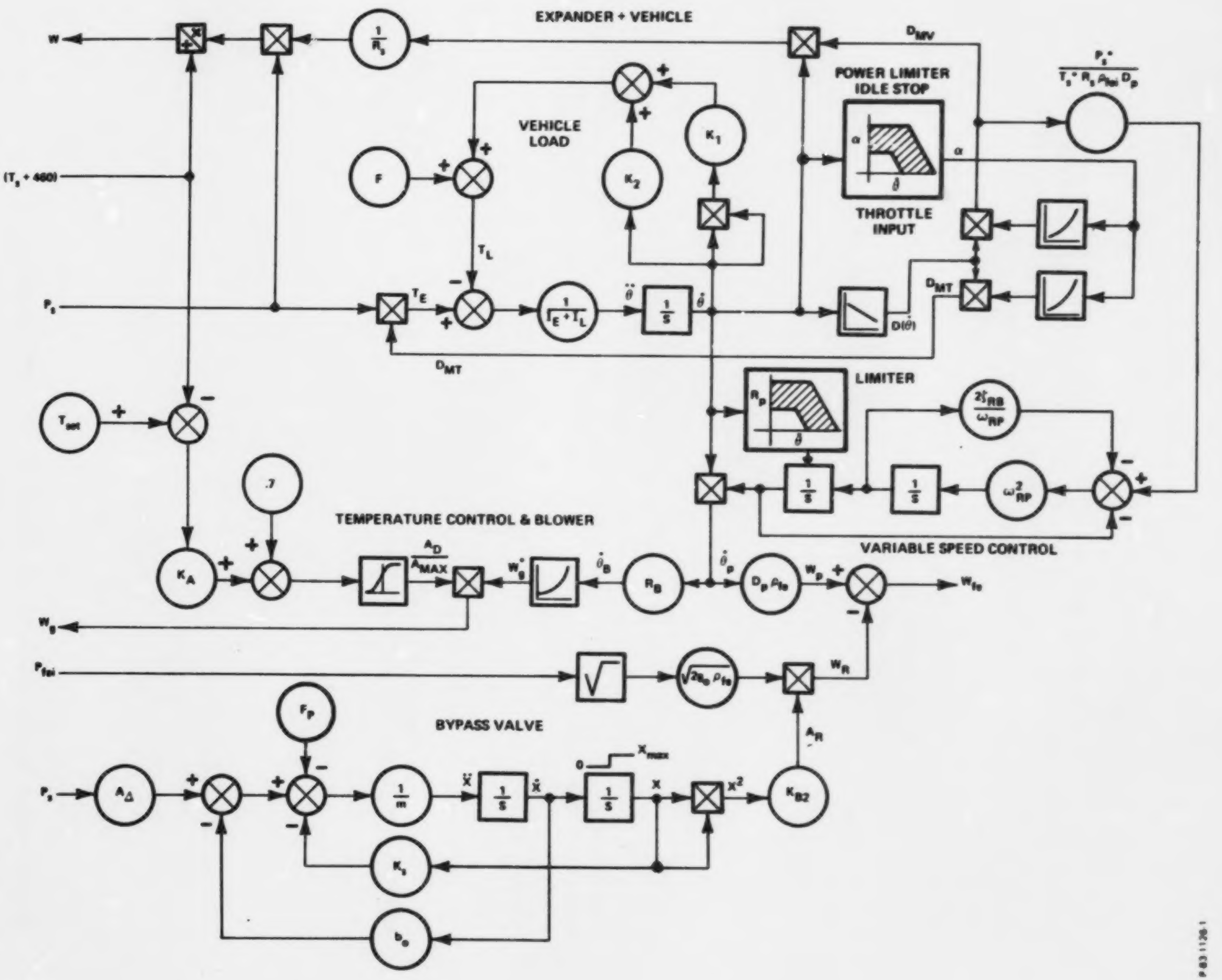
EXPANDER + VEHICLE
W
$(T_s + 460)$
P_s
$\frac{1}{R_s}$
D_{MV}
POWER LIMITER
IDLE STOP
THROTTLE
INPUT
α
θ
$\frac{P_s^*}{T_s^* R_s \rho_{fai} D_p}$
VEHICLE
LOAD
F
K_1
K_2
T_L
T_E
$\frac{1}{I_E + I_L}$
$\ddot{\theta}$
$\frac{1}{s}$
$\dot{\theta}$
$D(\dot{\theta})$
D_{MT}
T_{set}
LIMITER
R_p
$\frac{2\zeta_{RB}}{\omega_{RP}}$
ω_{RP}^2
VARIABLE SPEED CONTROL
.7
TEMPERATURE CONTROL & BLOWER
K_A
$\frac{A_D}{A_{MAX}}$
W_g^*
$\dot{\theta}_B$
R_B
$\dot{\theta}_p$
$D_p \rho_{fe}$
W_p
W_{fe}
W_g
P_{fai}
$\sqrt{2g_o \rho_{fe}}$
W_R
A_R
BYPASS VALVE
F_P
A_Δ
$\frac{1}{m}$
$\ddot{X}$
$\dot{X}$
X
X_{max}
0
X^2
K_{B2}
K_s
b_o
P83 1126 1

Figure 4-2 - Expander Vehicle and Auxiliaries - Information Flow Diagram

$$D_{MV} = D_{MV}\ (\alpha)\ D\ (\dot{\theta}) \tag{65}$$

The vehicle and accessory loads can be combined into a single second-order representation for preliminary control studies. A more elaborate model may be included at a future time as engine performance and auxiliary loads become more firmly defined.

$$T_L = K_1\ \ddot{\theta} + K_2\ \dot{\theta} + F \tag{66}$$

The vehicle and engine inertia are combined as reflected at the engine RPM.

$$\ddot{\theta} = \left(T_E - T_L\right) \frac{1}{I_E + I_L} \tag{67}$$

4.1.3 Auxiliaries and Flow Control Mechanization

The present simulation describes an engine-driven, combustion-air blower and feedpump operated through a variable-ratio transmission. The transmission ratio is controlled by a central controller. A simple, steam-pressure-operated, bypass valve is used to implement a closed-loop pressure control. The closed-loop temperature controller actuates an air damper valve to regulate the combustion gas flow. The separate fuel controller is assumed to maintain fuel-air ratio, and is not included in the present system simulation.

The pump speed is controlled by the variable-speed transmission, represented as a second-order system.

$$\dot{\theta}_P = R_P\ \dot{\theta} \tag{68}$$

$$R_P = \frac{D_{MV}\ \dfrac{P_s^*}{R_s\ T_s^*\ \rho_{fei}\ D_p}}{\dfrac{S^2}{\omega_{RP}^2} + \dfrac{2\phi_{ms}}{\omega_{RP}} S + 1} \tag{69}$$

Blower speed is directly proportional to the pump speed.

$$\dot{\theta}_B = R_B \dot{\theta}_p \tag{70}$$

Pump delivery is defined by pump speed

$$W_p = D_p \rho_{fei} \dot{\theta}_p \tag{71}$$

Steam-generator inlet flow is defined by conservation of mass

$$W_{fe} = W_p - W_R \tag{72}$$

The bypass flow is calculated on the basis of pressure, fluid properties and valve opening

$$W_R = A_R \sqrt{2 g_o \rho_{fei} P_{fei}} \tag{73}$$

The valve opening is defined by the geometry of the design and instantaneous valve position

$$A_R = K_{B2} x^2 \tag{74}$$

Valve position calculation is based on the solution of a second-order system

$$\ddot{X} = \frac{\Delta F}{m_{Dp}} \tag{75}$$

$$\Delta F = P_s A_\Delta - b_o \dot{x} - F_p - K_s x \tag{76}$$

The combustion gas flow is defined by blower speed, blower characteristics and air damper opening

$$W_g = W_g^* \left(\dot{\theta}_B\right) \frac{A_D}{A_{D\,max}} \tag{77}$$

where damper opening is controlled by the temperature error signal. The rapid time response of the damper system may be neglected for the initial evaluation.

$$\frac{A_D}{A_{max}} = K_A \left(T_{set} - T_s\right) \tag{78}$$

4.1.4 SES-5 Steam Generator and Expander Representation

In order to increase the solution speed of the overall hybrid-system simulation, several relationships were precomputed and the results of these calculations were used to program analog, nonlinear, function generators. In the following, results of these calculations, as applicable to the SES-5 steam generator, are presented.

The gas-to-metal heat transfer equations (15), (25), and (46) require the functions f_e (W_g), f_b (W_g), and f_s (W_g) as a function of gas flow, W_g. Figure 4-3 presents this information in the form currently used in the hybrid simulation.

The metal-to-fluid heat transfer coefficients, U_e and U_s, as a function of fluid flow, W_F, are shown in Figure 4-4. The functional relations are used in equations (3) and (50) to calculate metal-to-fluid heat flow in the economizer and the superheater. In the boiling section, a fixed heat transfer coefficient is used.

The expander D_{MT} and D_{MV} curves were generated on the basis of SES data describing expander performance at various operating conditions defined by valve angles from 20 to 70 degrees at 500, 1500, and 2500 RPM engine speeds. The 500 RPM data set was used to represent both the torque and volumetric coefficient maps of the engine in the hybrid simulation. Results are given in Figure 4-5. The speed correction curve, as used in equations (63) and (65), is given in Figure 4-6.

Engine losses, auxiliary power consumption, and vehicle load were combined into a single load-torque curve for the initial studies. A second-order least squares fit to this curve was used to represent loads to the engine in high or low gear. The following expressions were used to calculate total load.

Load = Engine Friction + Auxiliaries + Road Load

Auxiliaries = Feedpump + Burner + Fan Power

The engine friction horsepower load was defined as

$$\text{Engine Friction} = 4 \times 4.41 \times 10^{-5}\ \text{RPM}\ (11 + \text{RPM}/100)$$

Auxiliary horsepower loads were defined as

$$\text{Feedpump Power} = 2.42 \times 10^{-3} \times \text{Steam Flow (lb/hr)}$$

```
HX-GAS     11:01    02/04/72  FRI.

wGB=          .537

INPUT 4 SCALE FACTORS
? 1,1,1,1
   WG       FGE*WG      FGB*WG      FGS*WG      FGE      FGB      FGS
 .0268     .007181     .008533     .002461     .2674    .3178    .0917
 .0537     .013483     .016417     .004070     .2511    .3057    .0758
 .0805     .019303     .023775     .005461     .2396    .2952    .0678
 .1074     .024787     .030727     .006732     .2308    .2861    .0627
 .1342     .030014     .037353     .007923     .2236    .2782    .0590
 .1611     .035034     .043707     .009056     .2175    .2713    .0562
 .1879     .039880     .049830     .010142     .2122    .2651    .0540
 .2148     .044576     .055753     .011191     .2075    .2596    .0521
 .2416     .049142     .061500     .012210     .2034    .2545    .0505
 .2685     .053593     .067090     .013203     .1996    .2499    .0492
 .2953     .057939     .072540     .014173     .1962    .2456    .0480
 .3222     .062192     .077862     .015123     .1930    .2417    .0469
 .3490     .066359     .083067     .016056     .1901    .2380    .0460
 .3759     .070448     .088165     .016973     .1874    .2345    .0452
 .4027     .074464     .093164     .017876     .1849    .2313    .0444
 .4296     .078412     .098071     .018766     .1825    .2283    .0437
 .4564     .082297     .102893     .019644     .1803    .2254    .0430
 .4833     .086124     .107634     .020511     .1782    .2227    .0424
 .5101     .089895     .112301     .021368     .1762    .2201    .0419
 .5370     .093614 .   .116896     .022216     .1743    .2177    .0414
 .5638     .097283     .121425     .023055     .1725    .2154    .0409
 .5907     .100906     .125891     .023887     .1708    .2131    .0404
 .6175     .104485     .130297     .024710     .1692    .2110    .0400
 .6444     .108021     .134646     .025527     .1676    .2089    .0396
 .6712     .111518     .138940     .026336     .1661    .2070    .0392
 .6981     .114975     .143183     .027140     .1647    .2051    .0389
 .7249     .118396     .147377     .027937     .1633    .2033    .0385
 .7518     .121782     .151523     .028728     .1620    .2015    .0382
 .7786     .125134     .155624     .029515     .1607    .1999    .0379
 .8055     .128454     .159682     .030296     .1595    .1982    .0376
   CGE       CGB        CGS
 .2932     .326300     .355400
```

Figure 4-3 - Heat Transfer Coefficients for Gas-to-Metal Side

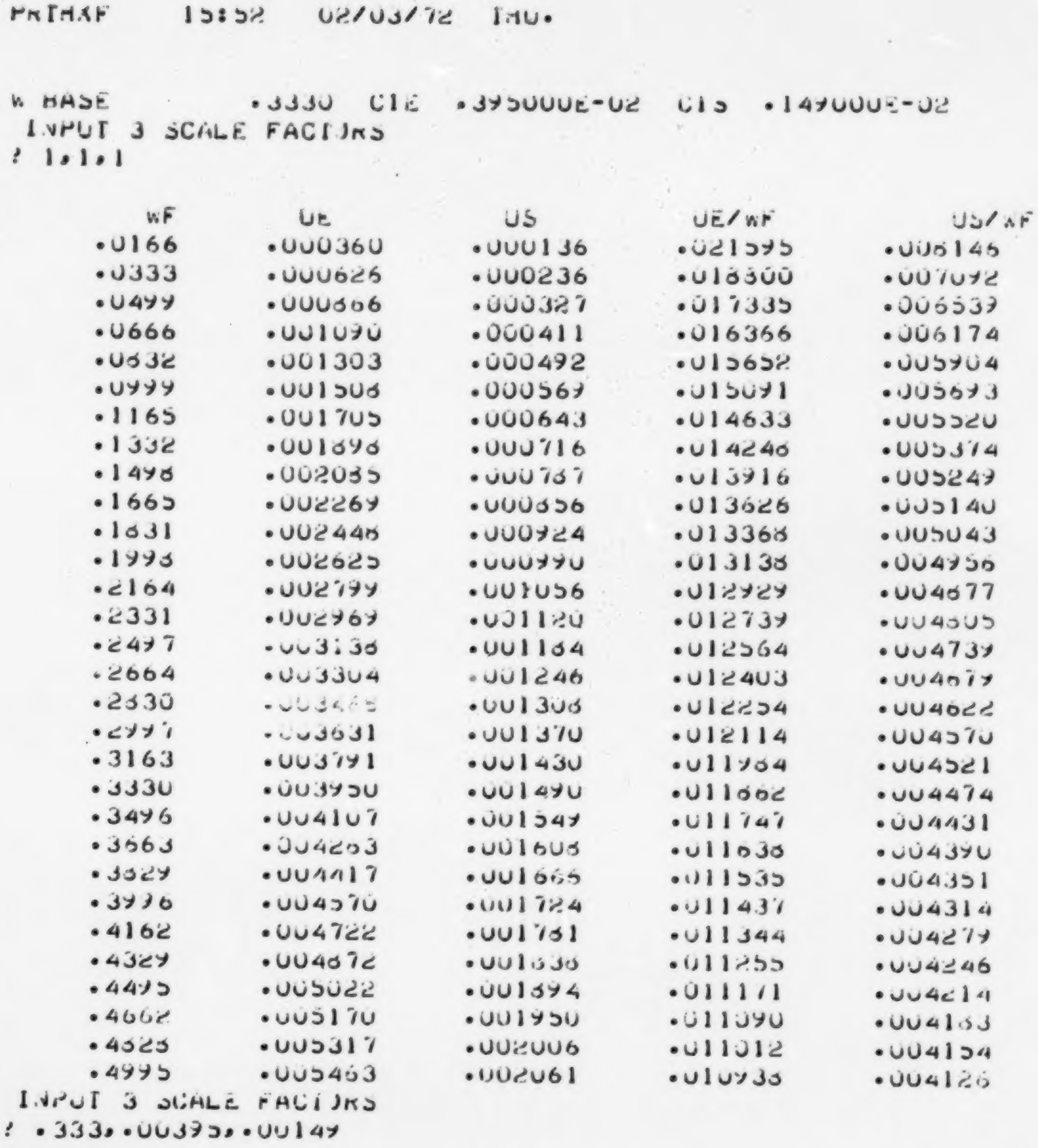

```
PRTHXF     15:52   02/03/72  THU.


W BASE          .3330  C1E  .395000E-02  C1S  .149000E-02
 INPUT 3 SCALE FACTORS
? 1,1,1

            WF           UE            US            UE/WF          US/WF
          .0166       .000360       .000136        .021595        .008146
          .0333       .000626       .000236        .018800        .007092
          .0499       .000866       .000327        .017335        .006539
          .0666       .001090       .000411        .016366        .006174
          .0832       .001303       .000492        .015652        .005904
          .0999       .001508       .000569        .015091        .005693
          .1165       .001705       .000643        .014633        .005520
          .1332       .001898       .000716        .014246        .005374
          .1498       .002085       .000787        .013916        .005249
          .1665       .002269       .000856        .013626        .005140
          .1831       .002448       .000924        .013368        .005043
          .1998       .002625       .000990        .013138        .004956
          .2164       .002799       .001056        .012929        .004877
          .2331       .002969       .001120        .012739        .004805
          .2497       .003138       .001184        .012564        .004739
          .2664       .003304       .001246        .012403        .004679
          .2830       .003465       .001308        .012254        .004622
          .2997       .003631       .001370        .012114        .004570
          .3163       .003791       .001430        .011984        .004521
          .3330       .003950       .001490        .011862        .004474
          .3496       .004107       .001549        .011747        .004431
          .3663       .004263       .001608        .011638        .004390
          .3829       .004417       .001665        .011535        .004351
          .3996       .004570       .001724        .011437        .004314
          .4162       .004722       .001781        .011344        .004279
          .4329       .004872       .001838        .011255        .004246
          .4495       .005022       .001894        .011171        .004214
          .4662       .005170       .001950        .011090        .004183
          .4828       .005317       .002006        .011012        .004154
          .4995       .005463       .002061        .010933        .004126
 INPUT 3 SCALE FACTORS
? .333,.00395,.00149
```

Figure 4-4 - Heat Transfer Coefficients for Metal-to-Fluid Side

```
PRTEXP     9:39   11/15/71  MØN.


INPUT FØR 500,1500,2500,XX,XX, RPMS
5 DMT FACTØRS
? 6.7878,5.8597,5.1582,1,1
5 DMV FACTØRS
? 3.3607,2.8611,2.4893,1,1
TS      1460.00    RS      1027.20    PS      1000.00    DP      1000.00
HPF         30.7493  TF     63025.358  DMVF       238.6666

 α   500.00      RPM
LEAD    IHP     T        DMT      DMV       WS    DMT/DMV NDMT  NDMV
 20.     10.13   1277.  1.2769    .5170   .0180   2.47 .1881  .1538
 30.     21.63   2726.  2.7265  1.1663   .0407   2.34 .4017  .3470
 40.     36.86   4646.  4.6462  2.1291   .0743   2.18 .6845  .6335
 50.     53.85   6788.  6.7878  3.3607   .1173   2.02 1.0000 1.0000
 60.     70.83   8928.  8.9282  4.8079   .1679   1.86 1.3153 1.4306
 70.     86.90  10954.  10.9538 6.4231    .2242   1.71 1.6137 1.9112

 α  1500.00      RPM
LEAD    IHP     T        DMT      DMV       WS    DMT/DMV NDMT  NDMV
 20.     24.91   1047.  1.0466    .4281   .0448   2.45 .1786  .1496
 30.     54.37   2284.  2.2845    .9765   .1023   2.34 .3899  .3413
 40.     94.21   3958.  3.9584  1.8235   .1910   2.17 .6755  .6373
 45.    116.25   4884.  4.8845  2.2988   .2408   2.12 .8336  .8035
 50.    139.46   5860.  5.8597  2.8611   .2997   2.05 1.0000 1.0000
 60.    185.09   7777.  7.7769  4.0969   .4291   1.90 1.3272 1.4319

 α  2500.00      RPM
LEAD    IHP     T        DMT      DMV       WS    DMT/DMV NDMT  NDMV
 20.     35.46    894.   .8940    .3655   .0638   2.45 .1733  .1468
 30.     78.51   1979.  1.9792    .8421   .1470   2.35 .3837  .3383
 35.    105.95   2671.  2.6710  1.1681   .2039   2.29 .5178  .4693
 40.    137.16   3458.  3.4578  1.5596   .2722   2.22 .6704  .6265
 45.    169.78   4280.  4.2802  1.9948   .3482   2.15 .8298  .8013
 50.    204.61   5158.  5.1582  2.4893   .4346   2.07 1.0000 1.0000
```

Figure 4-5 Expander D_{MT} and D_{MV} Calculation Results

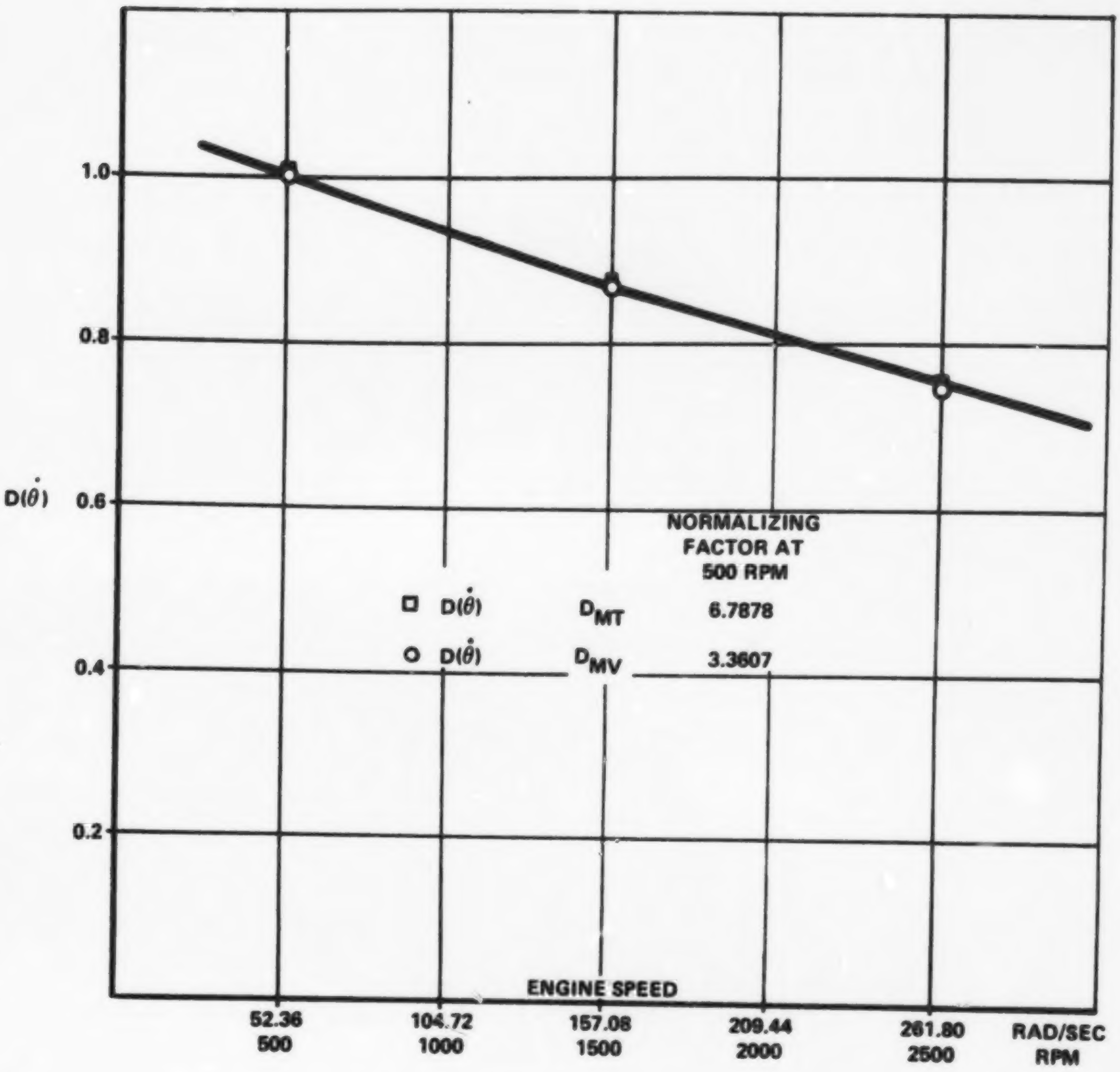

Figure 4-6 - Engine Speed Correction Curves

$$\text{Burner Power} = 0.68 + 1.18\,(\text{Steam flow (lb/hr)}/1290)^3$$

$$\text{Fan Power} = 2.084 - 5.94 \times 10^{-3}\ \text{RPM} + 4.36 \times 10^{-6}\ \text{RPM}^2$$

Road Load was defined in terms of grade and vehicle speed for a 4600 pound vehicle.

$$\text{Road Load} = V\ (\text{ft/sec})/550 \quad \Big[4600/\sqrt{1 + G^2\ (\%)}\ (G(\%)\ (G(\%) + 0.0154)$$

$$+\ 9.91 \times 10^{-2}\ V(\text{ft/sec}) + 1.44 \times 10^{-2}\ V^2\ (\text{ft/sec})\Big]$$

The conversion factors between engine RPM and vehicle speed were given as

RPM = 20.50 V(ft/sec)	Second Gear
RPM = 13.16 V(ft/sec)	High Gear

The composite load-torque is shown as a function of engine speed for the high-gear condition in Figure 4-7, and for the second-gear engagement in Figure 4-8. Least squares fits of both curves are also shown in Figures 4-9 and 4-10 respectively. The least squares fit representing the high-gear conditions is used at the present for the load torque in the current control system studies as required by equation (66).

Both the maximum and minimum values of the cut-off valve were limited as a function of engine speed as shown in Figure 4-11. The maximum limit is required to hold the expander steam consumption within the maximum output of the steam generator. The minimum setting provides the idle-speed regulation for the expander.

The vehicle ratio-drive settings are similarly controlled to avoid over-speeding of the auxiliaries and are shown in Figure 4-12. Maximum available ratio from the drive is 0.9 and the minimum is 0.3 for the design currently considered.

4.2 EXPERIMENTAL VERIFICATION FOR MODEL SES-4

During the early part of the program, experimental transient results of the SES Model 4 steam generator were compared with hybrid-computer results. The comparison indicates that the hybrid-computer program represents the dynamic characteristics of the SES vapor generator. The accuracy of the hybrid-computer simulation is satisfactory to serve as a design tool in the program. Figure 4-13 presents steam-generator, open-loop characteristics at 100 percent and 40 percent steady-state levels.

Figure 4-14 compares step-transient results in gas flow at the 0.0819 lb/sec fluid flow rate. The gas step change was adjusted to produce an outlet temperature change from 800°F to 1040°F to duplicate the experimental conditions designated as SES-1. During the change, both in the experimental and in the simulation, the throttle was manually controlled

```
GRADE         .00    PERCENT                   13.16

        MPH         RPM          RAD/SEC       WST
      FRICTION     ROAD          FAN     FEED P       BURNER      TOTAL      TORQUE

          5         96.51        10.106        .00706
        .20          .96        1.55        .05         .68        3.45     2251.418

         10        193.01        20.212        .00882
        .44         2.01        1.10        .06         .68        4.29     1401.833

         15        289.52        30.318        .01109
        .71         3.20         .73        .08         .68        5.40     1175.712

         20        386.03        40.425        .01404
       1.01         4.60         .44        .11         .68        6.83     1115.775

         25        482.53        50.531        .01778
       1.35         6.26         .23        .14         .68        8.66     1130.568

         30        579.04        60.637        .02245
       1.72         8.25         .10        .18         .68       10.93     1189.606

         35        675.55        70.743        .02818
       2.12        10.64         .06        .23         .68       13.72     1279.830

         40        772.05        80.849        .03509
       2.55        13.47         .09        .29         .68       17.09     1394.710

         45        868.56        90.955        .04333
       3.02        16.83         .21        .36         .68       21.09     1530.628

         50        965.07       101.061        .05301
       3.52        20.76         .41        .44         .68       25.81     1685.416

         55       1061.57       111.168        .06427
       4.05        25.33         .68        .54         .69       31.29     1857.705

         60       1158.08       121.274        .07724
       4.61        30.61        1.04        .65         .69       37.61     2046.805

         65       1254.59       131.380        .09205
       5.21        36.65        1.49        .78         .70       44.82     2251.504

         70       1351.09       141.486        .10884
       5.84        43.51        2.01        .92         .71       52.99     2471.998

         75       1447.60       151.592        .12774
       6.51        51.27        2.61       1.08         .73       62.19     2707.518

         80       1544.11       161.698        .14887
       7.20        59.97        3.30       1.26         .76       72.49     2953.802

         85       1640.61       171.804        .17242
       7.93        69.69        4.06       1.46         .80       83.95     3224.572

         90       1737.12       181.911        .19848
       8.69        80.48        4.91       1.68         .87       96.63     3506.030

         95       1833.63       192.017        .22721
       9.49        92.41        5.84       1.93         .96      110.62     3802.349

        100       1930.13       202.123        .25877
      10.32       105.54        6.84       2.20        1.09      125.99     4113.974

WST       907.2911       122.703
```

Figure 4-7 - Expander Load Tabulation - High Gear

```
GRADE          .00    PERCENT                    20.5

        MPH         RPM         RAD/SEC       WST
      FRICTION      ROAD        FAN     FEED P      BURNER     TOTAL      TORQUE

          5        150.33        15.743       .00680
        .33          .96       1.29        .05          .68       3.31     1368.059

         10        300.67        31.486       .00860
        .74         2.01        .69        .06          .68       4.19      877.375

         15        451.00        47.229       .01127
       1.23         3.20        .29        .08          .68       5.49      766.924

         20        601.33        62.971       .01496
       1.80         4.60        .09        .12          .68       7.28      763.155

         25        751.67        78.714       .01978
       2.46         6.26        .08        .16          .68       9.63      807.361

         30        902.00        94.457       .02587
       3.19         8.25        .27        .21          .68      12.59      879.974

         35       1052.33       110.200       .03336
       4.00        10.64        .65        .27          .68      16.24      972.610

         40       1202.67       125.943       .04237
       4.89        13.47       1.24        .35          .68      20.63     1031.035

         45       1353.00       141.686       .05305
       5.85        16.83       2.02        .44          .68      25.83     1203.075

         50       1503.33       157.429       .06551
       6.90        20.76       3.00        .55          .69      31.90     1337.207

         55       1653.67       173.171       .07990
       8.03        25.33       4.17        .67          .69      38.90     1482.607

         60       1804.00       188.914       .09634
       9.24        30.61       5.54        .81          .70      46.91     1638.715

         65       1954.33       204.657       .11497
      10.53        36.65       7.11        .97          .72      55.98     1805.165

         70       2104.67       220.400       .13592
      11.90        43.51       8.88       1.15          .74      66.16     1981.721

         75       2255.00       236.143       .15934
      13.35        51.27      10.84       1.35          .78      77.58     2160.248

         80       2405.33       251.886       .18536
      14.87        59.97      13.00       1.57          .83      90.25     2364.683

         85       2555.67       267.629       .21413
      16.48        69.69      15.35       1.82          .91     104.25     2571.033

         90       2706.00       283.371       .24581
      18.17        80.48      17.91       2.09         1.03     119.68     2787.367

         95       2856.33       299.114       .28054
      19.93        92.41      20.66       2.38         1.20     136.59     3013.816

        100       3005.67       314.857       .31851
      21.78       105.54      23.60       2.70         1.44     155.07     3250.576

WST     1115.9786       150.9261
? 32.6
```

Figure 4-8 - Expander Load Tabulation - Second Gear

```
NEXT? 3
ORDER? 2
COEFF           VALUE

 0               1753.54
 1              -15.0552
 2               .136385

NEXT? 5
ORDER? 2

OBS X           OBS Y          CALC Y          DIFF

 10.1061         2251.42        1615.32         636.102
 20.2123         1401.83        1504.95        -103.12
 30.3184         1175.71        1422.45        -246.74
 40.4246         1115.78        1367.81        -252.034
 50.5307         1130.57        1341.03        -210.457
 60.6369         1189.61        1342.1         -152.494
 70.743          1279.83        1371.04        -91.2053
 80.8492         1394.71        1427.83        -33.1169
 90.9553         1530.63        1512.48         18.1453
 101.062         1685.42        1625.           60.4204
 111.168         1857.71        1765.37         92.3412
 121.274         2046.6         1933.6          113.007
 131.38          2251.5         2129.69         121.817
 141.486         2472.          2353.64         118.362
 151.592         2707.82        2605.45         102.373
 161.698         2958.8         2885.11         73.6899
 171.805         3224.87        3192.64         32.232
 181.911         3506.03        3528.03        -21.9947
 192.017         3802.35        3891.27        -88.9238
 202.123         4113.97        4282.38        -168.401

NEXT? 7
ENTER ORDER,STARTING VALUE,ENDING VALUE,INTERVAL? 2,0,300,20
   X               Y

 0               1753.54
 20              1506.99
 40              1369.54
 60              1341.21
 80              1421.99
 100             1611.87
 120             1910.86
 140             2318.96
 160             2836.17
 180             3462.48
 200             4197.91
 220             5042.44
 240             5996.08
 260             7058.83
 280             8230.69
 300             9511.66
```

Figure 4-9 - Second-Order Load Curve Fitting - High Gear

```
COEFF            VALUE

 0                1034.99
 1               -4.03255
 2                3.62334 E-2

NEXT? 5
ORDER? 2

OBS X            OBS Y            CALC Y           DIFF

 15.7429          1388.06          980.484          407.575
 31.4857          877.375          943.941         -66.5658
 47.2286          766.924          925.357         -158.433
 62.9714          763.155          924.733         -161.578
 78.7143          807.361          942.069         -134.708
 94.4571          879.974          977.365         -97.3915
 110.2            972.61           1030.62         -58.0111
 125.943          1081.08          1101.84         -20.753
 141.686          1203.08          1191.01          12.064
 157.429          1337.21          1298.15          39.0572
 173.171          1482.61          1423.25          59.3608
 188.914          1638.71          1566.3           72.4124
 204.657          1805.16          1727.32          77.8466
 220.4            1981.72          1906.29          75.4269
 236.143          2168.25          2103.23          65.0176
 251.886          2364.68          2318.13          46.5562
 267.629          2571.03          2550.98          20.0498
 283.371          2787.37          2801.8          -14.4313
 299.114          3013.82          3070.58         -56.7596
 314.857          3250.58          3357.31         -106.735

NEXT? 7
ENTER ORDER,STARTING VALUE,ENDING VALUE,INTERVAL? 2,0,300,20
   X                 Y

 0                1034.99
 20               968.831
 40               931.66
 60               923.476
 80               944.278
 100              994.067
 120              1072.84
 140              1180.61
 160              1317.36
 180              1483.09
 200              1677.82
 220              1901.52
 240              2154.22
 260              2435.9
 280              2746.57
 300              3086.23
```

Figure 4-10 - Second Order Load Curve Fitting - Second Gear

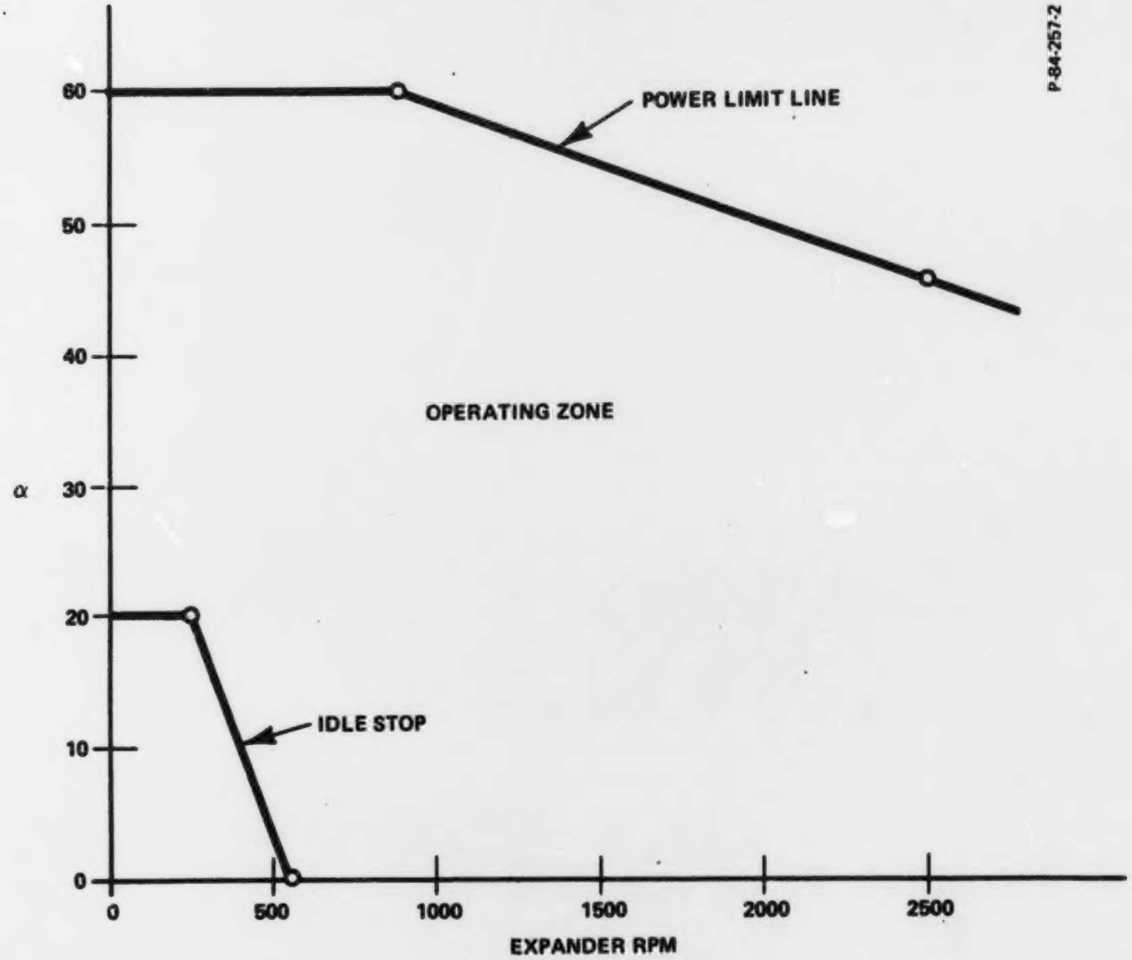

Figure 4-11 - Power Limiter and Idle Stop

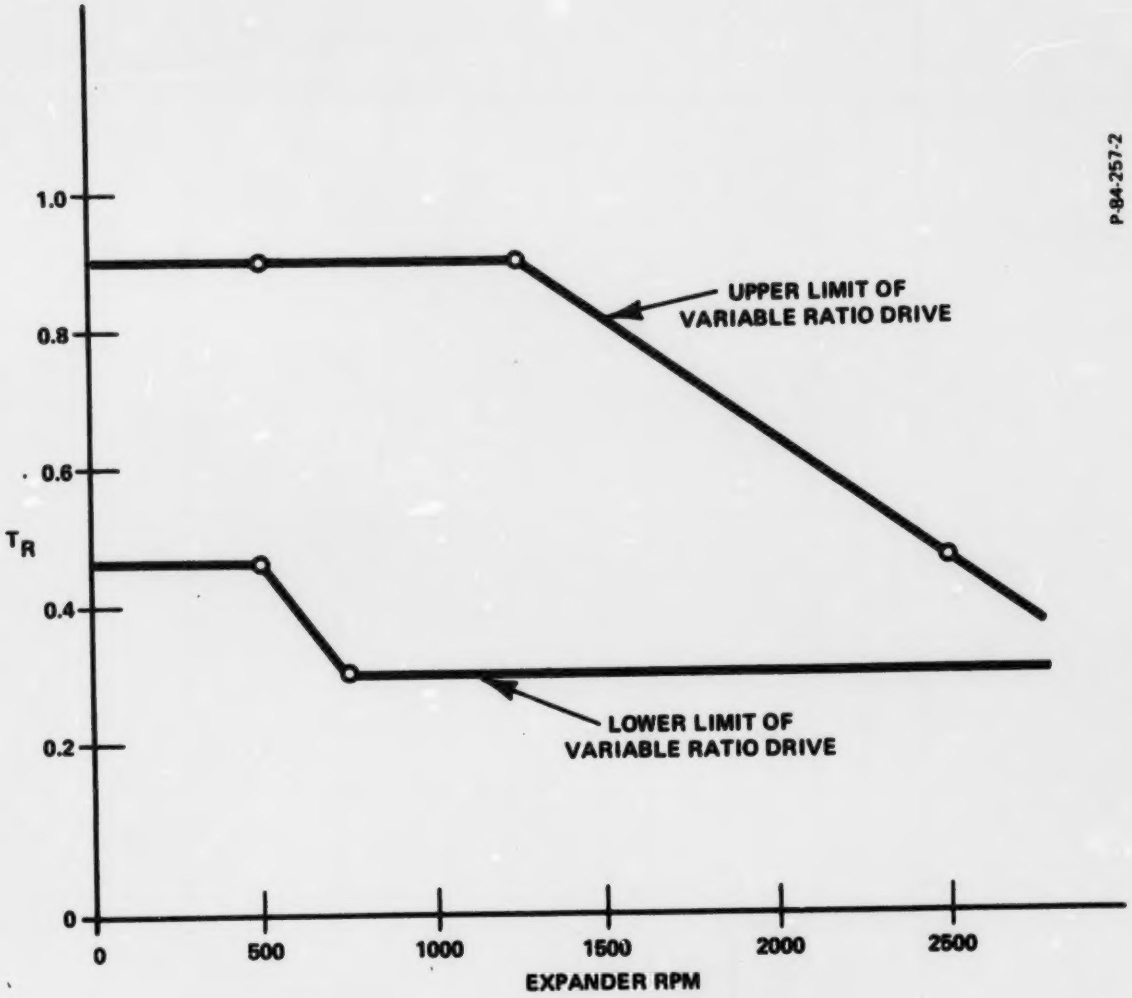

Figure 4-12 - Variable-Ratio Drive Limits

	FLOW LEVEL				
	100%		40%		
	SES EXPERIMENT	HYBRID RESULT	SES EXPERIMENT	HYBRID RESULT	UNITS
Super Heater Gas Outlet	1663	1764	1320	1426	°F
Economizer Gas Outlet	830	851	542	563	°F
Fluid Flow	0.211	0.211	0.0835	0.0835	lb/sec
Fluid Outlet	1000	1000	1000	1000	°F
Gas Inlet	3200	3200	3200	3200	°F
Gas Flow Rate	0.358	0.400	0.130	0.137	lb/sec

P-83-830-1

Figure 4-13 - Steam Generator Open Loop Characteristics

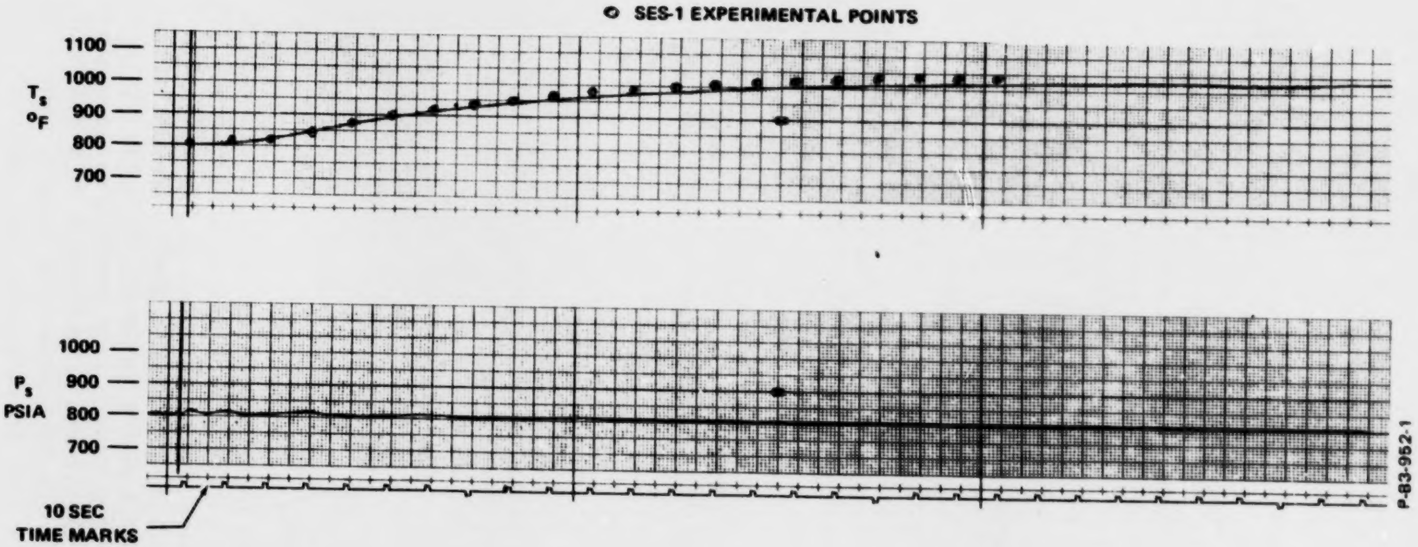

Figure 4-14 - Experimental and Hybrid Computer Transient Results Duplicating Experiment SES-1 at 0.0819 lb/sec Flow Rate

to maintain the steam outlet pressure at 800 psia. Figure 4-14 indicates excellent correlation between hybrid-computer results and the supporting SES experimental data points.

Figure 4-15 shows results of a similar transient at a higher steam flow rate of 0.1722 lb/sec. Again the throttle was manually controlled to maintain the steam-generator outlet pressure at 800 psia. Superposition of SES experimental data from the experiment designated as SES-9 again indicates good correlation. It must be noted that, during the experimental tests, a slight droop in the temperature occurred from the initial value. It is difficult to maintain a constant fluid-flow rate in the experimental test setup as pump delivery is sensitive to extraneous disturbances.

Figure 4-16 compares the hybrid-computer results with experimental data obtained in SES-10 experiment for a constant throttle setting. The agreement between the outlet steam temperature traces of the hybrid computer and the experiment is good. The system pressure for the step varied from 800 to 700 psia in the experiments and from 800 to about 745 psi in the computer prediction. This discrepancy between hybrid computer results and experimental data was resolved as a result of thermal drift in the steam flow control valve opening. In the experimental setup, thermal expansion of the valve body affects the valve opening and it is difficult to maintain a constant valve opening for temperature changes in excess of 200°F. Thermodynamic calculations verified the predictions of the hybrid computer, provided the throttle area was held constant.

The results of this direct comparison between experimental and analytical transient results verify the validity of the computer model. General shapes and physical relationships between temperature and pressure correspond closely between the analytical and experimental model.

One of the nonlinear characteristics of the steam generator is shown in Figure 4-17. In open-loop operation, the computed outlet steam temperature is shown as a function of combustion gas flow at 10, 30 and 100 percent fluid flow levels. The significant change in system gain over a 10 to 1 operating range is one of the contributing factors to the difficulty encountered when simple feedback control is applied to the control of the monotube steam generator.

4.3 PROTOTYPE RESULTS

The hybrid-computer model of the SES-5 steam generator was intergrated with the vehicle and engine-driven auxiliaries. The general schematic of the integrated system is shown in Figure 4-18. The information flow diagram includes a very simple predictive controller that sets the variable-speed auxiliary drive ratio on the basis of throttle position and engine speed. The pressure trim controller is a simple direct-acting bypass valve. The temperature trim control is a position-servo-actuated damper in series with the combustion air blower. The model was used to establish preliminary gain settings that provide stable operation in the

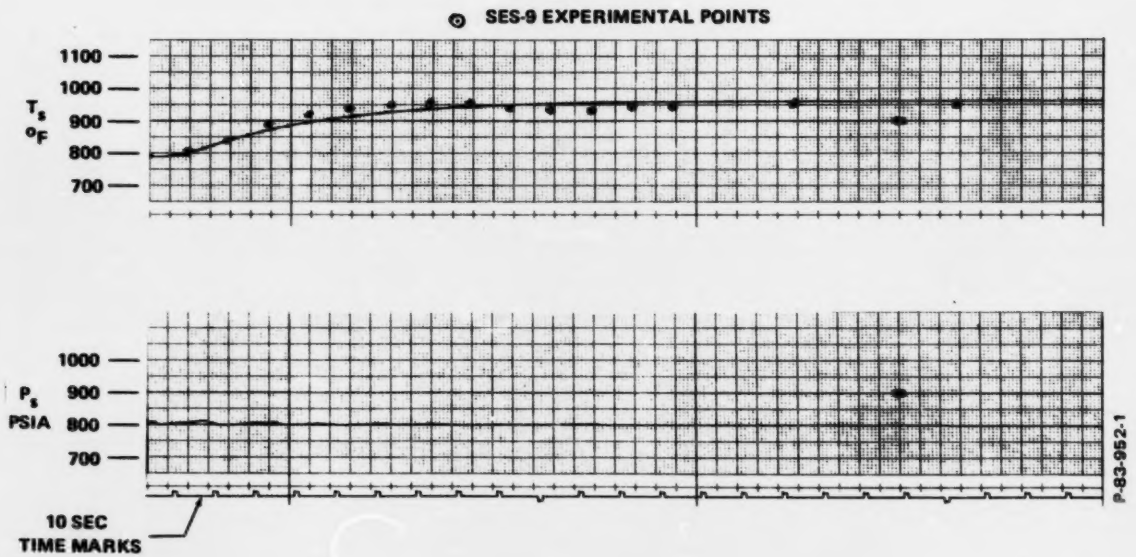

Figure 4-15 - Experimental and Hybrid Computer Transient Results Duplicating Experiment SES-9 at 0.1722 lb/sec Flow Rate

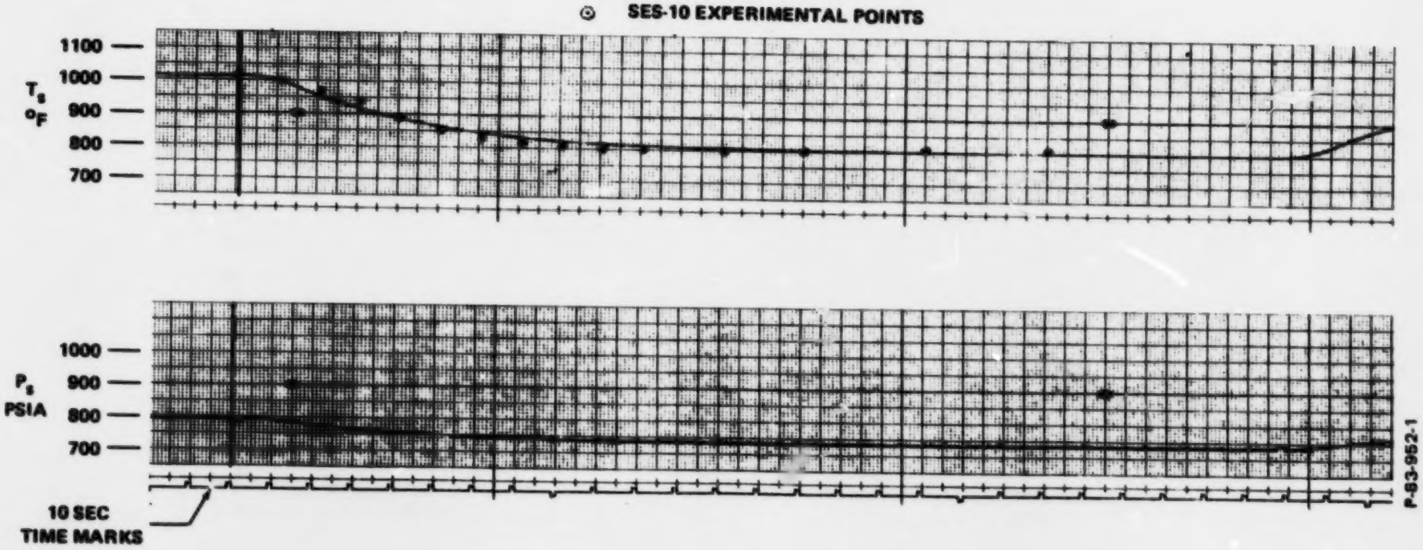

Figure 4-16 - Experimental and Hybrid Computer Transient Results Duplicating Experiment SES-10 at 0.1722 lb/sec Flow Rate

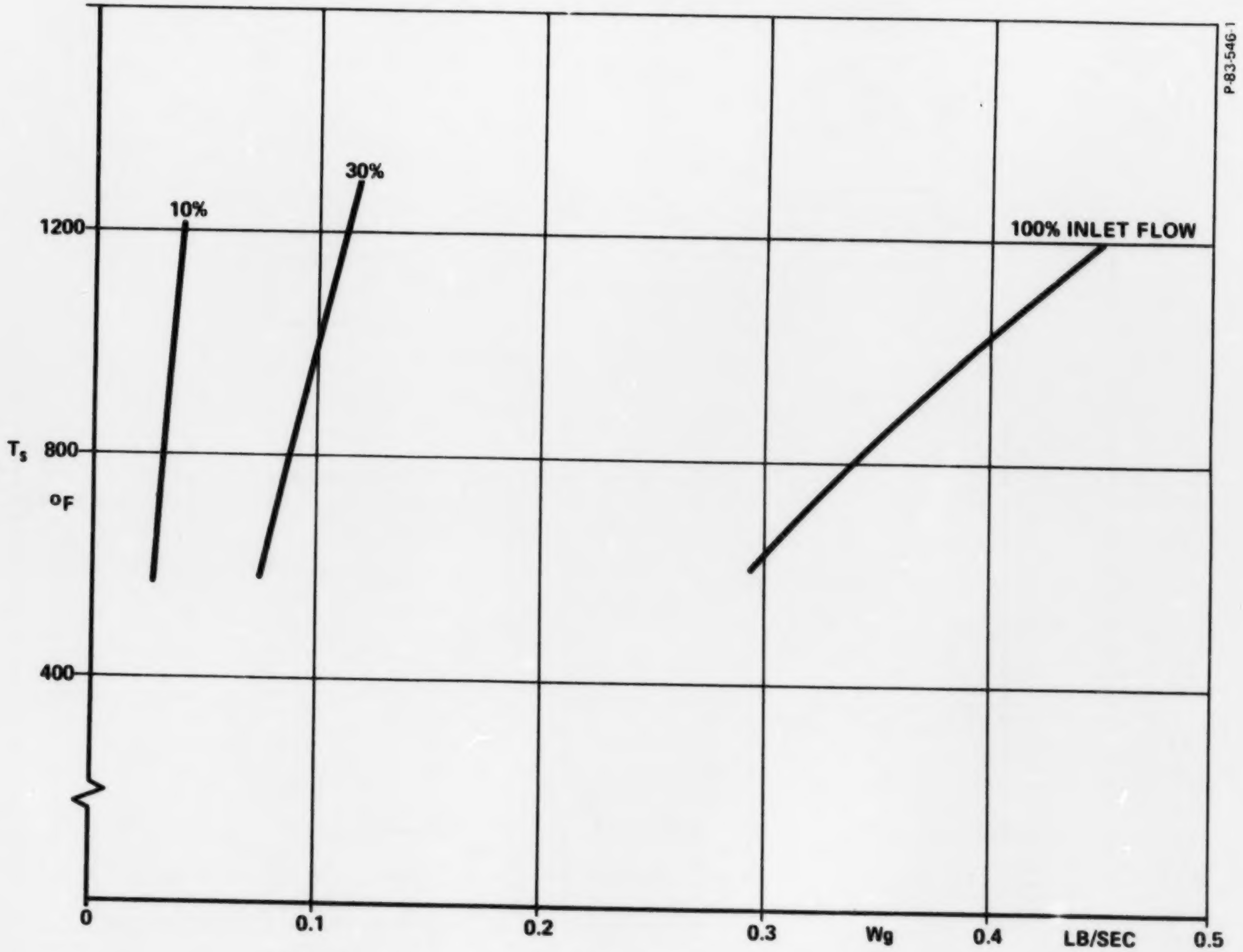

Figure 4-17- Steam Temperature Versus Gas Flow Rate

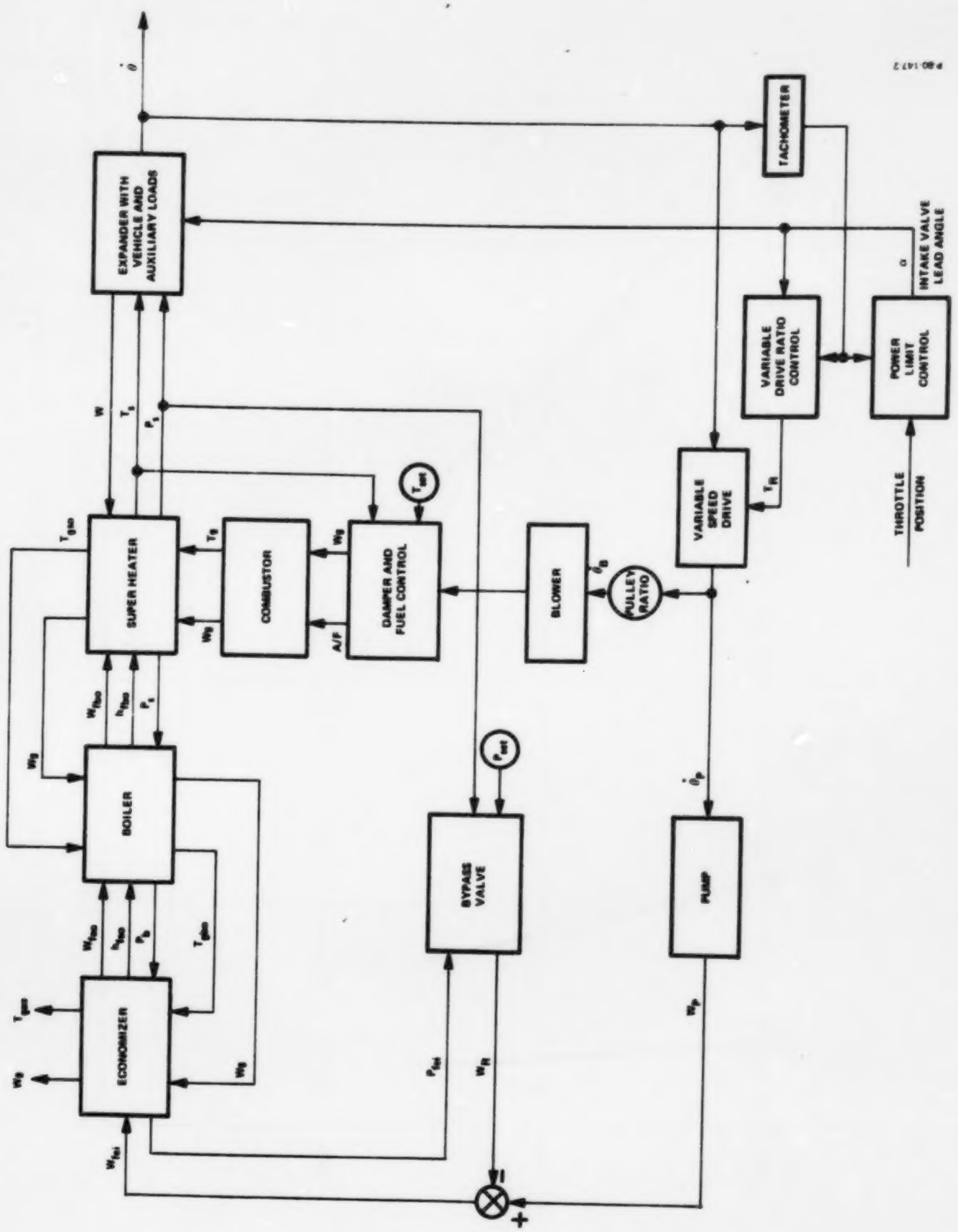
EXPANDER WITH VEHICLE AND AUXILIARY LOADS
θ̇
TACHOMETER
INTAKE VALVE LEAD ANGLE
α
VARIABLE DRIVE RATIO CONTROL
POWER LIMIT CONTROL
THROTTLE POSITION
VARIABLE SPEED DRIVE
T_R
W
T_S
P_S
T_gso
SUPER HEATER
T_g
W_g
COMBUSTOR
DAMPER AND FUEL CONTROL
T_set
A/F
BLOWER
θ̇_B
PULLEY RATIO
W_fbo
h_fbo
P_s
W_g
BOILER
BYPASS VALVE
P_set
PUMP
θ̇_p
W_feo
h_feo
P_b
T_gbo
ECONOMIZER
T_geo
W_g
W_g
W_fei
P_fei
W_R
W_p
-
+
P-80-1472

Figure 4-18 - Block Diagram of Hybrid Simulation;
Engine Driven Auxiliaries and Closed-Loop Control

pressure and temperature trim control loops and also to evaluate the operating characteristics of several bypass feedwater control designs.

Two prototype steam generator configurations were evaluated. The initial SES concept had a single boiler-section pass nearest to the burner. General evaluations of several control concepts were conducted using this model. The results of these investigations are reported under the designation of cross-counter flow model. The later design included the insertion of an additional pass of a bare-tube superheater pass directly located at the burner outlet. These results are described under the counterflow configuration.

4.3.1 Hybrid-Computer Results of Cross-Counter Flow Steam Generator Configuration Effect of Prediction Accuracy

Initial evaluations were conducted using an idealized predictive flow control system. In this idealized case it was assumed that a rapid-response (2 to 5 hertz bandpass) fuel and feedwater controller would be able to match the demanded fuel flow and feedwater flow commanded by the predictive controller. Using this idealized model of the predictive control system, the required prediction accuracy was evaluated. Results indicated that an 80 percent accuracy in the prediction is sufficient, and trim control operation was able to handle as much as 50 percent error in the predicted signal. With zero prediction, in other words with straight closed-loop control, pressure transients were controlled sufficiently by a bypass controller. However, the temperature errors in the non-predictive case become excessively large. This initial evaluation of the control concept also indicated the need of combustion air and feedwater pump capacity in excess of the steady-state requirements. This excess is mainly needed during acceleration. In the feedpump circuit, a sudden increase in the accelerator pedal may open the inlet valve to the expander at a rate faster than the feedwater system can follow. If no excess combustion gas and pumping capacity is available, then the initial steam pressure droop exists for an extended period of time. This reduces the maximum torque capability of the expander and limits the acceleration of the car.

On-Off Pressure Control

Operation of an on-off pressure controller was also evaluated. This pressure concept offers a very simple mechanization of the bypass concept. Over the required flow range of 20 to 1, excessive limit cycling was present. Pressure switch deadband was varied from 990 to 1010 psi, for a narrow-range design, to 900 to 1100 psi for a wide-range deadband evaluation. The speed of the bypass valve was slow and was varied from two to four seconds end-to-end travel time. Under these operating conditions, excessive pressure variations were present. The relatively slow-response bypass valve was to simulate an electrically operated bypass valve. The extréme limit cycle was evident at all conditions evaluated.

Proportional Pressure Control

An optimization of the bypass feedwater control, when combined with the simple predictive control of engine-driven auxiliaries, was carried out. This combination may offer the simplest and least expensive control configuration of the feedwater control system. Typical results describing this optimization study are given in Figures 4-19 through 4-24. The examples are given in order to illustrate the use of the hybrid-computer model for the control system optimization. In this type of control system, interaction is present between feedwater and fuel control. In addition, the relative capacity of combustion air blower and feedpump, as compared with steady-state engine demand, also influences the design and the performance of the power plant controls. A wide range of choices are practical in these areas. At the present time, the choices were not optimized. However, results presented are typical of the type of controls proposed for the prototype control mode.

Slow Bypass Valve

Figures 4-19 and 4-20 describe the operation of the bypass pressure control using a relatively slow bypass valve, requiring two seconds to travel from the fully opened to fully closed position. The two figures represent simultaneous recordings of 16 selected variables in the hybrid-computer simulation. The designations of the variables can be correlated with the schematic (Figure 4-18). Pressure control characteristics of the feedwater system, using a slow-response bypass valve, are described in Figures 4-19 and 4-20. The traces describe the response of the steam generator and the control system to a step change in throttle setting corresponding to approximately 40-70 mph vehicle speed range with the corresponding steam flow rates from 0.315 to 0.415 pounds per second. Wide excursion in steam pressure occurs during the transient. The slowly responding bypass valve is not able to cope with the rapidly varying steam flow. Pressure excursions of plus and minus 500 psi occur in this case. A slow temperature transient follows the pressure transient. Steady-state steam pressure varies from 1200 to 1020 psi. The offset is due to the fact that pump capacity is significantly larger than steady-state engine requirements. The bypass valve opening changes from 40 percent to 1 percent opening. In general, this indicates that at a minimum engine speed, low excess feedwater and combustion air flow is available. Figure 4-20 shows the corresponding metal temperature transients and boiler pressure transients. In addition, it may be seen that the predictive circuit changes the variable-speed drive ratio from 0.64 to 1.20 during the transient.

Fast Linear-Area Bypass Valve

A sufficient reduction of the pressure transient is achieved through the use of a faster bypass valve. Results are shown in Figures 4-21 and 4-22 for the new bypass valve design. The details of this design are shown in Section 3 under bypass valve. The traces indicate a

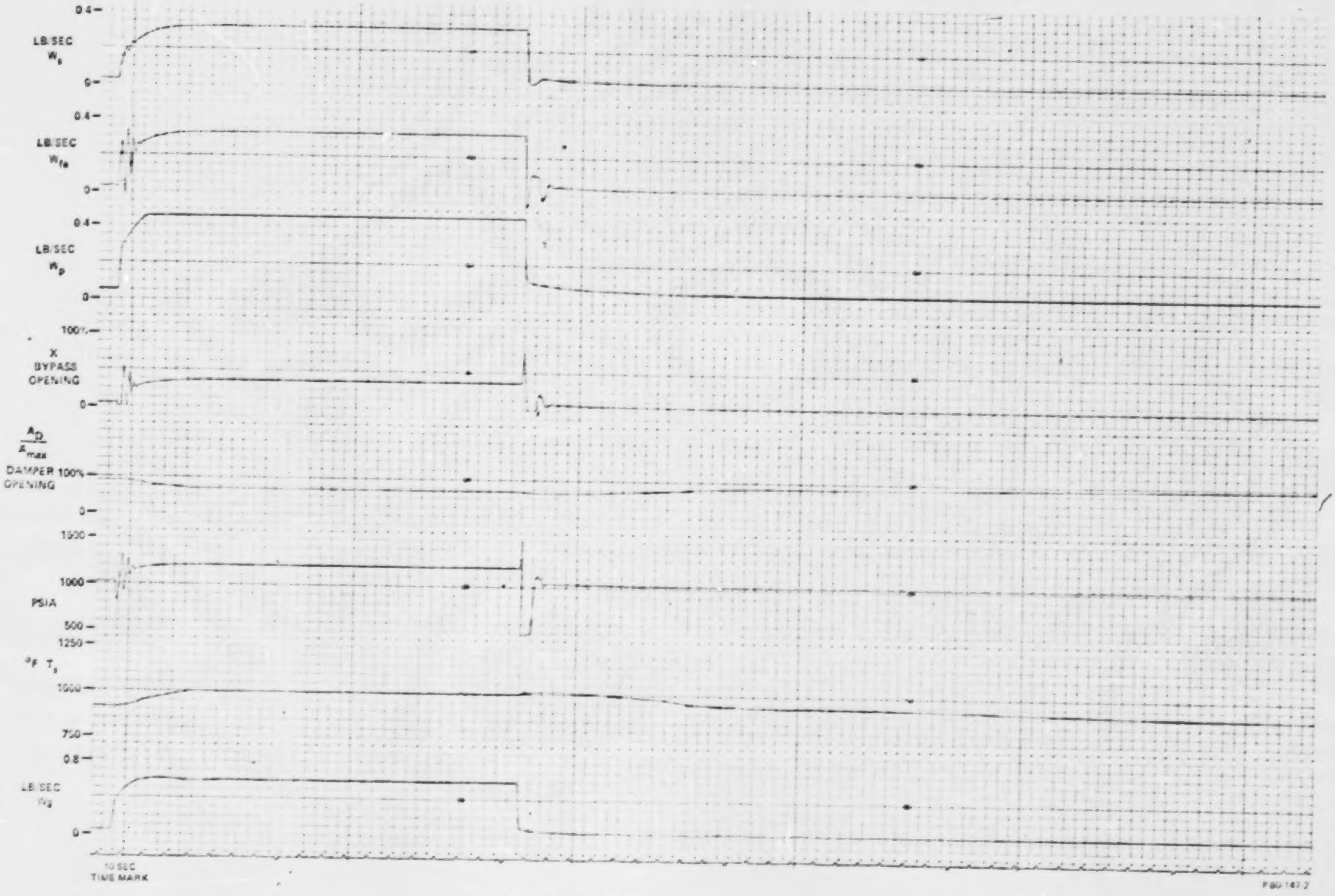

Figure 4-19 - Hybrid-Computer Results; Slow Bypass Valve

See following pages
for greater detail.

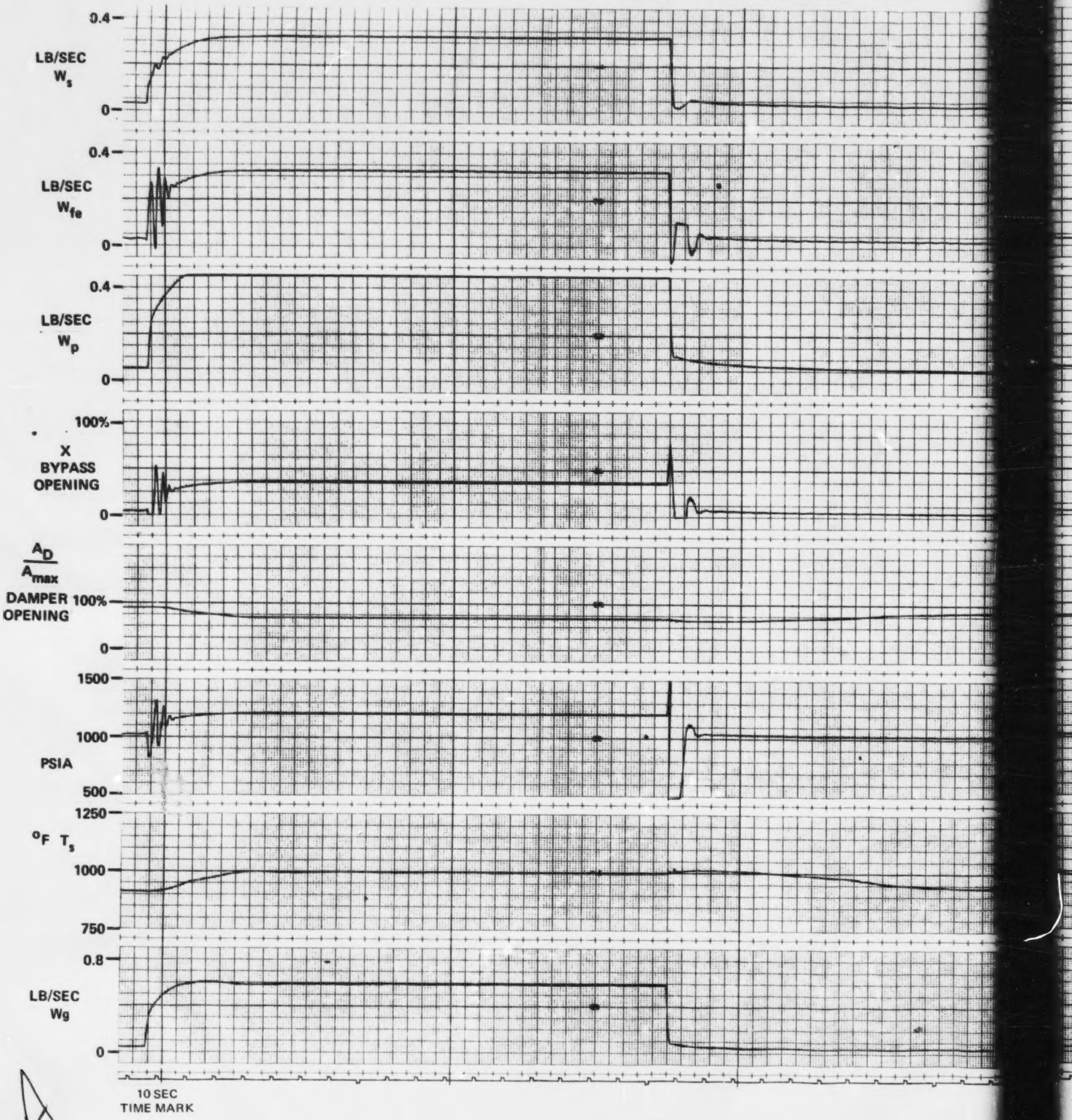

A

Figure 4-19 - Hybrid-Computer Results; Slow

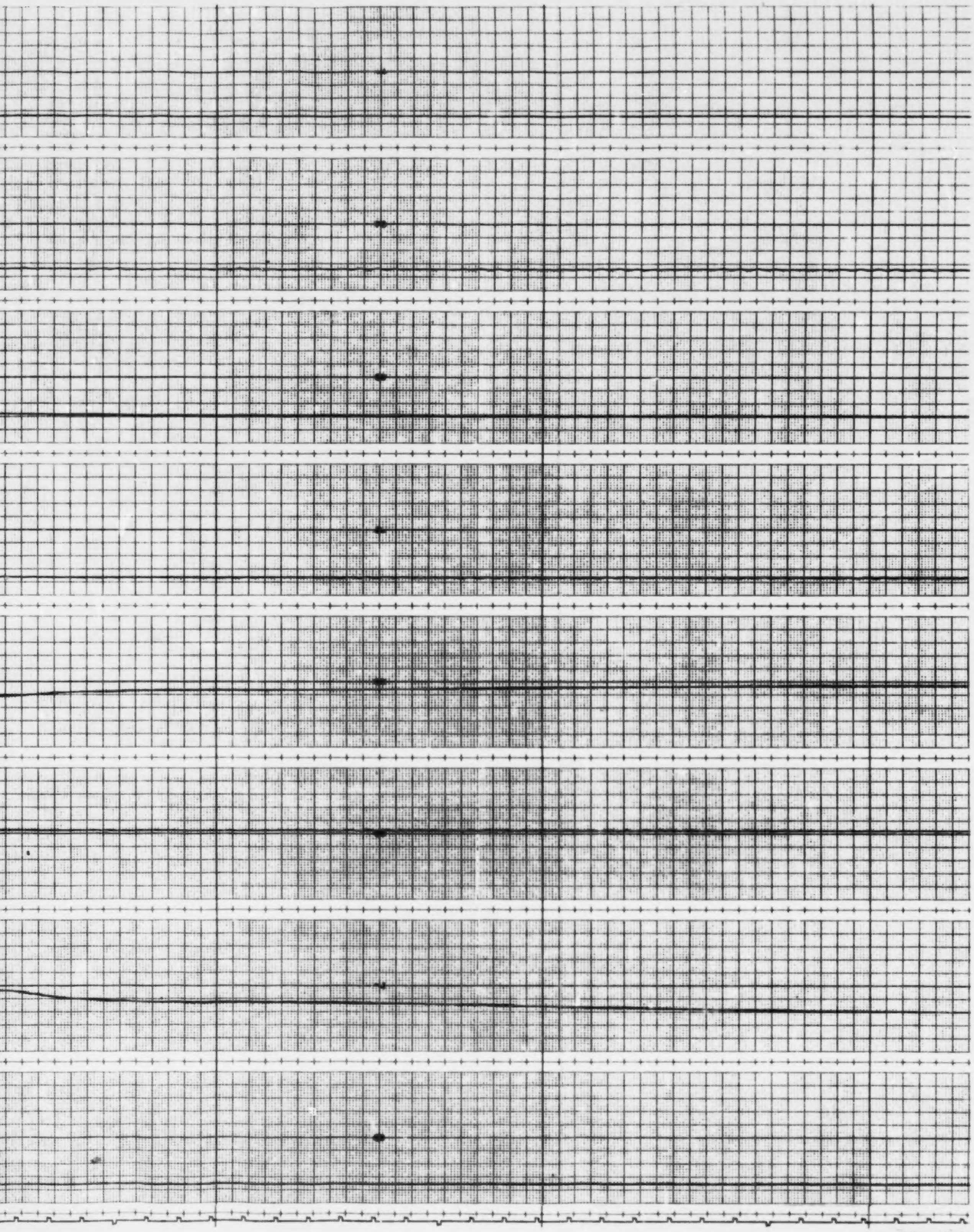

P-80-147-2

ter Results; Slow Bypass Valve

B

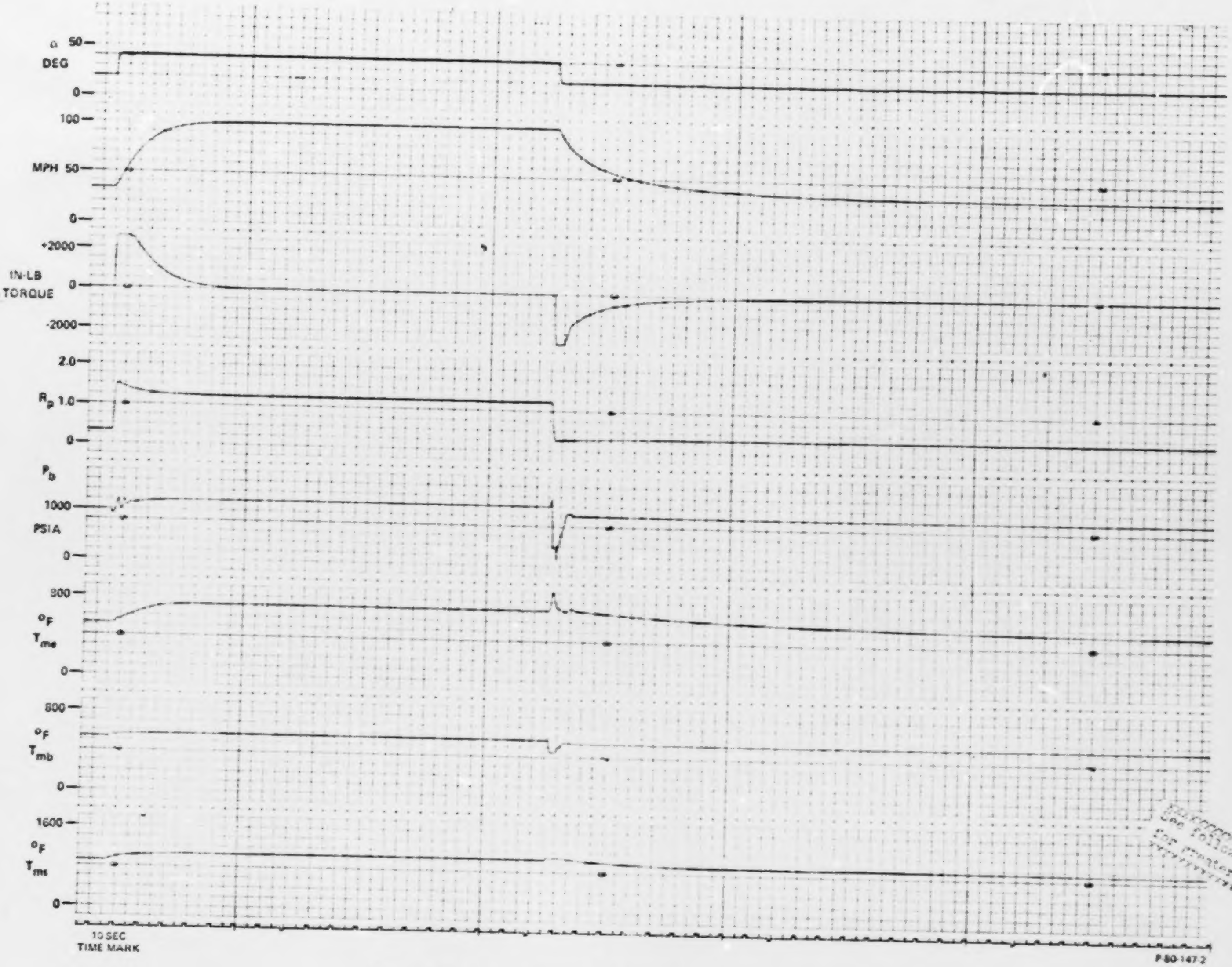

Figure 4-20 - Hybrid-Computer Results; Slew Bypass Valve

See following pages for greater detail.

Preceding page blank

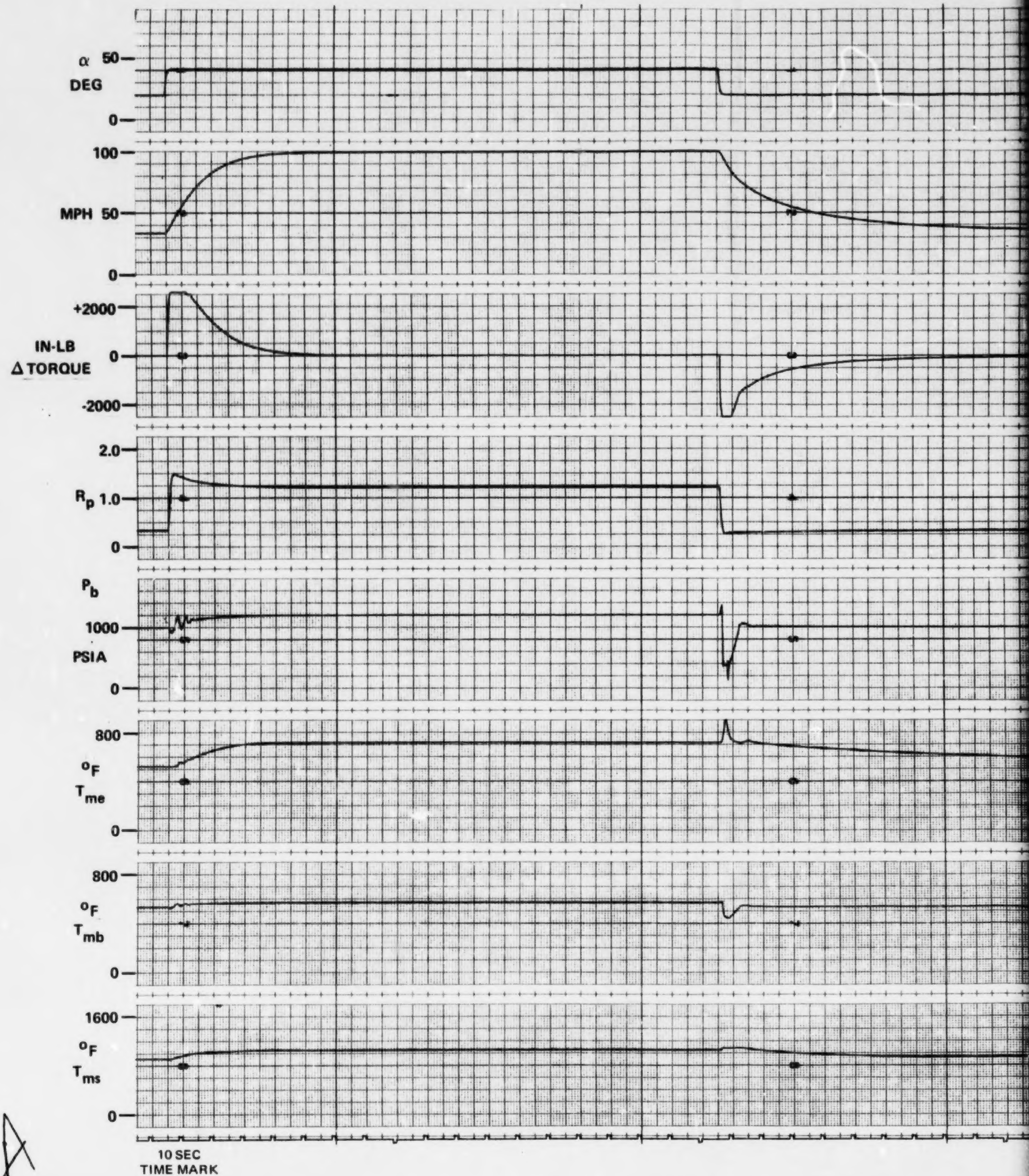

A

Figure 4-20 - Hybrid-Computer Results; Slow Bypass Va

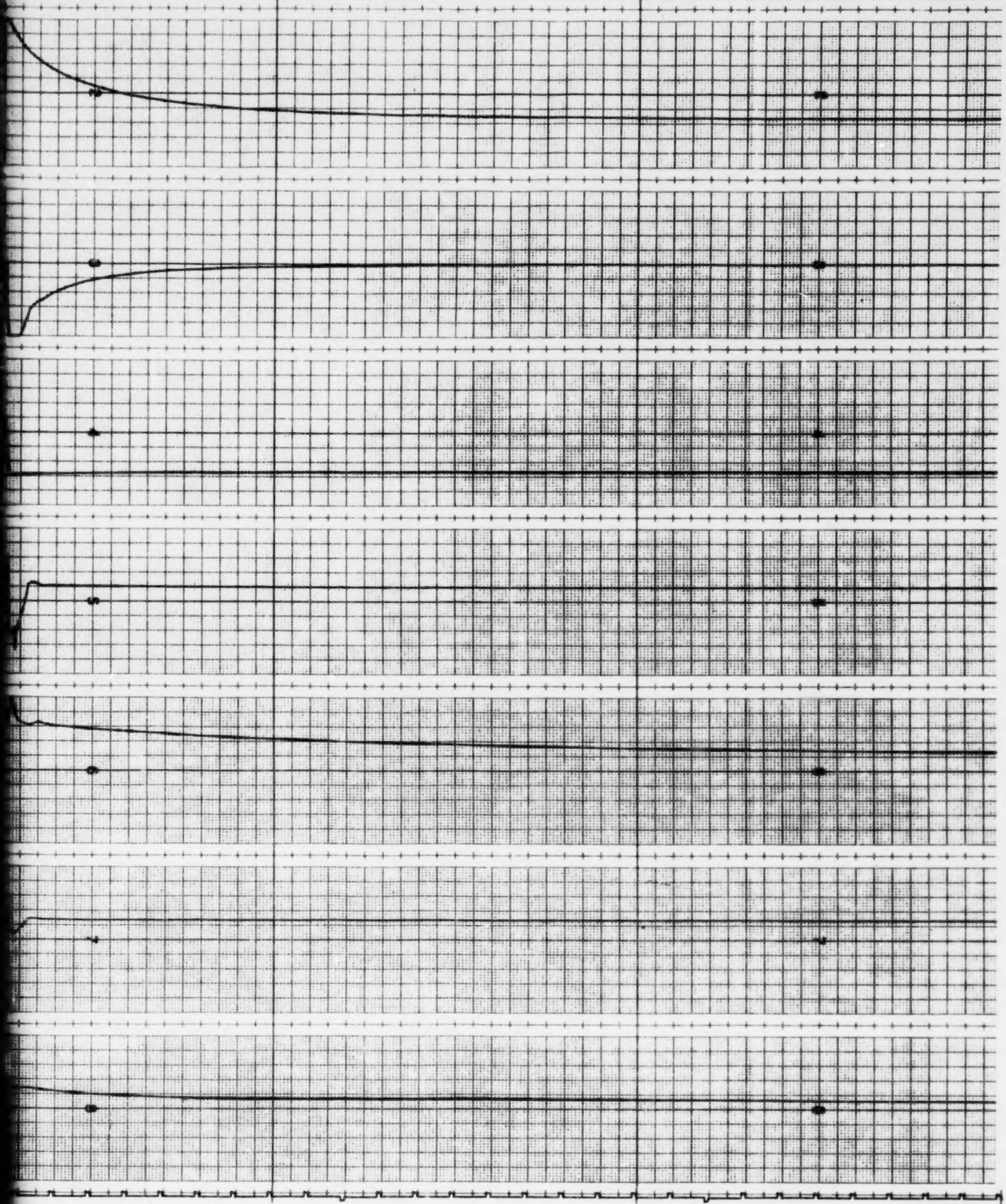

P-80-147-2

B

mputer Results; Slow Bypass Valve

Preceding page blank

1

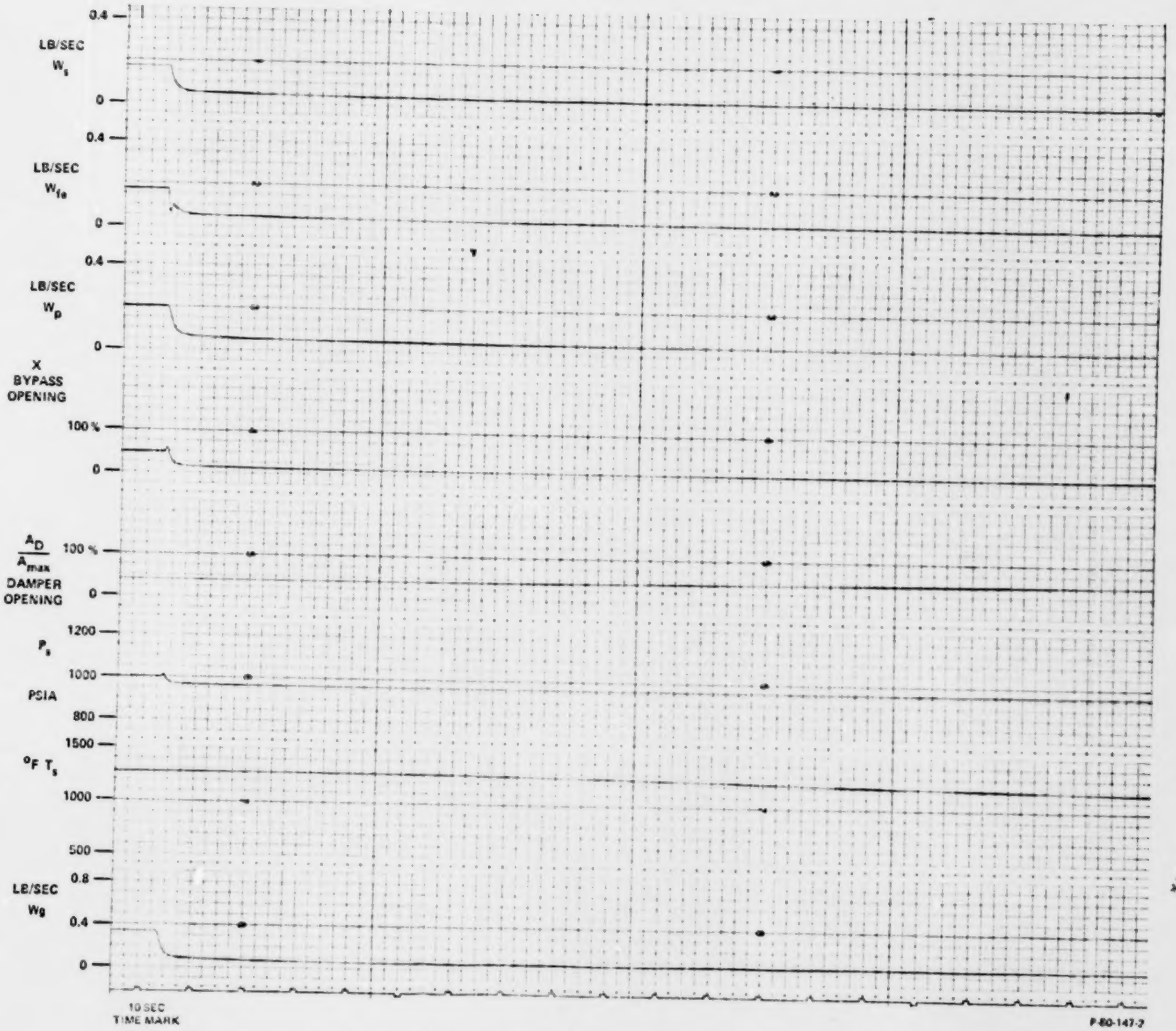

Figure 4-21 - Hybrid-Computer Results; Fast Linear Bypass Valve

See following pages for greater detail.

Preceding page blank

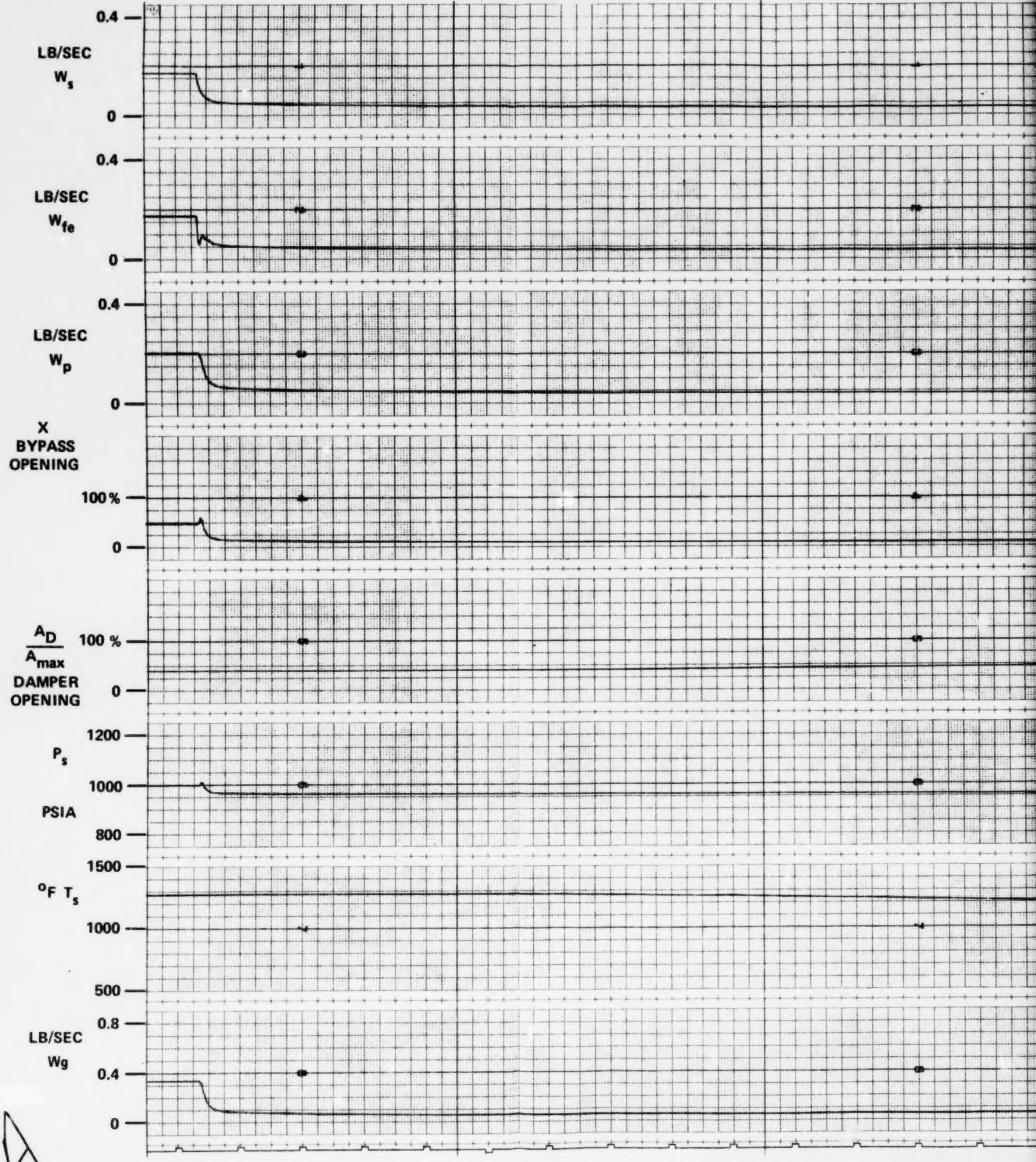

A

Figure 4-21 - Hybrid-Computer Results; Fast Linear Bypass Valve

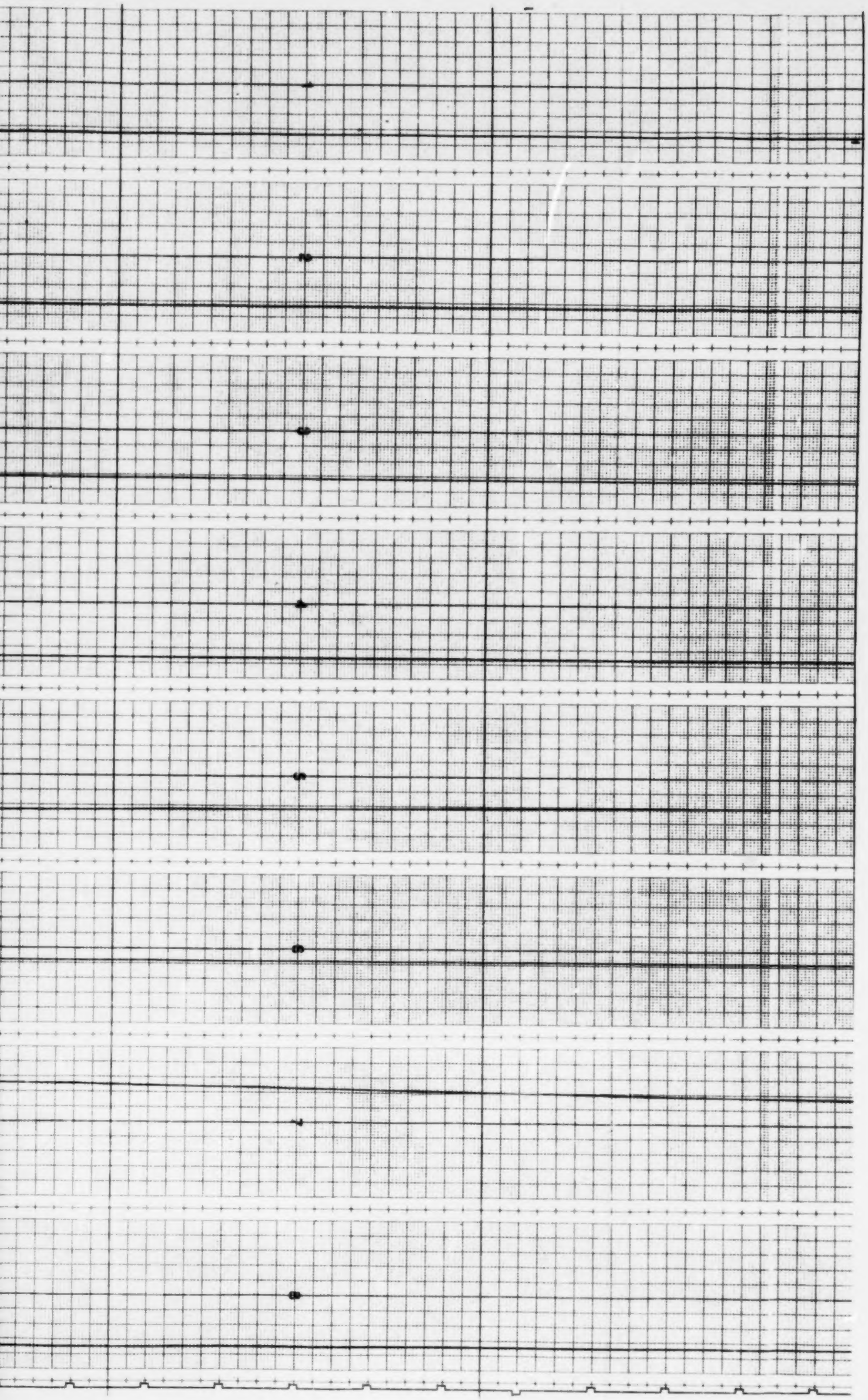

P-80-147-2

B

Results; Fast Linear Bypass Valve

Preceding page blank

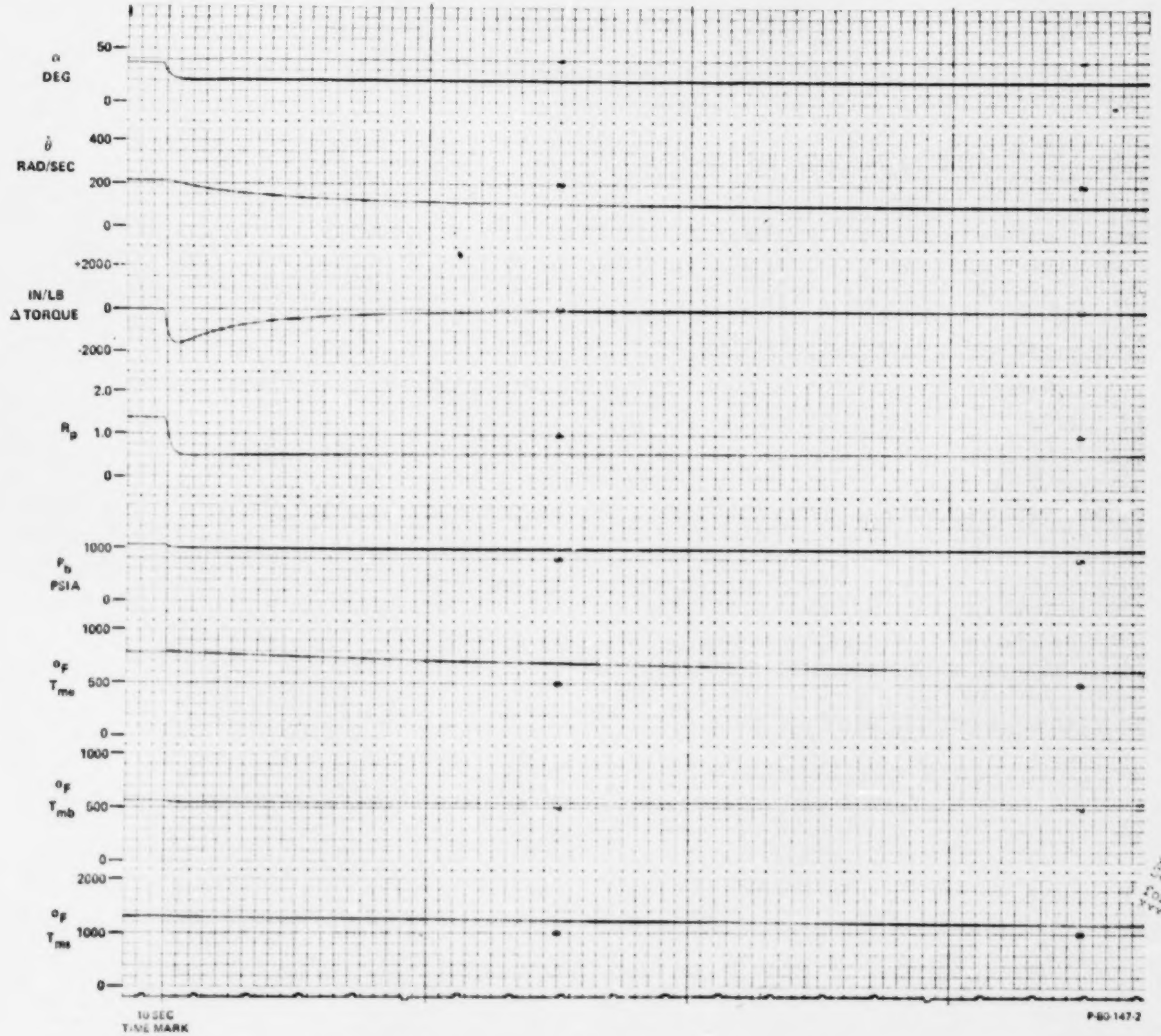

Figure 4-22 - Hybrid-Computer Results; Fast Linear Bypass Valve

See following pages for greater detail.

Preceding page blank

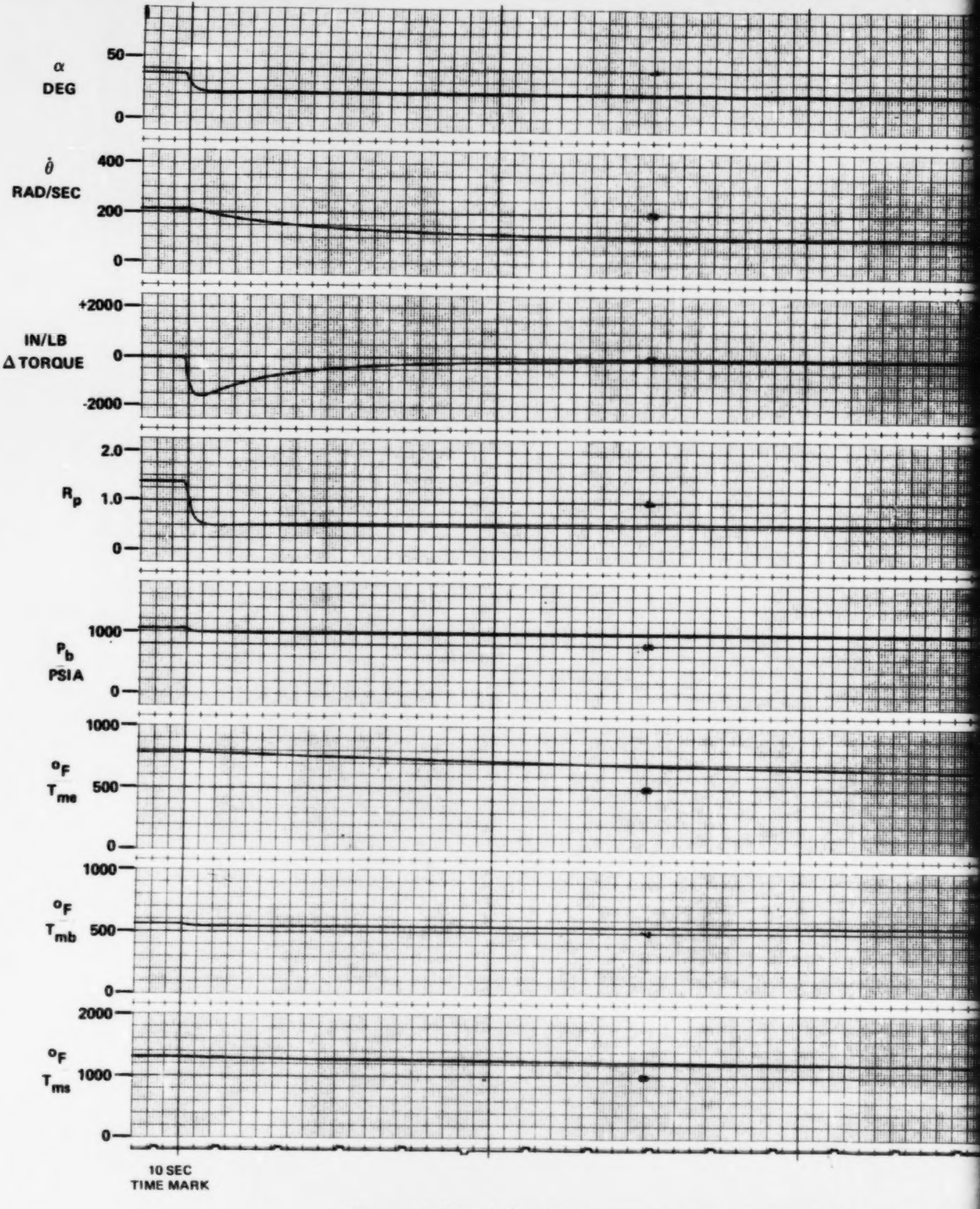

A

Figure 4-22 - Hybrid-Computer Results; Fast Linear Bypass Valv

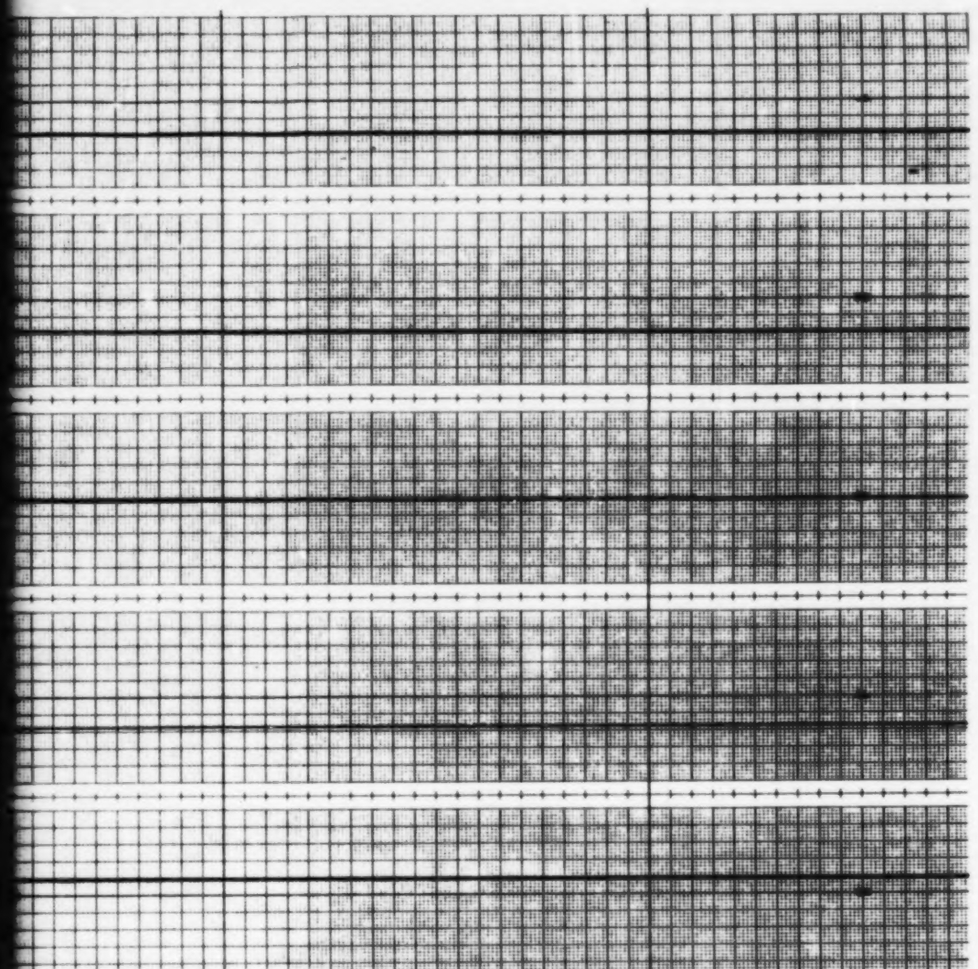

P-80-147-2

B

Results; Fast Linear Bypass Valve

Preceding page blank

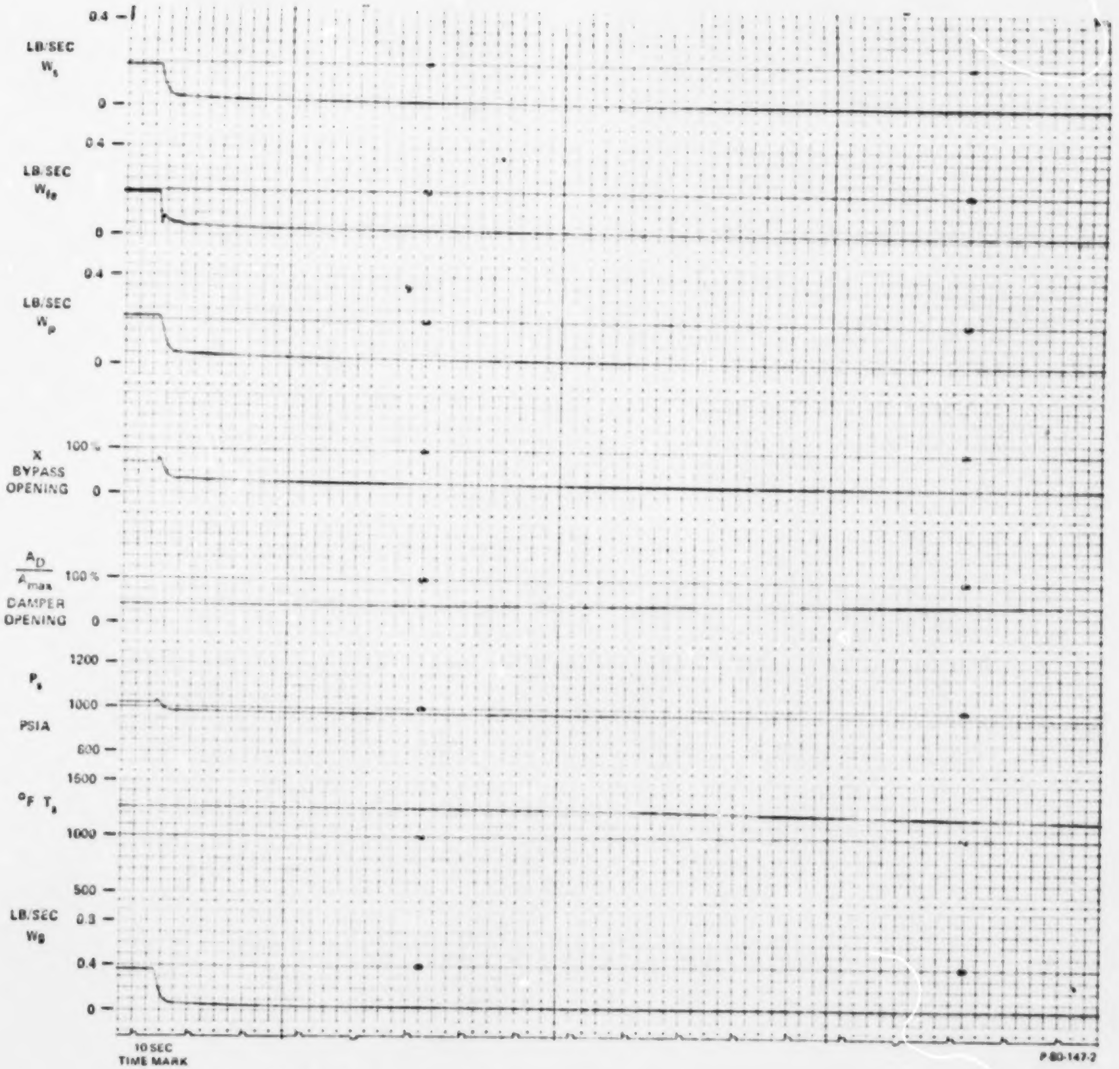

Figure 4-23 - Hybrid-Computer Results; Fast Equal-Percentage Bypass Valve

XXXXXXXXXXXXXXXXXX
See following pages
for greater detail.
YYYYYYYYYYYYYYYYYY

Preceding page blank

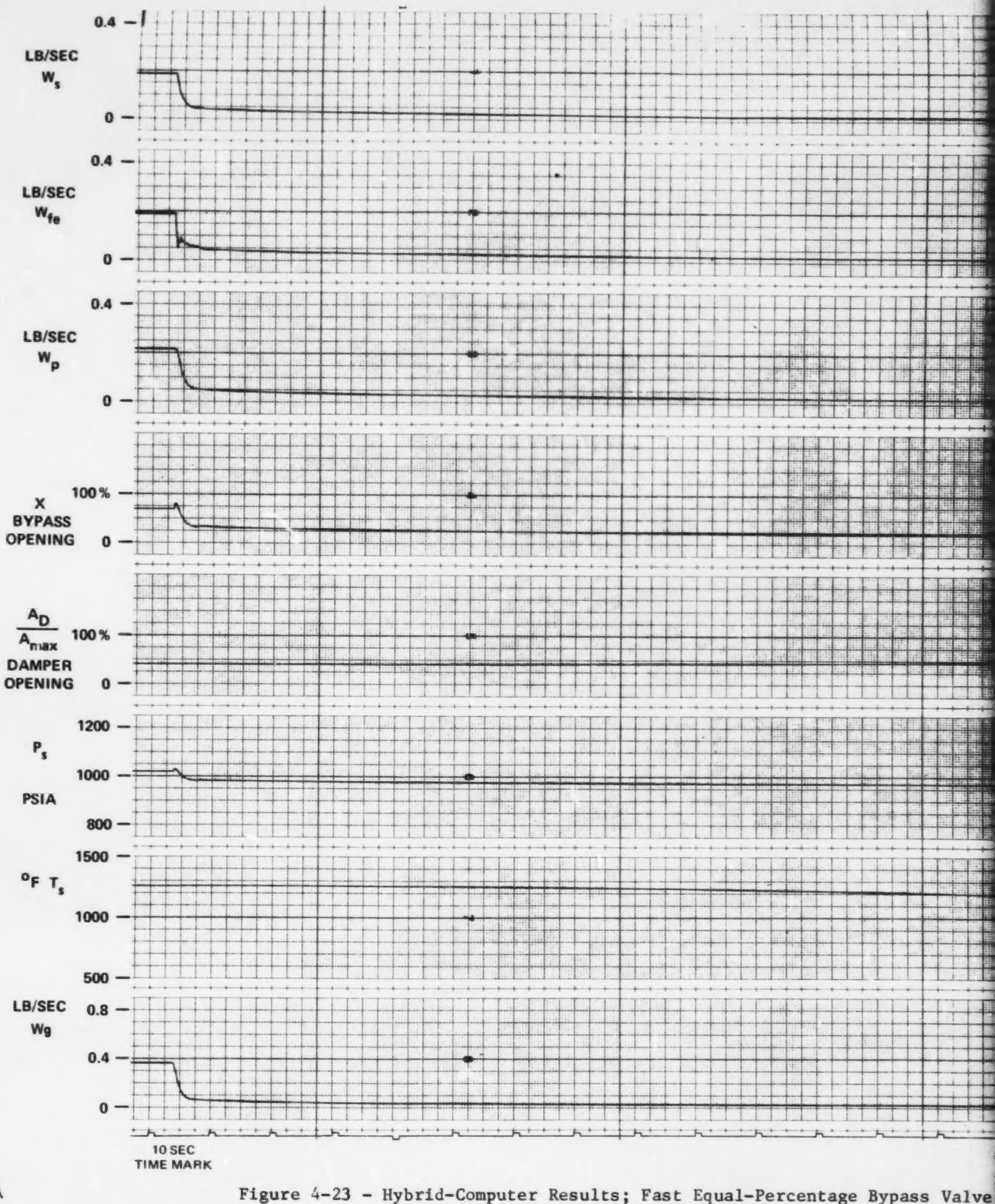

Figure 4-23 - Hybrid-Computer Results; Fast Equal-Percentage Bypass Valve

A

P-80-147-2

omputer Results; Fast Equal-Percentage Bypass Valve

B

Preceding page blank

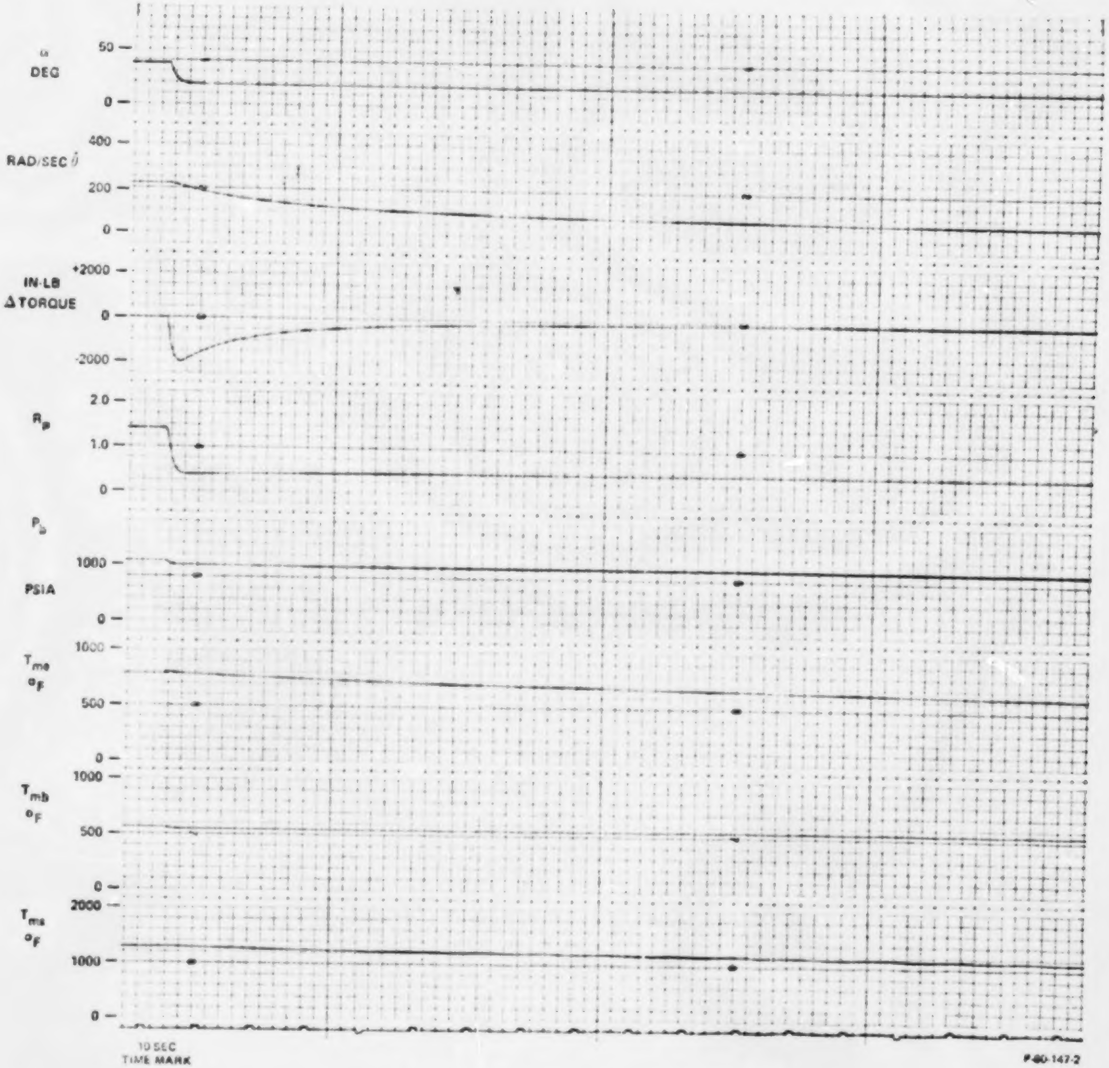

Figure 4-24 - Hybrid-Computer Results; Fast Equal-Percentage Bypass Valve

See following pages
for greater detail.

Preceding page blank

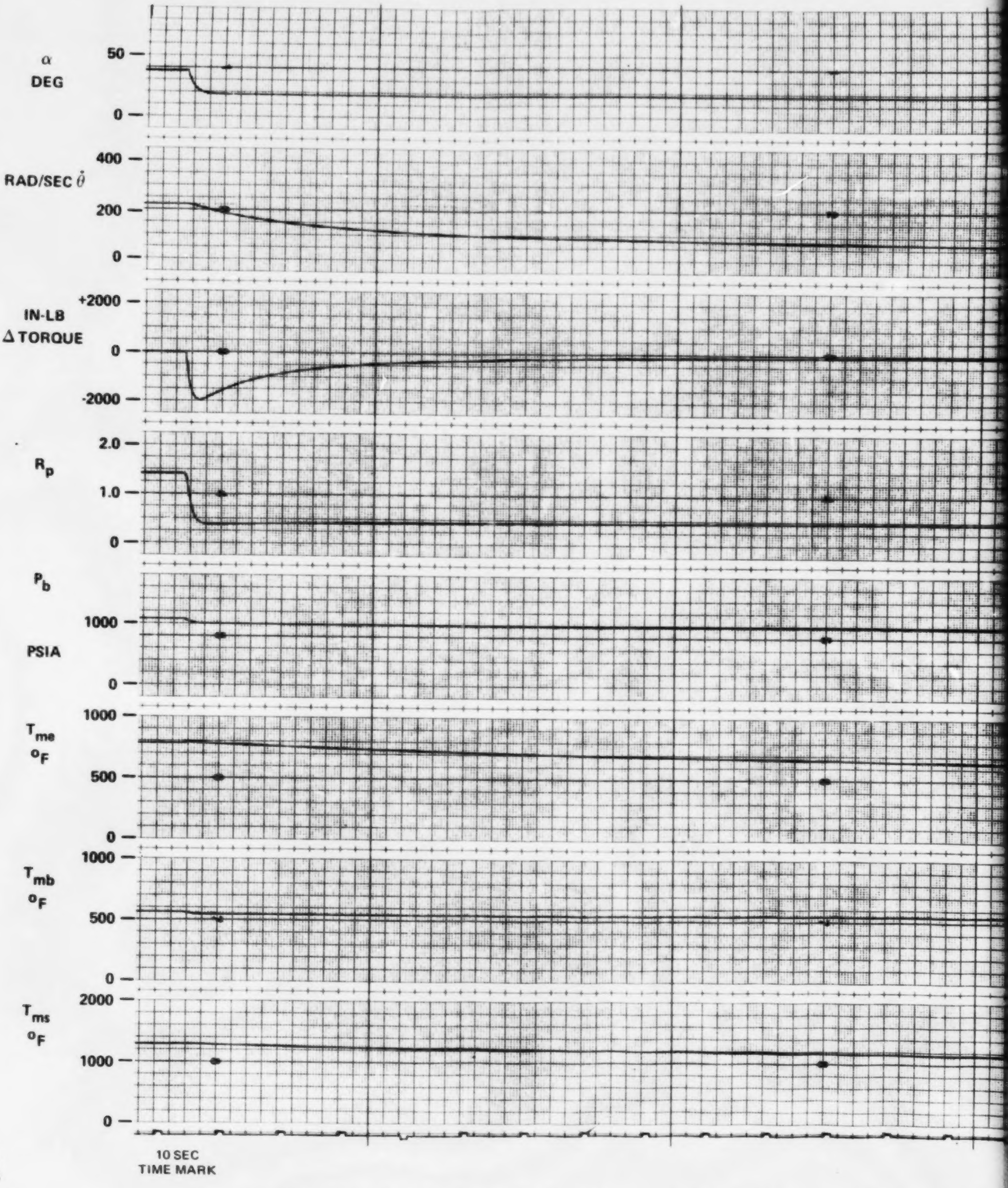

Figure 4-24 - Hybrid-Computer Results; Fast Equal-Percentage Bypass Valve

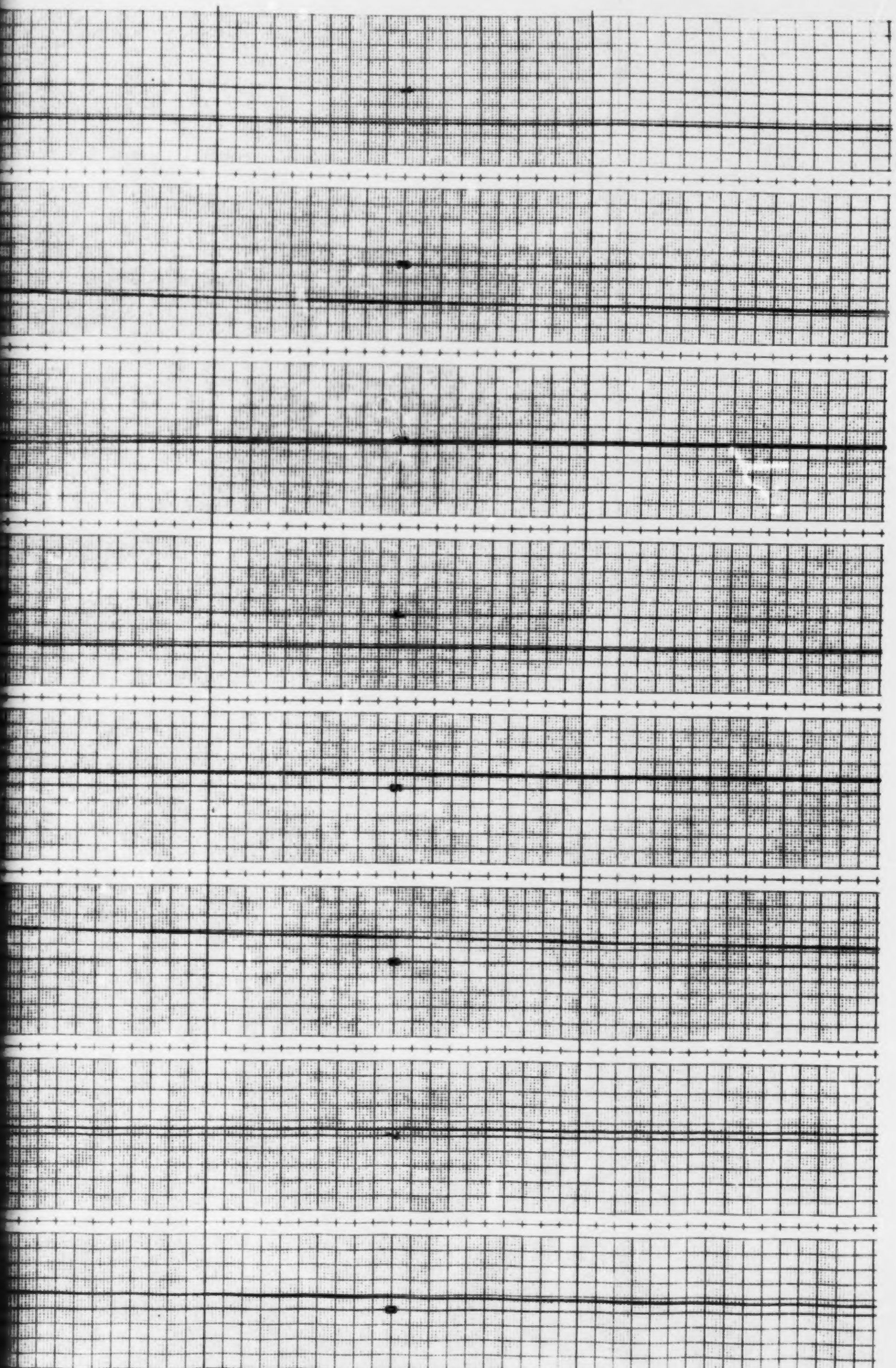

P-80-147-2

er Results; Fast Equal-Percentage Bypass Valve

B

Preceding page blank

linear scheduling between valve position and valve opening area. The results indicated that this type of a valve operates satisfactorily over a range of feedwater flow levels. However, at the very low flows, at the order of 3-5 percent of the full steam generator capacity, the gain of this type of a feedwater bypass valve becomes too high and unstable operation results. The steam pressure is controlled between 1000 and 960 psi during the transient. The maximum pressure excursion is 1010 psi and indicates a significant improvement over the previous design. The bypass opening varies from 50 to 10 percent opening. The variable-drive transmission ratio varies from 1.37 to 1.55 during the transient shown. The steam-flow steady-state levels vary from 0.16 to 0.015 for this transient.

Fast Equal-Percentage Bypass Valve

The performance of the feedwater control system can be improved at the low flow levels through the use of an equal-percentage valve opening. In this configuration the area of the bypass valve varies approximately as the square of the valve position. This can be achieved by the use of a taper-plug design as already described in Section 3. This is the configuration that was selected for experimental evaluation and for the facsimile system. Typical results are again shown in Figures 4-23 and 4-24. Typical operation is shown for a steam flow change from 0.195 to 0.007 pound per second. The minimum flow level is 1/50th of the rated 100 percent flow capacity of the SES-5 boiler. The steam pressure is controlled between 1020 to 960 psi. The variable transmission drive ratio is changed during the transient from 1.42 to 0.45. It appears that satisfactory steam-generator pressure control can be achieved through the use of the equal-percentage bypass flow controller.

The above results are shown mainly to illustrate the use of the hybrid computer in the optimization of control. However, in the selected traces, the steam temperature is too high. This was due to the relatively low proportional gain used in the trim temperature control. The high-excess, combustion-air-blower capacity required a nearly 50 percent closing of the damper. It became apparent during the evaluations that capacity matches between the combustion air blower delivery and the feedwater pump delivery must be carefully observed. The speed-flow characteristic of the feedwater pump is essentially linear, while the blower output-speed curve is highly nonlinear in the operating range. This suggests that for the blower characteristics currently used, it may be necessary to add a predictive signal to the air damper control in order to maintain an improved steam temperature control.

4.3.2 Hybrid-Computer Results of Counterflow Steam Generator Configuration

The hybrid-computer simulation was later modified to accommodate the changes due to the new SES-5 design of the steam generator. The effect of the additional fifth pass, which is a bare-tube superheater

Preceding page blank

section, and the change of the gas flow path that locates the new section directly at the burner phase, were evaluated. Perhaps the most significant effect stems from the differences between blower and pump output characteristics as a function of auxiliary drive shaft speeds. In general, combustion air blowers of the type considered for the present application have a strong exponential characteristic of flow versus shaft speed. On the otherhand, positive-displacement pumps have a nearly linear output versus speed characteristic. When additional restraints are imposed on the control design, then the design of the temperature and pressure control for the steam generator becomes increasingly more complex. An example of such an additional restraint is the need for a minimum differential-pressure drop across the combustion air circuit in order to reduce its sensitivity to ambient pressure disturbances at the inlet or exhaust of the combustor. A large number of parametric evaluations becomes essential to optimize the temperature and pressure control systems.

The interaction between the temperature and pressure control system is illustrated in Figures 4-25 through 4-28. In both instances the steam generator is operated at a low level. At this point the system time constants, both in the pressure and temperature control loop, become the longest. Closed-loop control under these conditions becomes the most difficult due to the slow but strong interaction between the temperature and pressure control system. In both cases a step change in engine demand is initiated by changing the cut-off position alpha. In both cases, the feedwater flow input is manually controlled to maintain the steam pressure at 1,000 psi, with a lower gain in the temperature trim control. As shown in Figures 4-25 and 4-26, the control of the pressure becomes very difficult as the changes in feedwater flow affect both the outlet pressure and temperature. When the temperature control is improved as shown in Figures 4-27 and 4-28, pressure control becomes less affected by temperature changes, thus significantly improved control over the outlet pressure can be achieved even at very low operating levels. The increased level of air damper activity is a direct result of the increased temperature gain. It is apparent that good prediction accuracy will be required at the low power levels to reduce the air damper activity and the resultant modulation of the combustion gas flow at the minimum operating levels. The examples shown are characteristic of the general results of the hybrid-computer simulation which appears to offer a very realistic tool for the optimization of the steam generator control system.

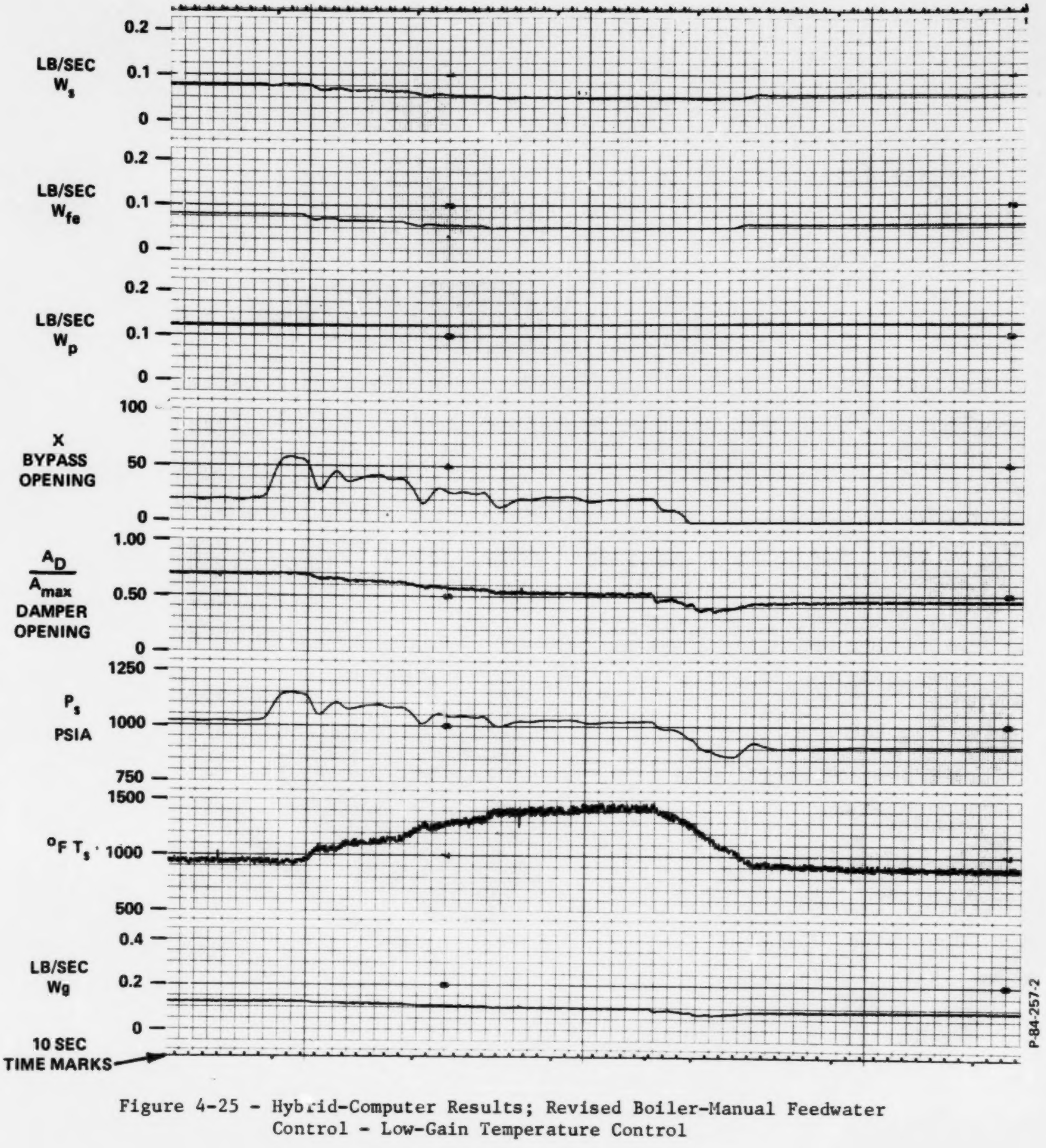

Figure 4-25 - Hybrid-Computer Results; Revised Boiler-Manual Feedwater Control - Low-Gain Temperature Control

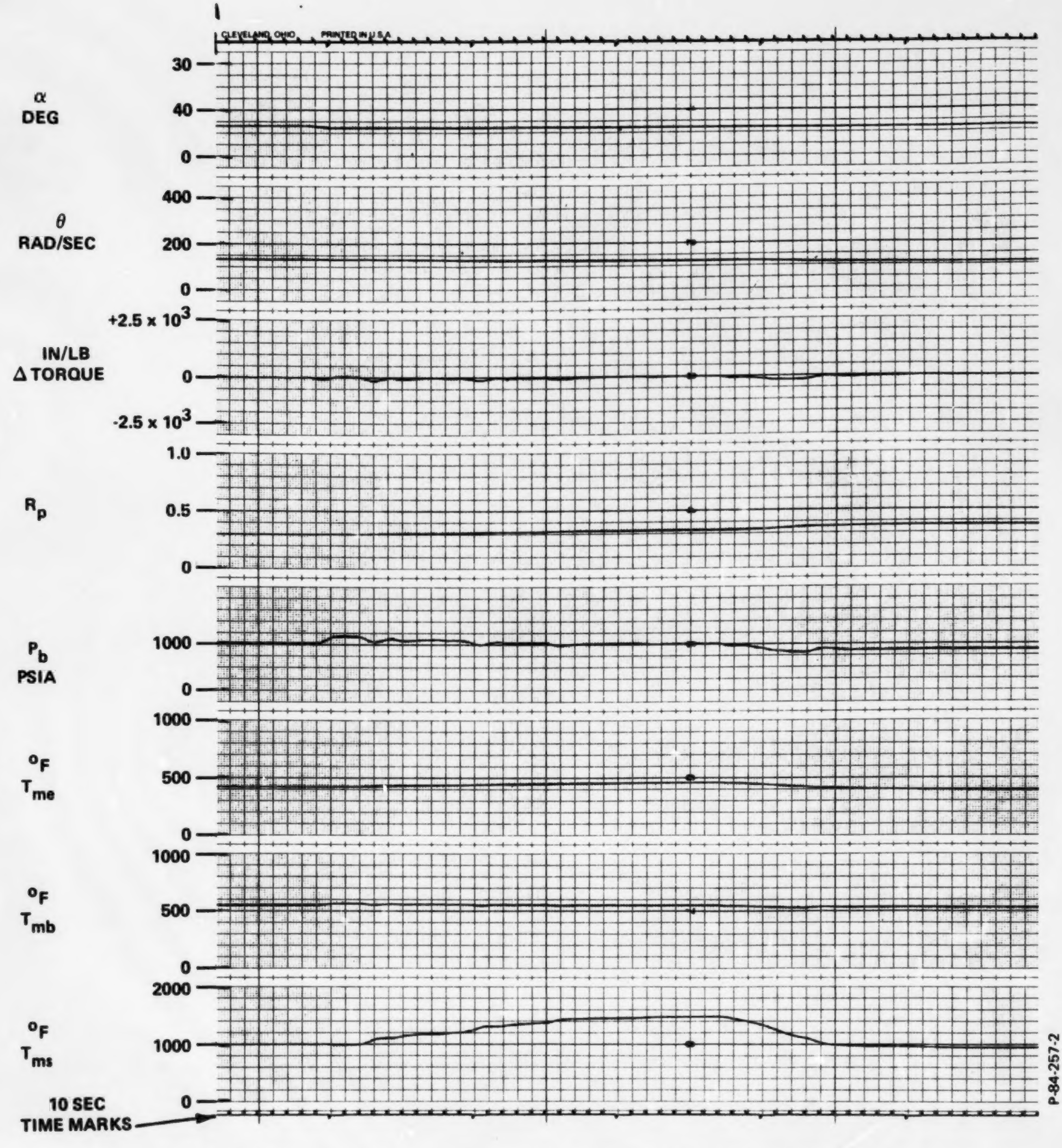

Figure 4-26 - Hybrid-Computer Results; Revised Boiler-Manual Feedwater Control - Low-Gain Temperature Control

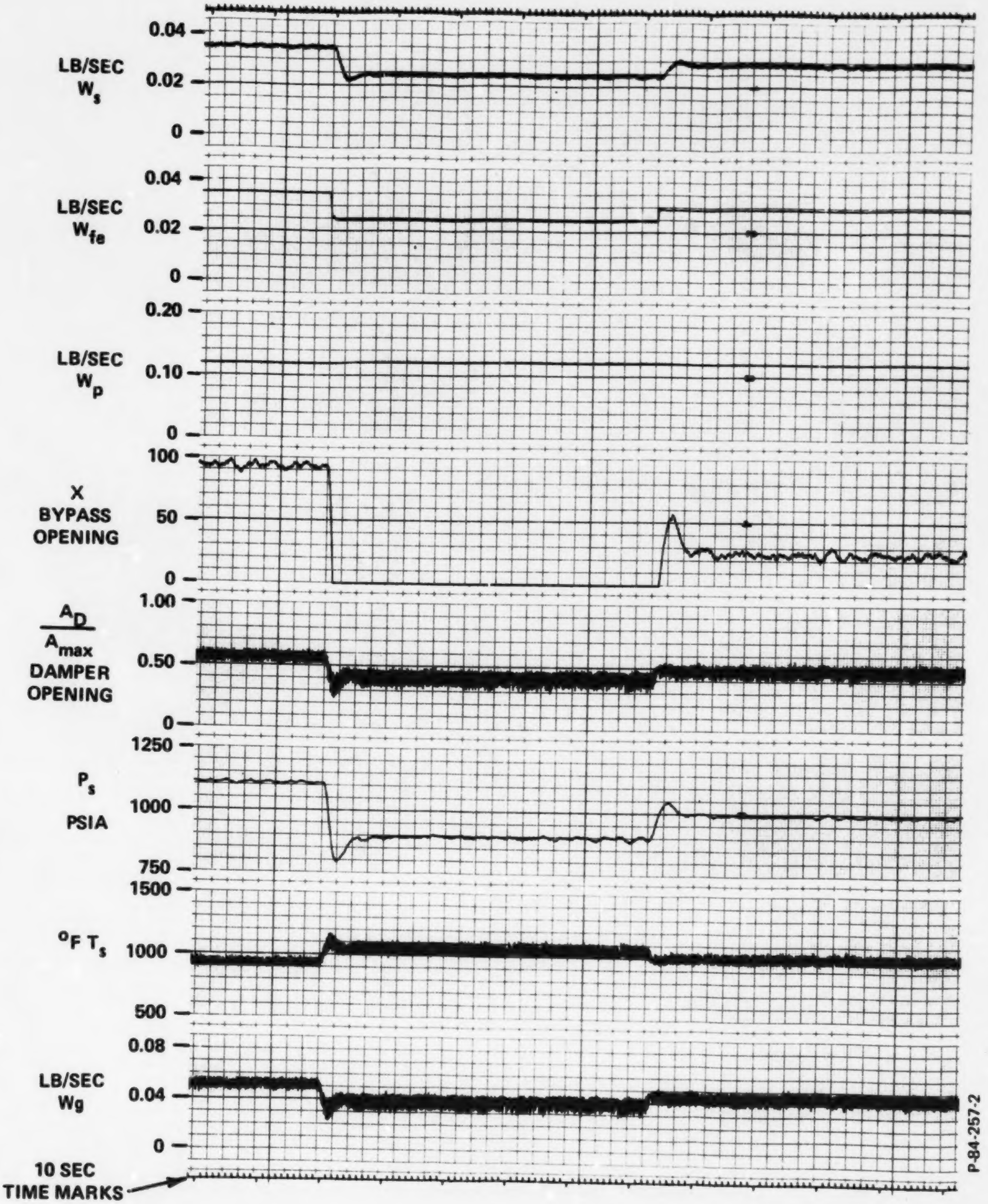

Figure 4-27 - Hybrid-Computer Results, Revised Boiler-Manual Feedwater Control - High-Gain Temperature Control

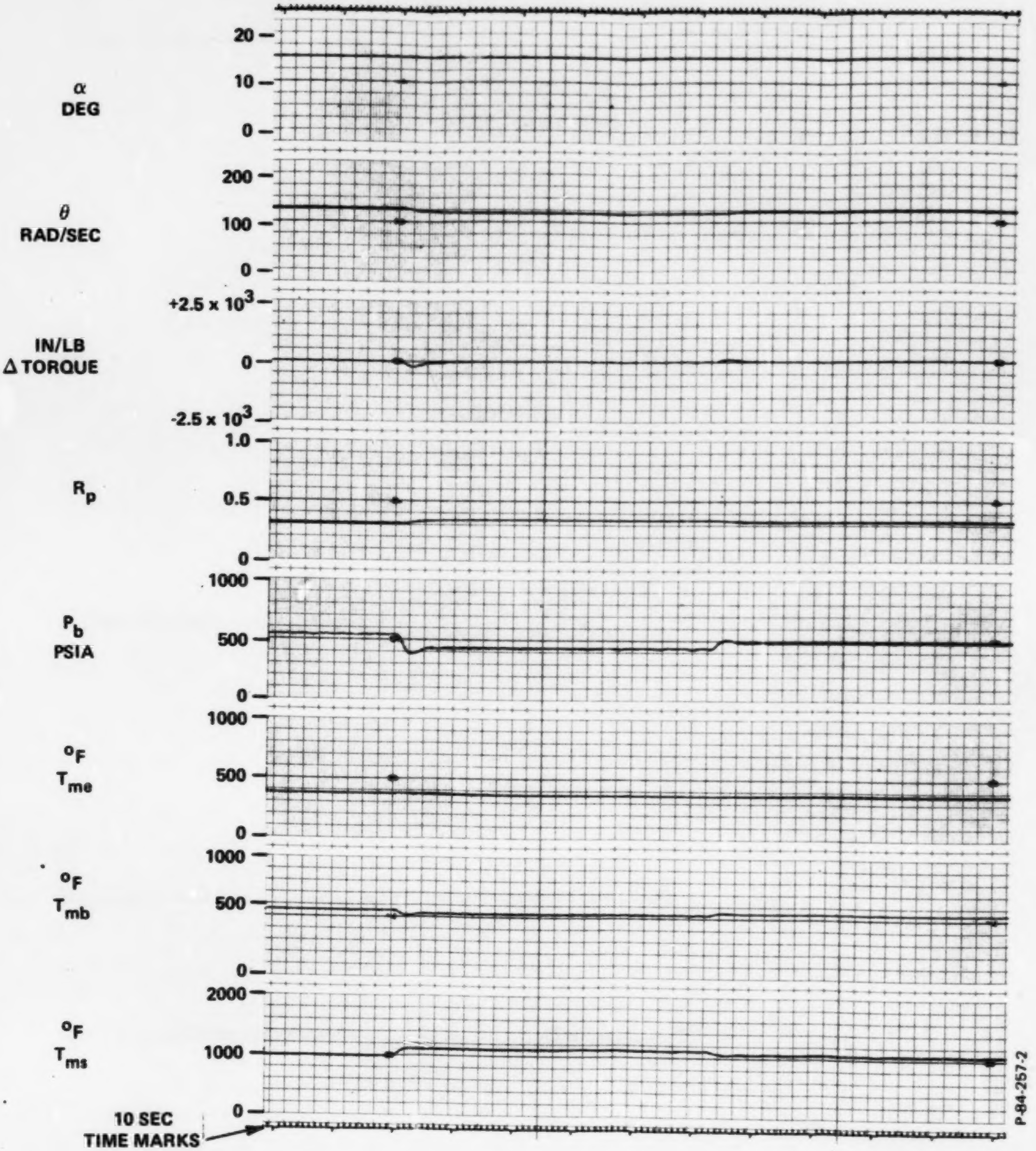

Figure 4-28 - Hybrid-Computer Results; Revised Boiler-Manual Feedwater Control - High-Gain Temperature Control

NOMENCLATURE

Symbol	Units	Value SES-5	 SES-4	Description
a	1/°F			Equation-of-state constant
A	lb/in^2	4267.5	4267.5	Equation-of-state coefficients, boiler
A_D	in^2			Air damper opening
$A_D max$	in^2			Maximum damper opening
A/F			19.0	Air-fuel ratio
A_{Hfe}	in^2	625	324	Heat transfer area, fluid side, economizer
A_{Hfb}	in^2	1150	312	Heat transfer area, fluid side, boiler
A_{Hfs}	in^2	373	288	Heat transfer area, fluid side, superheater
A_R	in^2	3.518×10^{-3}		Bypass flow area
A_Δ	in^2	0.169		Bypass differential area
A_T	in^2	0.05373		Flow area, throttle
A_{xb}	in^2	0.192	0.116	Flow area, boiler tube
A_{xe}	in^2	0.107	0.075	Flow area, economizer tubes
A_{xs}	in^2	0.192	0.116	Flow area, superheater
b				Equation-of-state constant
b_o	lb-sec/in	0.444		Bypass damping coefficient
B	lb/in-°F	-20.35	-20.35	Equation-of-state coefficients, boiler
c	°F			Equation-of-state constant
C	$lb/in^2-°F^2$	0.0527	0.0527	Equation-of-state coefficients, boiler
C_1	$^oR/sec$	0.4049		Superheated steam, gas coefficient

		Value		
Symbol	Units	SES-5	SES-4	Description
C_{1e}	btu/(in^2-sec-°F)	3.95×10^{-3}	3.86 x 10-3	Film coefficient, economizer, fluid side
C_{1s}	btu/(in^2-sec-°F)	1.49×10^{-3}	1.736×10^{-3}	Film coefficient, superheater, fluid side
C_d		0.80	0.80	Orifice coefficient, throttle
C_{fe}	btu/lb-°F	1.09	1.09	Specific heat, fluid, economizer
C_{gb}	btu/lb-°F	0.3263	0.434	Specific heat, gas, boiler
C_{ge}	btu/lb-°F	0.2932	0.287	Specific heat, gas, economizer
C_{gs}	btu/lb-°F	0.3554	0.310	Specific heat, gas, superheater
C_{mb}	btu/lb-°F	0.11	0.11	Specific heat, metal, boiler
C_{me}	btu/lb-°F	0.11	0.11	Specific heat, metal, economizer
C_{ms}	btu/lb-°F	0.11	0.11	Specific heat, metal, superheater
C_{ps}	btu/lb-°F	0.697	0.68	Specific heat, fluid, superheater
C_{Tps}	in/°F	1437	1437	Superheater conversion coefficient, temperature pressure
D	btu/lb-°F	1.26	1.26	Equation-of-state coefficients, boiler
D_b	in.	0.495	0.385	Boiler tube I.D.
D_e	in.	0.37	0.31	Diameter, economizer fluid tube

		Value		
Symbol	Units	SES-5	SES-4	Description
D_{MT} (α)	in^3-sec/rad			Expander torque constant
D_{MV} (α)	in^3-sec/rad			Expander volumetric constant
D_p	in^3/rad	0.0872	0.385	Water pump displacement coefficient
D_s	in.	0.495		Tube diameter, superheater
$D\ (\dot{\theta})$				Velocity coefficient, expander constants
E	btu/lb	148	148	Liquid, internal energy equation coefficient
F	in-lb	1399.2		Vehicle rolling resistance revised
f_b		4×10^{-3}	4×10^{-3}	Friction factor, boiler
$f_b(W_g)$				Boiler heat transfer function
f_e		4×10^{-3}	4×10^{-3}	Friction factor, economizer
$f_e(W_g)$				Economizer gas-to-metal heat transfer function
$f_1 \frac{P_M}{P_S}$				Flow function
F_p	lb	160.55		Bypass spring preload
f_s		4×10^{-3}	4×10^{-3}	Friction factor, superheater
$f_s\ (W_g)$				Superheater heat transfer function
g_o	in/sec^2	386	386	Gravitational constant for mass conversion
h_e	btu/lb			Enthalpy - average economizer

Symbol	Unit	Value		Description
		SES-5	SES-4	
h_{ei}	btu/lb	190.4	219	Enthalpy - economizer, inlet
h_{eo}	btu/lb			Enthalpy - economizer, outlet
h_{fb}	btu/lb			Enthalpy - fluid, boiler
f_{fbo}	btu/lb			Enthalpy - fluid, boiler outlet
h_{oe}	btu/lb	-51	-51	Enthalpy - baseline, economizer
h_{os}	btu/lb	864.35	825	Enthalpy - baseline, superheater
h_s	btu/lb			Enthalpy, superheater output
h_{fsi}	btu/lb	1187.8	1187.8	Enthalpy, superheater inlet
h_v	btu/lb			Enthalpy, vapor
I_E	in-lb-sec^2/rad	8		Engine inertia
I_L	in-lb-sec^2/rad	901		Reflected load inertia - High Gear
		371		Reflected load inertia - Second Gear
J	in-lb/btu	9335	9335	Thermal conversion coefficient
k		1.273	1.273	Ratio of specific heats, superheated steam
K_A	1/°F	3.5×10^{-3}		Damper positioner gain
K_E	in^2-°F/sec	0.3605		Simulated throttle admittance

Symbol	Unit	Value		Description
		SES-5	SES-4	
k_v				Expander velocity constant
K_s	lb/in	228		Bypass spring constant
K_1	in-lb-sec^2/rad^2	7.626×10^{-2}		Load torque - second order coefficient
K_2	in-lb-sec/rad	-0.0189		Load torque - speed coefficient
L_b	in.	739	265	Length of boiler
L_e	in.	538	336	Length of economizer
L_s	in.	240	240	Length of superheater
m_{DP}	lb-sec^2/in	2.163×10^{-4}		Mass of bypass valve
m_{fb}	lb			Mass of fluid, boiler
m_{fe}	lb	1.7	0.28	Mass of fluid, economizer
m_{fs}	lb	4.20×10^{-2}	2.08×10^{-2}	Mass of fluid, superheater
m_{mb}	lb	39.3×0.75	20	Mass of metal, boiler
m_{me}	lb	28.4×0.75	32.5	Mass of metal, economizer
m_{ms}	lb	7.8×0.75	22	Mass of metal, superheater
NTU_b		1.10		Heat transfer units, boiler
NTU_e		1.10		Heat transfer units, economizer
NTU_s		0.12		Heat transfer units, superheater
P_b	psia			Boiler pressure

Symbol	Unit	Value SES-5	 SES-4	Description
P_c	psia	20		Condenser pressure
P_{DP}	lb/in^2			Pressure, damping chamber
P_{ei}	psig			Pressure, economizer inlet
P_{eo}	psia			Pressure, economizer outlet
P_{fs}	psia			Average pressure, superheater
P_M	psia			Pressure, steam manifold
P_p	lb/in^2			Pressure, pump output
P_s	psia			Pressure, superheater outlet
P_s^*	psia	1000		Pressure, nominal, superheater outlet
Q_{gmb}	btu/sec			Heat flow, gas-to-metal, boiler
Q_{gme}	btu/sec			Heat flow, gas-to-metal, economizer
Q_{gms}	btu/sec			Heat flow, gas-to-metal, superheater
Q_{mfb}	btu/sec			Heat flow, metal-to-fluid, boiler
Q_{mfe}	btu/sec			Heat flow, metal-to-fluid, economizer
Q_{mfs}	btu/sec			Heat flow, metal-to-fluid, superheater
R_B		2.0		Variable-speed drive ratio - blower drive
R_p		0.3-0.9		Variable-speed drive ratio - pump drive

Symbol	Unit	Value SES-5	 SES-4	Description
R_s	in/^oR	1027.4	1027.4	Gas constant, superheated steam
R_v	in/^oR	1027.4	1024.4	Gas constant, vapor, superheater
T_E	in-lb			Torque output, expander
T_{fb}				Fluid temperature, boiler, average
T_{fe}	°F			Fluid temperature, economizer, average
T_{fei}	°F	220	220	Fluid temperature, economizer inlet
T_{feo}	°F			Fluid temperature, economizer outlet
T_{fs}	°F			Fluid temperature, superheater, average
T_{fsi}	°F			Fluid temperature, superheater inlet
T_g	°F	3200	3060	Gas temperature, burner output
T_{gbi}	°F			Gas temperature, boiler inlet
T_{gbo}	°F			Gas temperature, boiler outlet
T_{gei}	°F			Gas temperature, economizer inlet
T_{geo}	°F			Gas temperature, economizer outlet
T_{gsi}	°F			Gas temperature, superheater inlet
T_{gso}	°F			Gas temperature, superheater outlet

Symbol	Unit	Value SES-5	 SES-4	Description
T_L	in-lb			Load torque
T_{mb}	°F			Metal temperature, boiler, average
T_{me}	°F			Metal temperature, economizer, average
T_{ms}	°F			Metal temperature, superheater, average
T_s	°R	1460		Superheater outlet temperature
$T_s{}^*$	°R	1460		Nominal superheater outlet temperature
u_{fb}	btu/(sec in^2-°F)	1.929×10^{-2}	1.929×10^{-2}	Heat transfer coefficient, fluid side, boiler
u_{fe}	btu/(sec-in^2-°F)			Heat transfer coefficient, fluid side, economizer
U_{fs}	btu/lb			Fluid internal energy - superheater
u_{fs}	btu/sec-in^2-°F			Heat transfer coefficient, fluid side, superheater
u_{gb}	btu/sec-in^2-°F			Heat transfer units, boiler, gas side
u_{ge}	btu/sec-in^2-°F			Heat transfer coefficient, gas side, economizer
u_{gs}	btu/sec-in^2-°F			Heat transfer coefficient, gas side, superheater
U_{fb}	btu/lb			Internal energy, fluid, boiler

Symbol	Unit	Value		Description
		SES-5	SES-4	
U_L	btu/lb			Internal energy, liquid, boiler
V_b	in^3	142.1	35	Volume of boiler
V_{fb}	in^3/lb			Specific volume, fluid, boiler
V_L	in^3/lb	37.67	37.67	Mean specific volume of liquid, boiler
V_M	in^3	40		Manifold volume
V_s	in^3	46.1	30	Superheater volume
W	lb/sec			Fluid flow, expander
W_F	lb/sec	0.0277	0.0174	Fuel flow rate
W_{fbo}	lb/sec			Fluid flow, boiler outlet
W_{fe}	lb/sec			Fluid flow, economizer
W_{fe}^*	lb/sec	0.333	0.2153	Nominal fluid flow, superheater
W_{fei}	lb/sec			Fluid flow, economizer inlet
W_{feo}	lb/sec			Fluid flow, economizer outlet
W_{fs}	lb/sec			Average fluid flow rate, superheater
W_{fs}^*	lb/sec	0.333		Nominal fluid flow, superheater
W_g	lb/sec	0.537	0.3472	Gas flow rate
W_g^*	lb/sec			Blower delivery characteristics
W_{gb}^*	lb/sec	0.537	0.3472	Reference gas flow rate - boiler

Symbol	Unit	Value SES-5	 SES-4	Description
W_{ge}^*	lb/sec	0.537	0.3472	Reference gas flow rate - economizer (to be set until T_{fso} = 1000°F)
W_{gs}^*	lb/sec	0.537	0.3472	Reference gas flow rate - superheater
W_p	lb/sec			Pump output flow
W_R	lb/sec			Bypass flow
W_s	lb/sec			Steam flow, superheater outlet
x	in.	0-2.250		Bypass valve travel
α	degrees	0-60		Admission angle
ΔF	lb			Sum of bypass valve forces
Δh_{fe}	btu/lb			Enthalpy difference, fluid economizer
Δh_{ge}	btu/lb			Enthalpy change, economizer gas
ΔP_b	lb/in^2			Pressure drop, boiler
ρ_{fb}	lb/in^3			Average fluid density, boiler
ρ_{fb}^*	lb/in^3	1.389×10^{-3}	1.389×10^{-3}	Mean density of fluid in boiler
ρ_{fei}	lb/in^3	0.0346		Fluid density, economizer inlet
ρ_{fs}	lb/in^3			Fluid density, superheater
ρ_s^*	lb/in^3	6.944×10^{-4}	6.944×10^{-4}	Mean density, superheater

Symbol	Unit	Value		Description
		SES-5	SES-4	
θ	rad			Expander rotation
$\dot{\theta}$	rad/sec			Expander speed
$\ddot{\theta}$	rad/sec^2			Expander acceleration
$\dot{\theta}_B$	rad/sec			Blower speed
$\dot{\theta}_p$	rad/sec			Water pump speed
ϵ_b				Heat exchanger effectiveness coefficient, boiler
ϵ_e				Heat exchanger effectiveness coefficient, economizer
ϵ_s				Heat exchanger effectivness coefficient, superheater
τ_{eh}		8.7	24	Economic enthalpy time constant at nominal flow
τ_{bh}	sec	15.0	19.0	Boiler enthalpy time constant at nominal flow
τ_{sh}	sec	4.0	27	Superheater enthalpy time constant, at nominal flow
τ_{sp}	sec	0.068	0.068	Superheater, pressure buildup time constant
τ_{wb}	sec	0.008	0.008	Boiler, flow inertial time constant
ξ_{RP}		0.707		Variable drive damping ratio
ω_{RP}	rad/sec	3.14		Variable drive frequency response

SECTION 5

CONTROL-MODE SIMULATION EXPERIMENTS

In October 1971 the flow control mode concept was evaluated using the SES Model 4 burner and vapor-generator test setup. The experiments were designed to simulate, as much as practical, the closed-loop, hybrid-computer, design studies. Because of the limitations of the available experimental, vapor-generator, test bed, only the temperature control loop was implemented on the experimental test setup. The feedwater system and the steam throttle were controlled manually during the tests to maintain the vapor-generator pressure at the desired level. The temperature control of the vapor-generator outlet is the most critical control problem, because of the large thermal lag presented by the vapor-generator thermal inertia. The experimental results indicated an approximate 66°F control band for large-step fluid transients from 40 to 100 percent flow levels. The previously mentioned computer predictions indicated a 75°F control band for the same gain settings. This is considered to be good agreement between the hybrid-computer prediction and the experimental observations and indicates that the computer is an established tool for the control design studies.

In the following section, first the control-mode simulation experimental test setup is described in detail. Prior to the closed-loop steam-generator control tests, preliminary hardware design tests were conducted. These results are included in the section prior to the closed-loop steam-generator test results. In addition to the closed-loop testing, open-loop dynamic-response tests were conducted on the steam generator during the test period. The results of these transients tests are compared with hybrid-computer results and indicate good agreement between the analytical model and the experimental results, thus again verifying the accuracy of the hybrid computer model.

5.1 EXPERIMENTAL-SYSTEM DESCRIPTION

The general schematic of the control-mode simulation test setup is shown in Figure 5-1. The setup simulates the predictive flow-control mode of the vapor-generator outlet-temperature control. The basic system operation is as follows.

The feedwater flow is measured and this information is used to control the operating level of the burner. Relying on the known plant characteristics, a prediction curve is established for the open-loop control of the burner. At any flow level, the heat input to the vapor generator is adjusted to the appropriate steady-state level necessary to produce the desired steam-generator outlet temperature. The response of this predictive control loop can be made rapid compared to the thermal inertia of the vapor generator. Thus, the predictive control loop re-

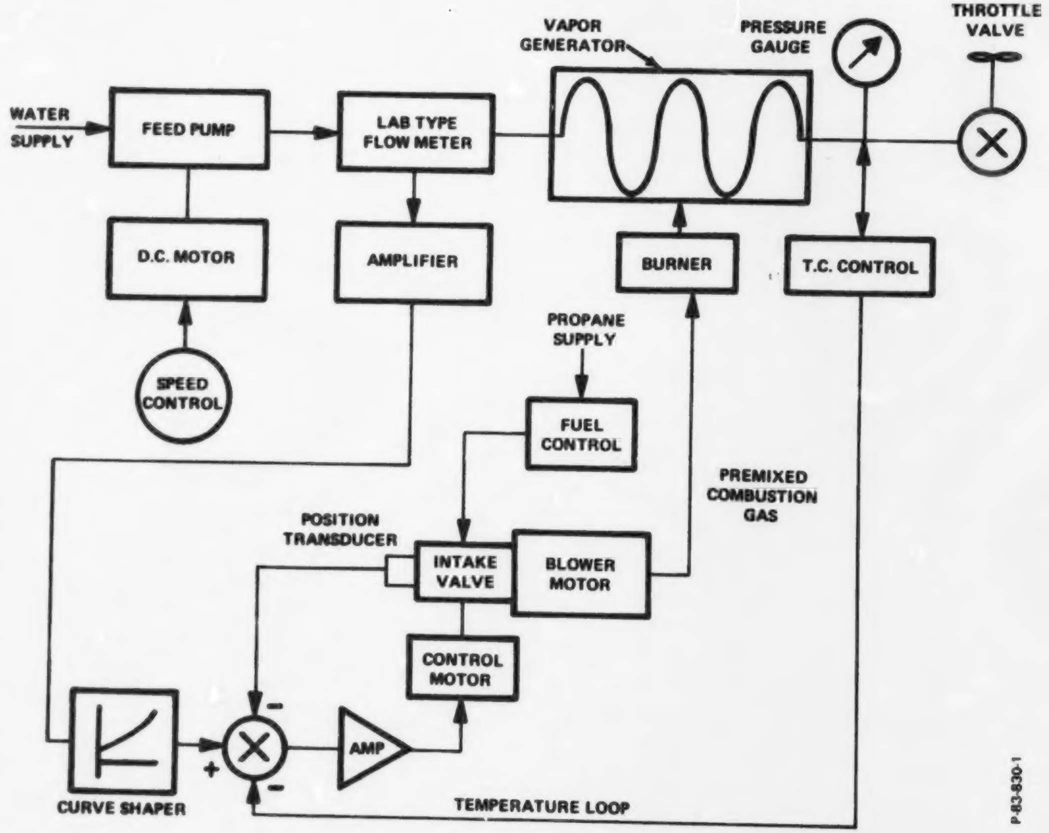
VAPOR GENERATOR
PRESSURE GAUGE
THROTTLE VALVE
WATER SUPPLY
FEED PUMP
LAB TYPE FLOW METER
D.C. MOTOR
AMPLIFIER
BURNER
T.C. CONTROL
SPEED CONTROL
PROPANE SUPPLY
FUEL CONTROL
PREMIXED COMBUSTION GAS
POSITION TRANSDUCER
INTAKE VALVE
BLOWER MOTOR
CONTROL MOTOR
AMP
+
-
-
CURVE SHAPER
TEMPERATURE LOOP
P-83-830-1

Figure 5-1 - Control-Mode Simulation Block Diagram

sponds to rapid large-scale changes in power levels as anticipated to occur during the operation of an automotive power plant. In order to correct for errors in predictions that may be caused by initial manufacturing tolerances of the plant, or because of changes in plant operating characteristics with time, a closed-loop temperature controller is added to the control scheme. The temperature controller measures the actual outlet temperature of the vapor generator, compares it to a desired set point and appropriately adjusts the combustion gas delivery. This controller may operate in a proportional control mode at the relatively low gain that is tolerable with the slow thermal response of the vapor generator. The controller will increase the burner heat output when the outlet temperature is below the desired set point and conversely decrease the burner output when the outlet temperature exceeds the set point. This control is secondary and operates at a much slower rate than the predictive control system.

The test setup, as shown in Figure 5-1, utilized the SES Model 4 vapor-generator test unit to the maximum extent. The feedwater is supplied through a variable-speed pump which is manually operated through a speed control. The flow delivered to the vapor generator was measured using a laboratory-type flowmeter. The flow information then was processed through a curve shaper and used to adjust the blower inlet valve position using an electric positioner. The blower motor operated at a constant speed. A separate fuel control, which is a part of the SES Model 4 for test setup, maintained fuel/air ratio. In order to maintain operating safety at or near critical gains, the intake valve was designed with a leakage path to prevent a flameout. The temperature controller was a commercially available process instrument and operated in a proportional mode only.

5.2 SIMULATION-HARDWARE-DESIGN TEST RESULTS

Prior to installation of the control hardware and mating with the SES Model 4 vapor generator, a number of design verification tests were conducted at the Bendix Research Laboratories to assure proper functioning of the control hardware and thus minimize the time requirements placed on the already heavily scheduled SES experimental test setup.

The general block diagram of this test setup is shown in Figure 5-2. The main combustion-gas control element is the inlet shutter assembly attached to the blower inlet. An electric positioning loop is used to set the shutter position to the desired level. In order to improve the overall linearity of the control system, the shutter was designed to produce an outlet area proportional to the square of the shutter position. The shutter and blower assembly is shown in Figure 5-3. The valve has 10 inlet orifices that are equilateral triangles at all times. As the inner orifices are rotated with relationship to the outer rectangular orifices, the equilateral triangular shape is maintained at all shutter positions.

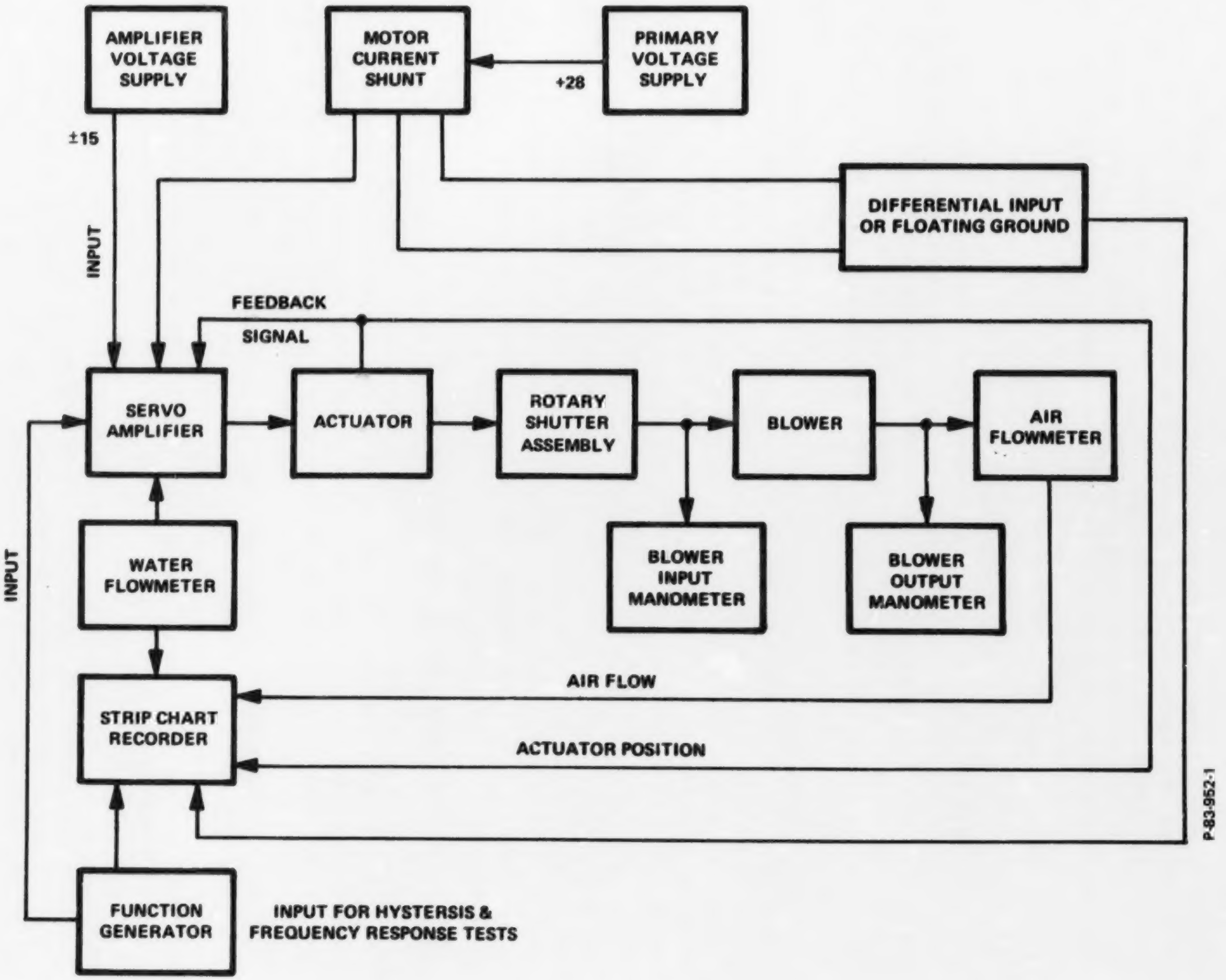
AMPLIFIER VOLTAGE SUPPLY
MOTOR CURRENT SHUNT
PRIMARY VOLTAGE SUPPLY
+28
±15
INPUT
DIFFERENTIAL INPUT OR FLOATING GROUND
FEEDBACK
SIGNAL
SERVO AMPLIFIER
ACTUATOR
ROTARY SHUTTER ASSEMBLY
BLOWER
AIR FLOWMETER
INPUT
WATER FLOWMETER
BLOWER INPUT MANOMETER
BLOWER OUTPUT MANOMETER
AIR FLOW
STRIP CHART RECORDER
ACTUATOR POSITION
P-83-952-1
FUNCTION GENERATOR
INPUT FOR HYSTERSIS & FREQUENCY RESPONSE TESTS

Figure 5-2 - Schematic of Rotary-Shutter Test Setup

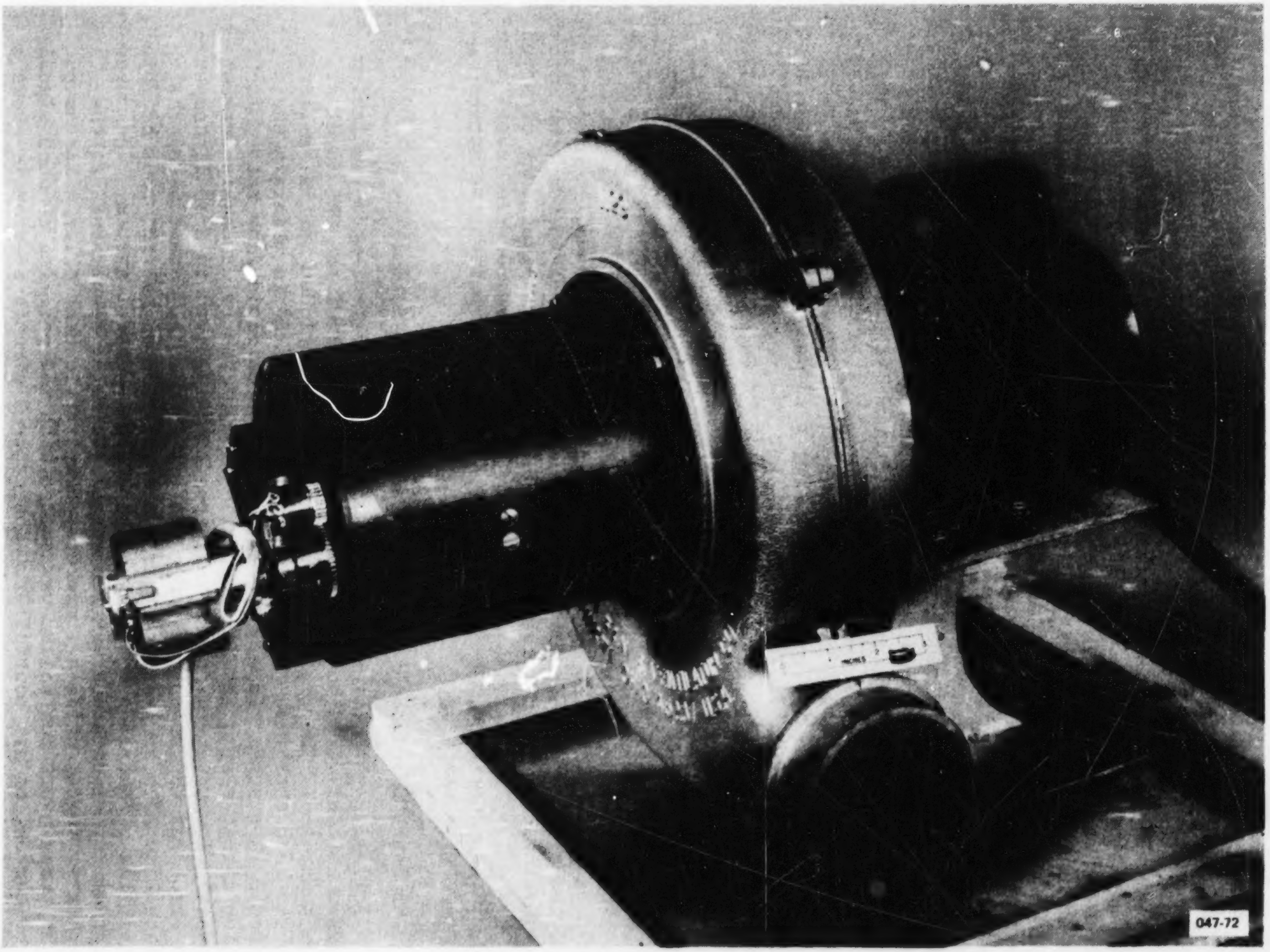

Figure 5-3 - Shutter and Blower Assembly

Blower outflow characteristics, as a function of static pressure, are shown in Figure 5-4. This curve was used for the combustion-air control design.

Experimental results describing blower outflow versus shutter positions are shown in Figure 5-5. The figure indicates a good linearity of the air control system in the operating range. Dynamic tests were also conducted to verify the predicted stability and frequency response of the shutter positioner loop. The block diagram of the shutter-position stability analysis is shown in Figure 5-6. Using this linearized model, the analytical prediction of the frequency response for the shutter position and loop is shown in Figure 5-7 indicating approximately 14 Hz at the -3 db point. A frequency-response test of the actual positioner servo was subsequently made. The results are given as the amplitude ratio versus frequency response plot in Figure 5-8. From this plot it is readily seen that the -3 db point occurs at approximately 13.5 Hz and is in excellent agreement with the prior calculations. The system response to a step input was also tested. The test data was recorded and the chart is shown in Figure 5-9. The rotary shutter was commanded to close and then to open, in each case, through an angle of 23 degrees. The slew rate achieved was 320 degrees per second with very good linearity and little overshoot. A 30 millisecond delay in the response of the air flow to the shutter movement may also be seen in the figure. The small reversal in motor current to correct the slight overshoot is also apparent.

To simulate anticipated input from the feedwater transducer, a turbine-type flowmeter was connected to a tap-water source and its output connected to the control-servo amplifier. The action of the shutter with this input was evaluated only qualitatively. The shutter actions observed were deemed satisfactory. Additional adjustments were deferred until such time as tests could be made at SES in conjunction with the burner and steam generator.

5.3 CLOSED-LOOP STEAM-GENERATOR TEST RESULTS

Following the design test evaluations, the control-mode simulation hardware was delivered to SES and installed to control the SES Model 4 vapor generator. The experimental test program included initial calibration tests to establish the shutter position required to maintain the desired outlet steam temperature as a function of fluid flow rate. It was found that a straight line approximation of the relationship between feedwater flow rate and intake valve position resulted in a small temperature error for the operating range tested. It was the intention of the test to have such an inaccuracy in the prediction signal and thus be able to test the closed-loop corrective temperature control system. The superheater outlet temperature was monitored as a metal temperature at the superheater outlet using a commercial temperature controller. The output of the temperature controller was summed with the position command signal of the combustion-air controller. The control circuit diagram is shown in Figure 5-10, and shows that the temperature error summing was accomp-

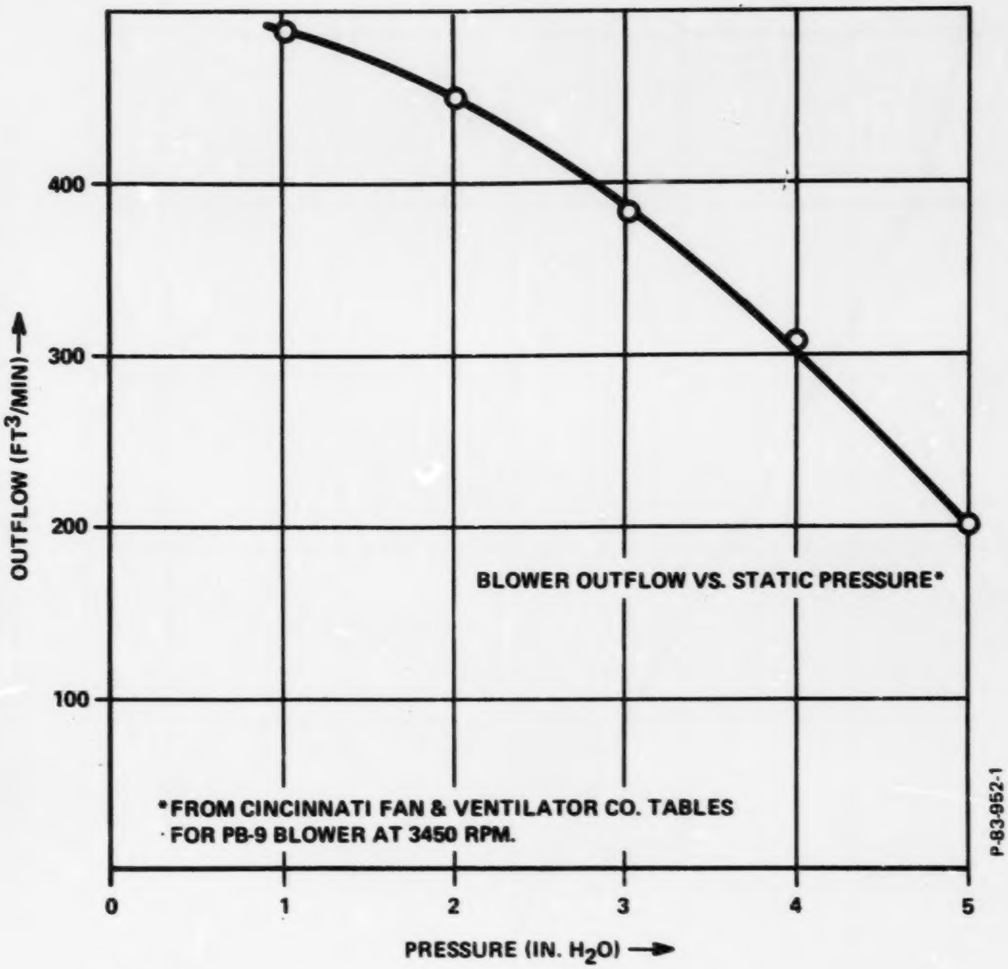

Figure 5-4 - Blower Outflow versus Static Pressure

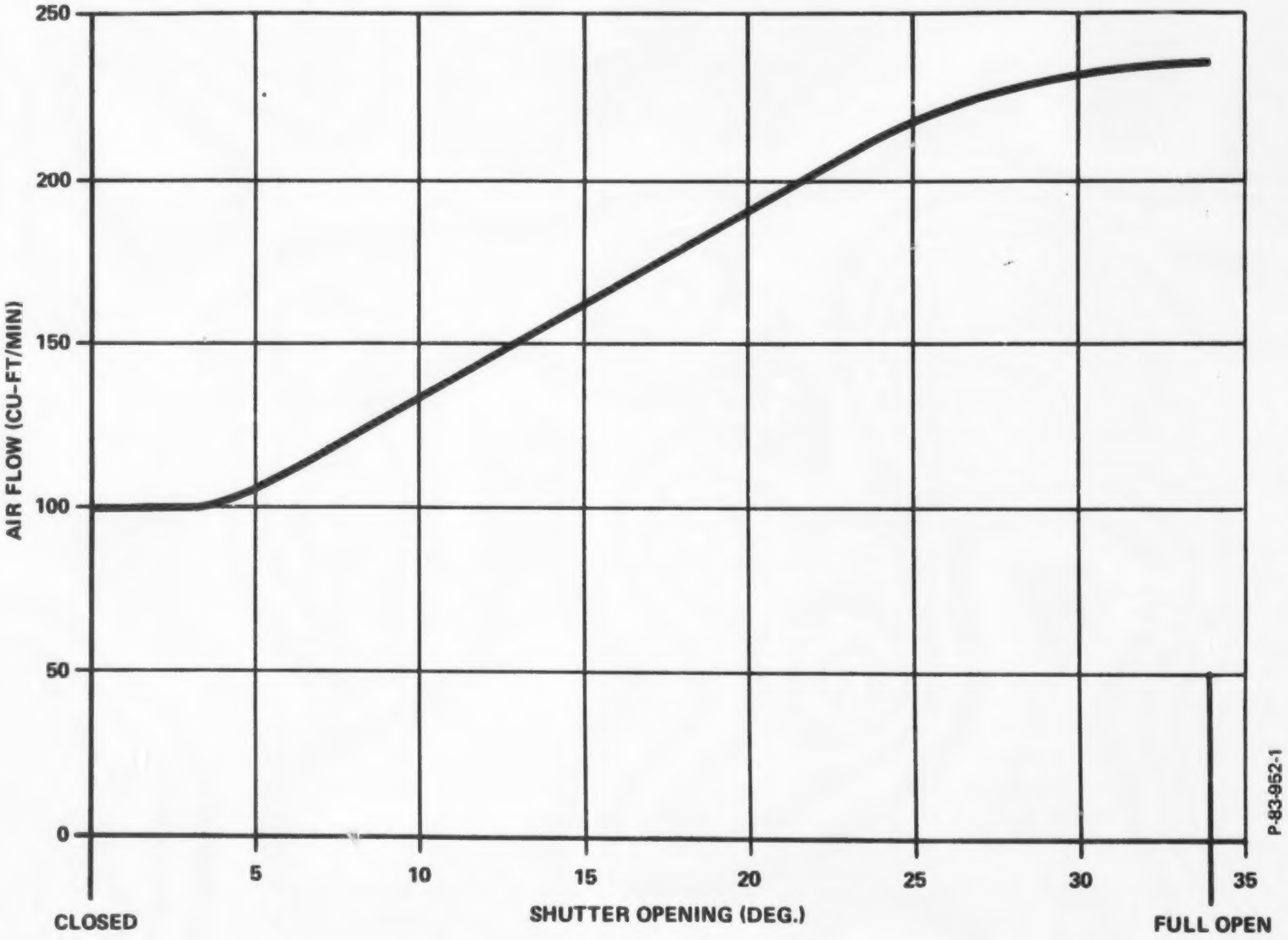

Figure 5-5 - Blower Outflow versus Shutter Position

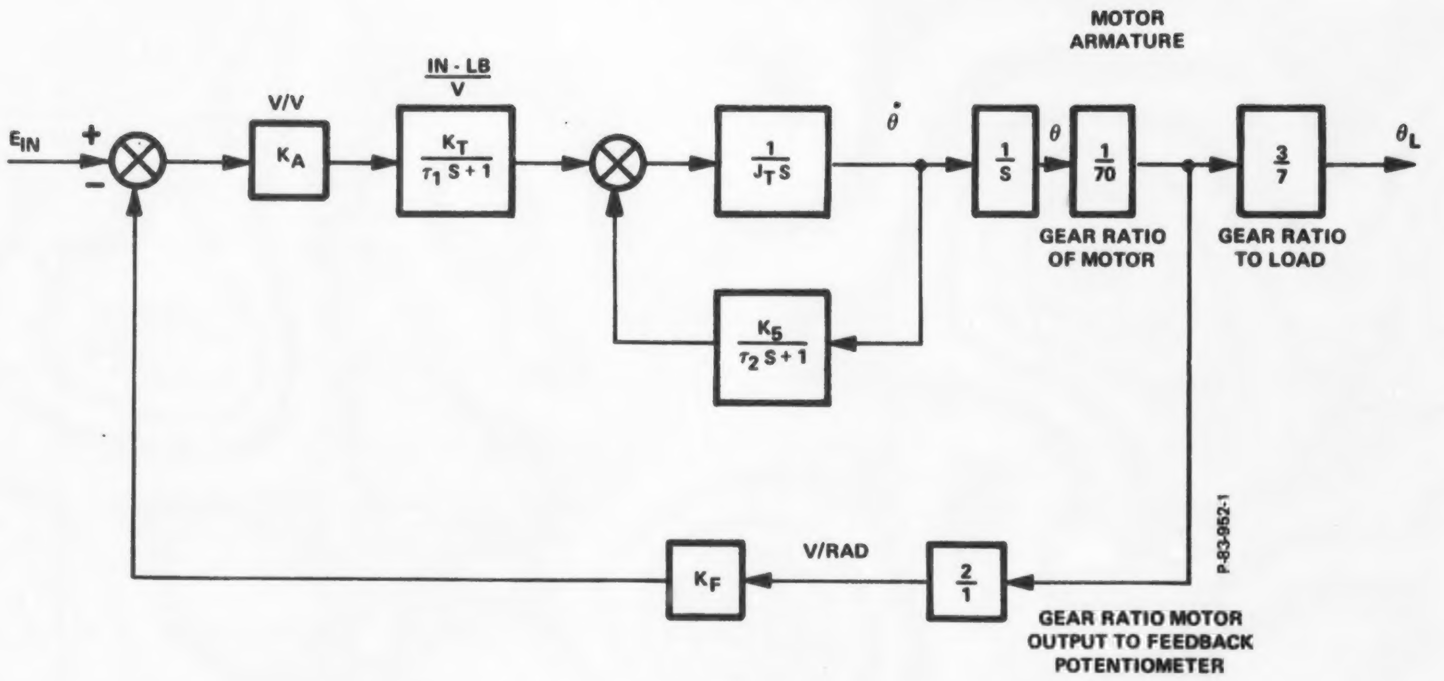
MOTOR
ARMATURE
IN - LB / V
V/V
E_{IN}
+
−
K_A
$\frac{K_T}{\tau_1 S+1}$
$\frac{1}{J_T S}$
$\dot{\theta}$
$\frac{1}{S}$
θ
$\frac{1}{70}$
$\frac{3}{7}$
θ_L
GEAR RATIO
OF MOTOR
GEAR RATIO
TO LOAD
$\frac{K_5}{\tau_2 S+1}$
P-83-952-1
V/RAD
K_F
$\frac{2}{1}$
GEAR RATIO MOTOR
OUTPUT TO FEEDBACK
POTENTIOMETER

Figure 5-6 - Block Diagram of Stability Analysis of Shutter Positioner

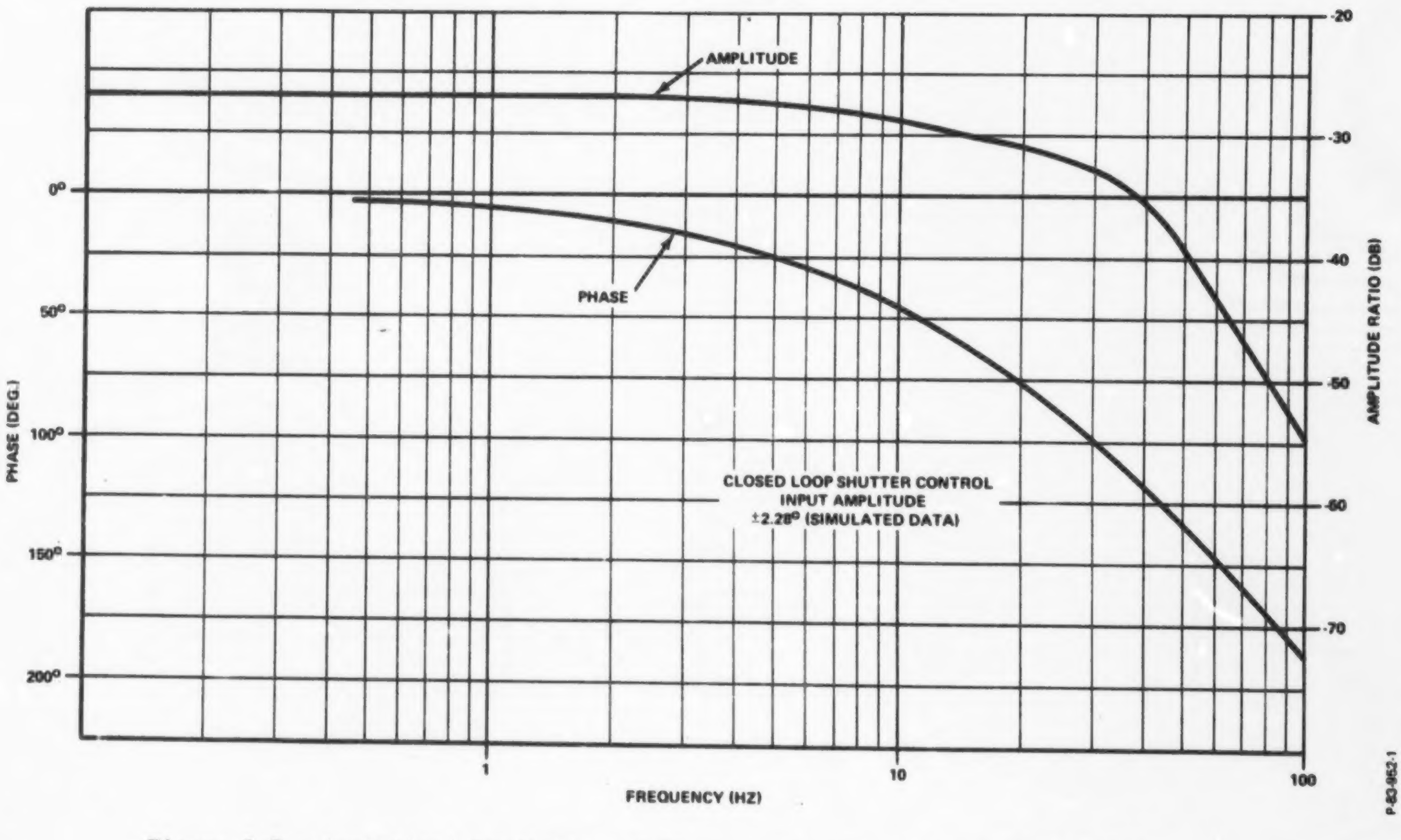

Figure 5-7 - Analytical Prediction of Frequency Response of Shutter Positioner

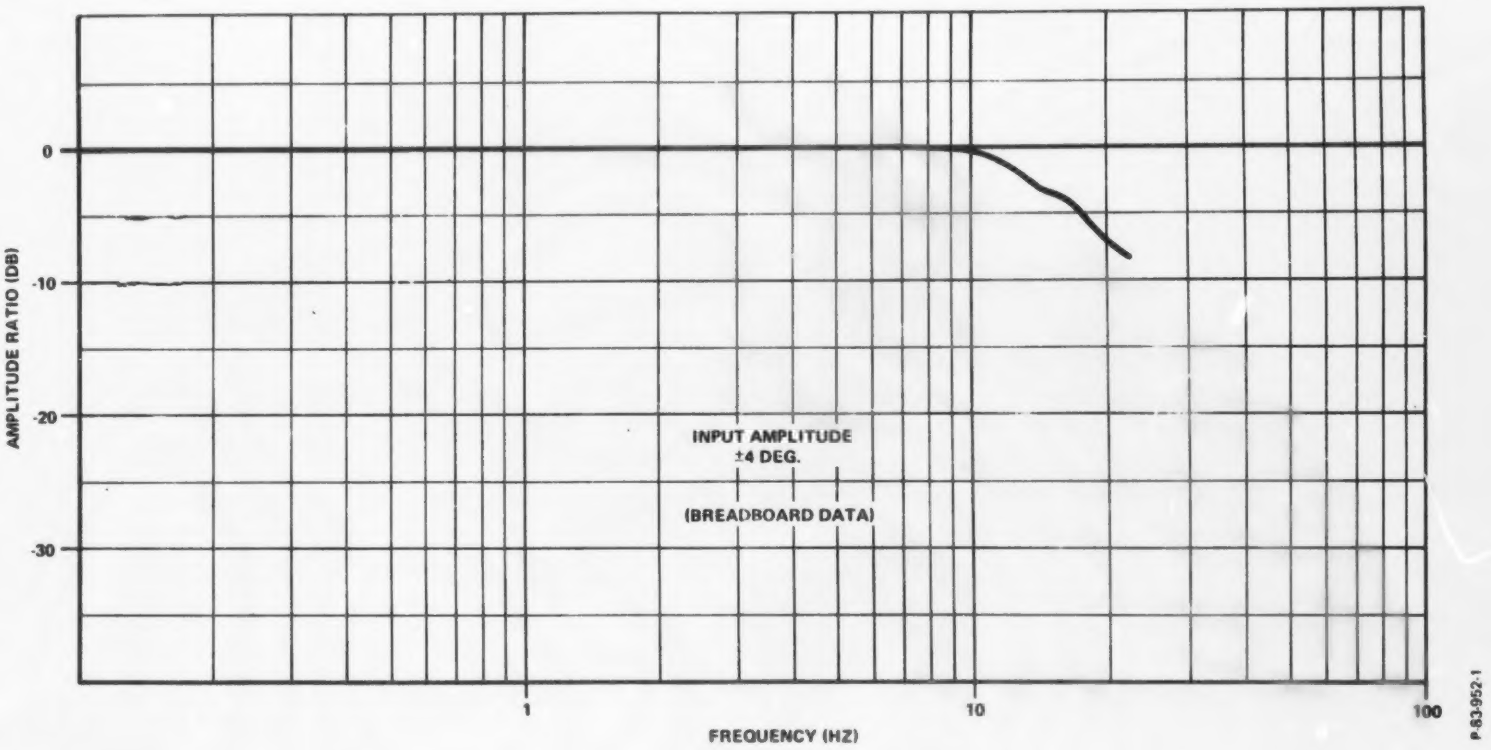

Figure 5-8 - Experimental Determination of Frequency Response of Shutter Positioner

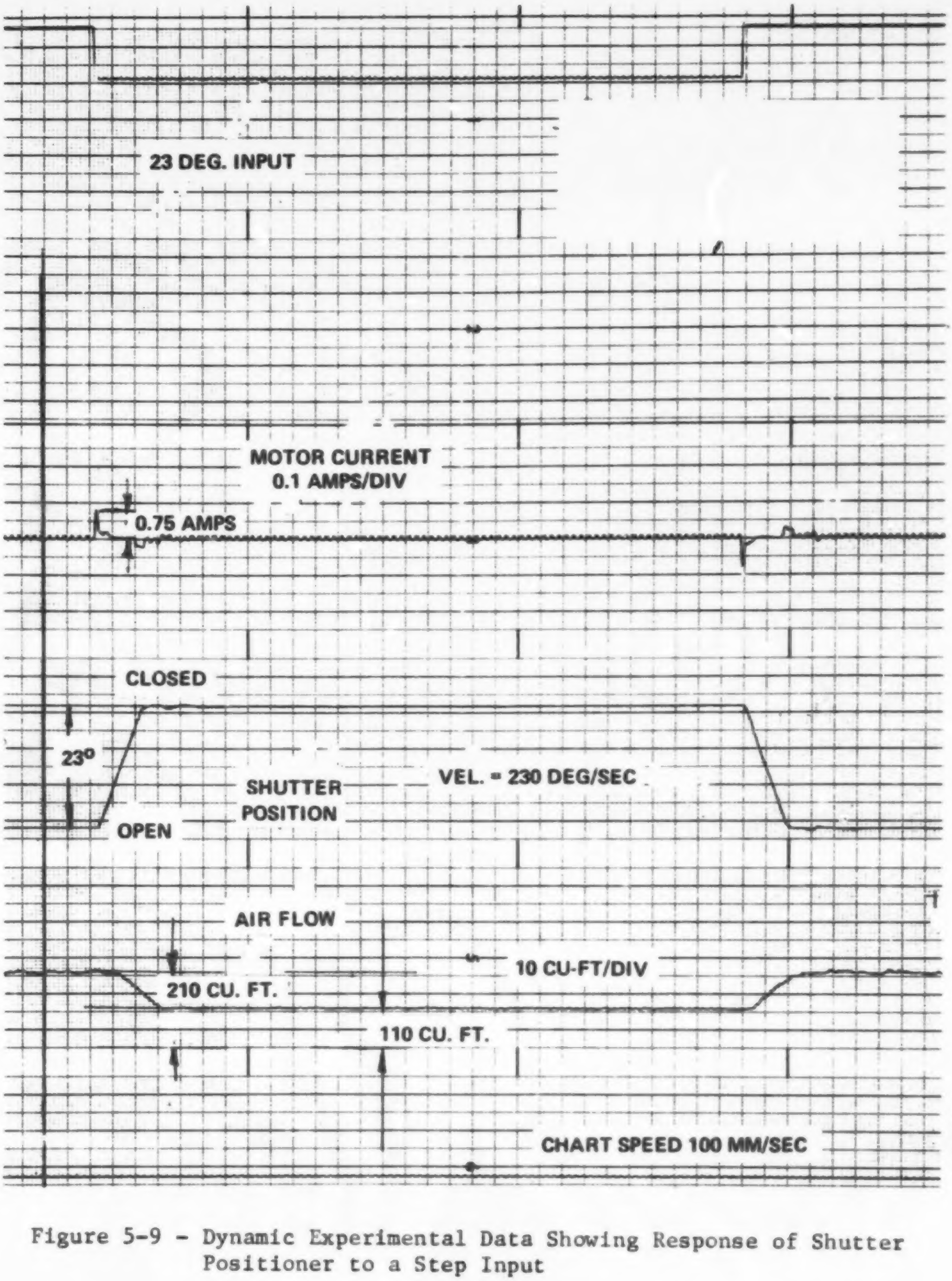

Figure 5-9 - Dynamic Experimental Data Showing Response of Shutter Positioner to a Step Input

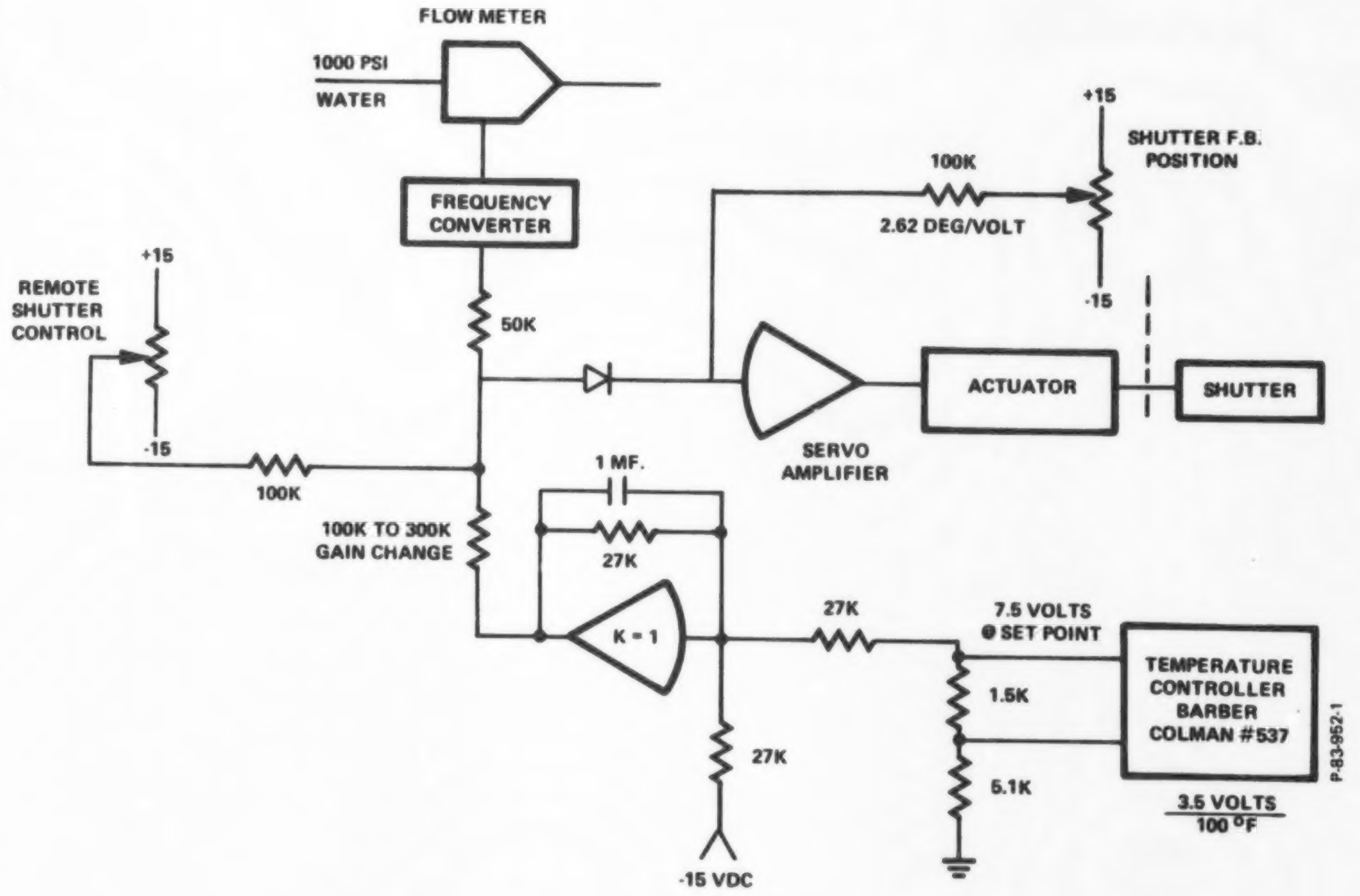
FLOW METER
1000 PSI
WATER
FREQUENCY CONVERTER
50K
REMOTE SHUTTER CONTROL
+15
-15
100K
100K TO 300K GAIN CHANGE
1 MF.
27K
K = 1
27K
-15 VDC
27K
7.5 VOLTS @ SET POINT
1.5K
5.1K
TEMPERATURE CONTROLLER BARBER COLMAN #537
3.5 VOLTS / 100 °F
P-83-952-1
SERVO AMPLIFIER
ACTUATOR
SHUTTER
100K
2.62 DEG/VOLT
+15
-15
SHUTTER F.B. POSITION

Figure 5-10 - Control Circuit Diagram

lished in such manner that if the superheater outlet temeprature exceeded the temperature set point, the intake valve was to close to a degree proportional to the temperature error. No derivative or integral temperature control signals were needed in the temperature control loop. The proportional control mode was selected in order to maintain the simplest type of control to be used in an automotive power plant.

Figure 5-11 shows the air flow/shutter position curve established for the experimental setup. Again, good linearity is indicated between air flow and water flow. The air flow was measured in arbitrary units defined in terms of the flue-gas differential pressure, as no direct measurement of combustion gases was practical. The estimated air flow control range is approximately 2:1 which is in good agreement with the preliminary open-loop tests conducted at Bendix Research Laboratories.

Following operating qualification tests of the control-mode simulation hardware, open-loop hot testing was conducted to determine the required shutter position for the predictor circuit. The predictor was selected to maintain the superheater outlet temperature at 800°F. The results of these tests are shown in Figure 5-12. Using the open-loop data, the straight-line shutter prediction curve, shown as a function of feedwater flow, was programmed. This simple prediction curve was used in all of the following closed-loop tests. Typical closed-loop data points are superimposed for comparison in Figure 5-12 and indicate slight deviation from the programmed straight line. This is the amount of prediction error that had to be corrected through the closed-loop temperature controller at the various parts of the operating range. As a reference, one millimeter of water-flow error corresponds to approximately 75°F superheater temperature deviation.

The control system, operating over a wider range, will require curve fitting between the predicted shutter position and the feedwater flow rate. The calculated combustion gas flow required to maintain 1000°F steam temperature is shown as a function of steam flow rate in Figure 5-13 for the entire anticipated operating rnage of the steam generator. It appears that the required performance could be achieved by fitting the function generator with three straight lines. This straight-line approximation would not result in prediction errors in excess of the correction capability of a proportional temperature-control loop.

Closed-loop stability of the steam temperature control was evaluated first. After the stability evaluation was completed, large step changes in water flow, corresponding to the total gas-flow control range of the control-mode simulation hardware, were conducted. At the completion of the testing, the proportional gain of the temperature loop was increased until the gain margin of the experimental setup was established. In the following, typical examples of the experimental results are presented.

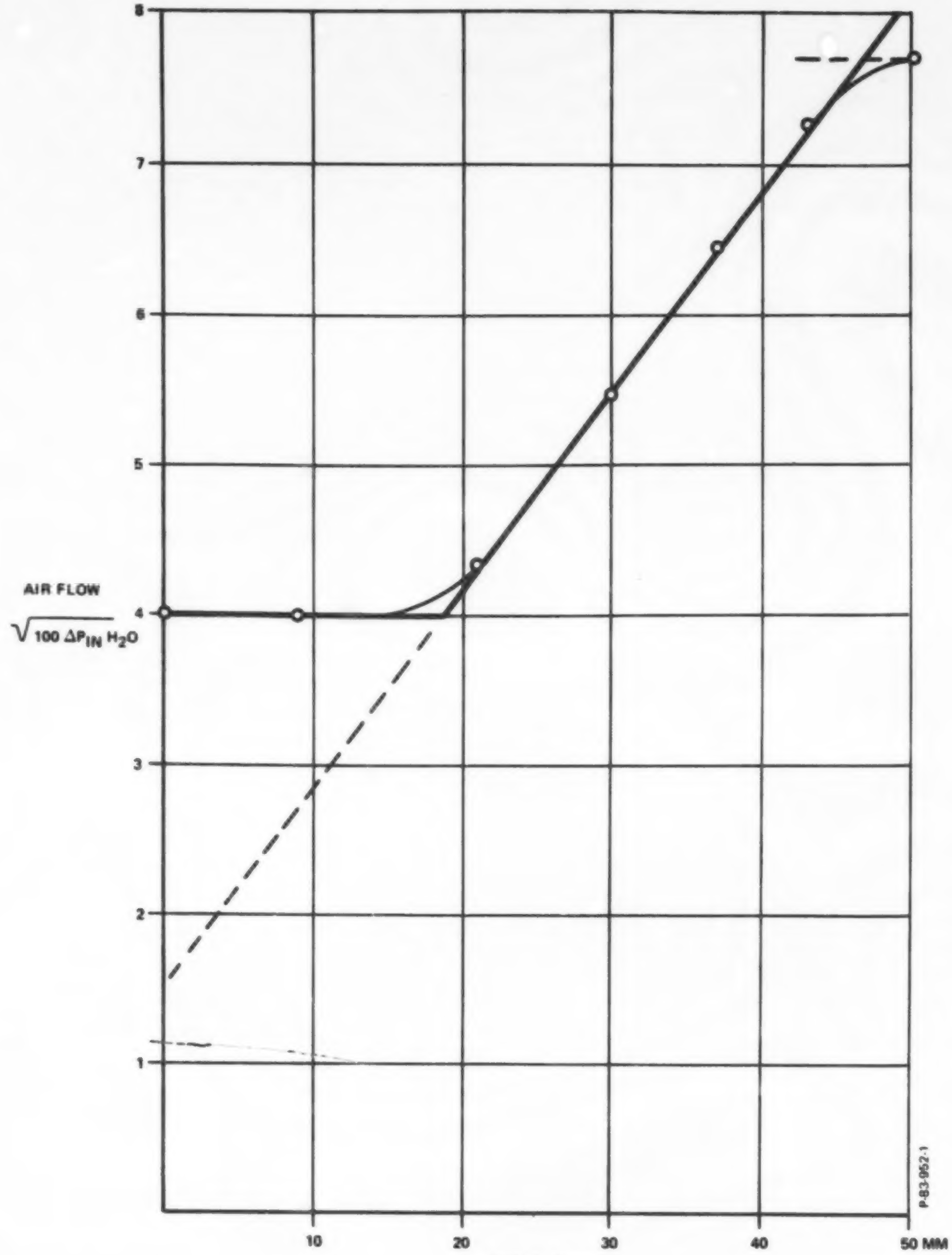

Figure 5-11 - Experimental Results of Airflow-Shutter Position Test

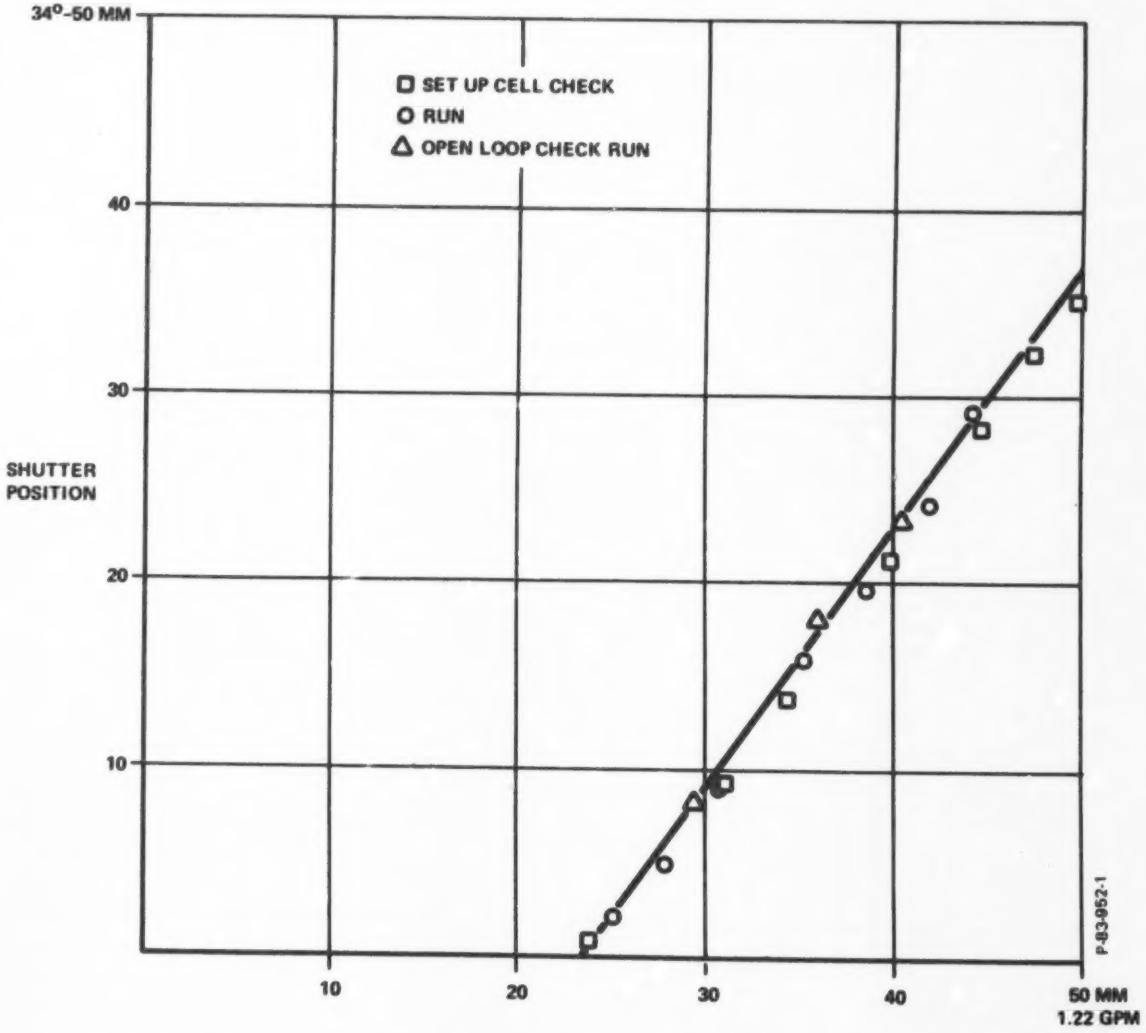

Figure 5-12 - Shutter Position Required to Maintain 800°F Superheater Outlet Temperature as a Function of Feedwater Flow

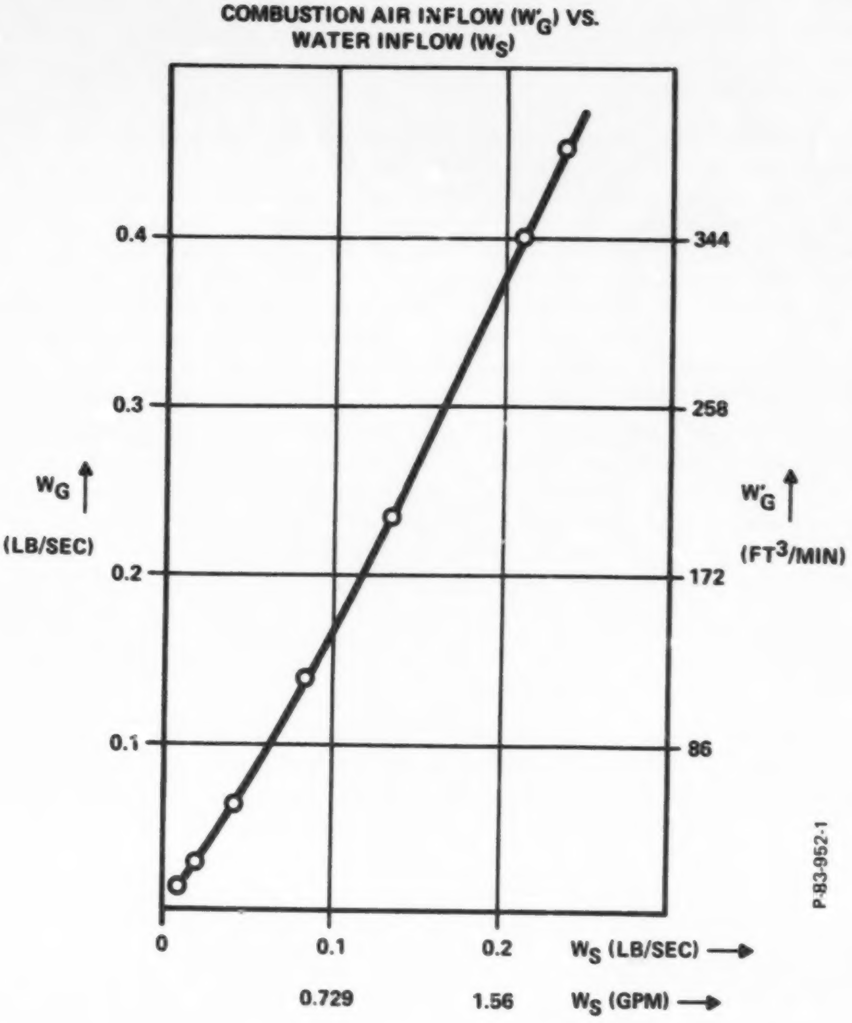

Figure 5-13 - Calculated Combustion-Gas Flow Required to Maintain 1000°F Steam Temperature as a Function of Steam Flow

A small step change in water flow is shown in Figure 5-14 for a reduction in water flow rate. The predictive loop immediately commands a reduction in air intake-valve position. It may be seen that the area of the combustion control valve closely follows the water flow changes. A temperature undershoot of -8°F and a maximum overshoot of +20°F is rapidly damped out. The total shift in the outlet steam temperature is approximately 4°F.

Closed-loop control characteristics of the predictive flow controller, in response to a large step change in water flow, is shown in Figure 5-15. Water flow is increased from the minimum to near the maximum operating level. It again may be observed that the predictor loop commands the combustion-air control area to correspond with water flow changes. A temperature excursion of +60°F overshoot and -6°F undershoot is again rapidly corrected. The total shift of the operating outlet temperature is -6°F for this large step input. Several other steps of input signals were used to verify this stable operation of the control system. In general, the results were similar to the example shown above.

The proportional gain of the temperature loop was increased in two steps to find the critical gain level for the experimental test setup. The critical point was reached at approximately three times the initial gain setting. The operating characteristics at this setting are shown in Figure 5-16. The temperature oscillations are slowly damped out, indicating a closed-loop proportional temperature gain near to the critical system gain at the operating conditions. The overshoot of the system is approximately 80°F and the undershoot is approximately 3°F. These results establish that the operating gain margin for the system corresponds to previous computer predictions.

The experimental closed-loop results presented clearly establish verification of the flow control mode as proposed for the temperature control system, and also that the hybrid computer model is a valid tool for the control system design of the steam generator.

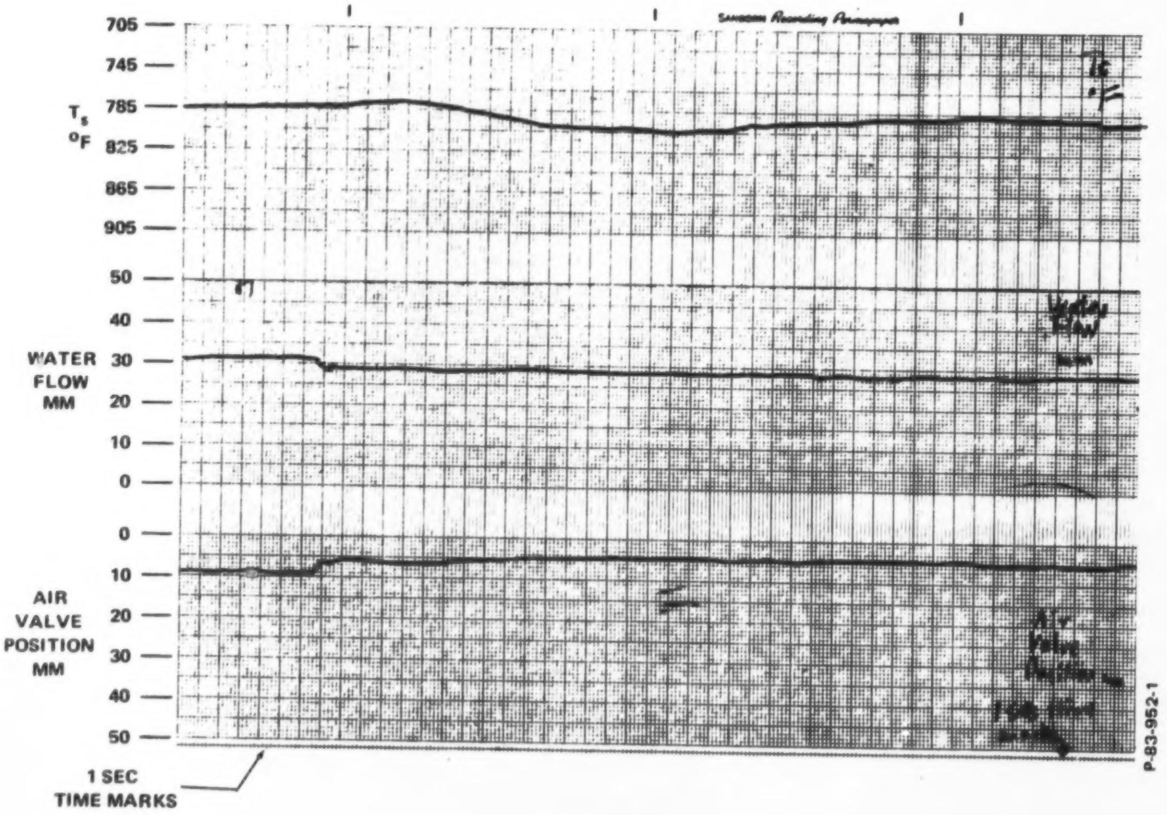

Figure 5-14 - Experimental Closed-Loop Temperature Control, Small Step Input in Water Flow at Design Gain

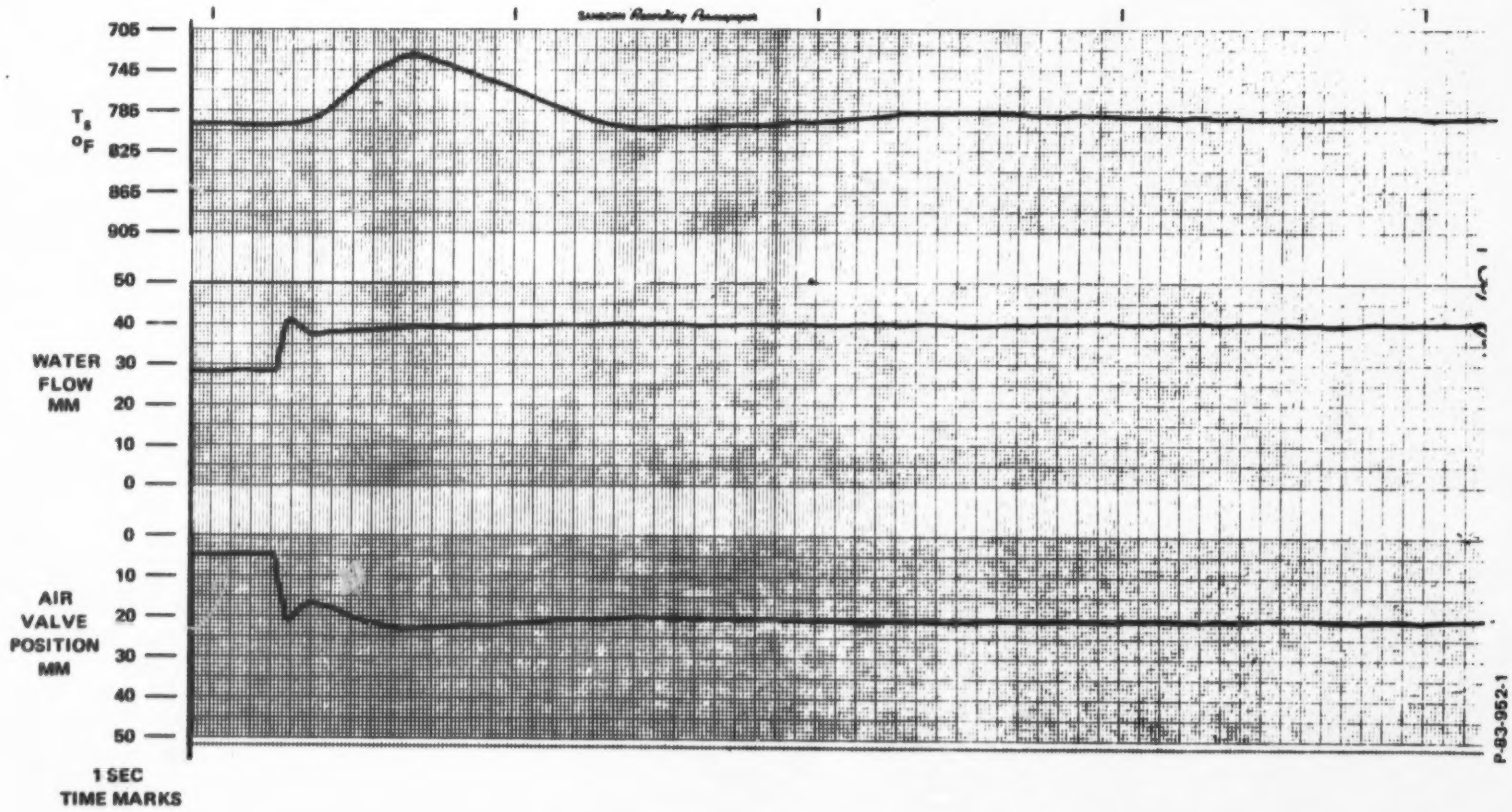

Figure 5-15 - Experimental Closed-Loop Temperature Control, Large Step Input in Water Flow at Design Gain

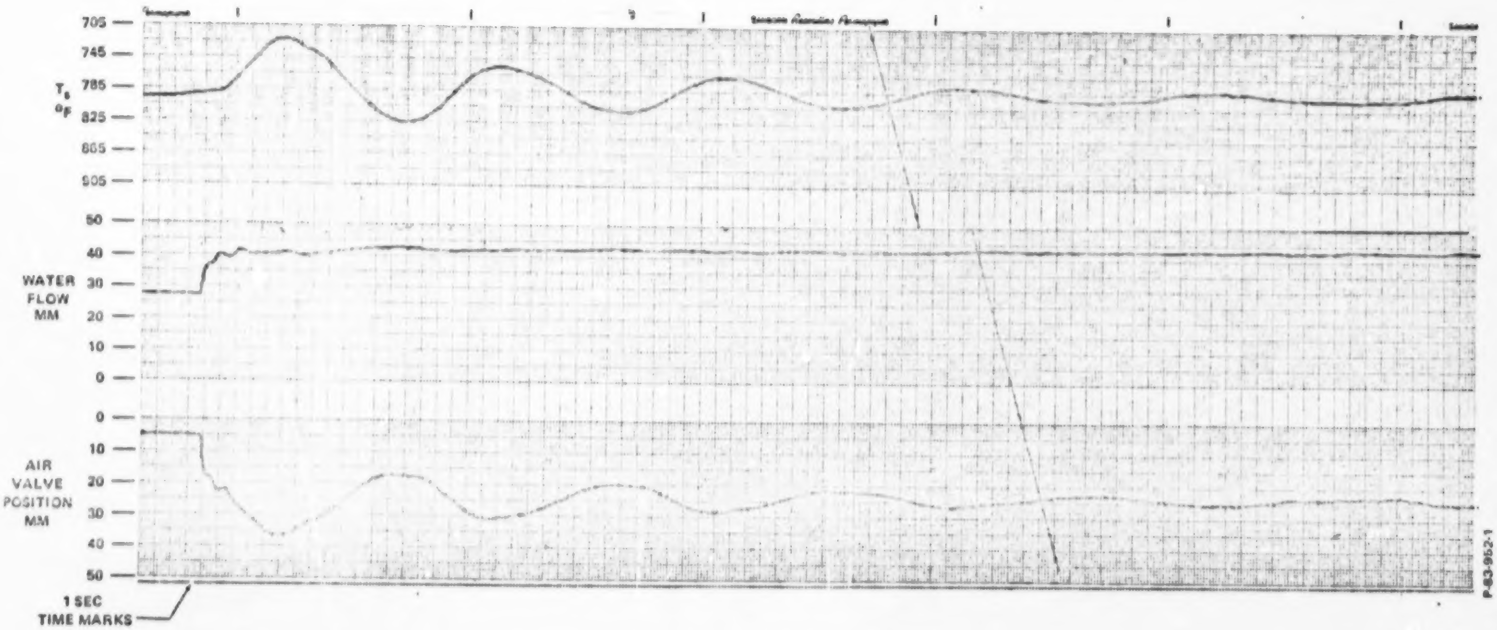

Figure 5-16 - Experimental Closed-Loop Temperature Control, Large Step from Low to High Water Flow near Critical Gain (3X Design)

xxxxxxxxxxxxxxxxxxxx
See following pages
for greater detail.
xxxxxxxxxxxxxxxxxxxx

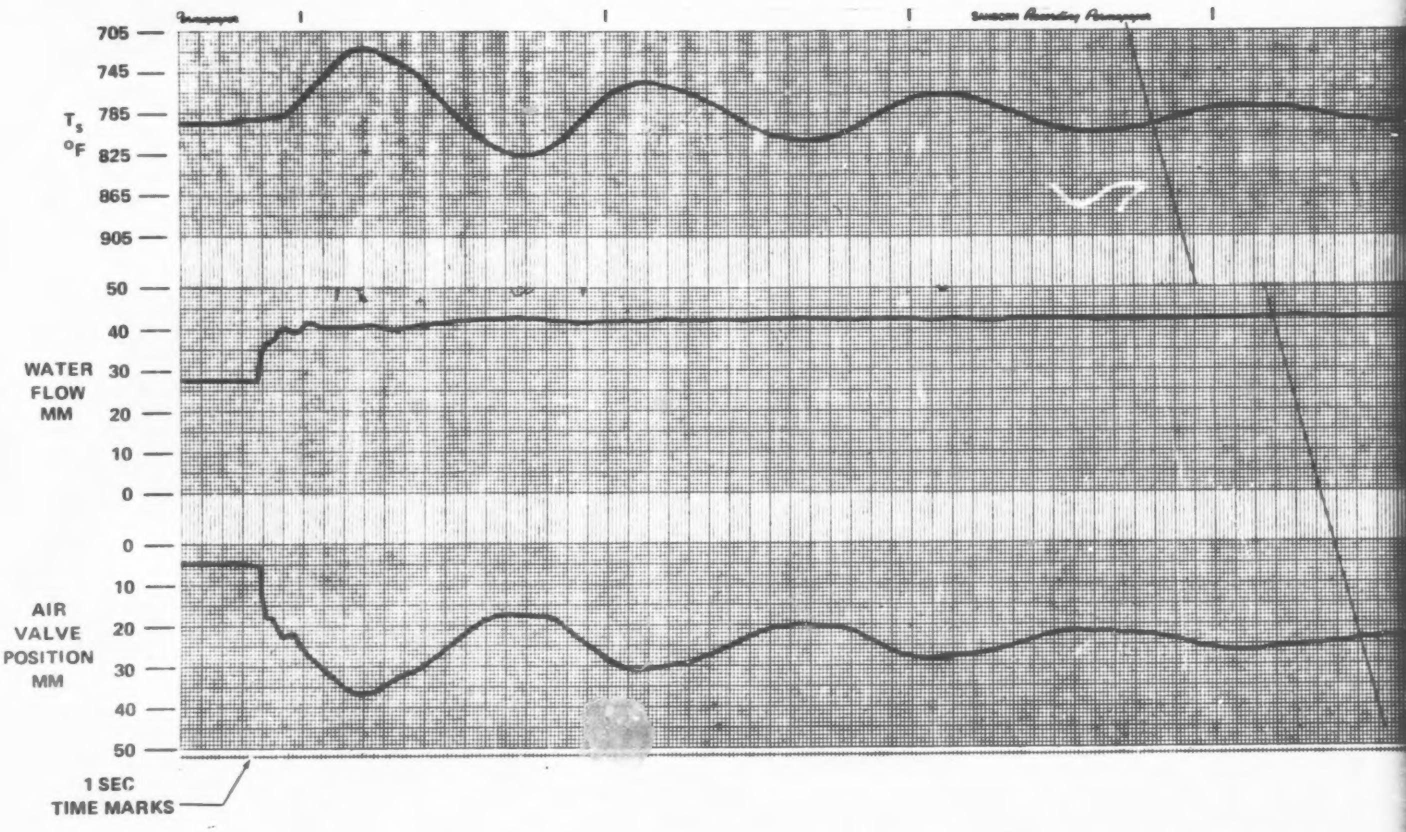

Figure 5-16 - Experimental Closed-Loop Temperature Control, Large
from Low to High Water Flow near Critical Gain (3X

A

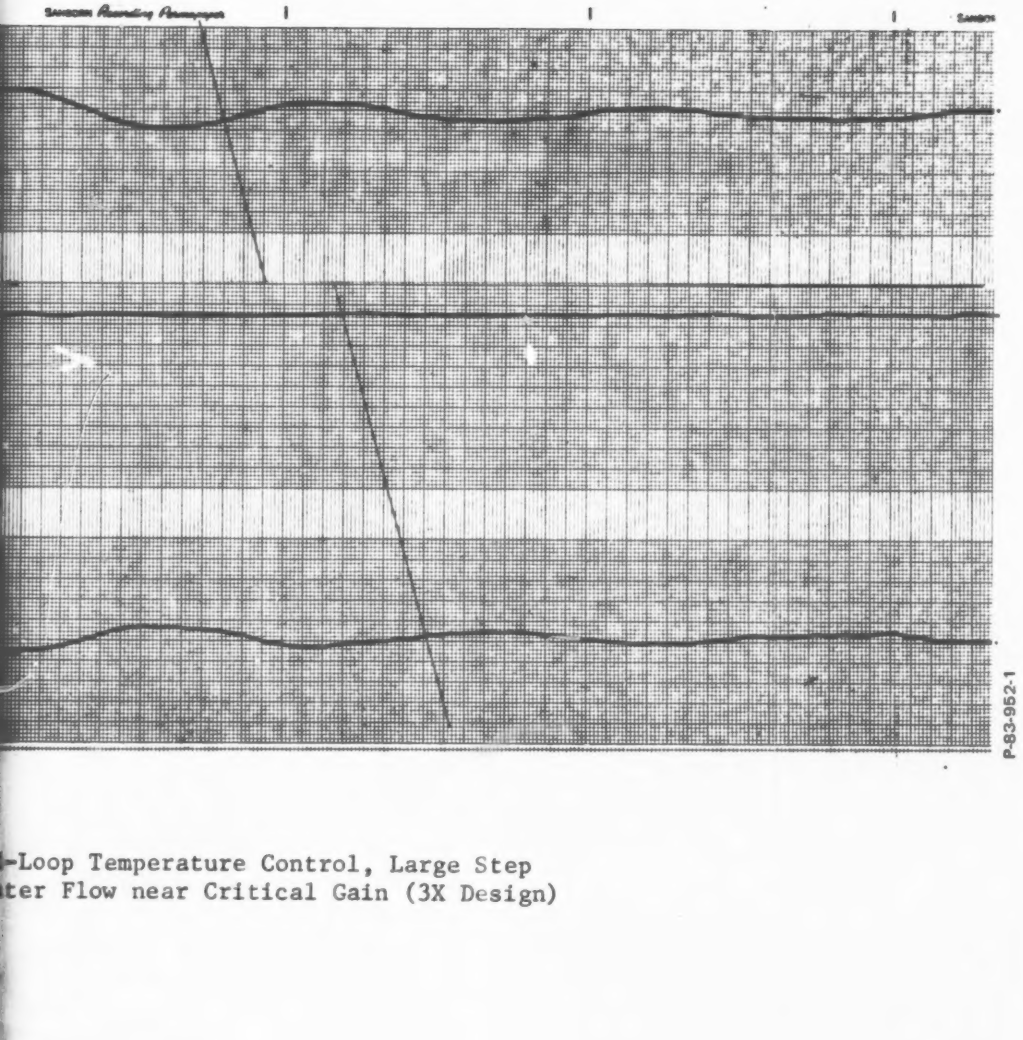

P-83-952-1

-Loop Temperature Control, Large Step
ter Flow near Critical Gain (3X Design)

B